UNIVERSITY OF LEEDS

Phenotypic and Functional Characterization of B-lineage cells Associated With Relapse and Response to B-cell Depletion Therapy for Rheumatoid Arthritis

Gururaj Arumugakani

November 2015

Submitted in accordance with the requirements for the degree of Doctor of Philosophy

Supervisors

Prof.Dennis McGonagle

Dr.Reuben Tooze

Section of Experimental Rheumatology

Leeds Institute of Molecular Medicine

&

Haematological Malignancy Diagnostic Service

Leeds Teaching Hospitals NHS Trust

The candidate confirms that the work submitted is his own and that appropriate credit has been given where reference has been made to the work of others.

Acknowledgements

I owe my deepest gratitude to many people for their invaluable help throughout my research.

I am extremely grateful to Professor Paul Emery for his continued direction and support in this work.

Firstly I would like to thank Dr Andy Rawstron, for his help and guidance in designing and setting up of complex flow cytometry panels and analysing the resultant data and also sharing his expertise in excel. He was also helpful with troubleshooting all flow cytometry related aspects of the project. I am grateful for his sharing of knowledge and preliminary data on long-lived plasma cells.

Ms.Ruth DeTute, Mr.Matthew Cullen and Ms.Fiona Bennett have all been of great help with day to day flow cytometry experiments.

I would like to thank Dr.Darren Newton for performing the Next generation sequencing of the IGHV regions and his guidance in performing the PCR for EBV detection.

I am grateful to Dr.Isabel Haro for synthesizing citrullinated peptides with biotin and fluorescent tags to be used in ELISA, ELISpot and flow cytometry.

Dr.Gina Doody was extremely helpful in troubleshooting various assays at different stages of the project.

Mrs Sophie Stephenson, Dr. Nicholas Barnes and Dr. Mario Cocco have been extremely helpful in instruction on culture techniques. Dr. Mario Cocco also demonstrated techniques of RNA extraction and quantification. Dr. Mathew Care helped with the analysis of gene expression data.

I would also like to thank Dr John Sinfield, for his support and guidance with preparing various buffers for the experiments and lyophilisation of the citrullinated peptides.

My sincere gratitude extends to all patients and normal control groups for donating blood samples.

Finally I would like to thank both my supervisors, Prof.Dennis McGonagle and Dr.Reuben Tooze for all their help and guidance at every stage of the project and support throughout.

Abstract

Background:

Clinical response to therapeutic B-cell depletion by anti-CD20 antibody in rheumatoid arthritis (RA) is not associated with robust depletion of disease specific anti-citrullinated protein antibodies (ACPA). This suggests pathogenesis mediated predominantly by short-lived antibody secreting cells or an antibody independent role of B-cells or both in RA. The persistence of ACPA post B-cell depletion is consistent with secretion from long-lived plasma cells (PC) and could be linked to non-response to B-cell depletion. The aim of this thesis was to delineate populations of B-cells and plasma cells linked to RA disease activity.

Results:

Autoreactive citrullinated protein-specific B-cells were detected using ELISA from supernatants of B cell culture but not by flow cytometry or ELISpot. RA patients relapsing following B-cell depletion showed an increased proportion of a memory B-cell subset in the peripheral blood. The in vitro stage of B-cell differentiation closest to this relapse associated subset secreted multiple proinflammatory mediators. A novel mode of contact-dependent B-NK cell interaction was noted, likely to be due to EBV latency in B-cells or a novel mode of B-cell regulation by NK cells. $CD19^{Neg}$ PCs had a longer recovery time following depletion and had a longer life span in an in vitro PC differentiation model system but were generated early, which suggests that CD19 negativity is a marker for potential to be long-lived rather than PC age.

Conclusions:

Memory B-cell subset distribution is skewed during clinical relapse in RA which reflects on-going B-cell activity/differentiation generating inflammatory mediators or pathogenic short-lived antibody secreting cells which explains response to B-cell depletion or anti-TNF therapy. In those patients where B-cell depletion does not achieve clinical response, $CD19^{Neg}$ long-lived PCs may have a pathogenic role. Agents targeting certain stages of B-cell differentiation or long-lived PCs can be therapeutic options in carefully selected patients.

Table of Contents

List of Tables

List of Figures

1 Glossary

7-AAD – 7-Amino-actinomycin D

ABC – Activated B-cell

ACPA – Anti-Citrullinated Protein/Peptide Antibodies

ACR – American College of Rheumatology

ADCC – Antibody-dependant cell-mediated cytotoxicity

ANA – Anti-nuclear antibody

APC – Allophycocyanin

ASC – Antibody-secreting Cell

BAFF – B-cell Activation Factor

BCDT – B-cell Depletion Therapy

BCR – B-cell receptor

BSA – Bovine Serum Albumin

CCP – Cyclic Citrullinated Peptide

CD – Cluster of Differentiation

CD40L – CD40 Ligand

CEACAM – Carcino Embryonic Antigen Cell Adhesion Molecule

CFFCP2 – Chimeric Fibrin-Fillagrin Citrullinated Peptide

CFFCP2-Mimo/ESP – Chimeric Fibrin-Fillagrin Citrullinated Peptide synthesized by Mimotopes or Spanish collaborator

Cit Fib – Citrullinated Fibrinogen

CST – Cytometer Setup and Tracking

CVID – Common Variable Immunodeficiency

CV – Coefficient of Variation

DMARD – Disease Modifying Anti-Rheumatic Drugs

dsDNA – Anti-double stranded DNA antibodies

EBNA – EBV Nuclear Antigen

EBV – Epstein Barr Virus

EDTA – Ethylenediaminetetraacetic acid

ELISA – Enzyme-Linked Immunosorbent Assay

ELISpot – Enzyme-Linked Immunosorbent Spot

EULAR – European League Against Rheumatism

FCS – Foetal Calf Serum

Fib – Fibrinogen

FITC – Fluorescein isothiocyanate

GO – Gene Ontology

HMDS – Haematological Malignancy Diagnostic Service

ICAM – Intercellular adhesion molecule

IFN – Interferon

Ig – Immunoglobulin

IgA – Immunoglobulin A

IgD – Immunoglobulin D

IgG – Immunoglobulin G

IGHV – Immunoglobulin heavy chain - variable region

IgM – Immunoglobulin M

IL – Interleukin

IMDM – Iscove's Modified Dulbecco's Medium

ITIM – Immunoreceptor tyrosine-based inhibitory motif

LEAF – Low Endotoxin, Azide Free

LFA – Lymphocyte Function-associated Antigen

LMP – Latent Membrane Protein

mAb – Monoclonal antibody

MALT – Mucosa Associated Lymphoid Tissue

MCF – Median Channel Fluorescence

MFI – Mean Fluorescence Intensity

mRNA – messenger ribonucleic acid

NK cells – Natural Killer cells

OD – Optical Density

PADI – Peptidyl Arginine Deiminase

PBLM – Plasmablast Like Memory B-cell

PBS – Phosphate Buffered Saline

PCR – Polymerase chain reaction

PCs – Plasma Cells

PE – Phycoerythrin

PI – Propidium Iodide

PMT – Photomultiplier Tube

QDot – Quantum Dot

RA – Rheumatoid Arthritis

RAMB – Relapse-associated memory B-cell subset ($CD24^{Neg}$ $CD84^{Neg}$ $CD95^{Pos}$ $LAIR1^{Neg}$)

SDS – Sodium Dodecyl Sulphate

SLAM – Signalling Lymphocyte Activation Molecule

SYK – Spleen Tyrosine Kinase

TBE – Tris Borate EDTA buffer

TMB – Tetramethylbenzidine

TNF – Tumour Necrosis Factor

UDMB – Usual-dominant memory B-cell subset ($CD24^{Pos}$ $CD84^{Pos}$ $CD95^{Neg}$ $LAIR1^{Pos}$)

XLA – X-linked Agammaglobulinemia

2 Background

Rheumatoid Arthritis (RA) is a chronic inflammatory polyarthritis where the primary target tissue within the joint is the synovium. The definitive diagnosis of RA is based on a score of >= 6/10 in the ACR-EULAR classification criteria which is based on the number of joints involved, positivity for autoantibodies, acute-phase reactants and duration of symptoms (1).

2.1.1 Epidemiology of RA

The estimated prevalence of RA is between 0.5-1% from North European and North-American studies with a mean annual incidence of 0.02-0.05% (2). RA is considered to be a multifactorial disease secondary to interaction between genetic and multiple environmental factors including age, sex, ethnicity, socioeconomic status, hormonal, dietary, infections and smoking, all considered to increase its risk. HLA-DRB1 genotype (shared epitope) and smoking are the most strongly associated risk factors (3).

2.1.2 Burden on self and society

RA is the most frequent cause of inflammatory joint pain with a female predominance of 3:1. The incidence is highest during the fourth and fifth decades of life (4). It causes severe joint pain, restricted functionality and mobility. Up to 40% of the patients lose their job within 5 years of disease onset, which is a significant personal economic burden. The health care costs are also significantly high in terms of number of hospital visits, time spent in hospitals and treatment costs. The recent NRAS report estimates the cost of RA to the UK economy at 8 billion GBP (5). There is also slightly increased mortality with a reduction in life span by 3-10 years (6).

2.1.3 Pathogenesis of RA

The presence of shared epitope – amino acid motif QKRAA in the HLA-DRB1 region confers increased susceptibility to auto-antibody positive RA (7) with a relative risk (RR) of 2.8 (3). The risk is enhanced with smoking (RR=7.5), other forms of bronchial injury like silica exposure and periodontitis. The peptidyl arginine deiminase enzyme (PADI) family which is released during bronchial damage or directly by P.gingivalis converts positively charged arginine residues on

self-proteins to neutrally charged citrulline. The recognition of such citrullinated proteins is enhanced by the presence of the shared epitope (8).

Single nucleotide polymorphisms in genes involved in lymphocyte signalling, co-stimulatory molecules, transcription factors, cytokines and their receptors have been linked with RA. The combination of environmental factors, epigenetic changes and presence of susceptibility genes induces post translational modification of self-proteins (citrullination and carbamylation) with resultant loss of tolerance to the modified proteins (9).

The adaptive immune system mounts responses to these modified proteins in the secondary lymphoid tissues and localises to the synovium through poorly understood mechanisms and initiates synovitis. The synovitis is perpetuated and maintained by positive feedback loops involving innate inflammatory cells, cytokines and other soluble pro-inflammatory mediators causing tissue damage locally with some systemic effects (8). Studies have shown that the inflamed synovial environment directly contributes to this by favouring the development of functional ectopic lymphoid structures that support autoantibody production which exacerbates disease chronicity (10).

The genetics of RA and presence of autoantibodies is suggestive of a key adaptive immunity component to the pathogenesis. Additionally, the remarkable clinical response to anti-TNF agents and anti-IL6 would imply a key role for cytokines and innate immunity. Cytokines also have systemic effects like release of acute phase proteins (IL6), cachexia (TNF- α) and accelerated vascular disease (11). Thus the clinical manifestations of RA represent a combined manifestation of adaptive and innate immune responses.

2.1.4 Role of autoantibodies in RA

Various autoantibodies have been described in RA and the first RA-associated antibody, rheumatoid factor (RF) was identified in 1937 (12). RF causes differential agglutination of normal and sensitised sheep RBCs which formed the basis of Rose-Waaler test (13). It was later found to be directed against the FC portion of IgG. IgM-RF is the commonly measured isotype and depending on the chosen cut-off value has a sensitivity of 60-80% but is limited by poor specificity (14). Transiently elevated IgM-RF is part of a normal immune response and

elevated RF is seen in a variety of other autoimmune disorders, infections and healthy people (15).

Anti-citrullinated protein antibodies (ACPA) are highly specific (98%) RA associated autoantibodies present in two-thirds of patients (16) and can precede disease onset by 4-5 years or occasionally longer (17). The diagnostic ACPA assays mostly detect IgG isotype using cyclized versions of citrullinated peptide (CCP) sequences from various proteins including α–enolase, vimentin, fillagrin, fibrinogen, collagen and keratin (18). The presence of ACPA positivity is associated with more severe disease and joint destruction (19). Therefore, RA could be perceived to be an autoantibody driven disease. However, a direct pathogenic role for ACPA remains unproven in humans so far as clinical remission is achieved without ACPA depletion although induction of ACPA has been shown to cause joint damage in mouse models (20).

2.1.5 Treatment of RA

Immunosuppression to down-modulate inflammatory cells and soluble mediators is the main stay of treatment for active RA. Disease modifying anti rheumatic drugs (DMARDs) including methotrexate (MTx), sulphasalazine, anti-malarial agent hydroxychloroquine and leflunomide alone or in combination with or without steroids are used as first-line agents. Anti-TNF agents, anti-Il6, B-cell depletion and co-stimulatory blockade in the form of monoclonal antibodies and fusion proteins have been used as the next step-up in therapy in case of DMARD failure. All the anti-TNF agents and biologic therapy are comparable in efficacy, but the IL-1R antagonist Anakinra is less effective (21).

2.1.6 Therapeutic B-cell depletion for RA

The clinical response achieved by B-cell depletion with therapeutic monoclonal anti-CD20 antibody (rituximab) for treatment of DMARD and anti-TNF failures in RA points towards a key role for B-lineage cells in the pathogenesis of RA (22). Rituximab directly depletes all B-lineage cells except plasmablasts, plasma cells and pre B-cells that do not express CD20.The B-cell depletion is mediated through 3 different mechanisms: complement mediated killing by activation of classical complement pathway, ADCC (Antibody-dependent cell mediated cytotoxicity), direct apoptosis by ligating CD20 (23). However, the mechanism by which B-cell depletion improves clinical symptoms remains unclear. ACPA levels decline initially, then plateau and continue to persist, and the change in ACPA levels does not predict clinical

response (24). This along with correlation of clinical response with B-cell depletion (25) implies a key role for B-cells which may or may not be related to the generation of ACPA secreting short-lived cells.

2.1.7 Other B-cell modulating agents for RA

There are other antibodies under clinical trials targeting pan-B cell molecules including anti-CD22 and anti-CD19 for treatment of RA. Belimumab is an antibody targeting the B-cell activation factor (BAFF) licensed for lupus and undergoing clinical trials for RA. Tocilizumab, an anti-IL6 antibody has been licensed for RA recently and is effective (26). IL-6 is required for plasma cell survival and Tocilizumab alters the peripheral blood memory B-cell compartment as well (27). Oral small molecules blocking the cytoplasmic tyrosine kinase SYK, which is a mediator of immunoreceptor signalling in B-cells, neutrophils, macrophages and mast cells have shown significant clinical response compared to placebo (28). Another small molecule targeting Janus Kinases (JAK) involved in signal transduction for multiple cytokines has been shown to be of comparable efficacy to the anti-TNF monoclonal antibody, Adalimumab for RA (29).

2.1.8 Rituximab – Mode of action

The mechanism of action of rituximab in RA and other autoantibody driven autoimmune diseases is still poorly understood. Potential mechanisms include:

- Depletion of pathogenic B-cells that mediate disease in an antibody independent fashion which could be antigen-specific secretion of inflammatory cytokines (TNF, IL6 (30)), co-stimulatory activity, increased antigen presentation or antigen independent.
- Depletion of short-lived plasmablasts that secrete potentially pathogenic short-lived autoantibodies including rheumatoid factor and ACPA and also have some B-cell functionalities including cytokine secretion and co-stimulatory activity (31).
- Depletion of short-lived plasma cells by depleting the B-cells and plasmablasts from which they originate.
- Depletion of non-B lineage cells like sub-populations of T-cells expressing CD20 with pro-inflammatory properties (32).

2.1.9 RA – Unmet needs

The response rate for anti-TNF agents is 60-70% and it is similar for rituximab. Recent EULAR recommendation advocates the early use of biologic agents (33) and combining biologics with DMARDs is more effective than DMARDs alone (34). Anti-TNF agents are preferred for seronegative RA, but currently there are no biomarkers to guide the choice between rituximab and anti-TNF for seropositive RA. However, it has been noted that use of multiple anti-TNF agents prior to rituximab reduces its efficacy (35). Therefore, it would be beneficial to identify markers that would predict response to B lineage targeting for seropositive RA. The levels of citrullinated protein-specific B-cells might be one such marker in predicting response to BCDT.

Poor response in the form of early relapse or lack of response to rituximab therapy could be secondary to multiple reasons:

1. Lack of depletion or early return of the pathogenic subset (antigen-specific or antigen independent)
2. Presence of cells which are unaffected by rituximab (CD20 negative plasmablasts or plasma cells)

Various predictors of better response to rituximab prior to commencement of therapy have been proposed and include low levels of type1 interferons, circulating BAFF levels and favourable Fcγ receptor III genotype (36). Chemokines such as CXCL13 are able to predict return of B-cells following B-cell depletion (37) and baseline circulating levels of miRNA-125b predicted good response (38). Recent studies have shown the levels of IgM RF, soluble CD23 and serum free light chains as markers of plasmablast differentiation correlate with B-cell depletion and response (39). One of the best available predictors of response to rituximab is the level of B-cell depletion in the initial 2 weeks after the first dose of rituximab. The persistence of plasmablasts or B-cells at this time point is a predictor of poor clinical response (25). Relapse is unlikely without return of B-cells once clinical response is achieved with B-cell depletion. However, in patients who have started regenerating B-cells, the clinical relapse is variable, which might theoretically relate to the re-emergence of ACPA-specific clones, but this is unproven. A proportion of patients reconstitute with high proportion of plasmablasts, which is likely to be due to incomplete depletion and predicts poor response (25). Currently there is no way of predicting relapse in the major proportion of patients who reconstitute their B-cell compartment in a

physiological manner with predominant naïve and transitional B-cells and low proportion of plasmablasts. Some centres have therefore resorted to administering rituximab regularly every 6 months even though most patients would not have needed any treatment at that point (40).

2.1.10 B-cell subsets

Naïve B-cells are generated from the differentiation of B-cell precursors in the bone marrow (BM) through an intermediate transitional stage, which can also be seen in peripheral blood. Transitional B-cells are the earliest stage of B-cells seen in peripheral blood under physiological conditions (41). Naïve B-cells recirculate between peripheral blood and secondary lymphoid organs (lymph nodes, spleen, mucosa associated lymphoid tissue (MALT), BM) and die in the absence of antigen encounter. When the naïve B-cells recognize an antigen they can respond by generating extrafollicular plasmablast foci generating short-lived antibody responses, or in the context of a T-dependent cognate interaction start the germinal centre (GC) reaction in the secondary lymphoid organs (42). In germinal centres, B-cells express high levels of BCL6, undergo multiple rounds of proliferation and somatic hypermutation of rearranged immunoglobulin genes (43). This is coupled with antigen-dependent affinity maturation to generate memory B-cells and antibody secreting plasmablasts with enhanced affinity for antigen, and in some cases class-switched immunoglobulin (44). Plasmablasts migrate to survival niches in the BM or MALT and complete differentiation into plasma cells whereas the quiescent memory B-cells continue recirculating or migrate to antigen draining tissues.

During the process of B-cell activation and differentiation distinct combinations of surface proteins are regulated by underlying genetic programmes. These allow characterisation of B-cell subsets and functional states. The surface marker profile of major subsets is given below:(45)

- Transitional – $CD19^{Pos}CD20^{+}CD27^{-}CD38^{++}CD24^{+}$
- Naïve – $CD19^{Pos}CD20^{+}CD27^{-}CD38^{+/-}$
- Memory - $CD19^{Pos}CD20^{+}CD27^{+}CD38^{+/-}$
- Plasmablasts - $CD19^{Pos}CD20^{-}CD27^{++}CD38^{++}$
- Plasma cells - $CD19^{Pos/-}CD20^{-}CD27^{++}CD38^{++}CD138^{+}$

2.1.11 Long-lived plasma cells

Evidence for the existence of long-lived PCs comes from animal models that have shown persistence of antigen-specific PCs in the absence of B-cells (46-48). The presence of long-lived PCs in humans is supported by the persistence of anti-viral antibodies including small pox (49, 50) and also the stable antimicrobial antibody levels in the absence of B-cells following therapeutic B-cell depletion for B-lymphoid neoplasms and autoimmune disorders (24). The therapeutic anti-CD20 monoclonal antibody rituximab, does not affect PCs since CD20 expression is lost during differentiation to plasmablasts and plasma cells. The levels of vaccine antibodies do not fall after treatment with rituximab where as there is a steep fall in levels of rheumatoid factor (24), which are good examples of antibodies secreted by long and short-lived PCs respectively. Since, there are no definitive phenotypic markers of short or long-lived PCs, identifying PCs secreting vaccine-specific antibodies in the absence of recent vaccination or infection is a potential way of identifying a long-lived PC.

Multiple factors have been described as determinants of PC longevity. Although plasmablasts can be generated from naïve, memory, germinal centre, marginal zone or follicular B-cells whether all of these heritages could generate long-lived PCs is not known. The nature of signals received by these cells in terms of the antigen, T-cell help and TLR stimulus also play a role. According to the model described by Radbruch et al., the heritage and instructions determine the competence of plasmablasts to become a long lived PC (51).

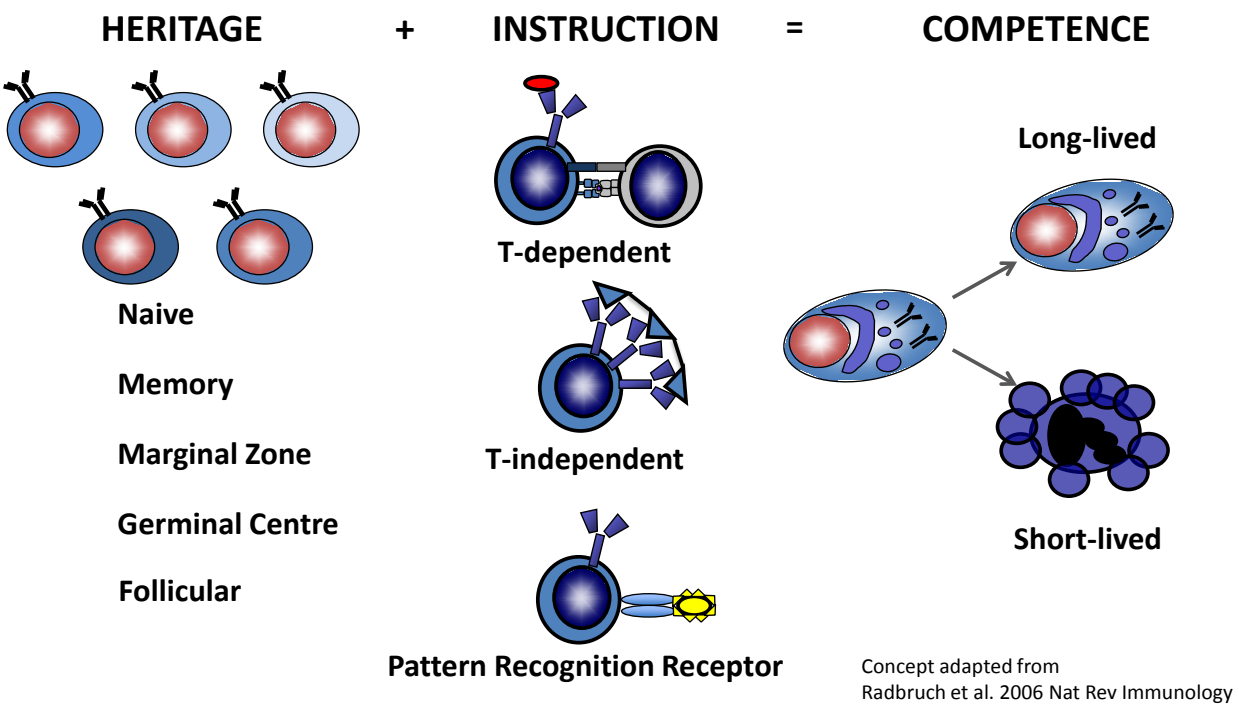

Figure 5.1-1 Competence of becoming a long-lived plasma cell

Plasmablasts can be generated from naïve, memory, marginal zone, germinal centre or follicular B-cells, but whether cells of all heritages can give rise to long-lived PCs is not known. This heritage along with instruction in the form of nature of antigen, T-cell help and TLR stimulus determines the competence to be a long-lived PC. *Pictures of the cells – courtesy of Dr.R.Tooze.*

The PCs reside in bone marrow niches that support their survival. The niche is constituted by molecular components such as SDF1, APRIL, BAFF etc. and cellular components such as stromal cells, eosinophils, DCs, neutrophils etc. To maintain the competence once differentiated to PCs, they should be able to home to the niche, reside there against competition and respond to the niche components (52).

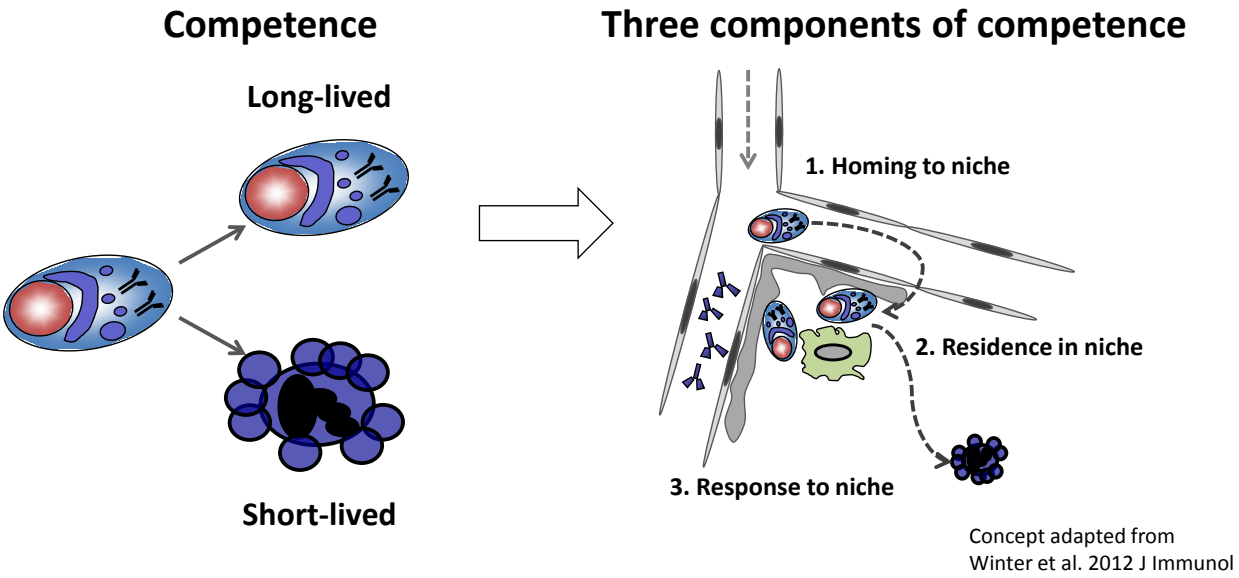

Figure 5.1-2 Maintaining competence of long-lived plasma cell

To maintain the competence of long-lived PC, the cells should be capable to homing to the niche, reside there against competition and respond to the niche. *Pictures of the cells – courtesy of Dr.R.Tooze.*

2.1.12 In vitro methods for generating plasma cells

The direct comparison of human and mouse plasma cells is difficult due to significant phenotypic differences, such as the lack of CD38 expression in mouse. Investigating the biology of human plasma cells in vivo to derive precursor-product relationships and establish lifespans is not readily feasible. Furthermore human plasma cells do not survive well in xenotransplant models, although these issues have been addressed with some modifications (53). Multiple in vitro model systems have been developed in the past as alternatives. One of the earliest developed models developed using CD40L transduced fibroblast established that exposure followed by removal of CD40L is essential for PC differentiation (54). Mouse stromal cells and IL6 were able to maintain viable plasma cells for short periods (55). Differentiation of B-cells to PCs has been achieved with plasmacytoid dendritic cells (DCs) due to their secretion of IFNα (56). IL21 was identified as a key cytokine to induce B-cell differentiation to PCs and also class-switching but not somatic hypermutation (57). TLR9 agonist unmethylated CpG DNA can induce

PC differentiation of naïve and memory B-cells in the absence of CD40L and BCR stimulus (58). A method using a 3-stage process to generate PCs with detailed characterisation has also been reported (59). However, none of the methods were able to maintain viable, functional plasma cells in vitro long-term. A recently described method uses the key essential factors identified from the above methods and is able to generate plasma cells with an estimated potential lifespan of 40 years (60).

2.1.13 Myeloma and long-lived plasma cells

Intuitively it may be considered that long-lived PCs that are linked to autoimmunity may share characteristics with PCs from malignant conditions given the longevity of the latter. Multiple myeloma is a monoclonal PC disorder that is preceded by a premalignant condition, monoclonal gammopathy of undetermined significance, MGUS. The MGUS PCs share phenotypic and genetic abnormalities of myeloma PCs and the key distinguishing factors are the tumour load in the bone marrow and end organ damage. Clear progression from the indolent MGUS to aggressive myeloma state is demonstrable. The normal counterpart of myeloma PCs is the post-GC, long-lived bone marrow PC but the cell of origin for these neoplastic PCs is still not completely understood (61, 62). Myeloma PCs subvert the survival factors of normal long-lived PCs which depend on bone marrow survival niches (51). While the presence of long-lived PCs is supported by observations related to antimicrobrial immunity (50) and also the stable antimicrobial antibody levels in the absence of B-cells following therapeutic B-cell depletion for B-lymphoid neoplasms and autoimmune disorders (24). However the phenotypic identification of this population has remained elusive. Direct evidence for extended PC lifespan in humans is lacking. While human PCs with extended lifespan can be generated in vitro (63), the mode of maintenance and regulation of long-lived PCs in vivo is not known (64). Animal studies support extended lifespans (47, 48) but comparisons are complicated due to the phenotypic differences with human PCs such as the lack of CD38 in murine PCs and maintenance of CD19 on many but not all human PCs. In vitro systems for generation of human PCs that can survive for prolonged periods provide tractable models (63) but cannot fully recapitulate in vivo biology. Thus in vivo correlative studies are an essential component of understanding human PC biology.

The PCs in myeloma are characteristically CD19 negative and show aberrant expression of CD56, CD45, CD27 and CD38 in addition to their clonality. Normal PCs are predominantly

CD19 positive but also include a proportion of CD19 negative polyclonal PCs (65). While the normal counterpart of myeloma PCs, the long-lived PC may share some characteristics it is not known whether normal $CD19^{Neg}$ PCs share extended similarities with myeloma PCs and how they differ from normal $CD19^{Pos}$ PCs.

2.1.14 B-cell subsets in autoimmunity

Flow cytometric phenotyping of peripheral blood B-cells has been successfully employed in the past to identify markers associated with autoimmune diseases and subsets correlating with response. Complement receptor 1&2 have been shown to be down-regulated on B-cells of RA and lupus patients (66). In lupus patients, an autoreactive population based on levels of CD19 expression and CXCR3 has been identified (67).The surface expression and function of leucocyte associated Ig like receptor (LAIR) 1 which mediates down modulation of various kinases and cell activation via its cytoplasmic tail containing ITIMs has been shown to be reduced in lupus B-cells (68). BCDT has helped to identify a previously undescribed late stage of transitional B-cells which would have been classified as mature naïve B-cells in the past but differ from naïve B-cells in terms of increased CD24 and IgM expression, reduced CD23 expression and functional immaturity demonstrated by increased apoptosis susceptibility (69). A recent study has shown that levels of CD95+ non-class switched memory B-cells is predictive of clinical response to rituximab (70). Thus several recent and prior studies point to alterations in peripheral blood B-cell populations as a means of identifying disease associated B-cell subsets and potential biomarkers of disease activity.

2.1.15 Identification of antigen-specific B-cells

The ability to robustly isolate antigen-specific B-lineage cells in RA has considerable potential for defining the cellular hierarchy in ACPA production. Identification of Ag-specific cells has been technically challenging so far irrespective of the techniques used and one of the main reasons is the low frequency of Ag-specific cells (1 in 10000 B-cells) (50). The limiting dilution method, which was used to determine the initial frequency of Ag-specific cells, employs culturing of serial fold dilution of cells followed by evaluation of the supernatant for secreted antibodies by ELISA (71). This method is limited by the inability to phenotype the antigen-specific B-cells, sensitivity of ELISA, lack of reproducibility and labour intensity.

Flow cytometry can also be used to detect Ag-specific cells by using a fluorescent-tagged antigen (71). This offers the chance to phenotype the antigen-specific cells using surface markers, isolate the cells by sorting for further analysis such as gene expression and sequencing the immunoglobulin gene but could be limited by sensitivity issues and non-specific binding. ELISpot is another technique where the antibodies secreted by the cells are captured on the surface, which are detected with a colorimetric agent as a spot. The number of spots roughly equals the number of antibody secreting cells and from the number of input cells, their frequency can be calculated. While this technique can be linked to phenotypic characterisation of the input cell population, it does not allow the subsequent functional evaluation of the secreting cell, unless modified in a fluorescent capture approach.

Another novel approach employed single cell sorting of B-cells with a chosen phenotype from synovial fluid or plasmablasts from peripheral blood of RA patients with active disease and sequencing their immunoglobulin gene. The sequence was then re-expressed in a hybridoma setting and the secreted antibody was tested for ACPA specificity (72). While this technique provides a gold standard definition of antigen specificity linked to a known rearranged immunoglobulin gene pair, it is limited by the expertise required for sequencing from single cells and the hybridoma setting required to express the immunoglobulin sequence.

2.1.16 Summary

Several lines of evidence point to a central role for B-cells and their plasma cell progeny in RA pathogenesis. However the definition of disease associated B-cell and plasma cell populations is incomplete. The overarching theme of this work was to undertake detailed phenotypic and functional characterisation of B-lineage cells associated with relapse and resistance to treatment with rituximab in RA, and assess the relationship to ACPA secretion and plasma cell longevity to build toward a more comprehensive view of B-cell populations in RA.

3 Aims and Hypothesis

Anti-citrullinated protein antibodies (ACPA) are highly specific (>95%) for diagnosing rheumatoid arthritis (RA) and correlate with disease severity. However, the direct pathogenicity of ACPA is unproven. Of note, ACPA typically precedes clinical symptoms of RA by a few years. Clinical responses in RA are achieved with B-cell depletion, indicating a central role for this lineage in RA pathogenesis, but ACPA persists although there may be some reduction in levels. This could be suggestive of an antibody independent role for B-cells, which could either be antigen-specific or independent of their specificity. Alternatively, short-lived plasma cells and plasmablasts or their secreted autoantibodies are pathogenic whereas the long-lived PCs and their secreted antibodies are not. Due to their lack of CD20 expression neither PCs nor plasmablasts are directly affected by anti-CD20 therapy, however the B-cells giving rise to the short-lived cells will be depleted, thus potentially arguing for a more important role for plasmablasts and short-lived PCs in disease pathogenesis.

Hypotheses:

I. Antigen-specific B-cells correlate better with clinical response than the levels of autoantibodies.
II. Pathogenic B-cells responsible for disease process in RA are enriched within B-cell subpopulations as characterised by flow cytometry.
III. Short-lived and long-lived PCs have different roles in RA pathogenesis.

The key aims of this work were:

I. To identify ACPA-specific B-cells to correlate with clinical relapse and response.
II. To phenotypically characterise the B-cell subsets during clinical relapse following rituximab to identify potential pathogenic and/or autoreactive B-lineage cells as markers of disease relapse and response to therapy.
III. Establishing a phenotype for long-lived PCs to assess the nature of PCs generated by above B-cell subsets from RA patients.
IV. To identify functional differences between normal & RA B-cells in generation and survival of plasmablasts and plasma cells.

4 Overview of Thesis

RA disease specific ACPA depletion is not required for clinical response and incomplete depletion of B-cells is associated with poor clinical response. Therefore, it was hypothesized that citrullinated-protein specific B-cells are pathogenic in RA. In the first section of the results various methods were employed to detect the citrullinated-protein specific B-cells from peripheral blood. Although autoreactive B-cells are unlikely to exhibit a distinct surface phenotype, it was hypothesized that the B-cell subsets that are expanded during relapse following rituximab are likely to contain the autoreactive cells. The second results chapter discusses data from extensive phenotyping of peripheral blood B-cells to identify subsets of B-cells that are altered during relapse post-rituximab. The third results chapter attempts to define the functional role of the subset identified from the B-cell phenotyping such as antigen-specificity, pro-inflammatory mediator secretion and fluctuation during a normal immune response. The fourth chapter describes the unexpected finding of B-cell interaction with other cell types particularly NK cells which can have potential relevance to RA pathogenesis and was initially observed with RA B-cells. The clinical response to B-cell depletion with maintenance of disease specific autoantibodies suggests that pathogenesis could be potentially mediated by short-lived antibodies and short-lived PCs that are indirectly depleted. The distinction between short- and long-lived PCs is that of a functional one so far and the final chapter aims to identify phenotypic markers for long-lived PCs.

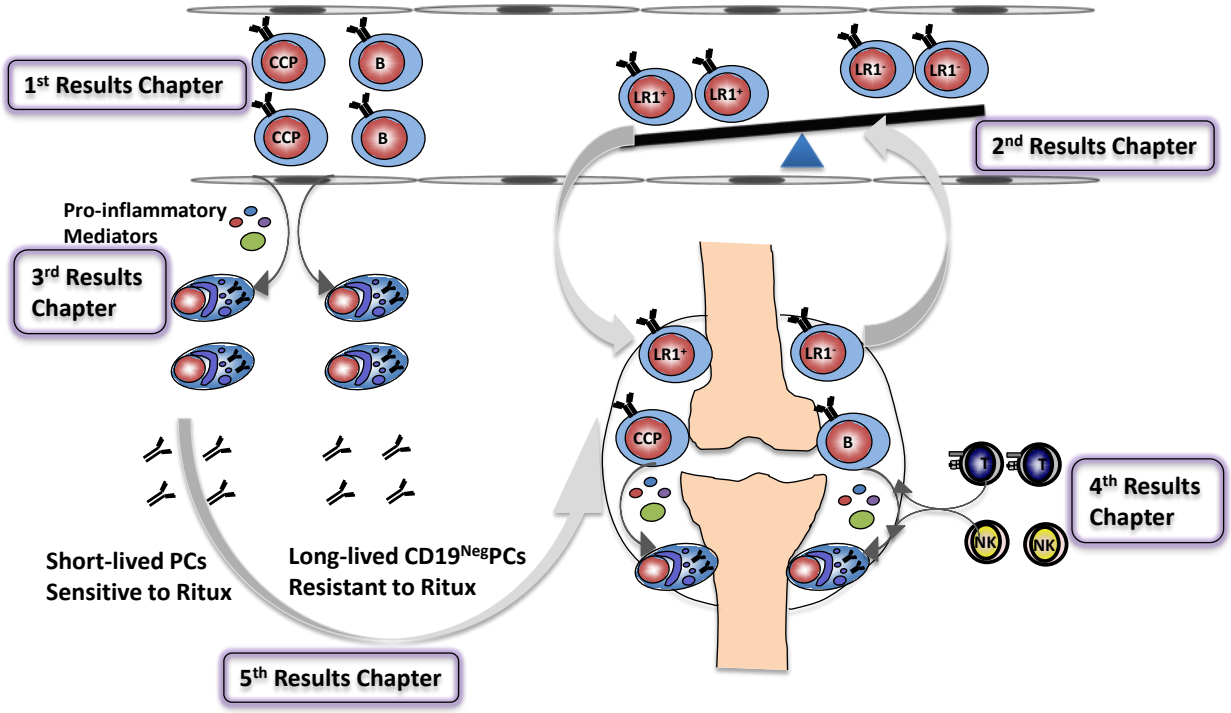

Figure 5.1-1 Overview of the sections of the thesis

The first results chapter aims to identify antigen-specific B-cells from peripheral blood. The second results chapter describes alterations in B-cell subsets during relapse post-rituximab which could be due to recruitment of pathogenic B-cells into the synovium or egress of pro-inflammatory cells from the joints. The third results chapter evaluates the functional role of the subsets identified in the previous chapter such as pro-inflammatory mediator secretion. The fourth results chapter describes B-cell interaction with NK cells which was an unexpected finding but might have relevance to RA pathogenesis. The final results chapter attempts to identify a surface phenotype to distinguish short and long-lived PCs which are likely to be differentially involved in RA pathogenesis. CCP – Citrullinated protein specific B-cells, B – B-cells, T – T-cells, NK – NK cells and LR1 – LAIR1.

5 Materials & Methods

5.1 Patients and Ethics

Samples were collected from RA patients managed at Leeds Teaching Hospitals NHS Trust and controls after informed written consent and was approved by Leeds (East) Research Ethics Committee (Ref: 04/Q1206/107). The use of waste clinical samples at HMDS from anonymous patients and controls was approved by the Leeds Teaching Hospitals Research Ethics Committee (Ref: 04/Q1107/40).

The MRC Myeloma IX trial was a multicentre, randomised phase III trial approved by the relevant institutional review boards. All patients provided written informed consent. Patients included in the analysis received high dose melphalan followed by autologous stem cell rescue. The detailed protocol of the trial has been described elsewhere (73). A six-colour panel of antibodies was used to analyse the PCs: CD138 APC (Miltenyi Biotec), CD45 APC-Cy7 (BD Pharmingen), CD38 PE-Cy7 (BD Pharmingen), and CD19 PerCP-Cy5.5 (BD Pharmingen).

A series of clinical trial studying the efficacy of Campath-1H for refractory CLL (74-76) were approved by the institutional review board and informed written consent was obtained from the patients

5.2 FACS staining

A volume equivalent of 1 million white cells from peripheral blood or bone marrow aspirate collected in EDTA tube was used. The required sample volume was calculated as follows:

$$Volume\ (\mu L) = \frac{1000}{White\ cell\ count\ (\times 10\text{^}9/L)}$$

For example, to obtain 1 million leucocytes from a sample with white cell count of $10X10^9$/L, 100 µL of sample would be required. The sample was treated with 8.6 g/L solution of ammonium chloride (Sigma Aldrich) for 10 minutes at 37^0C to lyse the red blood cells. Then cells were washed with 0.1% BSA in Facsflow (BD Biosciences) twice in 15 ml tubes (2000 rpm

for 4 minutes). Cells were then transferred to microtitre plates and incubated with the antibody cocktail for 20 minutes. For tests using a biotinylated antibody, 10 µL of Streptavidin pacific orange (50 µg/ml) (Invitrogen) was added at the end of 20 minutes and incubated for a further 5minutes. The samples were then washed twice with 0.1% BSA in Facsflow and resuspended in 300 µL of Facsflow in a tube. 500,000 – 1 million events were acquired on an 8-colour BD FACS Canto II or 11-colour LSRII Fortessa.

FACS Diva (Version 6.2/7, BD Biosciences) was used to analyse the data files. Data was analysed using Excel (Microsoft Office 2007/2010) and statistical analysis was performed with Graphpad Prism 5/6. Significance of difference in subsets between different patient groups was calculated using 1 way ANOVA (Analysis of Variance).

5.2.1 Antibody titration for flow cytometry

Antibodies were used at manufacturer recommended concentrations or the concentrations validated at the diagnostic HMDS laboratory. For antibodies which are not routinely used in HMDS, titration experiments were performed to establish the optimal dilution. In this example, CD19 PE-CF594 antibody was tested undiluted, 1 in 5 dilution and doubling dilutions till 1 in 640. An unstained sample was also included in the dilution series. CD20 antibody was used to identify B-cells and the level of fluorescence on B-cells and non-B lymphocytes were measured. The aim of titrating the antibodies is not only to achieve the best fluorescence signal in the cells of interest but also reduce the levels of non-specific fluorescence in the negative population. Signal to Noise ratio was calculated as follows:

$$Signal : Noise\ Ratio = \frac{CD19\ MFI\ of\ B - cells}{CD19\ MFI\ of\ non - B\ lymphocytes}$$

The dilution at which the fluorescence of the positive cells intersect the signal to noise ratio i.e, the dilution that provides the highest signal to noise ratio with the highest fluorescence was chosen. For CD19 PE-CF594 antibody in the example below, the optimal dilution is 1 in 5, which is 1 µL.

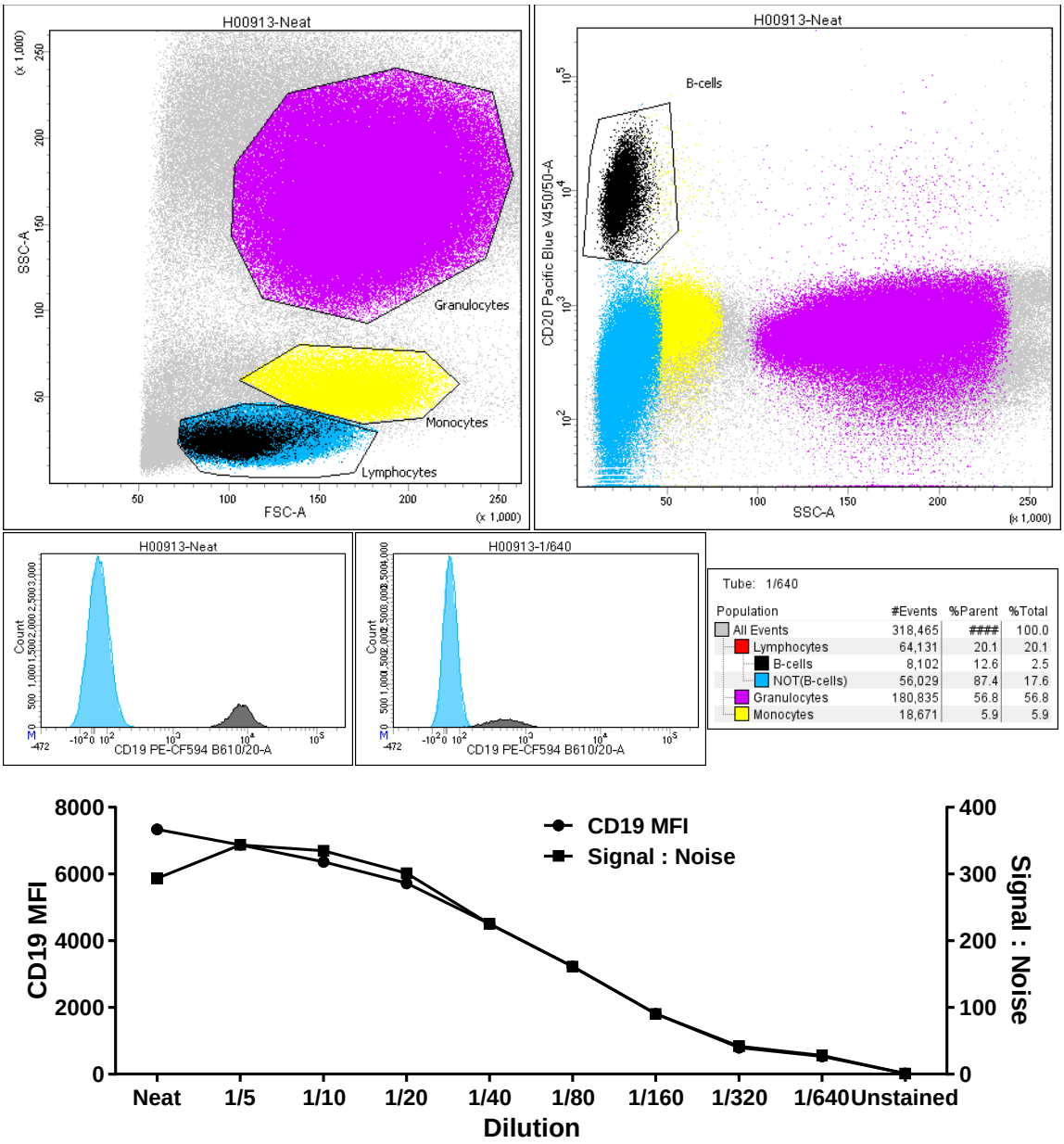

Figure 5.2-1 Titration of antibody for flow cytometry

Lymphocytes, monocytes (Yellow) and granulocytes (Purple) were gated based on their scatter profile and B-cells (Black) based on CD20 positivity. Inverse of the CD20 gate defined the non-B lymphocytes (Blue).
Histograms of B-cells and non-B lymphocytes at undiluted and maximal dilutions shown.
CD19MFI plotted on the left Y-axis (Circles) and signal to noise ratio on the right Y-axis (Squares) with dilutions shown on the X-axis.

5.2.2 Cell counting

Absolute cell counts of different lymphocyte subsets were obtained by dual platform methodology, the two platforms being – automated haematology cell counter and flow cytometer. Cell count of peripheral blood samples was performed on Sysmex K-1000 automated haematology analyser. This measured various parameters including – haemoglobin, platelet count, red cell count and white cell count with percentages and absolute counts of neutrophils, lymphocytes and monocytes. The absolute counts of various lymphocyte subsets were calculated from the proportion of that subset obtained by flow cytometry with the counts generated by sysmex as shown below:

$$B-cell\ count = \frac{B-cells\ as\ \%\ of\ lymphocytes \times Lymphocyte\ count\ from\ Sysmex}{100}$$

Plasmablasts, naïve and memory and B-cell counts from the diagnostic assay was used where available to calculate the absolute count of the B-cell subsets from RA patients.

For calculating the absolute counts of cells from tissue culture experiments CountBright absolute counting beads (Invitrogen) were used. 25 µL of CountBright beads were added to 300 µL of cell suspension and acquired on the flow cytometer. 5 µL of propidium iodide was added few minutes before sample acquisition to exclude dead cells. When the available sample volume was less than 300 µL, rest of the volume was substituted with FACSflow. The absolute cell count was calculated using the formula below:

$$Concentration(Cells/\mu L) = \frac{No.of\ Cell\ Events}{No.of\ Bead\ Events} \times \frac{Assigned\ Bead\ Count\ of\ the\ lot\ (beads/25\mu L)}{Volume\ of\ sample\ (\mu L)}$$

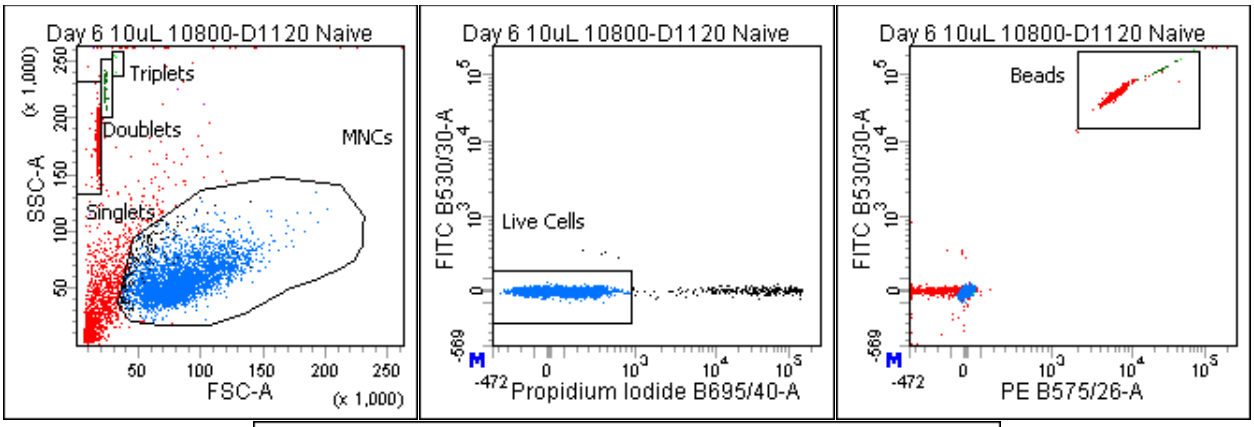

Tube: D1120 Naive

Population	#Events	%Parent	%Total
All Events	8,246	####	100.0
Time	8,246	100.0	100.0
MNCs	3,748	45.5	45.5
Live Cells	3,490	93.1	42.3
Beads	3,000	36.4	36.4
Singlets	2,971	36.0	36.0
Doublets	39	0.5	0.5
Triplets	6	0.1	0.1

Figure 5.2-2 Gating strategy for cell counts

The cells were gated based on their scatter profile and dead cells were excluded based on propidium iodide positivity. The beads were gated on their positivity in FITC and PE channels and bead doublets and triplets were identified based on their forward scatter profile. Thus the bead events were verified by both their fluorescence as well as scatter profile.

5.2.3 Flow cytometry panel for B-lineage cells during in vitro differentiation

For routine phenotyping of cells from the cell culture experiments, the panel shown in Table 5.2-1 with respective isotype controls were used. Non-specific binding was blocked with 25 µL of blocking buffer (50 µL normal mouse serum, 16.6 µL human IgG and 933 µL of 0.1% BSA in Facsflow to make 1 ml of blocking buffer) for 10 minutes before the antibody staining. Samples were washed with 0.1% BSA in Facsflow and then with annexin binding buffer (eBioscience). Samples were re-suspended in 100 µL of annexin binding buffer with 5 µL of Annexin-V FITC (eBioscience) along with 5 µL 7AAD (eBioscience) or propidium iodide (eBioscience) and incubated in the dark at room temperature for 10 minutes. Further 100 µL of annexin binding buffer was added and samples were kept at 4^0C till they are acquired in the flow cytometer.

Table 5.2-1 Antibody cocktail used for flow cytometric phenotyping of B-lineage cells during in vitro differentiation

Antibody cocktails were made up in multiples of 10 and 10 µL of the cocktail was used per test.

	4-colour Cocktail (µL)	Isotype Cocktail (µL)
CD19 PE	20	20
CD20 eFluor450	25	12.5
CD38 PE-Cy7	1	10
CD138 APC	20	30
0.1% BSA in Facsflow	34	27.5
Total for 10 Tests	100	100

The gating strategy for classifying the B-lineage cells during in vitro differentiation is shown in Figure 5.2-3. Live cells identified based on their scatter profile and annexin V and 7AAD negativity were subdivided $CD19^{Pos}CD20^{Neg}$, $CD19^{Pos}CD20^{Neg}$ and $CD19^{Neg}CD20^{Neg}$.

$CD20^{Neg}CD38^{Pos}$ cells were further subdivided into CD19 positive/negative plasma cells/ plasmablasts based on their expression of CD19 and CD138 respectively.

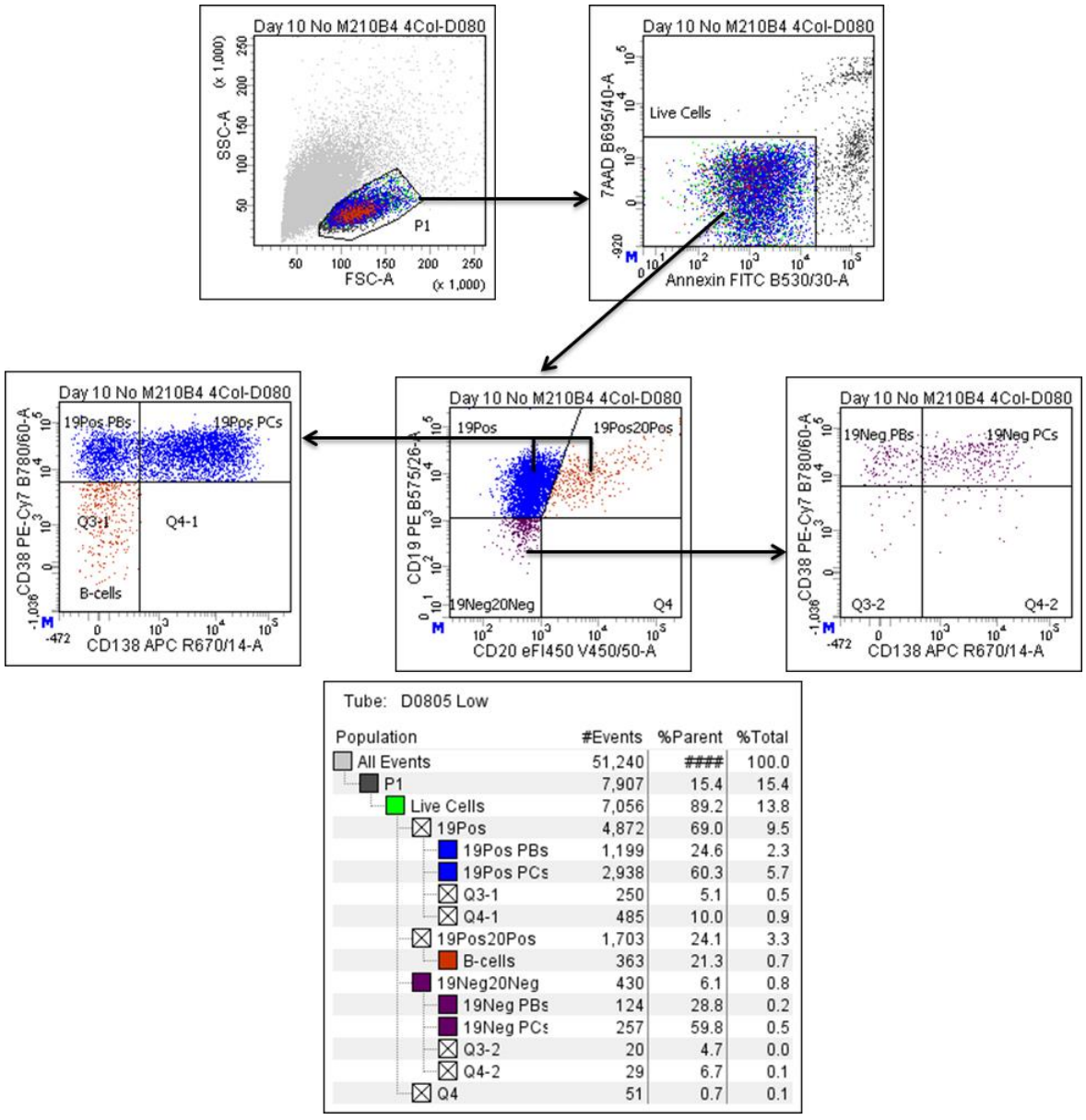

Tube: D0805 Low

Population	#Events	%Parent	%Total
All Events	51,240	####	100.0
P1	7,907	15.4	15.4
Live Cells	7,056	89.2	13.8
19Pos	4,872	69.0	9.5
19Pos PBs	1,199	24.6	2.3
19Pos PCs	2,938	60.3	5.7
Q3-1	250	5.1	0.5
Q4-1	485	10.0	0.9
19Pos20Pos	1,703	24.1	3.3
B-cells	363	21.3	0.7
19Neg20Neg	430	6.1	0.8
19Neg PBs	124	28.8	0.2
19Neg PCs	257	59.8	0.5
Q3-2	20	4.7	0.0
Q4-2	29	6.7	0.1
Q4	51	0.7	0.1

Figure 5.2-3 Gating Strategy for classification of B-lineage cells during in vitro B-cell differentiation

Live cells were identified based on their scatter profile and annexin V & 7AAD negativity. Live cells were subdivided into CD19 positive (Blue) and CD19&CD20 negative (Purple) cells which in turn were classified into plasma cells or plasmablasts based on CD138 expression. B-cells (Brown) were defined as CD19 and CD20 positive plus CD38 and CD138 negative. PB – Plasmablasts, PC – Plasma cell.

5.2.4 Plasma cell phenotyping

A 9-colour panel was used for evaluating surface expression of plasma cells: CD81 FITC (JS-81, BD Pharmingen), CD28 PE (L293; BD Biosciences), CD19 PerCP-Cy5.5 (SJ25C1; BD Biosciences), CD117 PE-Cy7 (104D2; BD Biosciences), CD138 APC (B-B4; Miltenyi), CD38 AF700 (HIT2; Biolegend), CD45 APC-H7 (2D1; BD Biosciences), CD56 BV421 (HCD56; Biolegend) and CD27 BV605 (O323; Biolegend).

Table 5.2-2 Antibody panel for surface phenotyping of plasma cells

27µL of the above antibody cocktail was used to stain one million cells.

Flurochrome	Antigen	Volume (µL)
FITC	CD81	5
PE	CD28	5
PerCp-Cy5.5	CD19	2.5
PE-Cy7	CD117	5
APC	CD138	1
AF700	CD38	2.5
APC-H7	CD45	2.5
BV421	CD56	1
BV605	CD27	2.5
Volume per Test		27

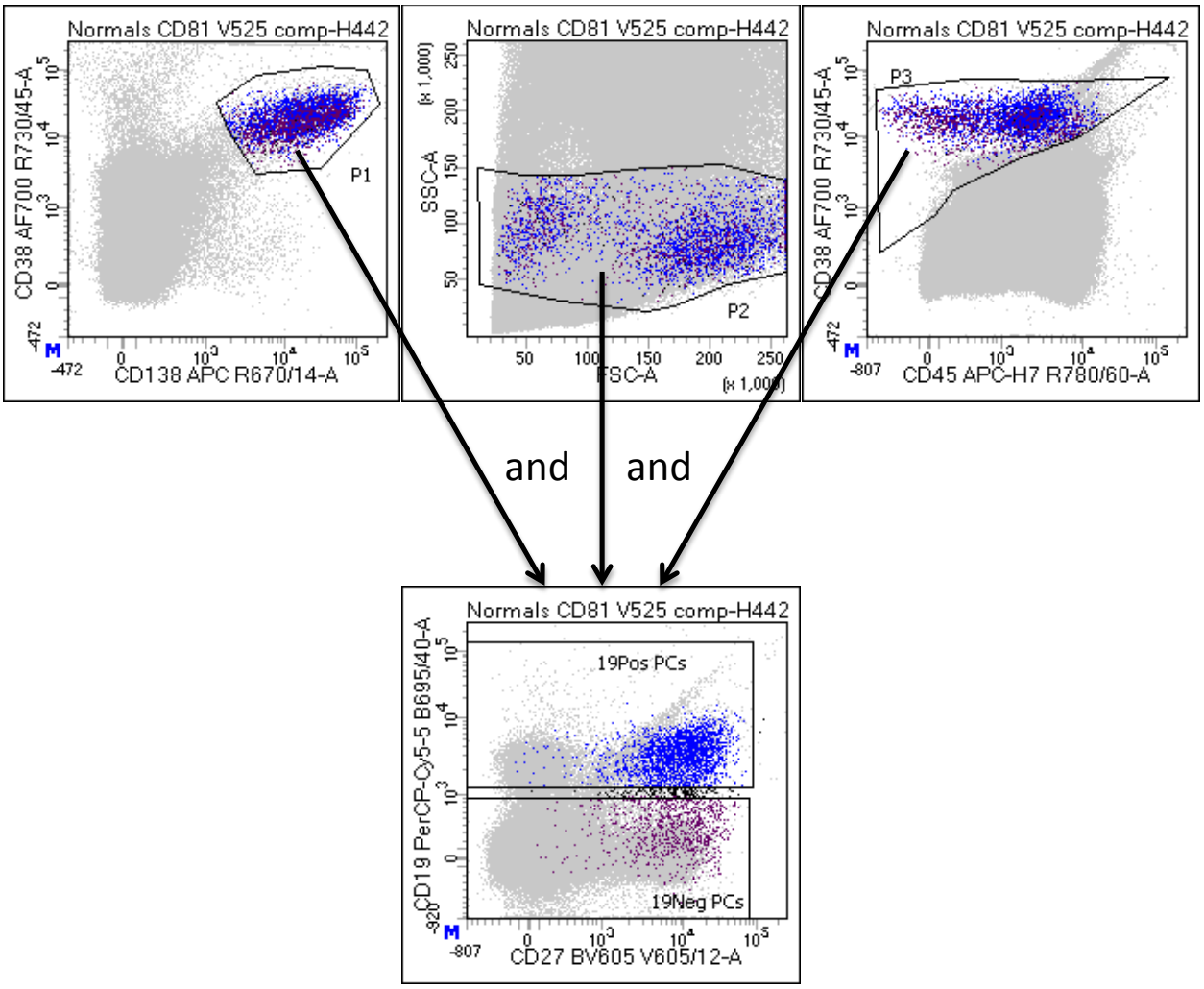

Tube: H4427

Population	#Events	%Parent	%Total
All Events	646,653	####	100.0
P2	111,170	17.2	17.2
P1	4,718	0.7	0.7
P3	9,807	1.5	1.5
P1 AND P2 AND P3 (PCs)	2,996	0.5	0.5
19Pos PCs	2,043	68.2	0.3
19Neg PCs	804	26.8	0.1

Figure 5.2-4 Gating strategy for identifying CD19^{Pos} and CD19^{Neg} plasma cells

Plasma cells were identified based on the expression of CD38, CD138, CD45 and their scatter profile as shown. Cells that met criteria P1, P2 and P3 were designated as plasma cells and were divided into 2 subsets based on their CD19 expression.

A six-color panel of antibodies was used to analyse the PCs from the Myeloma IX trial: CD138 APC (B-B4; Miltenyi Biotec), CD45 APC-Cy7 (2D1; BD Pharmingen, Oxford, United Kingdom), CD38 PE-Cy7 (HIT2; BD Pharmingen), and CD19 PerCP-Cy5.5 (HIB19; BD Pharmingen). Plasma cells were gated using CD38/CD138 and scatter profile. The level of CD19 staining by $CD19^{Neg}$ lymphocytes was used as threshold for CD19 expression by PCs.

Plasma cells from Campath trials were analysed retrospectively using markers from the panel designed for detection of residual CLL, comprising CD19 PE-Cy5 (FMC63, prepared in-house), CD5 APC (UCHT2, prepared in-house), CD20 FITC (B9E9, Coulter) and CD38 PE (HIT2, BD Biosciences). Plasma cells were gated using CD38/CD20 and light scatter characteristics and the CD19 threshold was set using $CD20^{Neg}CD5^{Pos}$ lymphocytes as a negative control.

5.2.5 Memory B-cell Phenotyping

The initial memory B-cell panel consisted of 8 surface markers which included four gating markers CD19, CD20, CD27 and CD38 and four markers for subset classification – CD24, CD84, CD95 and LAIR1. Subsequently, the antibody cocktail was modified to include IgM and IgD to identify class-switched B-cells as shown below.

Table 5.2-3 Antibody cocktails used for memory B-cell phenotyping

21.5 µL of the version 1 (V1) or 29 µL of version 2 (V2) of the antibody cocktail was used to stain one million cells. Residual antibody cocktails left after a week of preparation was not used for staining

Fluorochrome	Antigens V1	Volume (µL) V1	Antigens V2	Volume (µL) V2
FITC	CD24	5	CD24	5
PE	CD84	5	CD84	5
PerCp-Cy5.5	CD38	0.5	CD38	0.5
PE-Cy7	CD19	1	CD19	1
AF647/APC	CD27	5	IgM	5
AF700			IgD	5
APC-H7	CD20	2.5	CD20	2.5
BV421	CD95	1	CD95	1
Pacific Orange	LAIR1	1.5	LAIR1	1.5
BV605			CD27	2.5
Volume per Test		21.5		29

.

Lymphocytes were gated based on their scatter profile. CD19 and CD20 were used to identify the B-lineage cells. CD27 and CD38 were used to divide the B-cells into naïve, memory and plasmablast subsets. High levels of CD24 and CD38 expression was then used to distinguish the transitional B-cells from naïve B-cells.

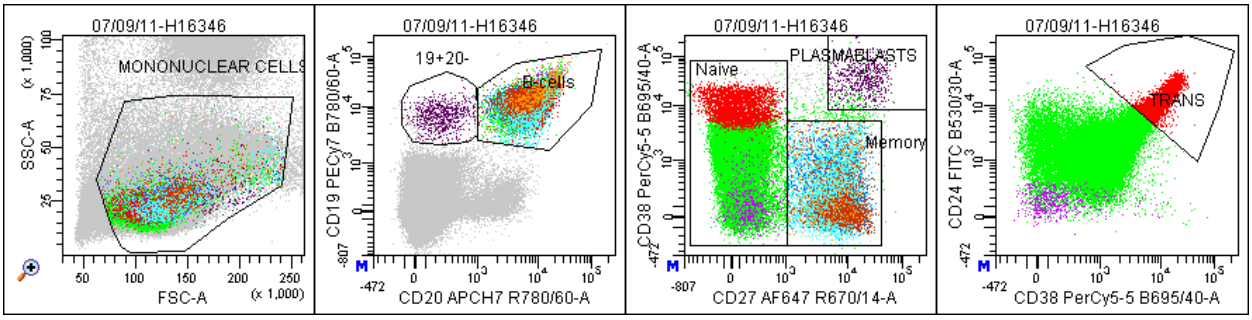

Figure 5.2-5 Gating strategy for defining B-cell subsets

Lymphocytes were gated based on their scatter profile and the B-cells were sub-classified as follows: Transitional B-cells (Red) – $CD19^{Pos}CD20^{+}CD27^{-}CD38^{++}CD24^{+}$, Naïve B-cells (Green) – $CD19^{Pos}CD20^{+}CD27^{-}CD38^{+/-}$, Memory B-cells (Blue) - $CD19^{Pos}CD20^{+}CD27^{+}CD38^{+/-}$, Plasmablasts (Purple) - $CD19^{Pos}CD20^{-}CD27^{++}CD38^{++}$

Plasmablasts ($24^-84^-95^+LAIR1^-$) and transitional B-cells ($24^+84^+95^-LAIR1^+$) were used to guide positive gating for 24, 84, 95 and LAIR1. With the help of two markers memory B-cells could be subdivided into 4 subsets. Each of these four subsets could be further subdivided into four subsets each based on the other 2 markers yielding 16 different subsets as shown in Figure 5.2-6.

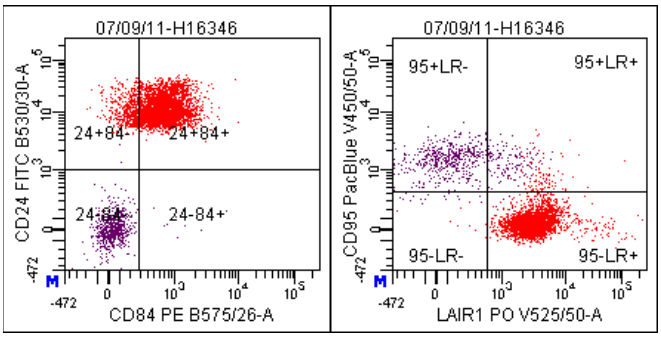

Tube: H16346

Population	#Events	%Parent	%Total
All Events	1,000,000	####	100.0
Time	1,000,000	100.0	100.0
MonoNuclear Cells	511,486	51.1	51.1
19+20-	956	0.2	0.1
Plasmablasts	761	79.6	0.1
B-cells	59,979	11.7	6.0
Naive & Transitional	49,065	81.8	4.9
Transitional	2,005	4.1	0.2
Memory	9,381	15.6	0.9
24+84-	3,303	35.2	0.3
24+84+	4,072	43.4	0.4
24-84-	1,586	16.9	0.2
24-84+	420	4.5	0.0
Lymphocytes	449,633	45.0	45.0
95+LR-	345,170	34.5	34.5
95+LR+	392,949	39.3	39.3
95-LR-	114,867	11.5	11.5
95-LR+	147,014	14.7	14.7
24+84- AND 95+LR-	1,444	0.1	0.1
24+84- AND 95+LR+	381	0.0	0.0
24+84- AND 95-LR-	876	0.1	0.1
24+84- AND 95-LR+	602	0.1	0.1
24+84+ AND 95+LR-	840	0.1	0.1
24+84+ AND 95+LR+	770	0.1	0.1
24+84+ AND 95-LR-	1,259	0.1	0.1
24+84+ AND 95-LR+	1,203	0.1	0.1
24-84- AND 95+LR-	1,216	0.1	0.1
24-84- AND 95+LR+	204	0.0	0.0
24-84- AND 95-LR-	113	0.0	0.0
24-84- AND 95-LR+	53	0.0	0.0
24-84+ AND 95+LR-	127	0.0	0.0
24-84+ AND 95+LR+	180	0.0	0.0
95-LR- AND 24-84+	20	0.0	0.0
95-LR+ AND 24-84+	93	0.0	0.0

Figure 5.2-6 Gating strategy for defining Memory B-cell subsets

Plasmablasts (in purple) known to be $CD24^-84^-95^+LAIR1^-$ and transitional B-cells (in red) known to be $24^+84^+95^-LAIR1^+$ were used to guide the placement of the quadrant gates to separate the positive and negative populations for the respective markers

5.2.6 Flow cytometry panel for detection of NK cells

For detection of NK cells and other non-B lineage cells noted during the in vitro differentiation of B-cells, an antibody panel was designed that could reliably detect NK cells and also identify B-cells, terminally differentiated antibody secreting cells which have reduced levels of CD19 expression and T-cells. A combination of CD16 PE (3G8, BD Pharmingen), CD56 V450 (B159, BD Horizon), CD19 V500 (HIB19, BD Horizon), CD27 FITC (M-T271, BD Pharmingen), CD3 PE-Cy7 (SK7, BD Biosciences), CD4 PerCp-Cy5.5 (SK3, BD Biosciences), CD8 APC (SK7, BD Biosciences) and CD45 APC-H7 (2D1, BD Biosciences) was used at the concentrations specified below.

Table 5.2-4 Antibody panel for detection of NK cell expansion during in vitro B-cell differentiation

24.1 µL of the antibody cocktail was used to stain up to one million cells.

Flurochrome	Antigen	Volume (µL)
FITC	CD27	5
PE	CD16	0.1
PerCp-Cy5.5	CD4	5
PE-Cy7	CD3	1
APC	CD8	0.5
APC-H7	CD45	2.5
V450	CD56	5
V500	CD19	5
Volume per Test		24.1

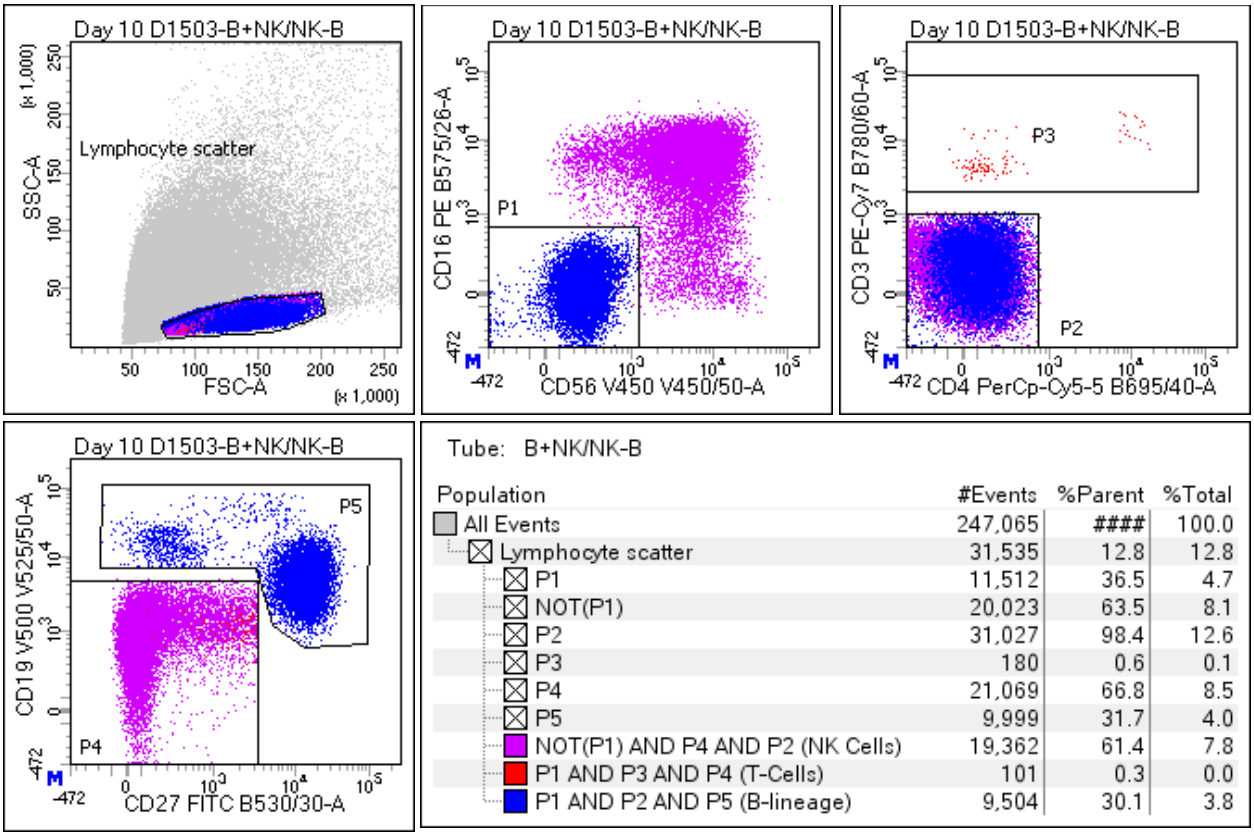

Figure 5.2-7 Gating strategy for detection of NK cells

Lymphocytes were identified based on their scatter profile and further sub-classfication was performed based on the following markers as shown in the table:

- B-lineage: $CD19^{Pos/Wk}$, $CD3^{Neg}$ $CD16^{Neg}$ $CD56^{Neg}$ $CD4^{-Neg}$ $CD27^{Pos/Neg}$
- NK-cells: $CD16/CD56^{Pos}$ $CD3^{Neg}$ $CD19^{Neg}$ $CD4^{Neg}$ $CD27^{Neg}$
- T-cells: $CD3^{Pos}$ $CD19^{Neg}$ $CD16^{Neg}$ $CD56^{Neg}$

5.2.7 Intracellular staining for flow cytometry

Intracellular staining was performed with BD Intrasure kit (BD Biosciences). Red cells were lysed using ammonium chloride and the cells were stained with surface antibodies as above. Once surface staining is completed further steps were carried out in FACS tubes. The cell pellet was resuspended in 100 µL of reagent A and incubated for 5 minutes in the dark at room temperature to fix the surface staining antibodies. 2ml of BD FACS lyse was added and incubated for 10 minutes in the dark at room temperature. Cells were pelleted and resuspended in 50 µL of reagent B which permeabilises the cell membrane for intracellular staining. Fluorochrome conjugated antibodies were added for intracellular staining at this stage and incubated for 15 minutes in the dark at room temperature. Cells were washed with 0.1%BSA in Facsflow and resuspended in 300 µL of Facsflow in a tube. 500,000 – 1 million events were acquired on an 8-colour BD FACS Canto or 11-colour LSRII Fortessa. The fixed and permeabilised cells were smaller in size compared to the surface stained cells and therefore the gain for forward scatter was adjusted accordingly.

For evaluation of intracellular expression of BCL2 and kappa/lambda ratio, surface staining was performed with CD95 PE (DX2, BD Pharmingen), CD4 PerCP-Cy5.5 (SK3; BD Biosciences),, CD19 PE-Cy7 (SJ25C1; BD Biosciences), CD138 APC (B-B4; Miltenyi), CD38 AF700 (HIT2; Biolegend), CD45 APC-H7 (2D1; BD Biosciences), CD56 BV421 (HCD56; Biolegend) and CD27 BV605 (O323; Biolegend).

Table 5.2-5 Antibody panel for intracellular staining of plasma cells

The antibodies marked as I/C (Intracellular) were used for intracellular staining after initial surface staining with rest of the antibodies in that panel.

Fluorochrome	Tube 1		Tube 2	
	Antigen	Volume (µL)	Antigen	Volume (µL)
FITC	BCL2 (I/C)	2	Lambda (I/C)	5
PE	CD95	5	CD95	5
PerCp-Cy5.5	CD4	5	CD4	5
PE-Cy7	CD19	1	CD19	1
APC	CD138	1	CD138	1
AF700	CD38	2.5	CD38	2.5
APC-H7	CD45	2.5	CD45	2.5
BV421/Pacific Blue	CD56	1	Kappa (I/C)	1
BV605	CD27	2.5	CD27	2.5

For intracellular stained cells, plasma cells were identified based on the surface expression of CD138, CD38 and CD45 as before, and subdivided further based on CD19 expression.

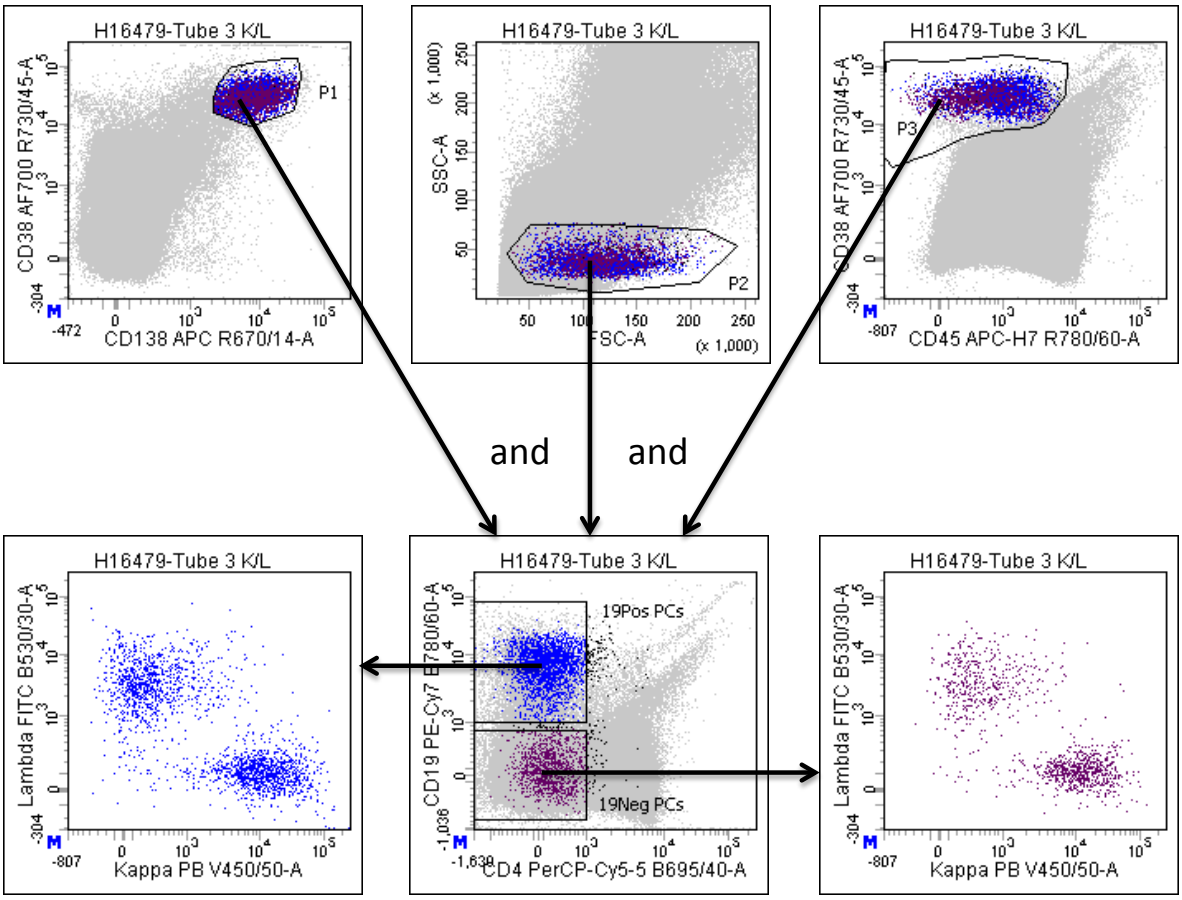

Tube: Tube 3 K/L

Population	#Events	%Parent	%Total
All Events	1,402,129	####	100.0
P1	4,547	0.3	0.3
P2	668,955	47.7	47.7
P3	5,602	0.4	0.4
P1 AND P2 AND P3 (PCs)	3,464	0.2	0.2
19Pos PCs	2,145	61.9	0.2
19Neg PCs	1,124	32.4	0.1

Figure 5.2-8 Gating strategy for evaluation of intracellular antigens expressed by plasma cells

Plasma cells were identified based on the expression of CD38, CD138, CD45 and their scatter profile as shown. Cells that met criteria P1, P2 and P3 were designated as plasma cells and were divided into 2 subsets based on their CD19 expression. Expression of intracellular kappa and lambda light chains by $CD19^{Pos}$ (Blue) and $CD19^{Neg}$ (Purple) plasma cells shown.

5.2.8 Choice of fluorochrome for antibodies

The fluorochrome conjugate for the different antibodies were chosen in such a way that rare channels were used for the backbone antigens (CD19, CD20, and CD38) and common channels like FITC, PE were allocated for rarer antigens. Antigens with high expression levels were chosen for conjugates with weaker fluorochromes and vice versa to achieve better resolution and reduce the levels of spectral overlap. Consideration was also given to allow for key markers to be allocated to a channel with good signal-to-noise ratio. For example, CD27 resolution is key to identify the major B-cell subsets and therefore placed on a common channel although it would occupy the potential space for a rare antigen.

5.2.9 Flow cytometry quality control

Polychromatic flow cytometry is a complex technology which requires various components to be optimized for reliable measurement of signals from multiple fluorochromes which can have a high degree of spectral overlap. Laser output, alignment, laser delay, photomultiplier tube (PMT) efficiency and optical filters are key components and need to be monitored regularly. Consistency is essential to ensure results are comparable between different samples and the same samples at different time points. Flow cytometry could be used to influence clinical decisions and therefore results should be precise and accurate. Two main methods were used on a daily basis to monitor the performance of the flow cytometer and thereby quality control.

BD cytometer setup and tracking (CST) beads (BD Biosciences) was used for the automated setup and tracking of cytometer performance. It contains equal quantities of dim, midrange and bright intensity beads. The dim beads are of 2 micron size and midrange and bright beads are 3 micron in size. The beads contain dyes covering the range of excitation and emission wavelengths of the cytometer. One drop of the CST bead mixture was added to 350 µL of FACSflow and acquired with the CST setup of BD FACSDiva software in the low flow setting. The MFI and robust CV of each bead is measured for all detectors in an automated fashion. The software calculates the optimal baseline PMT voltage for each channel based on the known fluorescence intensity of the beads. This baseline PMT voltage was used for setting up of all the experiments. On a day-to-day basis the software tries to adjust the PMT voltage to attain the target MFI of the beads and monitors for the change in PMT required to attain the target MFI.

When the CV is more than 6% or there is a change in PMT of more than 10% warnings are triggered.

Sphero rainbow calibration particles (Spherotech) were used, which contains mixture of 3µm-sized beads with 8 different fluorescence intensities. Each bead contains a mixture of fluorophores that enable excitation by laser wavelengths between 365nm to 650nm. The Beads fluoresce in all channels, which allows monitoring of the entire fluorescence range. One drop of the bead mixture was added to 350 µL of FACS buffer and acquired in the low flow setting. 20 minutes were allowed after switching on the flow cytometer before acquiring the sample. The PMT voltage that provided good resolution of the 8 different fluorescence intensities was set as baseline for each channel. CV and the MFI values of the highest peak for all the channels were monitored on a daily basis. The CV was maintained below 5% and change in MFI of more than 10% prompted further action. This method was used as a third party control to provide unbiased performance assessment and monitoring.

5.2.10 Flow cytometric compensation

Multiple fluorochromes excited by the same laser can be used in the same experiment. Most fluorochromes generate signals of wide wavelength. The signals generated by the fluorochromes are filtered to specified wavelength by band pass filters targeting the peak wavelengths before detection by photo-multiplier tubes (PMTs). However, since most fluorochromes have a wider wavelength spectrum than the respective filters, there is spillage of signals to the adjacent detectors. This can be established by running single fluorochrome stained samples and measuring the levels of signals detected by the other PMTs. This phenomenon is called spectral overlap when the fluorescence of one fluorochrome is detected by a detector which is dedicated to measure signal from a different fluorochrome.

To account for spectral overlap, signals detected from other fluorochromes are subtracted from the total signal detected by the PMT and this process is called compensation. This can be done in an automated fashion with FACSDiva software by running single stain tubes for all the fluorochromes to be used. For non-tandem conjugates like FITC, PE and APC, a generic antibody such as CD3 FITC can be used to calculate compensation values and does not require separate compensation for the other antibodies conjugated with the same fluorochrome, for

example, CD27 FITC or CD45 FITC. However, for tandem conjugates like PE-Cy7 and APC-H7 separate compensation setup tubes need to be performed for all individual antibodies even if they are attached to the same tandem conjugate due to variations in the ratio of components of the tandem conjugate. Compensation values are obtained by inverting the measured spectral overlap values of all fluorochromes in all detectors by matrix algebra which calculates simultaneous contributions of the spectral overlaps of each fluorochrome into every detector (77). The software then applies the compensation values to correct contributions from other fluorochromes into a given detector.

New compensation settings were created whenever there was any manipulation of the cytometer in the form of servicing of the equipment, changes to laser settings or alignment.

5.3 B-cell Selection

B-cells were purified using memory B-cell isolation kit (Miltenyi), according to manufacturer's instructions which enables purification of untouched B-cells by depletion of non-B lineage cells and plasmablasts. The kit contains a cocktail of biotinylated-antibodies against CD2, CD16, CD14, CD36, CD43 and CD235a to label T-cells, NK cells, monocytes, dendritic cells, granulocytes, platelets and erythroid cells. The labelled cells are depleted by passing through a column under a strong magnetic field after secondary labelling with anti-biotin microbeads.

5.3.1 Isolation of PBMCs by density centrifugation

- 20- 50 ml peripheral blood was collected in EDTA (EK3) purple tubes or crossmatch pink tubes
- 50 ml of blood was mixed with equal volume of sterile PBS at room temperature
- 17 ml of Lymphoprep at room temperature was placed into 3 x 50ml Falcon tubes
- 34 ml of blood/PBS mix was layered on to top of the Lymphoprep (NB: ratio 1 volume Lymphoprep to 2 volumes blood/PBS mix)
- Centrifuged at 2400rpm for 20 minutes at room temperature ~18^{0}C (acceleration 5, brake 0).
- The cloudy lymphocyte layer was removed gently with a plastic 3ml pastette (usually 2 times to get whole layer) and divided between 2 x 50 ml falcon tubes containing 10 ml cold PBS. (If the PBS is warm then clumping of sample may be noticed - probably due to the platelets. If this is the case then it was passed thru a 70 micron cell strainer at this point or later*).
- The volume was made up to 50 ml in each tube with cold PBS.
- Centrifuged at 1800rpm for 15 minutes at 4^{0}C.
- PBS was removed with stripette or decanted gently without disturbing the pellet.
- The cells were combined into one tube and washed with 50 ml cold PBS. (*passed through cell sieve if clumpy).
- Centrifuged at 1500rpm for 10 minutes at 4^{0}C.
- PBS was removed with stripette or decanted gently without disturbing the pellet.
- Cells were washed with 50 ml PBS at 4^{0}C.
- Centrifuged at 1500rpm for 10 minutes at 4^{0}C.

- PBS was removed with stripette or decanted gently without disturbing the pellet.
- Cells were washed with 15 ml ice cold MACS buffer (19 ml MACS rinsing solution + 1 ml MACS BSA stock solution). At this point cells were transferred to a 15 ml falcon tube and 10 µL was removed for counting before spinning.
- The 10 µL sample for counting was diluted 1:10 in PBS then 1:1 in trypan blue.
- Centrifuged at 1500rpm for 10 minutes at 4^0C.
- MACS buffer was removed with stripette then P1000 tip.
- The cell pellet was stored on ice until ready to label.
- Approximately 5-10 x 10^7 cells were isolated from 50 ml of blood.

5.3.2 Magnetic labelling of cells

The following protocol was used for selection with memory B cell isolation kit for 1x 10^8 cells or fewer (scaled up accordingly if greater than 1x10^8 cells):

- The cell pellet was resuspended in 400 µl of cold MACS buffer (same as above).
- 100 µl of the B cell Biotin-Antibody Cocktail was added and mixed well.
- Incubated for 20 minutes in the door of the fridge (not on ice).
- 300 µl of cold MACS buffer and 200 µl of Anti-Biotin Microbeads were added and mixed well.
- Incubated for 20-30 minutes in the door of the fridge (not on ice).
- Cells were washed by adding 10 ml of cold MACS buffer and centrifuged for 10 minutes at 1500rpm (whilst doing this step the column for MACS separation was prepared as below)
- The supernatant was completely removed and resuspended in 1 ml cold MACS buffer

5.3.3 Magnetic separation of cells

- The LD Column was placed in the magnetic field of a suitable MACS separator.
- The column was prepared by rinsing with 2 ml of cold MACS buffer.
- The cell suspension was applied onto the column.
- The unlabelled cells that pass through were collected in a clean 15 ml falcon tube.
- The column was washed twice with 1 ml of cold MACS buffer and flow through (effluent) was collected in the same tube.

- The 15 ml falcon tube now contains a pool of negatively selected (unlabelled) memory and naive B cells (total volume approximately 3 ml).
- The cells were counted with haemocytometer and resuspended in IMDM at the requisite concentrations.
- Approximately 2 – 8 x 10^6 total B cells (naïve + memory) were isolated from 50 mL of blood.

5.4 Tissue culture

24, 48 or 12 well flat-bottomed tissue culture plates (Corning) and IMDM supplemented with glutamax (Gibco) and 10% heat-inactivated FBS (HIFBS; Invitrogen) was used for tissue culture. For transwell experiments 24 well or 12 well transwell plates (clear polyester membrane, 0.4 µm pores, Corning) were used. The B-cells were cultured as per recently published protocol which is described below (60).

5.4.1 Reagents

The following reagents were used for in vitro studies:

Cytokines: Human IL-2 (Roche); IL-6, and IFN-α (Sigma); IL-21 (PeproTech).

Stimulation agents: Goat anti-human F(ab') 2 fragments (anti-IgM & IgG) (Jackson ImmunoResearch). R848 (Mabtech). Histidine-tagged recombinant human CD40L (R&D Systems); Monoclonal mouse IgG1 polyhistidine antibody (Clone AD1.1.10, R&D Systems).

Nutrients: Hybridomax hybridoma growth supplement (Gentaur); Lipid Mixture 1 chemically defined (200X) and MEM Amino Acids Solution (50X) (Sigma).

5.4.2 Preparation of irradiated CD40L (L-cells)

Day 0 - 1 vial of CD40L L-cells was thawed and seeded in 30 ml of IMDM with 10% HIFBS in a T175 flask.

Day 2 – The cells were trypsinized (6 ml of 1X Trypsin, neutralize with 14 ml of IMDM 10% HIFBS) and split and seeded in 4 x T175 flasks at a ratio of 1:6 (5 ml of trypsinized cells + 25 ml of IMDM with 10% HIFBS).

Day 4 – The cells were trypsinized (6 ml of 1X trypsin, neutralize with 14 ml of IMDM with 10% HIFBS) and passed through a cell strainer to avoid clumps into two 50 ml Falcon tubes.

The cells were counted and resuspended in 40 ml of fresh IMDM with 10% HIFBS in each tube at no more than 10^8 cells per tube.

The cells in falcon tubes were irradiated on ice twice at 25Gy for 45 minutes with gentle mixing in between.

Two 100 µl samples were tested by FACS (Unstained+anti-CD154) for CD154 expression.

The rest of the cells were frozen in aliquots (1.5 x 10^6/vial) in freezing media (90% IMDM 10% HIFBS, 10% DMSO).

Seeding 24 well plates to stimulate B-cells - 1 vial of CD40L L-cells was thawed and washed with 10 ml of IMDM with 10% HIFBS. The cells were resuspended in 12 ml of media, and plated 0.5 ml/well, 24 hours in advance and incubated at 37^0C. The L-cells adhere to the plate and the media can be removed before adding the B-cells for stimulation.

5.4.3 Preparation of irradiated mouse bone marrow stromal cells (M2-10B4)

M2-10B4 cells were grown in IMDM with 10% HIFBS in a T175 flask, split 1:10 twice a week and used up to passage 30.

M210B4 were irradiated in a flask when they are between 50-100% confluent at 57Gy for 57 minutes the day before plasmablast co-culture.

The media was removed from M210B4 and washed with 10ml of PBS.

3 ml of trypsin was added and left for 2-5 minutes.

7 ml media was added and the cells were transferred to 50 ml Falcon tube.

The cells were washed and plated at 1x10^6 cells / 24 well plate (0.5 ml media / well).

The plates were incubated at 37^0C until plasmablasts were ready.

M2-10B4 cells adhere to the plate and the media was removed before adding the plasmablasts.

5.4.4 B-cell differentiation of purified B-cells

The culture conditions for various stages of differentiation are as follows:

Days 0-3: For a 24 well plate, B-cells were cultured at 2.5×10^5/ml with IL-2 (20 U/ml), IL-21 (50 ng/ml), F(ab′)$_2$ goat anti-human IgM and IgG (10 µg/ml) on gamma-irradiated CD40L-expressing L cells (6.25 × 10^4/well). The number of cells and other reagents were reduced by half whilst using a 48 well plate. In experiments using soluble hCD40L, histidine-tagged recombinant human CD40L (50 ng/ml) was multimerised with monoclonal mouse IgG1 polyhistidine antibody (5 µg/ml) before or after adding to the rest of the culture media as

specified. In certain experiments, the TLR 7/8 agonist R848 (1 μg/ml) was used instead of CD40L stimulus.

Days 3-6: On day 3 cells were removed from CD40L layer and reseeded into fresh plates at 1×10^5/ml in media supplemented with IL-2 (20 U/ml), IL-21 (50 ng/ml), HybridoMax (11 μl/ml), Lipid Mixture 1 and MEM amino acids solution (both at 1× final concentration).

Day 6 onwards: Cells were reseeded into fresh plates at 2.5–5 $\times10^5$/ml in media supplemented with IL-6 (10 ng/ml), IL-21 (50 ng/ml), IFN-α (100 U/ml), HybridoMax (11 μl/ml), Lipid Mixture 1 and MEM amino acids solution (both at 1× final concentration).on gamma-irradiated M2-10B4 cells (4.16×10^4/well).

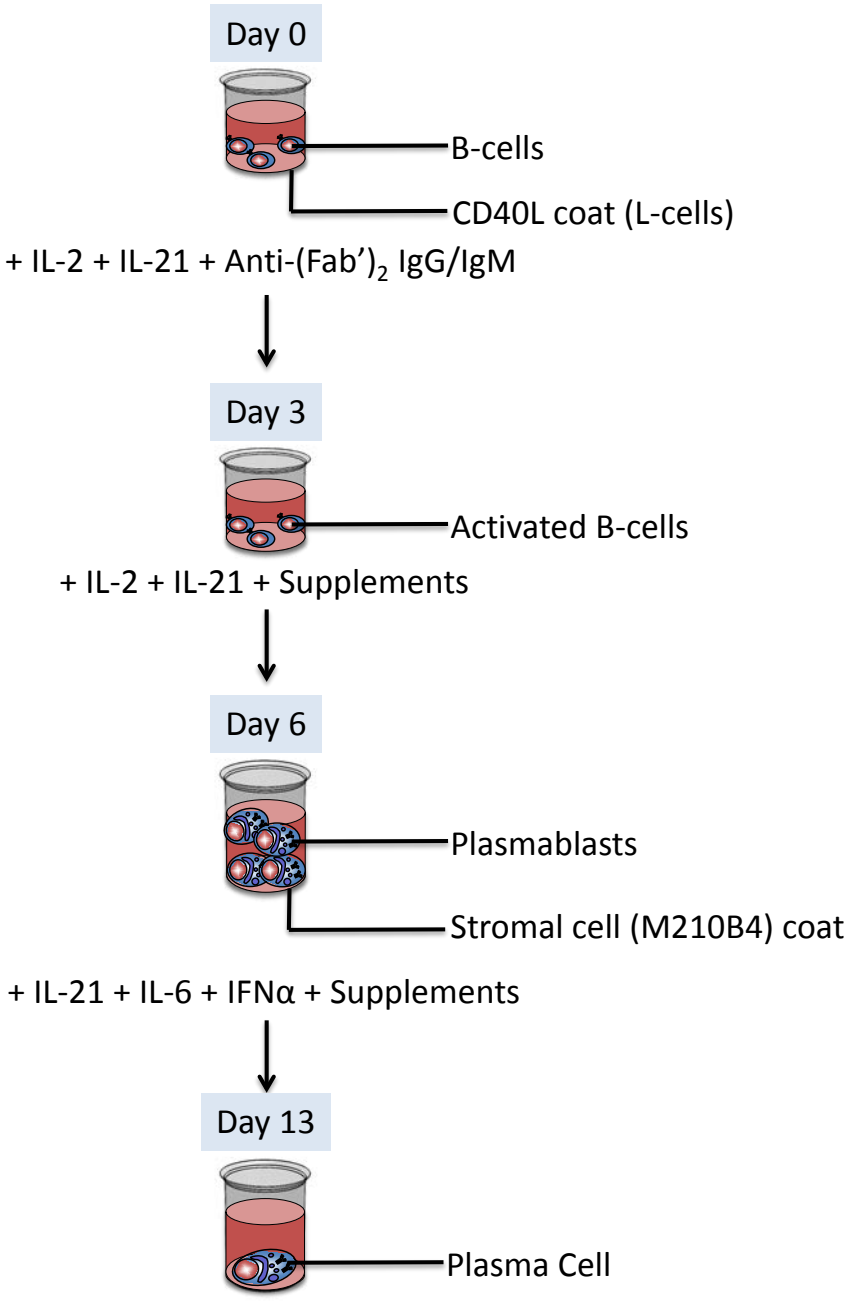

Figure 5.4-1 In vitro B-cell differentiation – schematic representation

B-cells are stimulated with BCR stimulus, CD40L and cytokines shown on day 0. Activated B-cells generated on day 3 are removed from CD40L and transferred to the shown conditions and differentiate to plasmablasts by day 6. With stromal cell and cytokine support majority of the plasmablasts mature into plasma cells by day 13. *Pictures of the cells – courtesy of Dr.R.Tooze.*

Long-term culture in transwells: For long-term culture, day 6 cells were seeded at 1.5 or 3×10^5/well into the upper chamber of 24 or 12 well transwell plate with the same day 6 conditions as above. The lower chamber was seeded with gamma-irradiated M2-10B4 cells (4.16×10^4/well and 8.32×10^4/well for 24 and 12 well plates respectively). IL-21 was withdrawn after day 13 and cells were re-fed by replacing half of the volume of media from the lower chamber twice a week with fresh media.

5.4.5 B-cell differentiation of whole PBMCS

For ELISpot to be used for routine diagnostic purposes, quicker turnaround time and the option to use PBMCs rather than selected B-cells is beneficial. Therefore stimulations of B-cells were performed according to ELISpot kit manufacturer's protocol (Mabtech, Sweden) which induces antibody secretion in 48-72 hours. PBMCs separated by density centrifugation were resuspended in 24 well plates at 1 million cells per well and stimulated with R848 (1 µg/mL) and rhIL2 (10 ng/mL) for 48-72 hours. The cells were then washed and used in ELISpot.

5.5 Synthesis of Citrullinated antigens

5.5.1 Citrullination of fibrinogen

Citrullinated fibrinogen (CitFib) was synthesized as previously described (10). Briefly, plasminogen-depleted human fibrinogen (Calbiochem) was incubated at 0.86mg/ml with 10 units of rabbit skeletal muscle peptidyl arginine deiminase (PADI) (Sigma-Aldrich) in 0.1 M Tris-HCl (pH 7.4), 10 mM $CaCl_2$, and 5 mM DTT for 2 h at 50°C. The reaction was stopped by inactivating PADI with 2% sodium dodecyl sulphate (SDS) and heating for 3 minutes at 100°C. CitFib was then purified using a 100kDa Amicon filter (Millipore) following manufacturer's instructions. CitFib was then biotinylated using NHS-LC biotin (Pierce Biotechnology) as per kit instructions. Human unmodified fibrinogen was also biotinylated to be used as control for CitFib.

5.5.2 Citrullinated cyclic peptides

The sequence of the peptides used in the second-generation CCP2 assay, which detects ACPA specific for RA is under patent, and not revealed by the manufacturers. It is thought to contain a mixture of peptides for improved sensitivity. Dr.Haro's lab (Unit of Synthesis and Biomedical Applications of Peptides IQAC-CSIC, Barcelona, Spain) have synthesized and evaluated a series of citrullinated peptide sequences from fibrin and fillagrin for their sensitivity and specificity for ACPA detection. From the best available fibrin and fillagrin sequences, a chimeric cyclic peptide CFFCP2 (Chimeric Fibrin-Fillagrin Citrullinated Peptide) was synthesized which was comparable if not slightly better than the commercial CCP2 diagnostic assay (78). This sequence was used to synthesize the peptide commercially (Mimotopes).

Synthesized CFFCP2 amino acid sequence:

Biotin-Ahx-HSTKRGHAKS**X**PV**X**GHQ*C*HQEST**X**GRSRGR*C*GRSGS-acid

Ahx = Aminohexanoic acid spacer, **X** = Citrulline, *C* = Site of cysteine residue used for cyclization

Biotinylated and direct Alexafluor647 conjugated versions of the citrullinated and arginine peptides synthesized by Dr.Haro's lab were used for ELISpot and flow cytometry (78).

5.6 Flow cytometric sorting of cell subsets

5.6.1 Plasma cell sorting

Clinical waste bone marrow samples which had been analysed at the Haematological Malignancies Diagnostic Service (HMDS) at Leeds and found to contain no malignant cells were chosen. Red blood cell lysis was performed by using 8.6 g/L ammonium chloride solution at a ratio of 10 ml for 1 ml of bone marrow. Plasma cells were then enriched in the sample by using CD138 microbeads (Miltenyi) following manufacturer's instructions. The enriched samples were stained with CD45 FITC (BD Biosciences), CD38 PE (BD Biosciences) and CD19 PE-Cy7 (BD Biosciences). Plasma cells with high expression of CD38 were sorted into $CD19^{hi}$ $CD45^{hi}$ and $CD19^{lo}$ $CD45^{lo}$ fractions with a high-speed MoFlo (Beckman Coulter) cell-sorter for further analysis.

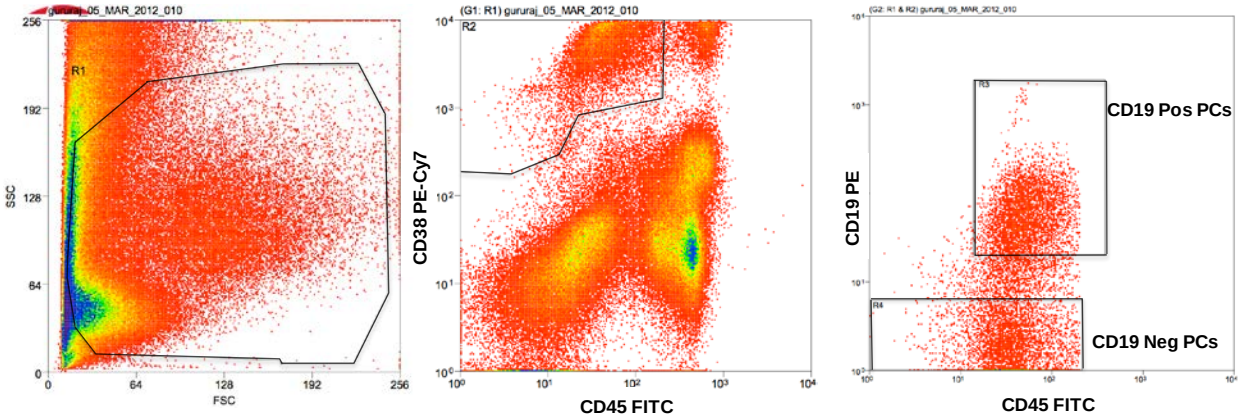

Figure 5.6-1 Gating strategy for Plasma cell sort

Bone marrow cells enriched by CD138 microbeads were initially gated on scatter properties followed by gating for cells positive for CD38 and weak CD45 to identify plasma cells. The PCs were sorted into $CD19^{Pos}$ and $CD19^{Neg}$ fractions.

5.6.2 Sorting of plasmablasts and memory B-cell subsets

Peripheral blood from patients and controls was subjected to treatment with 8.6 g/L ammonium chloride solution for 10 minutes at 37^0C at ratio of 10 ml per ml of blood. Ammonium chloride method was preferred to lymphoprep due to differential size and density of plasmablasts rendering them susceptible to loss during the density centrifugation. The cells were then stained

with CD19 PE-Cy7(BD Biosciences), CD38 PerCP-Cy5.5 (BD Biosciences), CD20 APC-H7 (BD Biosciences), CD24 FITC (BD Biosciences), CD84 PE (BD Biosciences), CD27 AF647(AbD Serotec), CD95 BV421 (Biolegend), LAIR1-biotin (Abcam) followed by streptavidin pacific orange (Invitrogen) for 10 minutes. The stained cells were sorted on BD influx cell sorter (BD Biosciences) platform into 4 fractions – Naïve B-cells, plasmablasts and 2 memory B-cell subsets. The sort compensation and setup was performed using BD FACS Sortware.

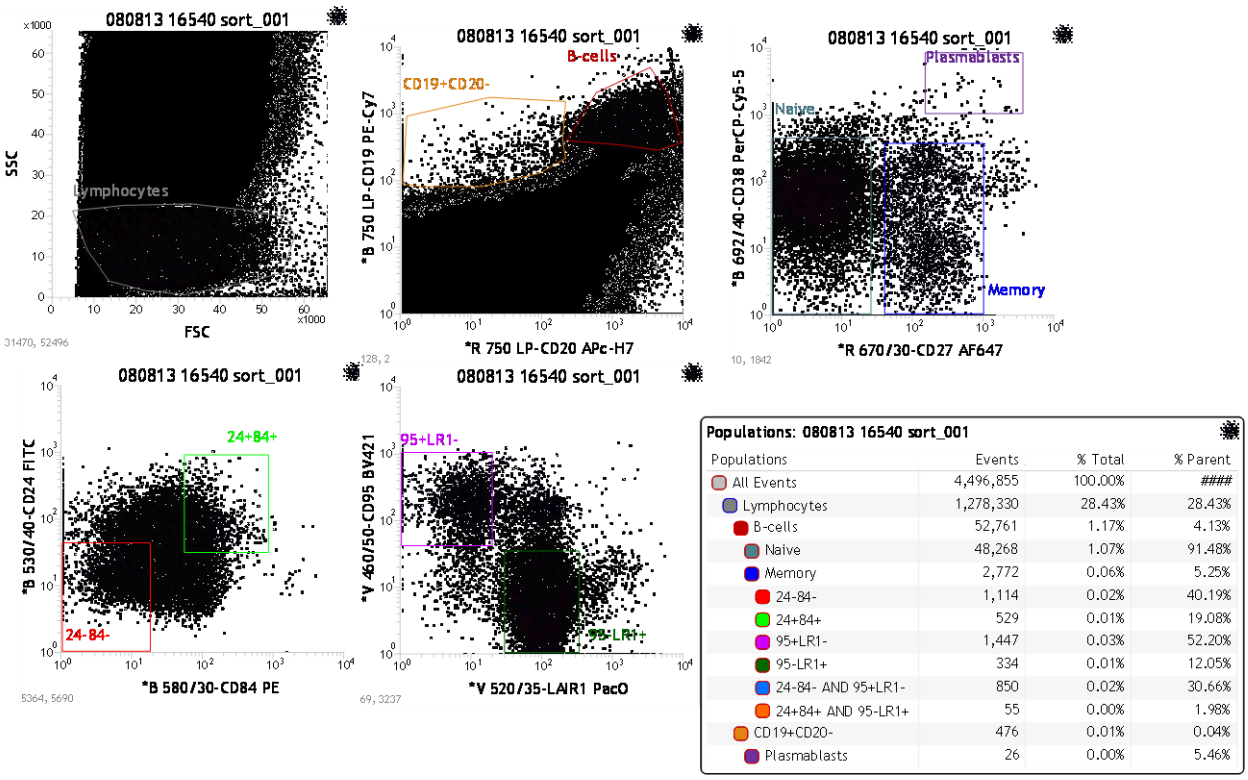

Figure 5.6-2 Gating strategy for flow sorting plasmablasts and memory B-cell subsets

Lymphocytes were gated based on their scatter profile and B-cells were defined as CD19 and CD20 positive. Naïve B-cells (Green) – CD27 negative, Memory B-cells (Blue) – CD27 positive, Plasmablasts (Purple) – CD19 positive, CD20 negative, CD27 and CD38 strong positive were gated subsequently. Memory B-cells were gated into CD24+CD84+, CD24-CD84-, CD95+LAIR1- and CD95-LAIR1+ subsets. Two of these gates were combined to sort the target memory B-cell subsets.

5.7 Next Generation Sequencing

Next generation sequencing of IGHV@ region from RNA of sorted $CD19^{Neg}$ & $CD19^{Pos}$ PCs was performed by Dr.Darren Newton using the Roche 454 GS Junior platform following manufacturer's instructions. RNA was extracted with TRIzol and reverse transcribed using Superscript II Reverse Transcriptase (Invitrogen). Ig H chain V (IGHV) regions were amplified from the cDNA with proofreading Phusion Flash polymerase (Finnzymes) using modified BIOMED-2 primers for framework 1 and common JH (79), with an incorporated 5′ M13 sequence. Purified amplicons generated by first-round PCR were amplified with a unique MID-tagged, M13-containing 454 amplicon sequencing primer. Libraries were quantified with Quant-iT pico-green (Biorad), mixed, and sequenced using the standard Roche 454 GSJunior sequencing protocol (GS Junior Titanium Series; Roche Applied Science). Resultant processed, split, trimmed data were analyzed using IMGT HighV-Quest software (80).

5.8 ELISA

ELISA was performed as per the standard protocol provided by the human IgG ELISA quantitation set (Bethyl laboratories, USA). 96 well plates (Nunc) were coated with 100 µl of antigen solution at concentration of 10 µg/ml for one hour. Wells coated with buffer alone or non-citrullinated version of the peptide were used as controls. The plate was washed and incubated with 200 µl of blocking solution (PBS + BSA) overnight at 4^0C. The wells were incubated with 100 µl of plasma or supernatant at described dilutions with appropriate positive and negative controls for 1 hour and the bound IgG was detected with anti-human IgG conjugated to HRP (Bethyl laboratories, USA). Tetramethylbenzidine (TMB) substrate was used for detection and the reaction was stopped with 0.18M H_2SO_4. The plate was read on a spectrometer (Dynex Revelation 4.04) at 450nm and also at 570nm as control.

5.9 ELISpot

ELISpot for antigen-specific B-cells was performed according to the kit protocol (Mabtech, Sweden). Briefly, PVDF membrane of the ELISpot plate was activated by 70% ethanol and was coated with 100 µl of 15 µg/ml of CFFCP2 or vaccine overnight at 4^0C. Anti-human IgG or anti-TNFα at the same concentration was used instead of CFFCP2 for detecting IgG or TNFα secreting cells. 200 µl of 10% FCS in IMDM was used for blocking followed by incubation with appropriate number of cells up to a maximum of 1 million in 100 µl of 10% FCS in IMDM per well. The cells were allowed to secrete for 8-12 hours and then removed by washing. Biotinylated anti-human IgG was used to identify secreted IgG and combination of Streptavidin-HRP and TMB substrate was used to detect the spots. When streptavidin (Invitrogen) was used to fix the biotinylated CFFCP2 peptide to the ELISpot plate, direct HRP conjugated anti-IgG (Bethyl laboratories, USA) was used. When anti-IgG was used as capture antibody to detect ACPA, the biotinylated peptides were used for detection with streptavidin HRP (Biolegend). Plates were read with AID Elispot reader version 5.0 (AID GmBH, Germany).

5.10 Polymerase chain reaction for detection of EBV

DNA was extracted using QiAamp DNA blood mini kit columns according to the manufacturer's protocol from day 6 plasmablasts that generated NK expansion. GM12878 and Raji cell lines were used as positive controls and HeLa was used as a negative control. 200 µl of sample containing 100,000 cells in PBS was added to 20 µl of Qiagen protease in a microcentrifuge tube. 200 µl of buffer AL was added and incubated at 56^0C for 10 minutes after vortexing. 200 µl of 96-100% ethanol was added and mixed by vortexing. After each vortexing step, the sample was briefly centrifuged to remove droplets from the lid. The mixture was transferred to the QIAamp mini spin column in a 2 ml collection tube and centrifuged at 8000rpm for 1min. The collection tube with the filtrate was discarded and replaced with a fresh tube. 500 µl of buffer AW1 was added and centrifuged again at 8000rpm for 1min. This step was repeated with buffer AW2 and the column was placed in a clean microcentrifuge tube after discarding the filtrate. The DNA from the column was eluted with distilled water.

EBNA2 (Epstein Barr Virus Nuclear Antigen) was detected by using nested PCR using the primers (Sigma) described before (81). The first round of PCR targets the common region of EBNA2 and generated an 801bp product. The product from the first PCR or primary DNA was used in the second PCR reaction which included two nested reactions targeting unique regions of EBV type 1 and EBV type 2.

Primers used for *EBNA2* PCR typing

	Primers	Sequence (5'-3')	Use in the PCR reaction
801bp expected	EBNA-2F	TGGAAACCCGTCACTCTC	1st reaction sense
	EBNA-2I	TAATGGCATAGGTGGAATG	1st reaction sntisense
	EBNA-2C	AGGGATGCCTGGACACAAGA	Nested reaction sense
250bp expected	EBNA-2G	GCCTCGGTTGTGACAGAG	Nested reaction antisense type-1
300bp expected	EBNA-2B	TTGAAGAGTATGTCCTAAGG	Nested reaction antisense type-2

Figure 5.10-1 Primers used for EBV EBNA2 PCR

The primers used for detection of EBV EBNA2 are shown. The first reaction generated 801bp product and the PCR product generated was used in the second nested reaction which generated a 250 or 300bp product depending on the EBV type.

1.5 mM and 3.5 mM concentrations of magnesium chloride and annealing temperatures of 56^0C, 58^0C, 60^0C and 62^0C were tested. The final reactions were performed with 1.5 mM magnesium chloride and annealing temperature of 60^0C.

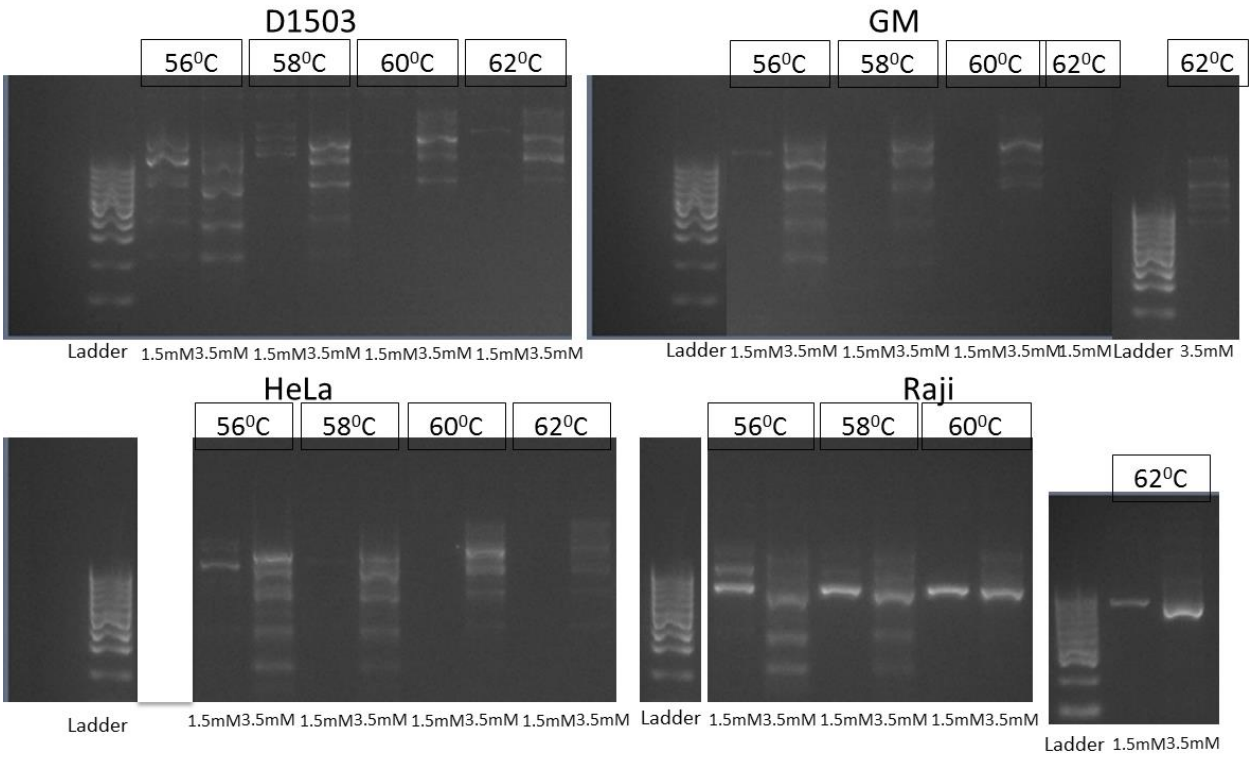

Figure 5.10-2 Optimisation of conditions for EBV EBNA2 PCR

DNA from control day 6 plasmablasts, 2 positive control cell lines (Raji, GM12878) and a negative control cell line (HeLa) was tested at 2 different magnesium chloride concentrations (1.5 and 3.5 mM – shown at the bottom) and 4 different annealing temperatures (56^0C, 58^0C, 60^0C and 62^0C – shown at the top). The primers used in the PCR reaction generated an 801bp product which was run on a 2% agarose gel and the PCR products were visualised with Gel Green.

10 µL of 2X Phusion Flash High-Fidelity master mix (Life Technologies) which contains Phusion Flash II DNA polymerase, deoxynucleotides and 2X reaction buffer which includes magnesium chloride was used per reaction. Each primer at 0.3 µM final concentration and 100 ng of DNA was added to the master mix and water was added to make up 20 µL reaction volume in 0.2 ml tubes. Thermocycler (Applied Biosystems) Cycling conditions: First reaction: 98^0C for 10 sec, followed by 35 cycles of 98^0C for 1 sec, 60^0C for 5 sec and 72^0C for 20 sec, followed by 72^0C

for 1 min. Second nested reaction: 98^{0}C for 10 sec, followed by 35 cycles of 98^{0}C for 1 sec, 60^{0}C for 5 sec and 72^{0}C for 10 sec, followed by 72^{0}C for 1 min.

The PCR products were run on 2% agarose gel in TBE and Gel Green (Cambridge Biosciences) was used for DNA staining. DNA bands of the appropriate size were excised from the agarose gel and purified with Zymoclean gel DNA recovery kit according to the kit protocol. Agarose dissolving buffer (ADB) at 3 times the volume of the gel containing DNA was added and incubated for 10 minutes at 50^{0}C. Once agarose melted, the contents were transferred to a Zymo-spin column in a collection tube. The column with collection tube was centrifuged at 8000rpm for 1 minute and the filtrate was discarded. This step was repeated with DNA wash buffer. After discarding the filtrate DNA was eluted into a clean tube using 20 µL of distilled water. Sanger sequencing of the PCR product was performed by Source Bioscience, Nottingham.

6 First Results Chapter: Detection of Antigen-specific B-lineage cells

Anti-citrullinated protein antibodies (ACPA) are highly specific for RA and correlates with severe disease and joint destruction. However, the direct pathogenic role for ACPA is not proven in humans and the lack of symptoms in the pre-clinical phase of RA characterised by positive ACPA remains unexplained (17). Baseline ACPA titre or drop in ACPA titre following BCDT does not correlate with clinical response. Baseline levels of B-lineage cells and their depletion have been shown to predict response to therapy. Therefore, the levels of autoreactive B-cells could be a better marker of response to and relapse following B-cell depletion for RA. Identification of this autoreactive anti-citrullinated protein-specific B-cells would allow direct monitoring of the pathogenic process at baseline and follow-up and offer a new mechanism to study antigen-specific B-cell dysregulation in RA. Specifically, detection by flow cytometry would also allow further phenotypic characterisation, which would shed light on the functional properties as well. Although ACPA-specific B-cells are unlikely to have a distinct surface phenotype compared to all other B-cells, they are likely to be enriched within subsets of B-cells with an activated phenotype particularly during active clinical disease and relapse post-BCDT. If ACPA-specific B-cells can be identified by surface phenotype with commercially available antibodies, that would allow better standardisation of the assay, since standardisation of antigens for universal access is much more complicated. The ultimate aim of this study to identify the autoreactive B-cells is to use it as a biomarker of response to B-cell depletion and predict relapse following rituximab.

If the frequency of antigen-specific cells is too low to be reliably detected by flow cytometry, in vitro expansion to generate PCs could be employed followed by a technique to detect antigen-specific plasma cells. ELISA allows quantification of ACPA secreted by PCs and ELISPot allows numerical enumeration of the ACPA secreting cells. Developing the technique to identify the antigen specificity of PCs could also be useful in differentiating short and long-lived PCs since RA pathogenesis is likely to be mediated by short-lived plasmablasts and PCs. There might also be a pathogenic role for long-lived PCs in a proportion of RA patients who fail to respond even after total B-cell depletion and in other autoimmune conditions. In the absence of recent vaccination or infection, vaccine specific antibodies are secreted by long-lived PCs and this fact

can be exploited for their identification. The purpose of the work presented in this chapter was therefore to address these interlinked questions.

Antigens used in commercial assays for detection of ACPA are not readily available. The citrullinated proteins cannot be generated by recombinant protein expression methodologies since citrulline is a non-standard amino acid which is not incorporated into proteins during protein synthesis as it is not encoded in the genome. The in vivo citrullinated proteins are derived from post-translational modification and can be generated in vitro by enzymatic citrullination of proteins. The alternative is to chemically synthesize peptides from the sequences available in the public domain, similar to the peptides used in commercially available ELISA for ACPA detection. The citrullinated fibrinogen synthesized in-house (as described in methods section 5.5.1) and commercially synthesized CFFCP2 peptide were initially evaluated by ELISA as shown in Table 6.1-1. The sensitivity of citrullinated fibrinogen was lower than that of the CFFCP2 peptide. ACPA can be directed against multiple other citrullinated proteins such as vimentin, enolase and fillagrin. The peptide contains an epitope that is common between multiple proteins and therefore likely to have a wider detection range. Due to the lower sensitivity and the multiple quality control steps required when every single batch of the protein is citrullinated and biotinylated, the synthetic peptides were preferred. The commercially synthesized CFFCP2-Mimo peptide gave a false positive result for one of the samples tested. Therefore, a series of ACPA negative samples from patients with other autoantibody positive conditions were tested with the peptide. Samples which were positive for certain autoantibodies such as anti-dsDNA showed a higher degree of non-specific binding as seen in Table 6.1-2. The CFFCP2-Mimo peptide identified all the 13 ACPA negative samples.

After the sensitivity and specificity of the CFFCP2 peptide was established, it was tested by flow cytometry by using streptavidin-pacific orange for detection. The streptavidin-pacific orange was used after the cells were exposed to the peptide and was also tried by pre-incubation with the peptide before exposure to the cells. The peptide was used in excess to ensure adequate tetramerisation. Non-specific binding was observed when streptavidin-pacific orange without peptide was used as a negative control. The non-specific binding could be due to streptavidin or pacific orange.

To avoid this non-specific binding, directly fluorochrome-tagged peptides were obtained from Dr.Haro's lab for testing by flow cytometry. When tested by ELISA, the sensitivity and specificity of the peptide was not affected by flurochrome (AF647) tagging, lyophilisation for long-term storage or indirect binding of the biotinylated peptide to the ELISA plate with streptavidin (Figure 6.2-3). There were a higher proportion of positive B-cells by flow cytometry in the ACPA negative patient compared to ACPA positive RA patients, which is suggestive of non-specific binding by the AF647 tagged peptide (Figure 6.2-4). This was also apparent when the AF647 tagged citrullinated and arginine versions of the peptide were tested in parallel as they showed similar proportions of positive cells. A similar level of positivity was noted with lower concentration of the AF647 tagged peptide which suggests that the non-specific binding was not concentration related (Figure 6.2-5).

The lack of citrullinated protein specific B-cells could be multifactorial. ACPA specific B-cells can be detected from peripheral blood as proven by ELISA from culture supernatants (Table 6.3-1) but their frequency can be variable as evidenced by the lack of detection in a significant proportion of the samples. The frequency of antigen specific B-cells could be below the level of detection by flow cytometry since it is reported to be 1 in 10000 during steady state for vaccine antigens (50). The frequency could be higher during an active immune response due to expansion of the antigen-specific cells or reduced due to their recruitment to secondary and tertiary lymphoid organs depending on the stage of the immune response. To assess this further, samples from bone marrow and synovium of RA patients with active disease have to be analysed. Bone marrow sampling and synovial biopsy require expertise and although low, carries a higher risk of complications compared to peripheral blood sampling. It also causes significant morbidity to the patients. The results cannot be reliably interpreted in the absence of a positive control. If detection of antigen-specific cells requires bone marrow or synovial tissue sampling it will preclude the use of the assay as a routine biomarker to predict response and relapse. However a technical explanation such as the possibility of non-specific binding masking the underlying specific binding cannot be entirely excluded. The non-specific binding could be peptide or flurochrome related or a combination of both.

Simple tetramerisation of the peptide with streptavidin was not effective for flow cytometric detection of the antigen-specific cells (Figure 6.2-1). However this concept has been demonstrated in mice to be efficient in detecting antigen-specific B-cells after multiple

modifications (82). This method utilises pre-enrichment for B-cells to improve the sensitivity and titration to identify the optimal concentration where the unbound peptide is minimal. Steps were also included in that study (82)to remove unbound peptides and peptide-free streptavidin and pre-incubation with unconjugated streptavidin was used to prevent non-specific binding to streptavidin. Although these methodologies can be performed, they require multiple validation steps and requires considerable time and expertise to setup. This would not be easily transferable to a robust diagnostic assay. The method ultimately required sequencing of the immunoglobulin genes of the positive cells and their re-expression to synthesize immunoglobulins to prove their specificity. This methodology requires considerable expertise which was not available locally and requires setting up. Therefore, flow cytometric detection was not pursued further and other methods of detection of antigen-specific B-cells were sought.

ELISpot was pursued as an alternative method for detecting citrullinated protein specific B-cells since the antigen is likely to be in a similar conformation to ELISA. In vivo generated antibody secreting cells can be directly assayed for their antigen specificity. Antigen-specific B-cells from the periphery can be expanded in vitro and the antibody secreting cells generated can be assayed thereby providing an option to circumvent their low frequency. The ELISpot technique was validated by detection of IgG and vaccine specific antibodies by plasma cells (Figure 6.3-1). ACPA secretion by PCs generated in vitro from RA patients B-cells was not detectable by ELISpot using two different biotinylated CFFCP peptides (Figure 6.3-2). For this assay to be useful in the clinical setting it has to have a lower turnaround time and be less resource intensive. Since the standard B-cell differentiation protocol requires 10 to 14 days to generate plasma cells and also requires B-cell purification, other alternatives were sought that can be quicker and would not require cell selection strategies. The ELISpot kit protocol recommends 24 – 48 hour culture of PBMCs with R848 and IL2 to generate antibody secreting cells (described in detail in methods section 5.4.4). ACPA secretion by the antibody secreting cells generated by this shortened protocol was not detectable by ELISpot (Figure 6.3-3). The citrullinated peptides were also tried as detection agents by capturing the secreted IgG with anti-IgG on the ELISpot plate. When tested for the presence of peptides bound to the ELISpot plates using an ELISA type technique, IgG was detectable but not ACPA from positive control serum. This raises the possibility of lack of binding of the peptide to the ELISpot plate. This could potentially be circumvented by using streptavidin to attach the peptides to the ELISpot plate. Analysis of the supernatants by ELISA revealed ACPA secretion by one out of the three RA patient samples in

each of the above two experiments (Table 6.3-1). This confirms the presence of citrullinated protein specific B-cells in the peripheral blood but their frequency is quite variable as evidenced by the lack of ACPA secretion in 4/6 samples.

The key issue that affected optimal quality control of the flow cytometry and ELISpot assays was the lack of a positive control. Dr.Malmstrom's group have sorted class-switched memory B-cells from synovium of active RA patients and generated monoclonal ACPA secreting cells (72). Such hybridoma cells can provide an ideal positive control. The other option is to EBV transform B-cells from RA patients to immortalise them and continue maintaining colonies that exhibit the appropriate antigen specificity. Robinson's lab at Stanford school of Medicine have generated citrullinated peptide tetramers which have been used to flow cytometrically sort B-cells. They have proven the sorted B-cells to be citrullinated protein specific by re-expression of the immunoglobulin mRNA (Verbal communication 2015). In a collaborative project Robinson's lab have agreed to provide samples of the peptide tetramers for evaluation of putative autoreactive B-cells by flow cytometry.

In summary, this chapter describes the various methodologies that were employed to identify the citrullinated protein specific B-lineage cells that are likely to play a key role in RA pathogenesis.

6.1 Generation and evaluation of antigens for ACPA detection

Antigens used in the commercial second generation CCP assay (CCP2) are not readily available due to patent restrictions. Therefore citrullinated fibrinogen was synthesized in house. The PADI enzyme used for citrullination is not cost-effective since it is able to citrullinate only small quantities of fibrinogen. Therefore attempts were made to synthesize peptides similar to CCP2 which has better sensitivity than fibrinogen. A biotinylated version of CFFCP2 was synthesized commercially by Mimotopes and non-biotinylated CFFCP2 was provided by Dr.Haro's lab in Spain. Further direct fluorochrome labelled, biotinylated and non-biotinylated versions of the citrullinated and arginine peptides were synthesized by Dr.Haro's lab.

6.1.1 ELISA of commercial CFFCP2 & citrullinated fibrinogen

Eight patient samples including 4 high positives (>300), 2 negatives (<0.5) and 2 moderate positives (50-100) were assayed on a diagnostic platform (Immunocap, Phadia). These samples

were used to compare commercially synthesized CFFCP2 (CFFCP2-Mimo) and CFFCP2 obtained from the collaborator (CFFCP2-Esp) by ELISA. The same samples were used to verify the in vitro citrullination of fibrinogen performed in house using previously described technique (10). Blank wells coated with buffer were used as negative controls for the peptides and non-citrullinated fibrinogen was used for citrullinated fibrinogen. ELISA was performed according to the kit protocol (Bethyl laboratories, USA) as described in detail in the methods section 5.8. Both peptides were comparable in their optical density (OD) values for all the samples except one. Although, the citrullinated fibrinogen was quite specific and identified both negatives, the sensitivity was 83.3% of the commercial CCP2 assay and missed a strong positive sample. Therefore, citrullinated fibrinogen has lower sensitivity compared to the chimeric peptide.

Table 6.1-1 Comparison of 2 Cyclic citrullinated peptides and citrullinated fibrinogen

The CCP value was determined by a commercial diagnostic assay for the 8 RA samples and the values are given in arbitrary units determined by the manufacturer (Immunocap, Phadia). CFFCP2-ESP is the synthetic peptide obtained from our collaborator in Spain (Dr.Haro's lab) and CFFCP2-Mimo is the commercially synthesized peptide. Avg OD is the average of the duplicates in ELISA. Binding to the blank well (Blank OD) was used to account for non-specific binding for the CFFCP2 and non-citrullinated fibrinogen (Fib) was used for the citrullinated fibrinogen (Cit Fib). The biotinylated versions of the proteins and peptides were tested in this ELISA since those were the versions to be used in flow cytometry. a) Raw ELISA data from the samples. b) Average optical density with the baseline signal subtracted.

a)

	CCP Value	Buffer		CFFCP2-ESP		CFFCP2-Mimo		Biot Cit Fib		Biot Fibrin	
1/100 RA1	>300	0.202	0.228	3.236	3.251	3.299	3.186	1.296	1.265	0.28	0.268
1/100 RA2	>300	0.245	0.247	3.156	3.128	3.182	3.076	1.789	1.812	0.349	0.34
1/100 RA3	>300	0.104	0.097	2.811	2.971	3.108	3.027	0.855	0.834	0.149	0.144
1/100 RA4	>300	0.594	0.606	3.073	3.092	3.189	3.091	0.66	0.653	0.635	0.71
1/100 RA5	<0.5	0.532	0.579	0.734	0.744	0.855	0.839	0.523	0.502	0.575	0.559
1/100 RA6	<0.5	0.653	0.659	0.472	0.474	1.756	1.749	0.513	0.502	0.683	0.669
1/100 RA7	59	0.127	0.11	1.302	1.193	1.535	1.502	0.45	0.42	0.163	0.165
1/100 RA8	95.9	0.262	0.434	2.989	2.92	3.214	3.094	0.479	0.456	0.317	0.302

b)

Sample	CCP Value (Units/mL)	CFFCP2 - ESP (Avg OD – Blank)	CFFCP2 - Mimo (Avg OD – Blank)	Biot Cit Fib (Avg OD – Fib)
1/100 RA1	**>300**	3.03	3.03	1.01
1/100 RA2	**>300**	2.90	2.88	1.46
1/100 RA3	**>300**	2.79	2.97	0.70
1/100 RA4	**>300**	2.48	2.54	-0.02
1/100 RA5	**<0.5**	0.18	0.29	-0.05
1/100 RA6	**<0.5**	-0.18	1.10	-0.17
1/100 RA7	**59**	1.13	1.40	0.27
1/100 RA8	**95.9**	2.61	2.81	0.16

.

6.1.2 Evaluation of negative controls for CFFCP2 ELISA

There was disparity between the two peptides in identifying a known negative sample with commercially synthesized Mimo peptide showing false-positivity. Therefore further negative samples from different clinical settings were chosen to evaluate the CFFCP2-Mimo further. ELISA was perfomed according to the kit protocol (Bethyl laboratories, USA) as described in detail in the methods section 5.8. Anti-nuclear antibody (ANA) negative samples had a lower OD value compared to ANA positive samples since they are less likely to have other autoantibodies and proteins with non-specific binding. Anti-dsDNA antibodies in particular caused higher non-specific binding whereas Anti-Ro antibodies were less so. The CFFCP2-Mimo was less sensitive towards the lower end of the reference range.

Table 6.1-2 Evaluation of specificity of the citrullinated peptide CFFCP2-Mimo

Luminex value was determined by a commercial diagnostic assay (BioRad) for the RA samples and the values are expressed in arbitrary units/ml. Levels above 3 are considered positive. OD-Blank was calculated as the difference in average of optical density of the wells coated with CFFCP2 and blank wells. ND = Not done, ANA = Anti-nuclear antibody, dsDNA = Anti-double stranded DNA antibodies, Ro = Anti-Ro52 antibodies.

Sample	Blank Coat OD		OD		OD-Blank	Luminex value	
Diluent	0.008	0.007	0.013	0.015	0.0065	N/A	
RA 1	0.159	0.159	3.361	3.326	3.1845	>300	
RA 5	0.584	0.586	0.853	0.839	0.261	<0.5	
RA 8	0.141	0.148	2.831	2.807	2.6745	95.9	
RA 9	0.192	0.191	0.283	0.317	0.1085	<0.5	ANA ND
RA 10	0.092	0.092	0.165	0.168	0.0745	<0.5	GP Sample
RA 11	0.074	0.068	0.139	0.129	0.063	<0.5	
RA 15	0.093	0.087	0.124	0.123	0.0335	<0.5	ANA Neg
RA 16	0.107	0.097	0.131	0.13	0.0285	<0.5	GP Sample
RA 17	0.13	0.124	0.127	0.125	-0.001	<0.5	
RA 21	0.089	0.089	0.152	0.148	0.061	<0.5	ANA Neg
RA 22	0.132	0.135	0.162	0.168	0.0315	<0.5	Clinic
RA 23	0.171	0.167	0.364	0.364	0.195	<0.5	dsDNA
RA 24	0.294	0.271	0.485	0.464	0.192	<0.5	Pos
RA 25	0.216	0.224	0.276	0.293	0.0645	<0.5	
RA 26	0.125	0.14	0.32	0.304	0.1795	<0.5	Ro Pos
RA 27	0.265	0.297	0.289	0.307	0.017	<0.5	
RA 28	0.225	0.233	0.22	0.238	0	14.2	
RA 29	0.133	0.138	1.161	1.291	1.0905	26.2	
RA 30	0.173	0.173	0.374	0.399	0.2135	8.5	

The lower sensitivity of CFFCP2-Mimo peptide could be peptide dependent or sample dependent. Patients with higher ACPA titre possibly have a wider coverage of epitopes whereas those with lower titres may have a restricted repertoire, which is not covered by the peptide.

6.2 Detection of antigen-specific B-cells by flow cytometry

Flow cytometry can be used as a quick tool to identify cell populations of interest. If ACPA-specific B-cells can be identified by FACS, it would allow easy monitoring and quantification of their levels in peripheral blood and could present a biomarker to predict relapse and response to therapy. This would also allow for further functional evaluation of these cells following flow sorting.

6.2.1 CCP-specific B-cells were not detectable by FACS using citrullinated fibrinogen or commercially synthesized CFFCP2 peptide

PBMCs from 2 RA patients with active disease and 1 RA patient relapsing after rituximab who were all known ACPA positive were selected along with a control sample. The relapsing patient's peripheral blood contained only plasmablasts from the B-lineage. The PBMCs were surface stained with CD19 PE-Cy7, CD20 APC-H7, CD38 PerCP-Cy5.5, CD27 AF647 and then prepared with intrasure (BD Biosciences) for intracellular staining. 5 µg of biotinylated-CFFCP2 peptide (1 mg/ml) was incubated for 20 minutes and 0.05 µg of Streptavidin-Pacific orange (10µl of 50 µg/ml) was added or pre-incubated mixture of CCP/ Streptavidin-Pacific orange was used. Streptavidin-Pacific orange without CCP was used as a negative control. No positive staining was detected by either method with intracellular staining. The molecular mass of the biotinylated peptide is 4224 g/mol. Therefore, 5 µg contains (5 µg) ***/*** (4224 g/mol) **X** 6.022 X 10^{23} molecules. The exact molecular mass of streptavidin pacific orange is not provided by the manufacturer but similar flurochrome-tagged streptavidin's molecular mass is 60000 g/mol. Therefore, 0.05 µg contains (0.05 µg) ***/*** (60000 g/mol) **X** 6.022 X 10^{23} molecules. Streptavidin has four biotin binding sites and the peptide was in excess to saturate all the binding sites.

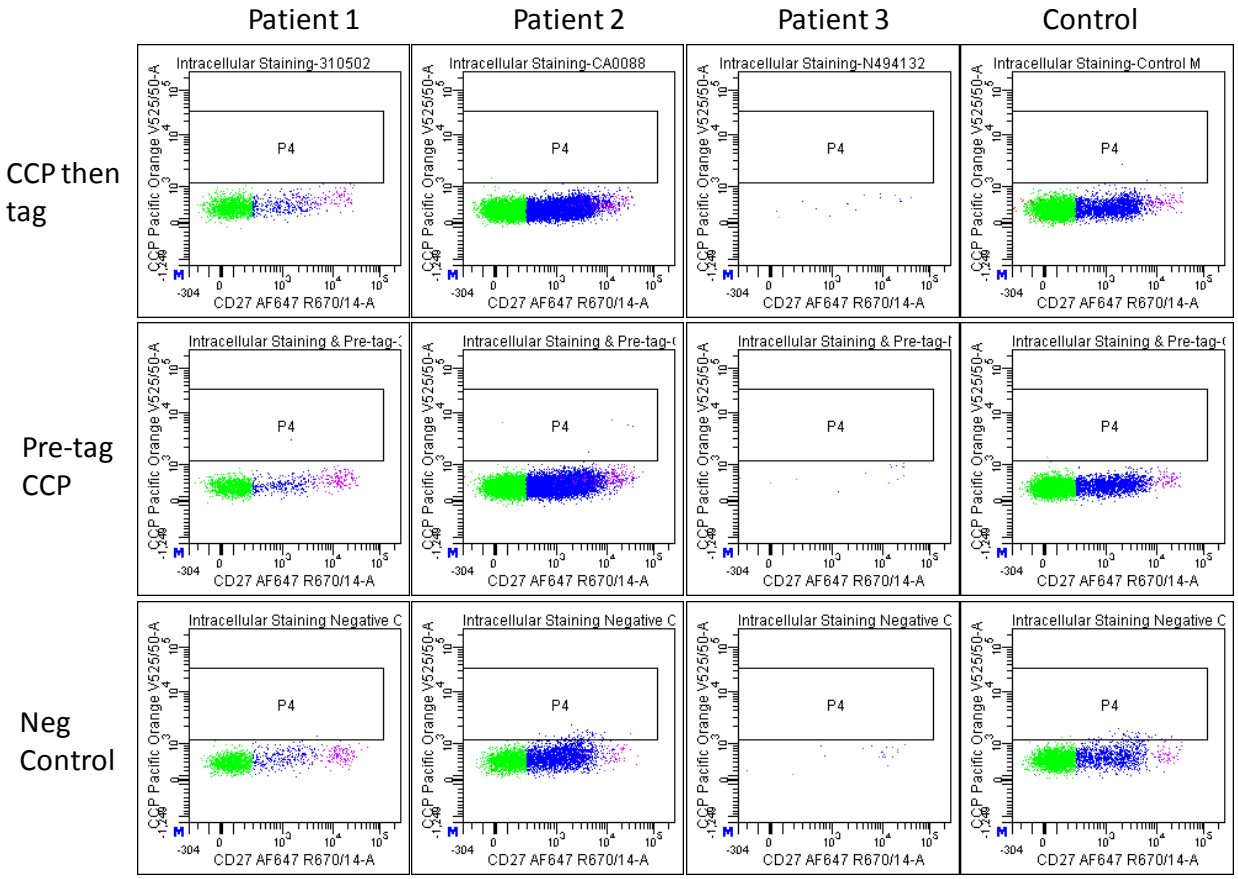

Figure 6.2-1 Intracellular staining with CCP

Patients 1&2 are active RA patients with no previous BCDT; patient 3 was relapsing post-BCDT with predominantly plasmablasts. For “CCP then tag” the cells were incubated with 5 µg of the biotinylated peptide before adding 0.05 µg of the Streptavidin pacific orange tag. For “Pre-tag CCP”, the cells were incubated with pre-mixed peptide (5 µg) and streptavidin pacific orange (0.05 µg). For negative control streptavidin pacific orange without the peptide was used. B-cells were defined based on their scatter profile and CD19 and CD20 dual positivity. The level of CD27 expression was used to subclassify B-cells into naïve (Green) and memory (Blue). Plasmablasts (Purple) were gated based on their scatter profile, $CD19^{Pos}CD20^{Neg}CD27^{Hi}$ and $CD38^{Hi}$.

For surface staining, 5 µg of biotinylated-CFFCP2 peptide was added at the same time as other surface staining antibodies followed by 0.05 µg Streptavidin-Pacific orange or the pre-incubated biotinylated-CFFCP2 (5 µg) / Streptavidin-Pacific orange (0.05 µg) mixture. Streptavidin-Pacific orange without any CFFCP2 used as a negative control showed equivalent or higher binding than with CFFCP2 in the 2 RA patients with active disease. The presence of CCP-binding to surface of plasmablasts is likely to be non-specific since there was no binding detected by intracellular staining. The non-specific binding was worse with pre-tagging the peptide with Streptavidin-Pacific orange.

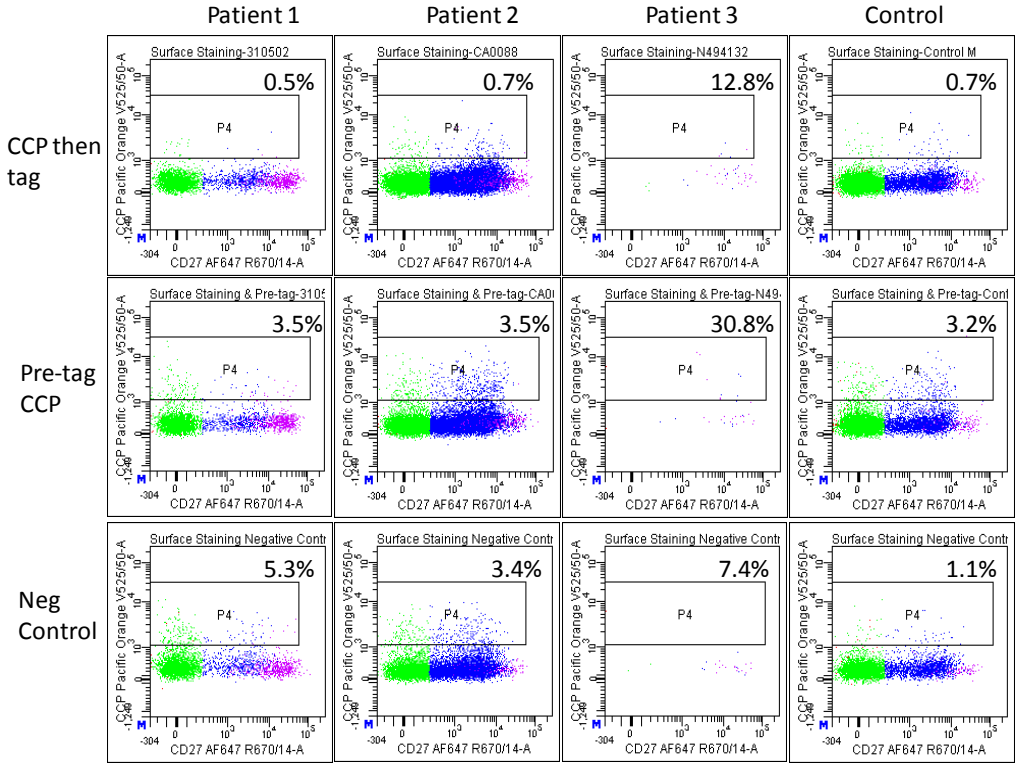

Figure 6.2-2 Surface staining with CCP

Patients 1&2 are active RA patients with no previous BCDT; patient 3 was relapsing post-BCDT with predominantly plasmablasts. For “CCP then tag” the cells were incubated with 5 µg of the peptide before adding 0.05 µg of the Streptavidin pacific orange tag. For “Pre-tag CCP”, the cells were incubated with pre-mixed peptide (5 µg) and streptavidin pacific orange (0.05 µg). For negative control streptavidin pacific orange without the peptide was used. CCP positive cells shown as a percentage of total B-cells. B-cells were defined based on their scatter profile and CD19 and CD20 dual positivity. The level of CD27 expression was used to subclassify B-cells into naïve (Green) and memory (Blue). Plasmablasts (Purple) were gated based on their scatter profile, $CD19^{Pos}CD20^{Neg}CD27^{Hi}$ and $CD38^{Hi}$.

6.2.2 Detection of CCP-specific B-cells using fluorochrome-tagged CFFCP2 peptide

CFFCP2 peptide directly conjugated with the fluorochrome AF647 was synthesized by Dr.Isabel Haro's lab in Spain. The detailed methodology for synthesizing the peptide has been previously described (78). The peptide was also generated with biotin tag to allow for a choice of conjugates and can also be used in ELISA. Non-citrullinated versions of the peptide with native arginine instead of the citrulline were also generated to be used as negative controls. The CFFCP2-AF647 peptide was validated by ELISA before using it for flow cytometry. The biotinylated peptides were bound to the ELISA plate with a streptavidin coat to test whether this additional protein binding interferes with the binding of the peptide when used in other methodologies like FACS and ELISpot. Serum from RA patients with very high levels, moderate levels and no ACPA were used as controls along with commercially sourced positive and negative controls used in the diagnostic laboratory. ELISA was performed according to the kit protocol (Bethyl laboratories, USA) as described in detail in the methods section 5.8. The optical density values (OD) of non-citrullinated version (Arg-CFFCP2) was subtracted from those obtained with the citrullinated version to calculate the final OD shown in Figure 6.2-3. Results obtained with AF647 conjugated CFFCP2 peptide was satisfactory for all the controls and correlated with those obtained with streptavidin-tagged CFFCP2 peptide. The OD for AF647 tagged CFFCP2 was lower which is likely to be due to the inherent fluorescence of AF647. The peptide solution was aliquoted and lyophilised for long-term storage. The lyophilisation process, fluorochrome tagging or streptavidin binding did not affect the sensitivity or specificity of the peptide for ELISA.

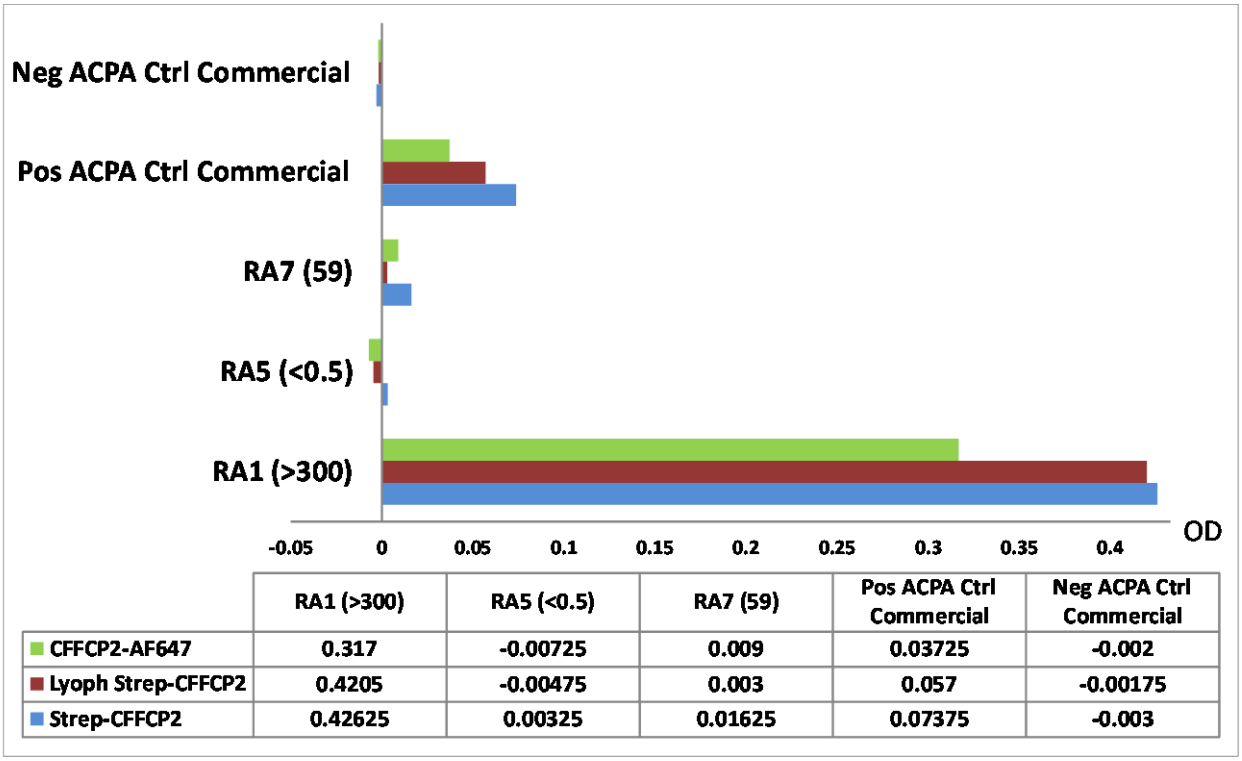

	RA1 (>300)	RA5 (<0.5)	RA7 (59)	Pos ACPA Ctrl Commercial	Neg ACPA Ctrl Commercial
CFFCP2-AF647	0.317	-0.00725	0.009	0.03725	-0.002
Lyoph Strep-CFFCP2	0.4205	-0.00475	0.003	0.057	-0.00175
Strep-CFFCP2	0.42625	0.00325	0.01625	0.07375	-0.003

Figure 6.2-3 ELISA of AF647 fluorochrome and streptavidin-tagged CFFCP2 peptide

Optical density values obtained by subtracting the arginine peptide values from the citrullinated peptide are shown. Commercially available positive and negative ACPA controls and samples from RA patients were used. The values in brackets are arbitrary units of level of ACPA antibodies detected on a diagnostic platform (Unicap).

Peripheral blood mononuclear cells from 4 RA patients with active disease, one patient stable on anti-TNF and one SLE patient were stained with 5 µg of CFFCP2-AF647 and 5 µg of biotinylated Arg-CFFCP2 + 0.05 µg streptavidin pacific orange. The arginine peptide served as a negative control to exclude non-specific binding to the peptide. Therefore, cells which were positive for both peptides were excluded as false-positives. 1-2% of the B-cells from the RA patients showed positive staining with CFFCP2-AF647. The lupus patient whose serum had been tested to be negative for ACPA had the highest proportion of positive B-cells (2%). The positive staining noted therefore is likely to be non-specific. 80% of the CFFCP2 positive B-cells were IgD positive in all samples except the SLE patient which was 75%. This reflects the higher non-specific binding by naïve B-cells rather than presence of higher proportion of autoreactive B-cells within the naïve B-cell compartment.

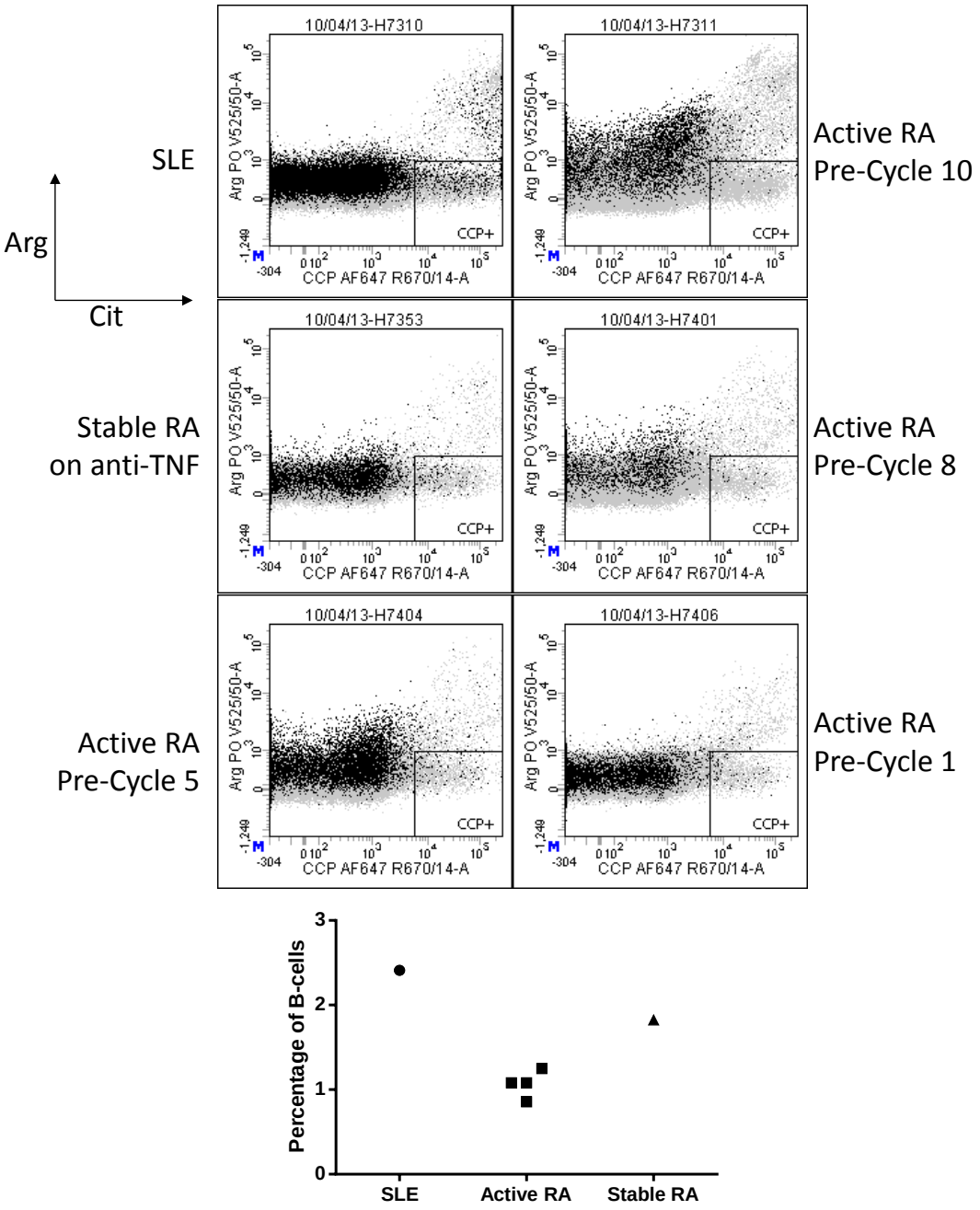

Figure 6.2-4 Detection of citrullinated protein-specific B-cells by flow cytometry

Lymphocytes (grey) were gated based on their scatter profile and B-cells (black) were identified by their expression of CD19. Intensity of staining with the citrullinated peptide is represented on the X-axis and the native arginine peptide on the y-axis. Cycle number of rituximab therapy for the active RA patients is given. The SLE patient was ACPA negative. CCP positive B-cells as a percentage of total B-cells shown.

Since there was high degree of non-specific binding with the fluorochrome-tagged peptide, cells were stained with increasing dilutions of the peptide. There was little change in the proportion of positive cells between 5 and 0.5 µg concentrations.

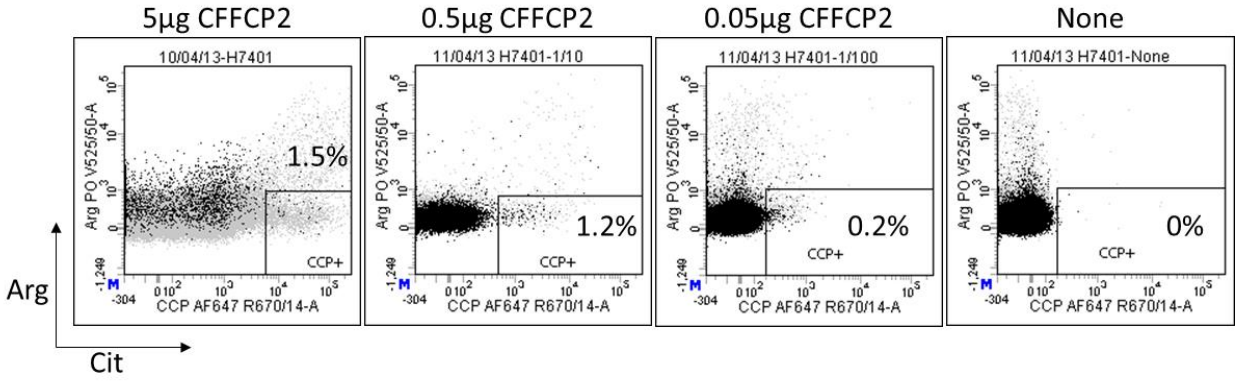

Figure 6.2-5 Titration of the AF647-tagged citrullinated peptide

Lymphocytes (grey) were gated based on their scatter profile and B-cells (black) were identified by their expression of CD19. Intensity of staining with the citrullinated or arginine versions of the cyclic peptides tagged with AF647 is represented on the X-axis. Biotinylated version of the arginine peptide with streptavidin pacific orange as the fluorochrome was used as additional negative control and is represented along the y-axis. CCP positive B-cells represented as percentage of total B-cells.

One of the active RA patient's samples with positive ACPA was stained with citrullinated and the arginine versions of the direct AF647 tagged peptide to assess the specificity. Both versions of the peptide showed similar levels of positivity in B-cells as shown in Figure 6.2-6. The non-specific binding could be due to the fluorochrome conjugate or directed against other amino acids in the cyclic peptide.

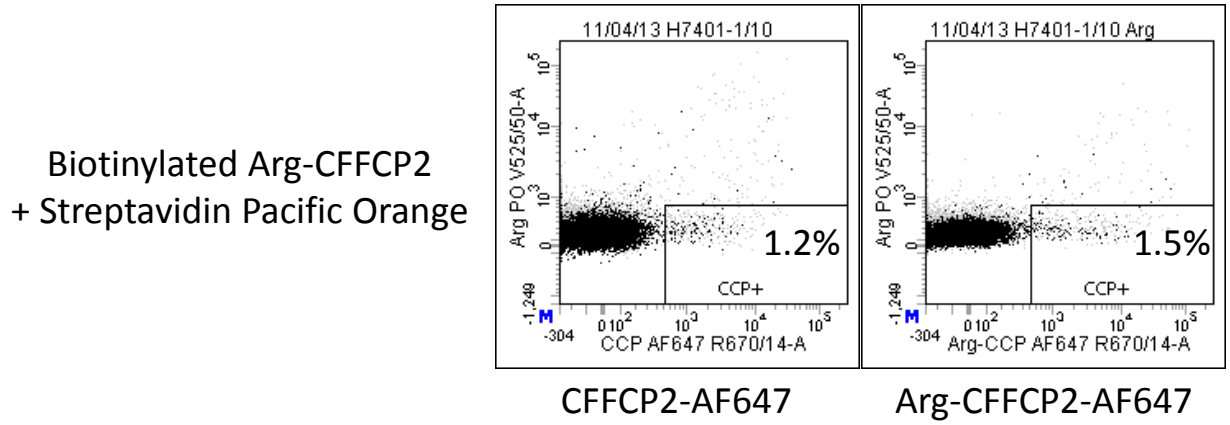

Figure 6.2-6 Non-specific binding by the AF647-tagged citrullinated peptide

Lymphocytes (grey) were gated based on their scatter profile and B-cells (black) were identified by their expression of CD19. Intensity of staining with the citrullinated or arginine versions of the cyclic peptides tagged with AF647 is represented on the X-axis. Biotinylated version of the arginine peptide with streptavidin pacific orange as the fluorochrome was used as additional negative control and is represented along the y-axis.

Citrullinated fibrinogen and the CFFCP2 peptides were able to identify ACPA by ELISA. Modifications to the peptide in terms of biotinylation, direct fluorochrome tagging and biotin-streptavidin tag did not interfere with its activity in ELISA. The cyclic citrullinated peptides were not reliable in detecting CCP-specific B-cells by flow cytometry. It is possible that the peptides are not sufficiently sensitive to detect the CCP-specific B-cells at all, and the staining seen was non-specific. Alternatively, the peptides might need binding to a solid phase for their optimal conformational state for binding and being in liquid phase when used in flow cytometry is suboptimal. The autoreactive B-cells might have higher degree of non-specific binding limiting their detection. The high degree of non-specific binding by the peptides could be related to folding pattern, ionic or hydrophobic interactions. Unfortunately, a positive control for flow cytometry is not available which makes quality control of the assay challenging. Due to these issues, flow cytometric detection of CCP-specific B-cells was not pursued further. The only definitive way to confirm the detection of autoreactive cells by this assay is to single cell sort the positive B-cells, sequence the whole immunoglobulin gene and re-express in a hybridoma (83). The immunoglobulin secreted could then be analysed for ACPA. However this highly technical process was not established locally, and was not pursued as an option in this work.

6.3 Detection of antigen-specific B-cells by ELISpot

The detection of antigen-specific B-cells by flow cytometry was unsuccessful and therefore alternative techniques were sought. One such technique is ELISpot which is more sensitive than ELISA. ELISpot also allows for quantification, and the frequency of secreting cells can be calculated from the input cell numbers. However, it does not allow selection of cells for further analysis although novel techniques using photodegradable hydrogels have been developed to capture the secreting cells (84). ELISpot can be used to define the antigen specificity of peripheral blood antibody secreting cells like plasmablasts or bone marrow plasma cells. Alternatively, B-cells can be expanded and differentiated in vitro to generate antibody secreting cells and assayed by ELISpot. If B-cells predominating during relapse can be identified based on surface phenotype, they can be sorted by flow cytometry and antibody secreting cells generated in vitro could be assayed.

6.3.1 ELISpot for detection of vaccine specific plasma cells

To establish the technical ability to detect antigen specific B-cells by ELISpot, plasma cells enriched by CD138 magnetic beads (Miltenyi) from clinical waste bone marrow samples were tested for secretion of antibodies against two vaccines. In the absence of recent vaccination or infection, the vaccine specificity is also a useful marker of long-lived PCs. Trivalent vaccine Revaxis (Diphtheria, Polio, Tetanus) and pentavalent vaccine Pediacell (Diphtheria, Polio, Tetanus, Pertussis, Haemophilus Influenzae type b) were coated onto the ELISpot plates at 15 mg/ml. Blank wells and CFFCP coated wells were used as negative controls whilst anti-IgG coated wells were used as positive controls. The spots were developed as described in the methods section 5.9. The positive control IgG spots were discrete when numbers of cells plated were optimal as in the case of control in vitro derived plasma cells and BM PCs1. When the number of cells is higher, the spots tend to merge in BM PCs 2 and 3 as shown in Figure 6.3-1. There were more spots in the pentavalent vaccine wells for BM PCs 2 and 3 compared to the trivalent vaccine wells (10 Vs 7 and 20 Vs 12) as expected in triplicates. There were no spots seen in the uncoated wells, which excludes non-specific binding.

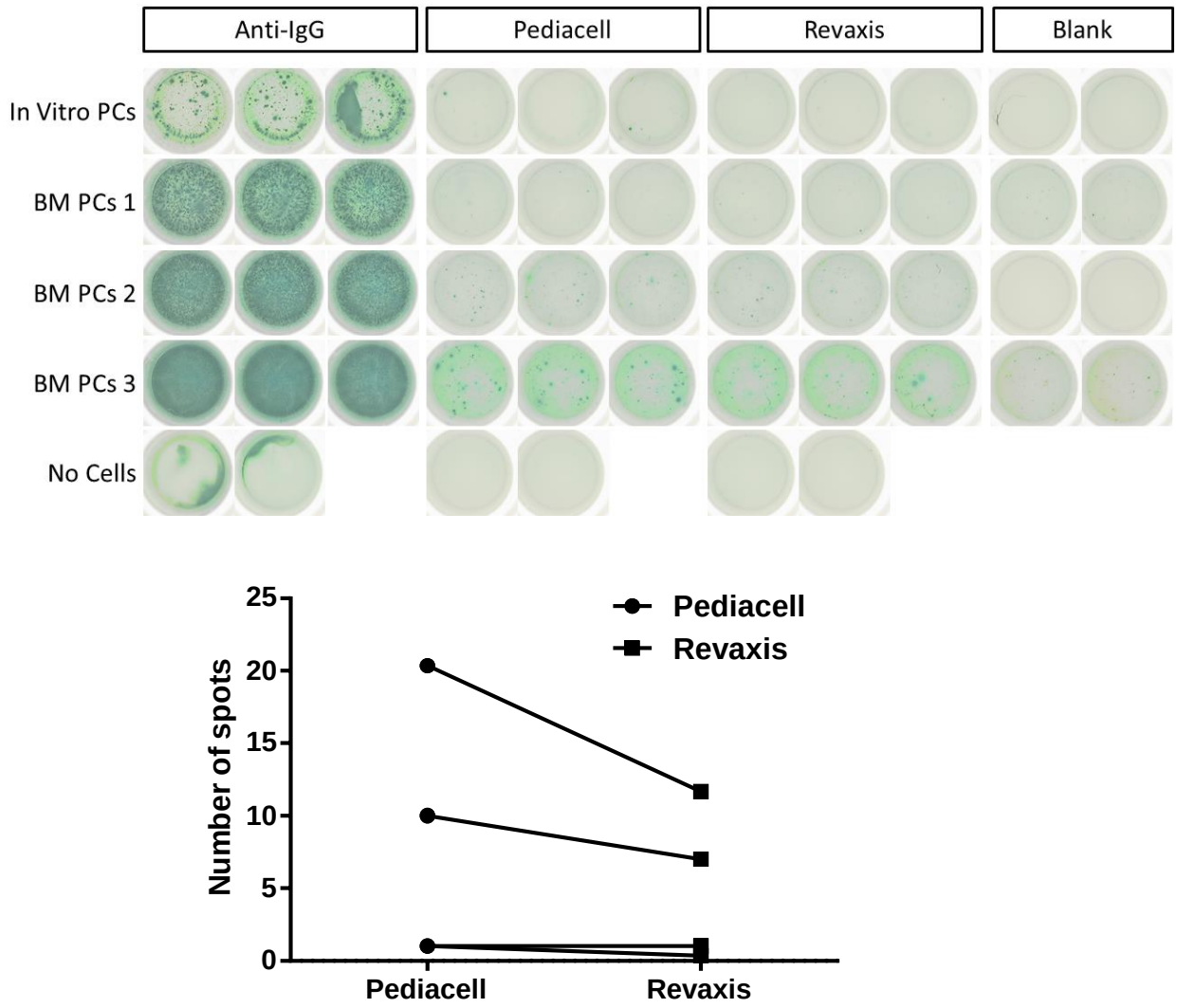

Figure 6.3-1 ELISpot for vaccine-specific plasma cells

In vitro generated PCs (Using protocol described in Figure 5.4-1) from a control (Row 1) and magnetically selected CD138 positive PCs from surplus bone marrow samples of patients (Rows 2-4) investigated for haematological malignancies were incubated for 8 hours. The spots were detected with anti-IgG biotin and streptavidin HRP (as described in the methods section 5.9). The labels at the top represent the primary coating of the well and the labels on the side represent the samples added. The average number of spots in triplicates is shown in the graph for the 4 samples. Revaxis - Trivalent vaccine (Diphtheria, Polio, Tetanus), Pediacell - Pentavalent vaccine (Diphtheria, Polio, Tetanus, Pertussis, Haemophilus Influenzae type b). These findings demonstrate ability to detect antigen-specific PCs.

6.3.2 ELISpot for CCP-specific plasma cells

Peripheral blood B-cells from one healthy control and 3 ACPA+ RA patients were differentiated using standard protocol as shown in Figure 5.4-1. An alternative condition using TLR 7/8 agonist R848 instead of CD40L stimulus was also included. The rest of the culture conditions remained the same. The cells differentiated into plasmablasts by day 6 and on day 10 consisted of a mixture of plasmablasts and plasma cells. These day 10 cells were plated on to ELISpot plates coated with the citrullinated peptides as shown in Figure 6.3-2 and incubated for 8 hours. The spots were detected with anti-IgG and streptavidin-HRP as described in methods section 5.9. IgG secretion was detected in all samples but there was no evidence of ACPA secretion in any of the samples by ELISpot. The supernatants were tested for ACPA by ELISA and only RA2012 was positive. CCP coated beads used in the diagnostic assay (Biorad) was also tried as the capture agent by coating it on the plate which did not detect ACPA secretion either.

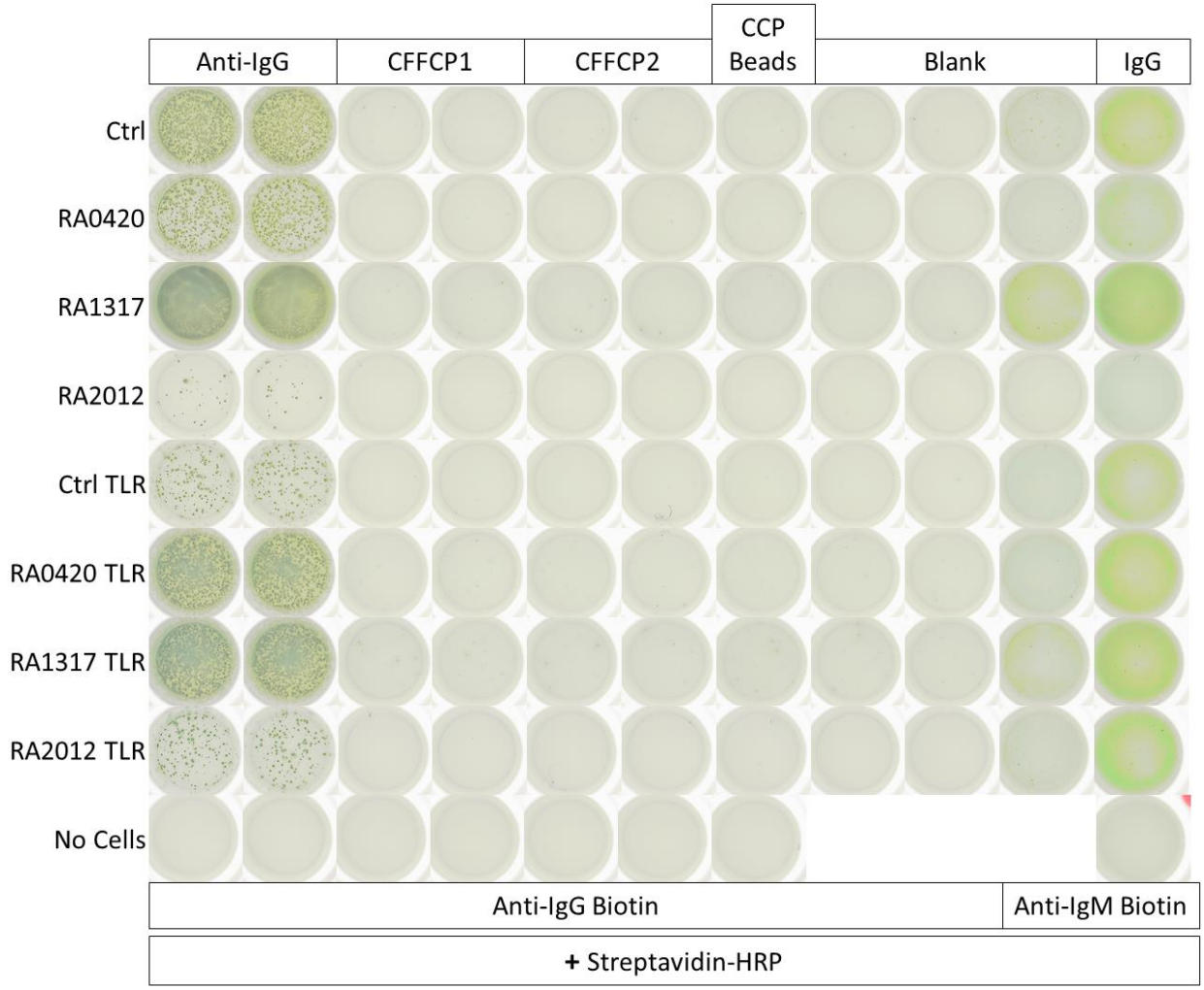

Figure 6.3-2 ELISpot for ACPA secretion by day 10 in vitro differentiated PCs

Peripheral blood B-cells from 1 control and 3 ACPA positive RA patients (Serum positive) were differentiated in vitro to antibody secreting cells by day 10 (Using protocol described in Figure 5.4-1) and were incubated for eight hours in the plate at 37^0C. The labels at the top represent the primary coating of the well and the labels on the side represent the samples added. The labels at the bottom denote the detection reagents used. Only supernatant of RA2012 was positive by ELISA.

The above protocol involves B-cell selection and change of culture conditions twice after the initial setup to generate plasma cells which takes 10 to 13 days in total. So, alternative methodologies which can use PBMCs that require less time and manipulation were sought. One such methodology described in the ELISpot kit protocol was used to generate antibody secreting cells. PBMCs from 1 control and 3 ACPA-positive RA patients were stimulated with

R848 and IL2 using the ELISpot kit protocol (Mabtech) (as described in methods section 5.4.5) and the generated antibody secreting cells on day 6 were incubated for eight hours in the plate at 37^0C.. The spots were developed as described in the methods section 5.9. The control and RA0513 showed some spots (not obvious in the picture below) but the corresponding uncoated wells also showed spots and therefore non-specific binding could not be ruled out. Biotinylated CFFCP2 was tried as a detection agent on captured IgG (columns 1 and 2) which did not detect ACPA either. In the bottom 4 rows instead of cells, plasma isolated on day 0 was used to detect IgG and ACPA similar to the ELISA technique. IgG was detectable from plasma with anti-IgG coat (columns 3,4) but ACPA was not detected by CFFCP coat (columns 5,6). This is suggestive of a lack of binding of CFFCP to the ELISpot plate.

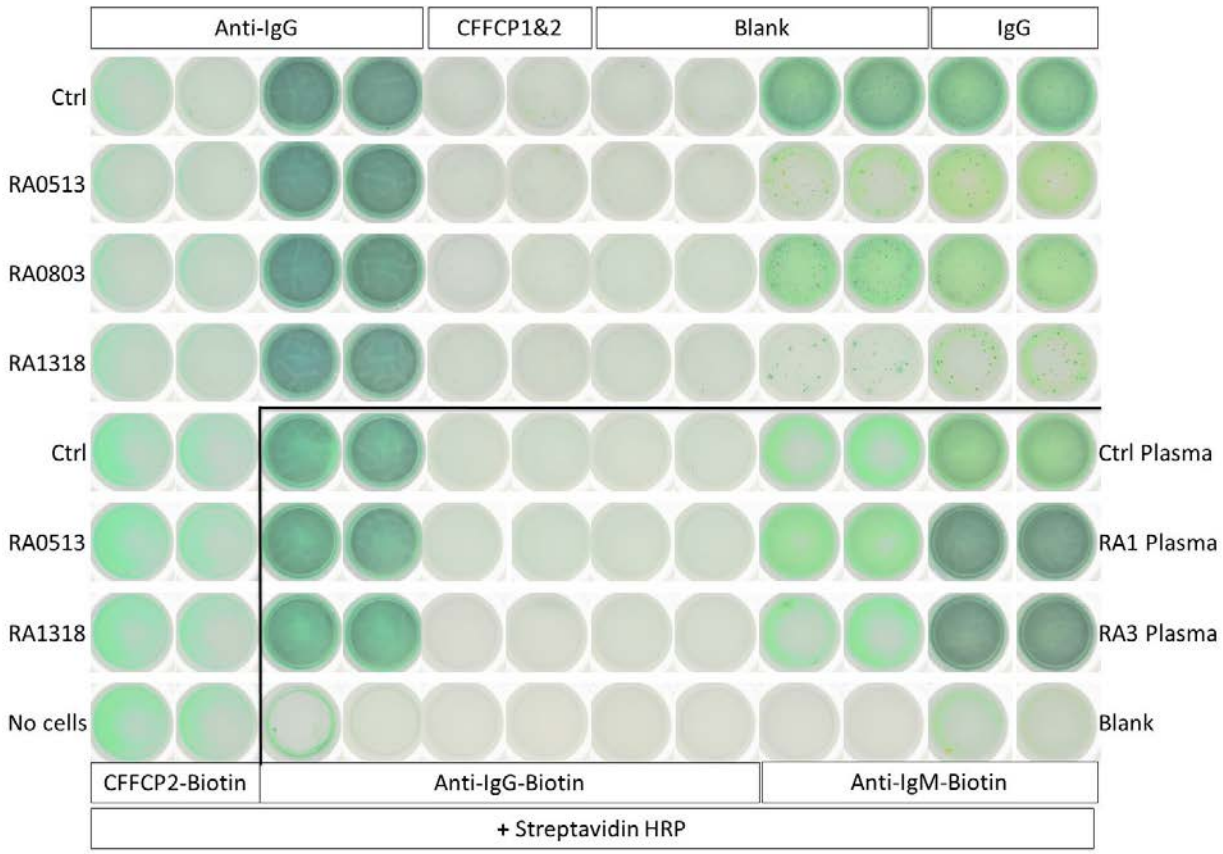

Figure 6.3-3 ELISpot for ACPA-specific PCs with day 6 TLR stimulated PBMCs

Peripheral blood mononuclear cells from a control and 3 ACPA+ RA patients stimulated with TLR agonist R848 and IL2 (as described in methods section 5.4.5) and tested on day 6 when differentiation to antibody secreting cells has occurred. The cells were incubated for eight hours in the plate at 37^0C and spots were developed as described in the methods section 5.9. The labels at the top represent the primary coating of the well and the labels on the side represent the samples added. The labels at the bottom represent the sample added to the bottom 4 rows. In the first 2 columns of the bottom 4 rows biotinylated CFFCP2 was used for detection instead of anti-IgG biotin.

6.3.3 In vitro ACPA secretion by peripheral blood B-cells from RA patients

B-cells from 3 ACPA positive RA patients and a control were cultured under standard protocol using BCR and CD40L stimulus as shown in Figure 5.4-1. When the undiluted supernatants were tested by ELISA (as described in methods section 5.8), there was detectable ACPA on day 6 and day 10 in one out of the three patients. In a separate experiment PBMCs from 3 ACPA positive RA patients and a control were stimulated with IL2 and R848, a TLR7 agonist as described in methods section 5.4.5. On day 6 ACPA was detected from the supernatant in one out of the three patients. However ACPA secreting cells were not detectable with these samples when tested by ELISpot as seen in Figure 6.3-2 and Figure 6.3-3. The in vitro secretion of ACPA did not correlate with serum ACPA titre or disease activity within these samples.

Table 6.3-1 Secretion of ACPA by peripheral blood B-cells in vitro and corresponding clinical details

The top half of first table shows data from supernatant derived from B-cells differentiated using the B-cell receptor/CD40L stimulus (Figure 5.4-1). The bottom half shows data from supernatant derived from PBMCs cultured using toll-like receptor stimulus (R848 1 µg/ml) (Methods section 5.4.5). The second table shows the clinical details of the RA patients. The samples showing in vitro ACPA secretion are highlighted. MTx – Methotrexate, HCQ – Hydroxychloroquine, SSZ – Sulphasalazine, Depomed – Depomedrone, Pred – Prednisolone.

OD

IgG		Buffer		CFFCP2-ESP							
Day 10 1/100		Day 10 Neat		Day 10 Neat		Day 6 Neat		Day 0 Plasma 1/100			
0.68	0.69	0.02	0.02	0.02	0.02	0.05	0.05	0.23	0.18	D2626	BCR/CD40L/B-cell
1.92	1.90	0.00	0.01	0.00	0.01	0.03	0.03	3.30	3.35	RA0420	
0.61	0.59	0.04	0.04	0.04	0.02	0.04	0.04	0.40	0.43	RA1317	
2.11	2.16	0.02	0.03	0.87	0.84	1.00	0.95	3.38	3.28	RA2012	
2.10	2.13	0.03	0.03	0.02	0.02	0.01	0.00	0.05	0.06	D2005	PBMC/TLR
2.00	2.10	0.04	0.04	0.10	0.10	0.08	0.08	3.12	3.11	RA0513	
2.14	2.07	0.01	0.02	0.31	0.31	0.00	0.01	3.12	3.11	RA0803	
0.86	0.78	0.08	0.08	0.02	0.04	0.02	0.00	2.10	2.06	RA1318	
Day 6 1/100		Day 6 Neat		Day 6 Neat		Day 3 Neat		Day 0 Plasma 1/100			

	Age	Active Disease	Medn	CRP	ESR	WCC	CCP	RF
RA1317	62/F	Yes	MTx, HCQ, SSZ	31	50	9.88	15	23
RA0420	35/M	Yes	Depomed	5	7	5.02	>300	Neg
RA2012	57/F	Yes	MTx, Pred	5		8.68	340	213
RA0803	63/F	No	MTx, HCQ	5	19	8.59	340	166
RA1318	54/F	No	MTx, Pred	12	44	5.23	312	Ro, La Pos. dsDNA-70
RA0513	40/F	Rx started 1/12 earlier	MTx, Depomed	23	31	9.74	142	

6.4 Summary and discussion

The sensitivity and specificity of the antigen peptide (CFFCP2) for detecting citrullinated protein-specific cells was comparable to the diagnostic CCP2 assay when tested by ELISA. The citrullinated fibrinogen generated in house although specific, had lower sensitivity and therefore was not pursued further. It was not possible to detect antigen-specific cells by flow cytometry due to low sensitivity and non-specific binding. An improved approach utilizing tetrameric antigen, may however make this feasible in the future (82). ELISpot detected vaccine specific PCs, but ACPA-secreting cells were not detected, possibly due to lack of CFFCP binding to the ELISpot plate. Trying the peptide as a probe or attaching it indirectly to the plate could circumvent this lack of binding.

The detection of ACPA from PBMC culture supernatant could be attributed to direct secretion of ACPA by peripheral blood plasmablasts. However, ACPA was detected in the supernatant when purified B-cells were differentiated to antibody secreting cells. The negative selection kit used for purifying B-cells depletes plasmablasts and therefore ACPA is likely to be derived from in vitro differentiated antibody secreting cells generated from peripheral blood B-cells. This confirms the presence of citrullinated protein-specific B-cells in the peripheral blood. It was interesting to note that ACPA secretion by ELISA was not demonstrable in 4 out of 6 RA peripheral blood samples tested, the reasons for which could be multi-factorial. Although the frequency of citrullinated protein-specific B-cells is not known, for vaccine antigens it is estimated to be 1 in 10000 (50) which is likely to be a significant limiting factor for their detection. The sensitivity of ELISA is possibly not adequate for ACPA detection from supernatants and it is not known whether co-secretion of RF or other proteins in the supernatant can affect ACPA detection. Recently published study demonstrated in vitro secretion of ACPA only after five-fold concentration of the supernatants which resulted in decreased specificity as evidenced by detection of ACPA from healthy donor culture supernatants (85). Citrullinated protein-specific B-cells could be recruited to secondary lymphoid structures and synovium which can reduce their frequency in peripheral blood. Therefore, the lack of ACPA detection from supernatants is likely to be due to technical limitations and other variables rather than absence of citrullinated protein-specific B-cells.

The detection of long-lived PCs by their antigen specificity is complicated by the vast array of potential antigen specificities that may need to be considered. The vaccine specific PCs when identified by ELISpot cannot be isolated for further phenotypic or gene expression analysis. A technique combining laser capture microdissection and a fluorophore for detection could make the isolation of ELISpot positive cells possible. However, if the long-lived PCs can be characterised phenotypically by other methods such as flow cytometry, ELISpot can then be used for detecting vaccine-specific PCs within the subset which would confirm their long life span.

7 Second Results Chapter: Phenotypic characterisation of cells associated with RA relapse post rituximab therapy

B-cell depletion therapy in RA has re-invigorated research into the autoimmune mechanisms in RA particularly mediated by B-lineage cells. The initial aim of work in this chapter was to identify the broad B-cell subset (naïve, memory or plasmablast) that is most likely to contain the pathogenic population, which might then be further sub-classified with additional markers to improve specificity. An increased proportion of a certain subset selectively during relapse would be suggestive of its role in pathogenesis, and this clinical context was therefore the major focus of subsequent study. Since antigen specific B-cells were difficult to identify directly by flow cytometry from the whole B-cell population, it was reasoned that identification of a relapse associated and thus potentially pathogenic B-cell subset would facilitate the identification of antigen specific B-cells. Previous studies done in Leeds had shown strong correlation of baseline plasmablasts with clinical response and that persistence of plasmablasts 2 weeks post-rituximab predicted poor clinical response (25, 86). Therefore, initial attempts were targeted towards identifying subsets amongst plasmablasts.

Patients treated with rituximab had a higher proportion of naïve B-cells and reduced absolute numbers of all the 3 tested subsets – naïve, memory and plasmablasts (Figure 6.4-1). This was likely to be due to the direct effect of B-cell depletion by rituximab rather than secondary to the process. Therefore, it was hypothesized that the major subsets needed further subclassification to identify differential proportions in relapsing patients. Since the pathogenic B-cells can potentially be present in any of the three major B-cell subsets – naïve, memory or plasmablasts all the three were sub-classified into 4 further subsets based on expression of IgM and LAIR1 (naïve and memory) or CD138 and LAIR1 (plasmablasts). This revealed heterogeneity within all the 3 tested B-cell subsets. However, only the heterogeneity within memory B-cells was significantly different in relapsing patients which cannot be explained by the direct B-cell depleting effect of rituximab (Figure 6.4-2). The significant differential heterogeneity was due to expansion of LAIR1 negative cells within the memory B-cells. However, if the LAIR1 negative cells were analysed as a proportion of total B-cells, this differential level within the relapsing patients was not evident Figure 6.4-3. Therefore, memory B-cells were pursued as the subset

with differential expansion of subpopulations during RA relapse post-rituximab containing potentially pathogenic cells.

As noted above the major subsets were quite heterogeneous and therefore the plan was to sub-classify memory B-cells into as many populations as possible by flow cytometry which can then be merged if necessary depending on subsequent clinical correlation. 34 markers which are expressed on the surface of B-lineage cells that are likely to indicate an active immune response such as activation markers, costimulatory and regulatory molecules, cytokine and chemokine receptors and markers associated with stages of B-cell life cycle were assessed. The markers which were expressed by between 90% and 10% of the memory B-cells were deemed to be heterogeneous (Figure 6.4-4). 19 out of the 34 surface markers were heterogeneously distributed and considered for further analysis. Due to technical limitations the number of markers that can be used was restricted to four. LAIR1 was already demonstrated to be of clinical relevance and three other markers - CD24, CD84 and CD95 which do not have a similar surface expression profile to any of the other selected markers were chosen.

When the memory B-cells were analysed for the concomitant expression of these four surface markers, 16 subsets could be defined as shown in Figure 6.4-6. The subset distribution pattern in RA patients relapsing post-rituximab was distinct compared to other patient groups and controls. The dominant memory B-cell subset was $CD24^{-}CD84^{-}CD95^{+}LAIR1^{-}$ in patients relapsing post-rituximab whereas it was the polar opposite $CD24^{+}CD84^{+}CD95^{-}LAIR1^{+}$ subset in the other patient groups as shown in Figure 6.4-7. The proportion of $CD24^{-}CD84^{-}CD95^{+}LAIR1^{-}$ was significantly elevated in patients relapsing post-rituximab compared to controls, rituximab naïve patients with active disease and patients in remission with biologics. This increase in proportion was not seen during B-cell reconstitution in other conditions where B-cells are therapeutically depleted such as B-cell neoplasms and campath pre-renal transplant (Figure 6.4-8). The absolute number of cells is usually the preferred index since proportions can be skewed by increase in the subset of interest or decrease in the other subsets. However, in patients relapsing post-rituximab, the B-cell numbers are reduced due to the depletion of B-cells and therefore exhibit lower absolute count of all the subsets. Therefore, the absolute counts are not comparable with other patient groups who were not exposed to rituximab (Figure 6.4-10).

The above dataset contained only 3 patients who were in remission post-rituximab. The clinical review of patients receiving rituximab therapy is setup in such a way that they are reviewed only

if they have clinical symptoms. Therefore, it was difficult to capture the cohort of patients who are in remission post-rituximab. Further efforts were made to collect samples from patients who were more than 6 months since the last dose of rituximab. This revealed that patients who were in remission did not exhibit skewing of the memory B-cell subset distribution but could be skewed by other intercurrent illnesses (**Error! Reference source not found.**).

Further evaluation of this $CD24^{-}CD84^{-}CD95^{+}LAIR1^{-}$ memory B-cell subset was performed to understand the functional relevance of these cells in the RA disease process. The initial assessment was that of their immunoglobulin isotype which revealed that this subset of memory B-cells were predominantly class-switched whereas the polar opposite usually dominant $CD24^{+}CD84^{+}CD95^{-}LAIR1^{+}$ subset was predominantly of the IgM/IgD isotype (Figure 6.4-11). The surface phenotype of this relapse associated memory B-cell subset was compared with plasmablasts, since persistence of plasmablasts were shown to be predictive of poor response to rituximab in previous work done in Leeds (25). The plasmablasts were similar in terms of CD24, CD84, CD95 and LAIR1 expression but lack CD20 and express very high levels of CD38 compared to memory B-cells (Figure 6.4-12). From sequential monitoring of the surface expression, CD24, CD84 and LAIR1 expression is lost and CD95 is gained following activation of B-cells before they differentiate to plasmablasts (Figure 8.2-1). Therefore, it was hypothesized that these cells could be in the stage of transition to plasmablasts. However, by definition plasmablasts are antibody secreting cells and also express CD38 but lack CD20 and therefore different. Results from further functional evaluation of these cells are discussed in the next chapter.

In summary, this chapter describes the classification of B-cells into broader subsets followed by further subclassification to identify cell populations that are elevated during clinical relapse and are likely to be related to RA pathogenesis.

7.1.1 Identifying candidate B-cell subsets

BCDT provides an excellent opportunity to study autoreactive B-lineage cells since the population which preferentially expands during relapse after depletion is likely to contain pathogenic cells. 12 patients who were relapsing after rituximab therapy were chosen along with 7 rituximab naïve RA patients with active disease and 21 disease controls. CD19, CD20, CD27 and CD38 were used to classify the B-cells into 3 broad subsets – naïve, memory B-cells and plasmablasts. IgM and LAIR1 identified four further subsets each in naïve and memory B-cells and for plasmablasts CD138 was used instead of IgM. Transitional B-cells were not separated from naïve B-cells in this analysis.

Patients treated with rituximab were found to have lower total number of B-cells and an associated reduction in the absolute numbers of all subsets as seen in Figure 6.4-1. This makes the comparison of the absolute numbers of different subsets between patient groups inaccurate. The relative change in proportion of a subset is more comparable and an increase of a particular subset in the context of clinical relapse would suggest a possible role in pathogenesis.

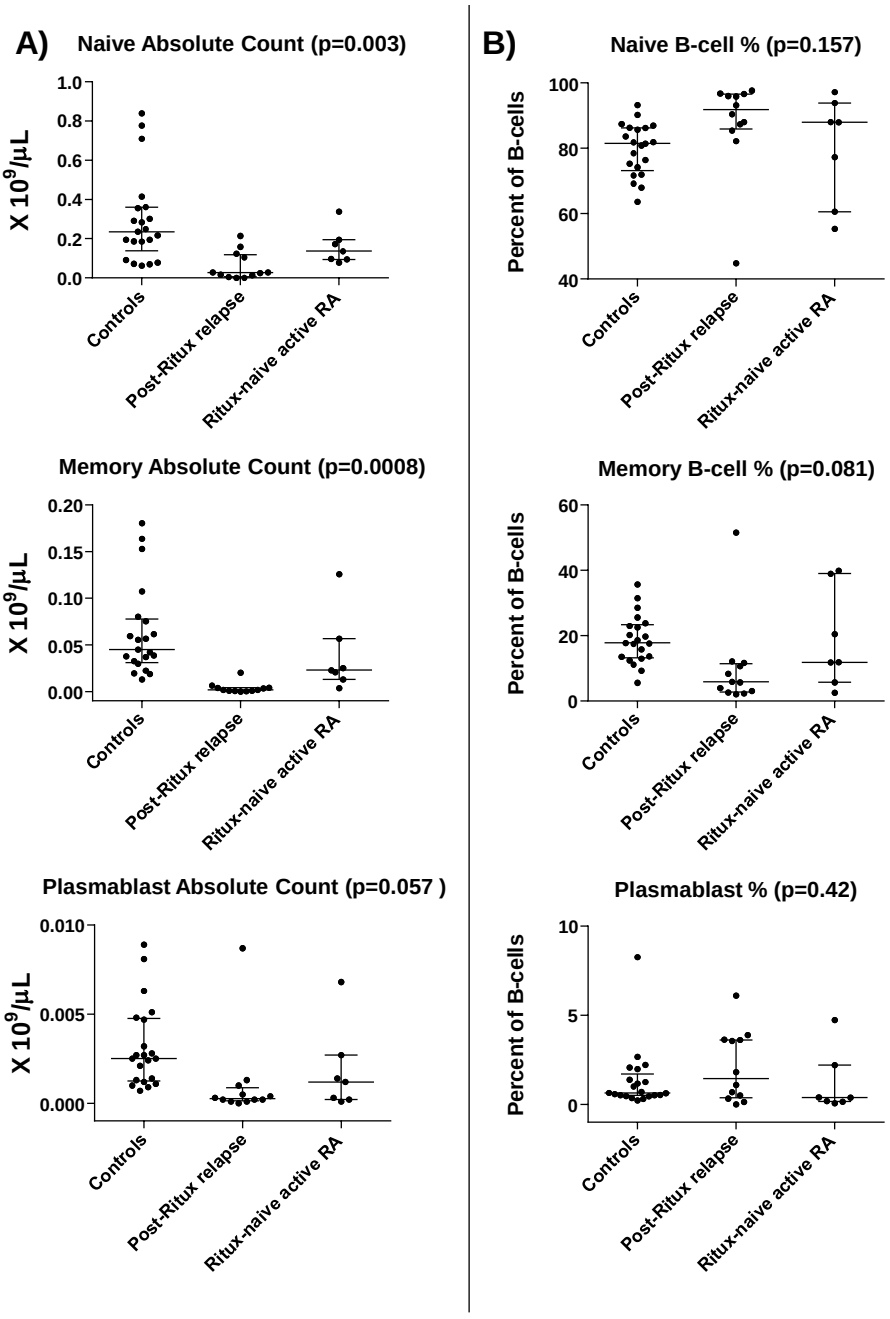

Figure 6.4-1 Proportion and absolute numbers of naïve, memory and plasmablasts in controls, active rituximab-naïve RA and patients relapsing post-rituximab

The dots represent individual patients and the bars represent median with 25th and 75th centiles. Figure B) shows naïve, memory and plasmablast subsets as a proportion of total B-cells and figure A) shows the absolute cell numbers. Each plot shows data for 3 patient groups – controls (n=21), patients relapsing post-rituximab (n=12) and active rituximab-naïve RA (n=7) from left to right.

The plasmablasts, which were the initial cells of interest based on previous work done in Leeds, had nearly identical subset distribution between the three groups. There was differential heterogeneity within the naïve B-cell subsets between the 3 groups mainly due to high proportion of IgM positive cells in relapsing patients. This is likely to be due to the presence of higher proportion of immature/transitional B-cells with high surface IgM (45) within the naïve B-cell subset in relapsing patients secondary to B-cell depletion by rituximab.

The IgM-LAIR1- memory B-cell subset was elevated in relapsing patients and the differential heterogeneity in distribution of memory B-cells among patient groups is likely to be more informative compared to naïve B-cells and plasmablasts. This heterogeneity seen in memory B-cells was not evident amongst plasmablasts. The absence of heterogeneity amongst plasmablasts could be due to convergence in phenotype when the memory B-cells differentiate into plasmablasts or that the plasmablasts are primarily derived directly from germinal centre or naïve B-cells. However the data would suggest that identification of heterogeneity in plasmablasts that correlates with the clinical status would require a different set of surface markers.

Figure 6.4-2 Distribution of subpopulations of the naïve, memory and plasmablast subsets compared between controls, rituximab-naïve RA patients with active disease and patients relapsing post-rituximab

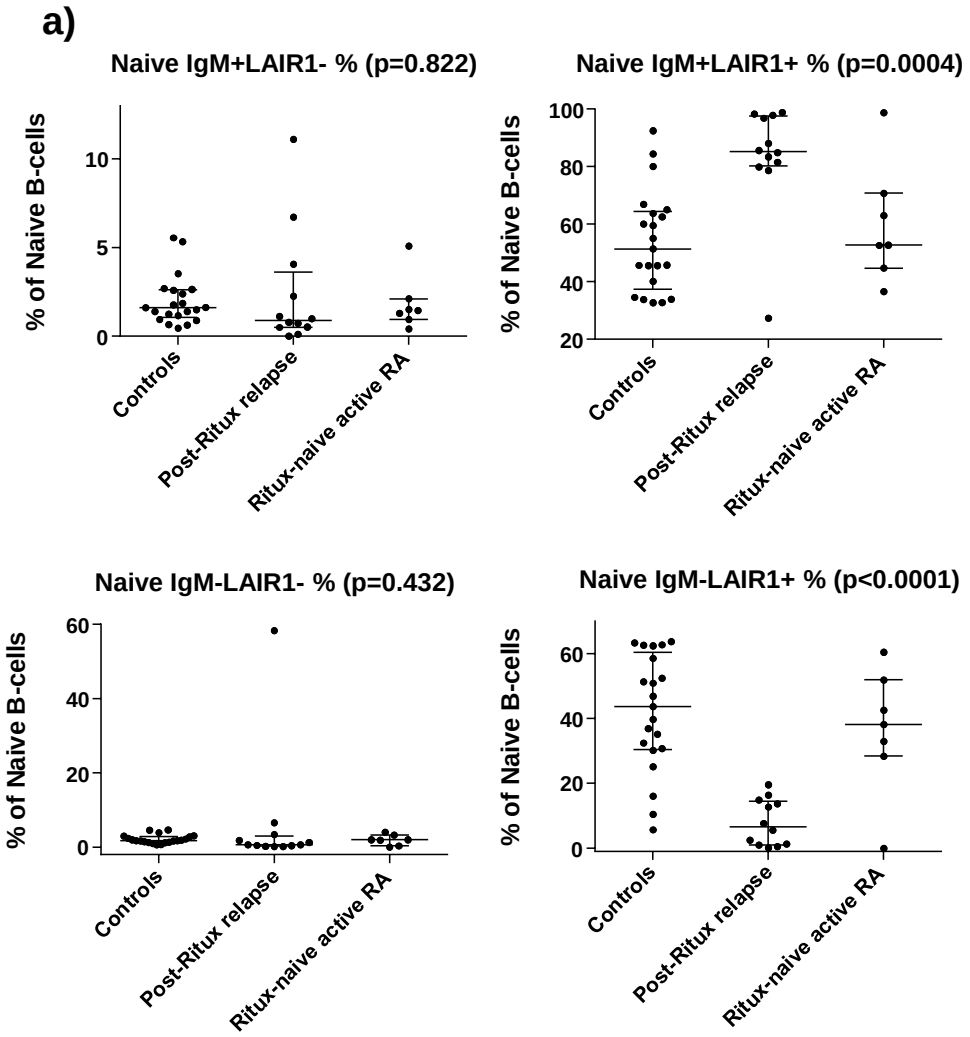

b)

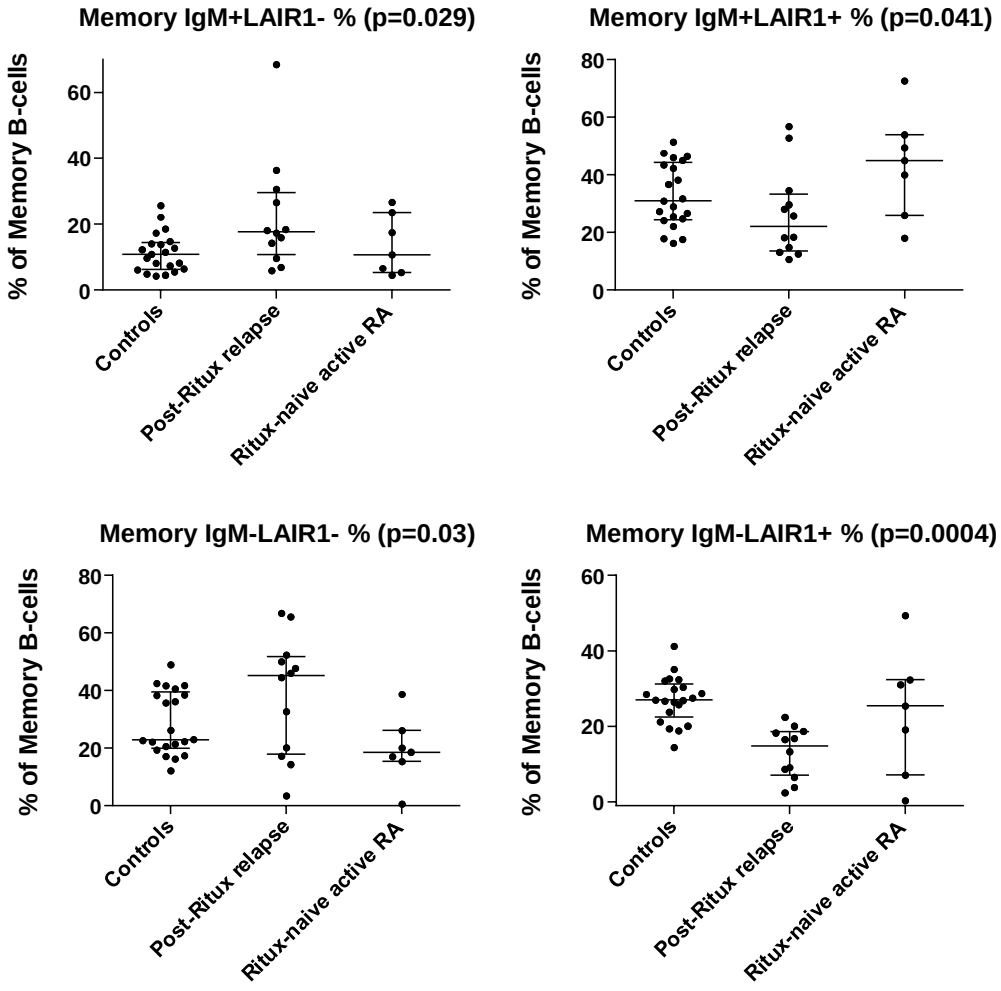
Memory IgM+LAIR1- % (p=0.029)
% of Memory B-cells
0
20
40
60
Controls
Post-Ritux relapse
Ritux-naive active RA
Memory IgM+LAIR1+ % (p=0.041)
% of Memory B-cells
0
20
40
60
80
Controls
Post-Ritux relapse
Ritux-naive active RA
Memory IgM-LAIR1- % (p=0.03)
% of Memory B-cells
0
20
40
60
80
Controls
Post-Ritux relapse
Ritux-naive active RA
Memory IgM-LAIR1+ % (p=0.0004)
% of Memory B-cells
0
20
40
60
Controls
Post-Ritux relapse
Ritux-naive active RA

c)

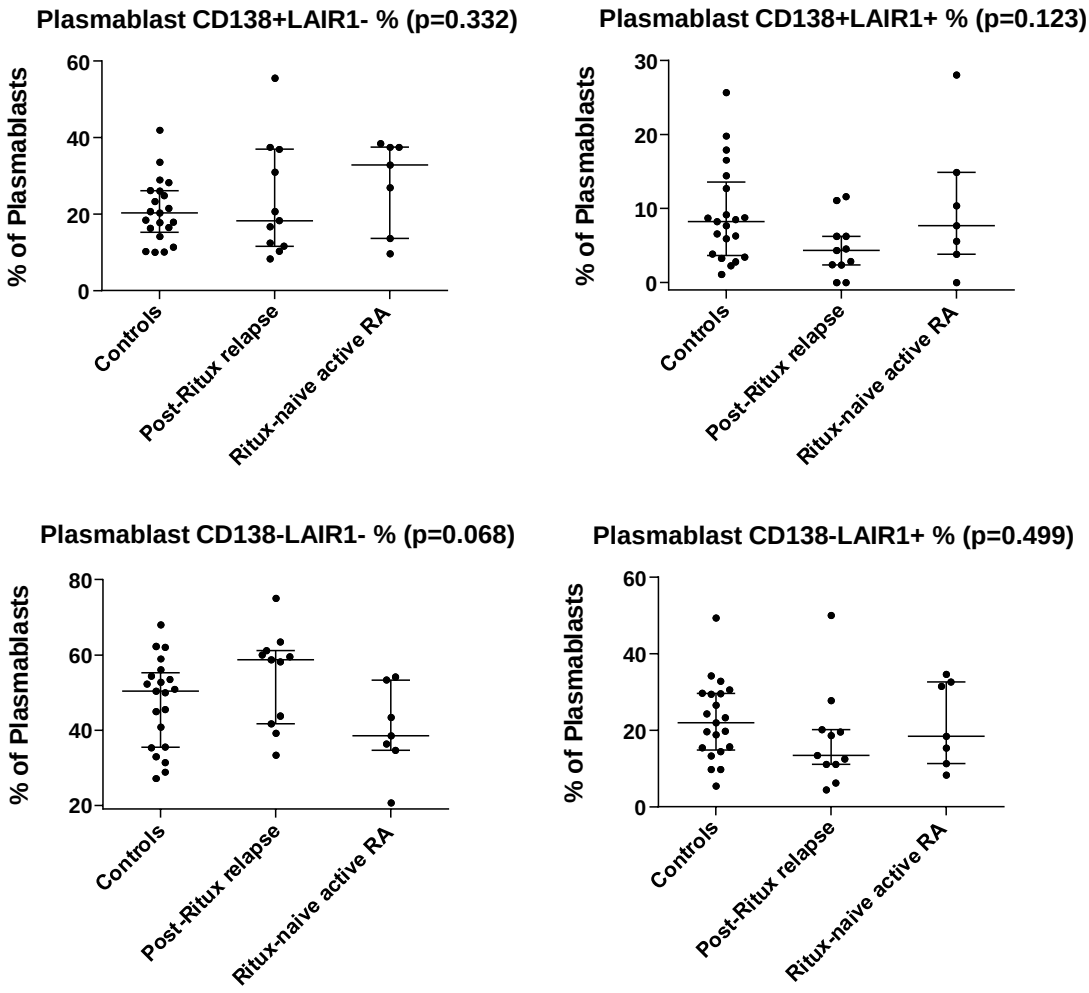

The dots represent individual patients and the bars represent median with 25th and 75th centiles. a) naïve B-cell subsets, b) memory B-cell subsets and c) plasmablast subsets. Each plot shows data for 3 patient groups – controls (n=21), patients relapsing post-rituximab (n=12) and active rituximab-naïve RA (n=7) from left to right. Only the significant p values for difference between the three groups (1 way ANOVA) are given within brackets.

When the total B-cell surface expression is examined, there is no significant difference in LAIR expression. The figure below shows the importance of classifying B-cells into naïve, memory and plasmablasts for analysing surface expression of markers. Evaluation of LAIR1 on total B-cells masks the significant difference in expression of LAIR1 on memory B-cells amongst relapsing patients. Although the lower sample numbers for rituximab naïve patients (n=7) can introduce sampling errors, the main aim for this section of the study is to identify the gross B-cell subset based on the presence of heterogeneity and identified memory B-cells as the key subset. This was confirmed subsequently with larger sample numbers and significant differences in memory B-cell subsets were demonstrated as shown in Figure 6.4-8.

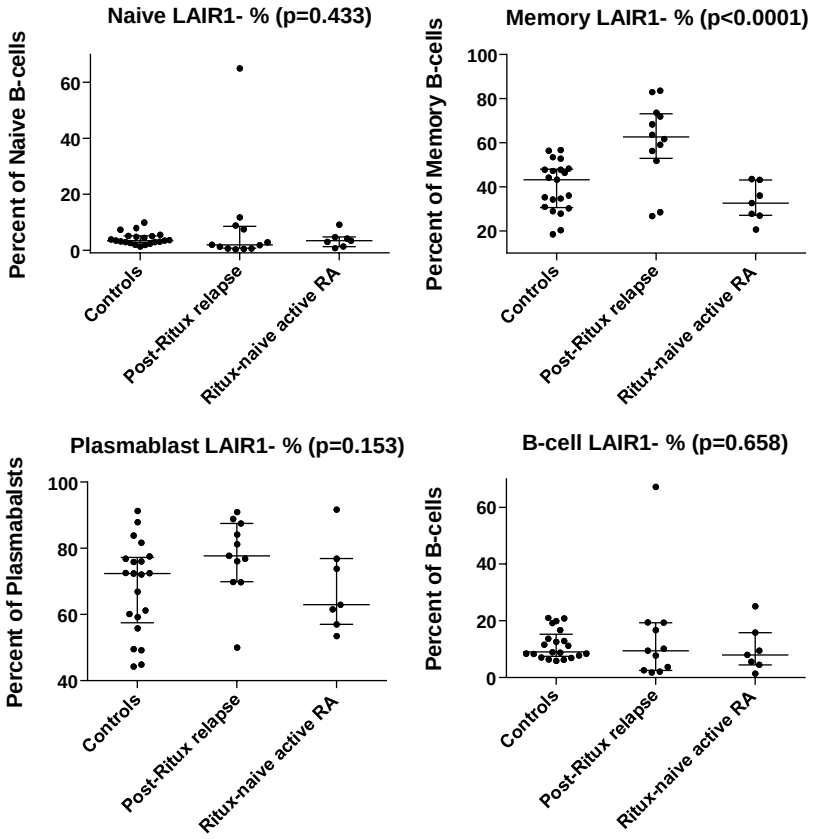

Figure 6.4-3 Proportion of LAIR1$^-$ cells within naïve, memory and plasmablast subsets and total B-cells

The dots represent individual patients and the bars represent median with 25th and 75th centiles. Each plot shows data for 3 patient groups – controls (n=21), patients relapsing post-rituximab (n=12) and active rituximab-naïve RA (n=7) from left to right. Only the significant p value (1 way ANOVA) is given within brackets.

7.1.2 Markers tested for heterogeneity within B-cell subsets

Autoreactive B-cells expanded during active disease are likely to be of an activated phenotype with downregulation of inhibitory receptors. In selected cases 34 further markers known to be expressed by B-cells with a potential role in pathogenesis were chosen initially. Markers chosen include:

- Activation markers – CD69, CD25, CD95, HLA-DR
- Co-stimulatory molecules – CD80, CD86
- Regulatory molecules – LAIR1, CD84
- Cytokine receptors – CD25, CD126
- Chemokine receptors – CD184, CD185, CD196
- Markers for stage of differentiation – CD5, CD10, CD138

Having shown that the memory B-cells exhibited greater heterogeneity and differences related to clinical state, the markers shown in Figure 6.4-4 were analysed for the presence of heterogeneity within the memory B-cell subset in 3 controls. B-cells were defined by their scatter profile and co-expression of CD19 and CD20. Memory B-cells were then identified by their CD27 positivity. The surface markers which were expressed by more than 90% of the memory B-cells and less than 10% of the memory B-cells were not considered for further analysis since they are likely to be expressed by all or none of the memory B-cells respectively. The rest of the markers were heterogeneous in distribution amongst memory B-cells, and many of these markers did not co-segregate. In other words when memory B-cells are divided into two fractions based on one marker, another marker would divide each of those fractions into two further fractions yielding four fractions in total. If two markers co-segregated, it would yield only two fractions but if they don't four fractions can be visualised. Since many of the markers did not co-segregate, this is suggestive of great heterogeneity within the memory B-cells. Among these, four markers (CD24, CD84, CD95 and LAIR1) which are non-redundant were chosen for further analysis. The number of markers that could be chosen was also restricted by the practical consideration that only 4 spare channels were available given the need for 4 channels dedicated to backbone markers.

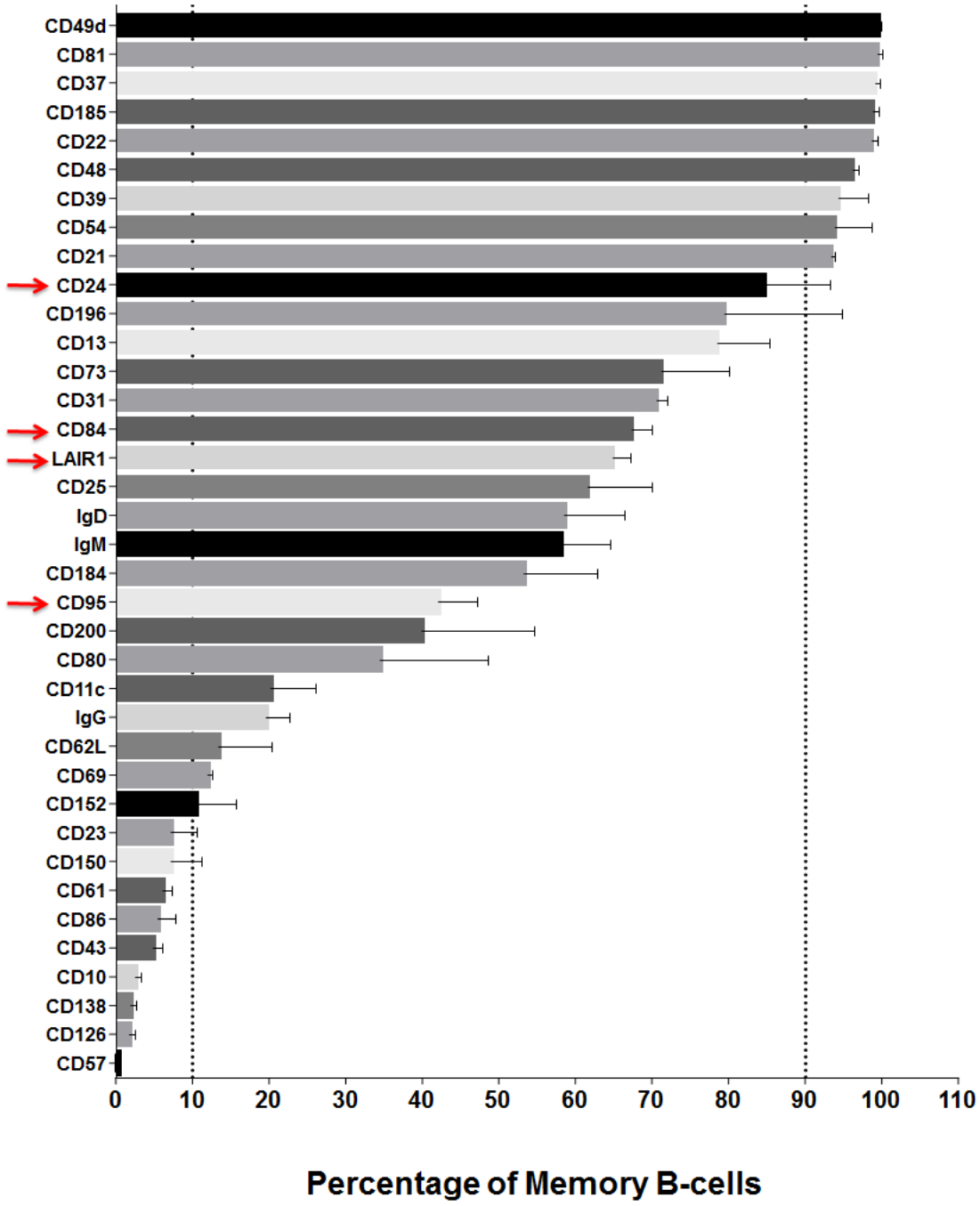

Figure 6.4-4 List of markers tested for heterogeneity within memory B-cells.

B-cells were identified based on their scatter profile and CD19 and CD20 dual positivity. Memory B-cells were then gated based on their CD27 positivity. Memory B-cell subsets defined by positivity for the marker on the left expressed as percentage of memory B-cells. Red arrows indicate markers that were heterogeneous and chosen for further analysis. Data shown from 3 healthy controls.

The presence of heterogeneity and redundancy in surface marker expression by memory B-cells is shown in the figure below.

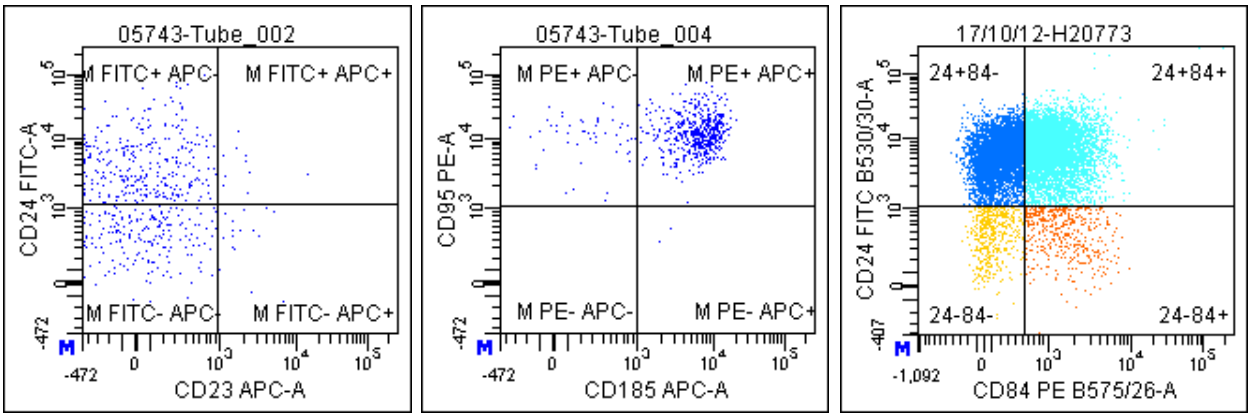

Figure 6.4-5 Examples of heterogeneous distribution of markers and redundancy

Representative flow cytometry plots of memory B-cells defined based on their scatter profile and positivity for CD19, CD20 and CD27.The first plot shows heterogeneity in expression of CD24 by memory B-cells bu they are homogeneous for CD23 expression. The second plot shows CD95 and CD185 have similar expression profile on memory B-cells and therefore only one of the markers is required making the other one redundant. The third plot shows expression pattern of non-redundant markers CD24 and CD84.

7.1.3 16 different memory B-cell subsets identifiable based on 4 surface markers

Memory B-cells are heterogeneous for expression of all these 4 markers and the expression patterns are non-overlapping. Therefore, each of the four subsets identified based on 2 markers could be subdivided into 4 further subsets as shown below. Thus it was possible to segregate the memory B-cells into 16 different fractions. For further analysis, each one of the CD24/CD84 quadrants was combined with each of the four CD95/LAIR1 quadrants as part of the gating strategy to generate the 16 subsets.

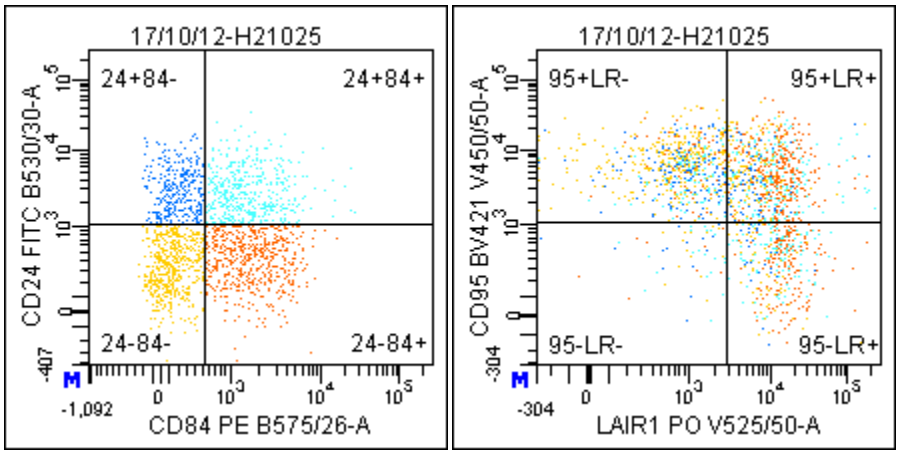

Figure 6.4-6 Non-overlapping pattern of heterogeneity of expression of CD24, CD84, CD95 and LAIR1 by memory B-cells

Representative flow cytometry plots of memory B-cells defined based on their scatter profile and positivity for CD19, CD20 and CD27. Cells from each CD24/CD84 quadrant coded with a different colour in the first plot are distributed at least in 3 different CD95/LAIR1 quadrants in the second plot. This schematically shows that the heterogeneity for these markers is non-overlapping.

7.1.4 RA patients relapsing post rituximab depletion show a skewed distribution of memory B-cell subsets compared to controls and untreated patients

22 rituximab naïve patients with active disease, 18 patients relapsing post-rituximab and 9 patients in remission with or without rituximab were analysed. 10 controls were also included. The control group consisted of 6 females (Average age 48.5) and 4 males (Average age 50). The patient group consisted of 43 females (Average age 54) and 9 males (Average age 62). Most patients who have been treated with rituximab had undergone 1-3 cycles of therapy and 1 patient with 4 cycles, 2 patients with 5 cycles and 1 patient with 9 cycles. The patients who were in remission were post-rituximab (n=3) or on anti-TNF (n=4) or anti-IL6 (n=2) therapy.

Clinical Status	No. of patients
Control	10
Active Disease Anti-CD20 Naïve	22
Relapse post Anti-CD20	18
Remission (With or without Anti-CD20)	9

No. of cycles	No. of patients
1	4
2	5
3	5
4	1
5	2
9	1

Table 6.4-1 Clinical status of patients included for memory B-cell subset characterization

The first table shows the clinical status of the patients and the number of cycles of therapy undergone by rituximab treated patients is given in the second table.

The peripheral blood memory B-cells were analysed by flow cytometry. Memory B-cells were defined based on their scatter profile and co-expression of CD19, CD20 and CD27 as shown in Figure 5.2-5. The memory B-cells were further sub-classified as shown in Figure 5.2-6. The memory subset distribution profile of the different patient groups shows the predominance of $CD24^{+}CD84^{+}CD95^{-}LAIR1^{+}$ subset in steady state and among controls which is replaced by a predominance of the reciprocal $CD24^{-}CD84^{-}CD95^{+}LAIR1^{-}$ subset during relapse.

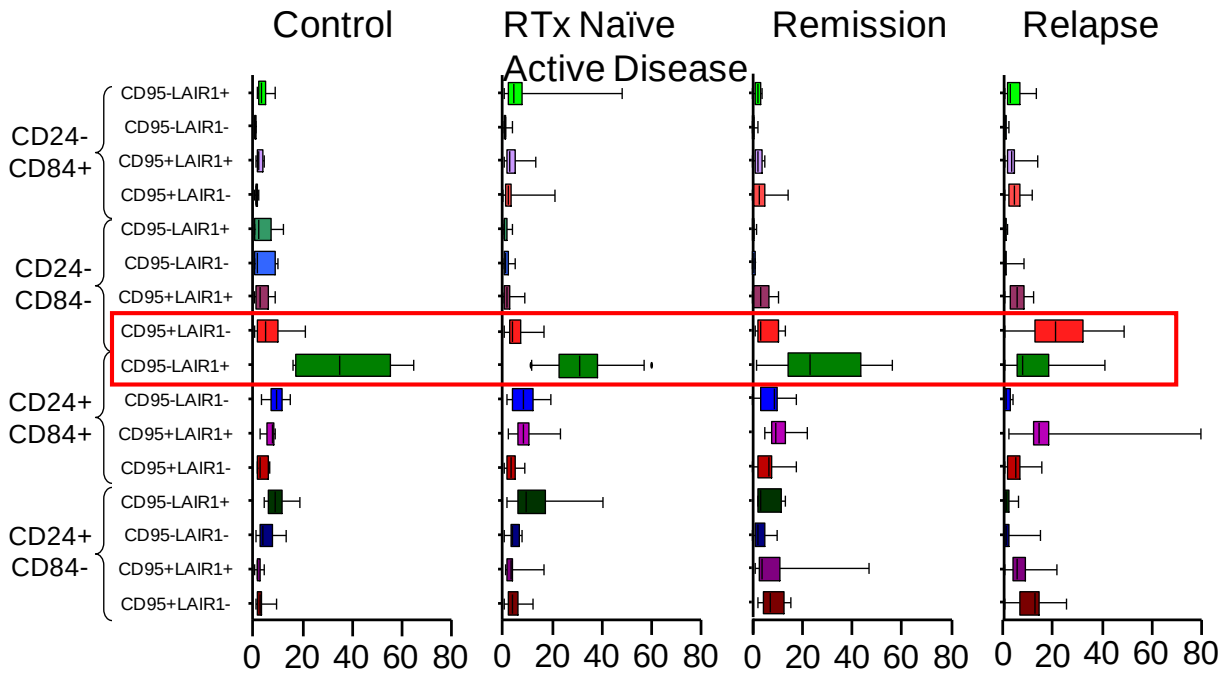

Figure 6.4-7 The distribution of the 16 memory B-cell subsets in different patient groups

The central line represents the median, boxes represent the 25th and 75th quartile and whiskers indicate the minimum and maximum data points. The subset depicted in green ($CD24^{+}CD84^{+}CD95^{-}LAIR1^{+}$) is the dominant subset in controls (n=10), active RA patients who are rituximab naïve (n=22) and remission (n=9) and the reciprocal subset depicted in red ($CD24^{-}CD84^{-}CD95^{+}LAIR1^{-}$) is dominant in patients relapsing post-rituximab (n=18). Memory B-cells were gated based on their scatter profile and $CD19^{+}CD20^{+}CD27^{+}$. The memory B-cells were then sub-divided based on the expression of CD24, CD84, CD95 and LAIR1.

7.1.5 RA patients relapsing post-rituximab therapy have a significantly higher proportion of $CD24^{-}CD84^{-}CD95^{+}LAIR1^{-}$ memory B-cells which is not solely due to direct B-cell depletion

The dataset in Table 6.4-1 was analysed for the proportion of $CD24^{-}CD84^{-}CD95^{+}LAIR1^{-}$ memory B-cell subset (defined as shown in Figure 5.2-6) for comparison between the different patient groups. The patients relapsing post-rituximab have significantly higher proportion of $CD24^{-}CD84^{-}CD95^{+}LAIR1^{-}$ memory B-cells compared to controls ($p=0.029$), active disease with no previous rituximab ($p<0.0001$) and patients in remission ($p=0.0013$).

One possible explanation for the skewed memory B-cell distribution seen in patients relapsing post-rituximab could be a direct effect of B-cell depletion irrespective of the underlying disease process. The skewed memory B-cell distribution noted in RA could be the normal reconstitution pattern if B-cells are depleted. To exclude this possibility, the memory B-cell subset distribution in 19 lymphoma patients 12–18 months since last dose of rituximab and 4 renal transplant recipients 3-6 months post campath therapy were analysed. The included patients had rituximab for B-cell neoplasms including follicular lymphoma, chronic lymphocytic leukaemia, diffuse large B-cell lymphoma or mantle cell lymphoma and all these patients were in remission at the time of sample collection. The key difference in rituximab usage is the much higher dose in lymphomas and continued immunosuppression with DMARDs like methotrexate for RA. The B-cell reconstitution in lymphoma patients treated with rituximab is delayed up to 12-18 months due to the higher dose and repeated cycles (87). Therefore the 12-18 month time point was chosen for the evaluation of these samples. Campath-1H is a therapeutic monoclonal antibody directed against CD52 which depletes B-cells and T-cells. The B-cell numbers recover earlier following campath-1H therapy compared to rituximab and return to baseline in 3 months although mainly with transitional B-cells (88). The proportion of $CD24^{-}CD84^{-}CD95^{+}LAIR1^{-}$ memory B-cells was significantly elevated in RA patients relapsing post rituximab compared to the lymphoma patients treated with rituximab ($p<0.0001$) and post-Campath therapy ($p=0.022$). The other instances of B-cell reconstitution after B-cell depletion did not exhibit this skewing of memory B-cell subsets which suggests that the skewing is specific to the RA disease process.

Therefore, the $CD24^{-}CD84^{-}CD95^{+}LAIR1^{-}$ subset is referred to as relapse associated memory B-cell subset (RAMB). The polar opposite $CD24^{+}CD84^{+}CD95^{-}LAIR1^{+}$ subset which is the dominant subset in controls is referred to as usual dominant memory B-cell subset (UDMB).

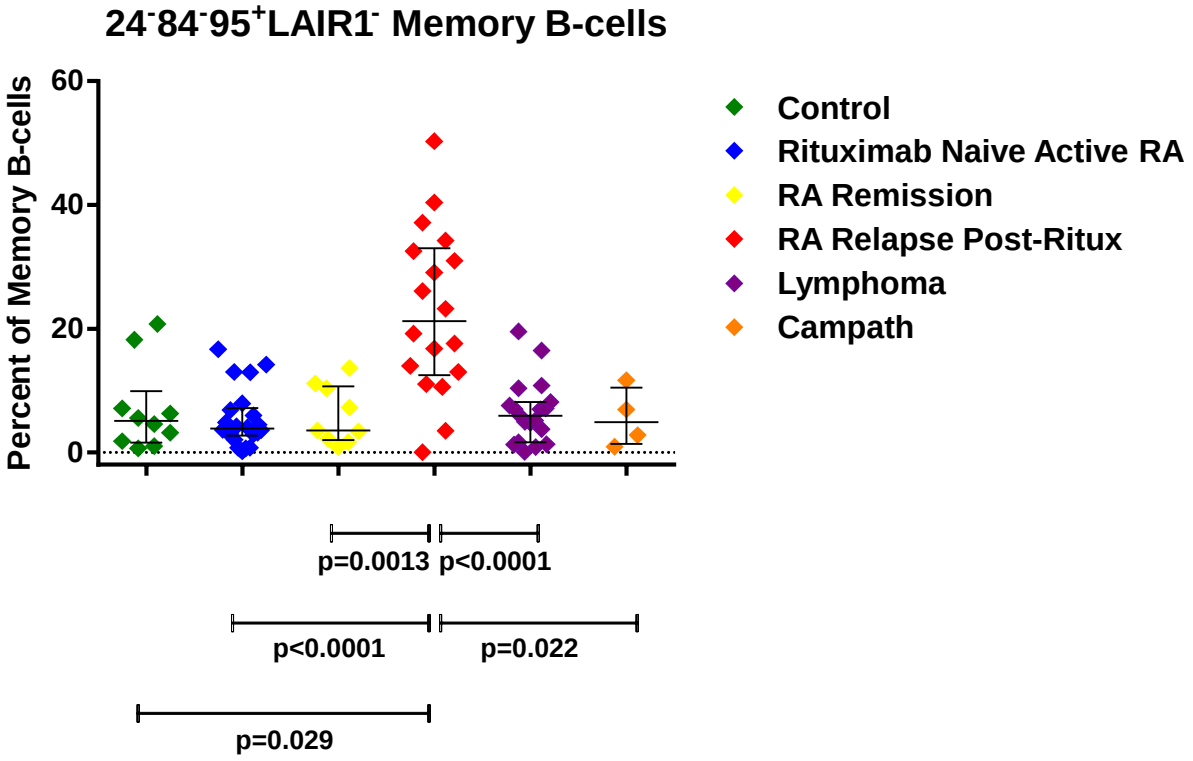

Figure 6.4-8 Proportion of $CD24^{-}CD84^{-}CD95^{+}LAIR1^{-}$ memory B-cells in different patient groups

The spots represent individual patients, the central line represents the median and the extreme lines represent 25th and 75th quartiles. P value for comparison between multiple groups was calculated by 1way ANOVA and two-tailed t test was used to compare between two groups. Controls (n=10), Rituximab naïve active disease (n=22), Remission (n=9), Relapse post-rituximab (n=18), Rituximab for Lymphoma (n=19) and Campath-1H (n=4). Memory B-cells were gated based on their scatter profile and $CD19^{+}CD20^{+}CD27^{+}$. The memory B-cells were then sub-divided based on the expression of CD24, CD84, CD95 and LAIR1.

The dataset was analysed for the difference between patient groups if the major B-cell subsets were compared. This significant difference between patient groups cannot be recapitulated by simpler subset evaluation of naïve, memory B-cells and plasmablasts (Gating strategy as described in Figure 5.2-5). There was no difference in the proportion of plasmablasts between the three groups shown ($p=0.1244$). There was a reduction in proportion of memory B-cells ($p=0.009$) and increase in proportion of transitional B-cells ($p<0.0001$) as expected due to the B-cell depletion effect of rituximab. The proportion of naïve B-cells ($p=0.029$) were reduced in patients treated with rituximab due to the higher proportion of transitional B-cells. Therefore, analysis of the proportion of major B-cell subsets did not reveal preferential increase in any of them during relapse to suggest the presence of a pathogenic subset.

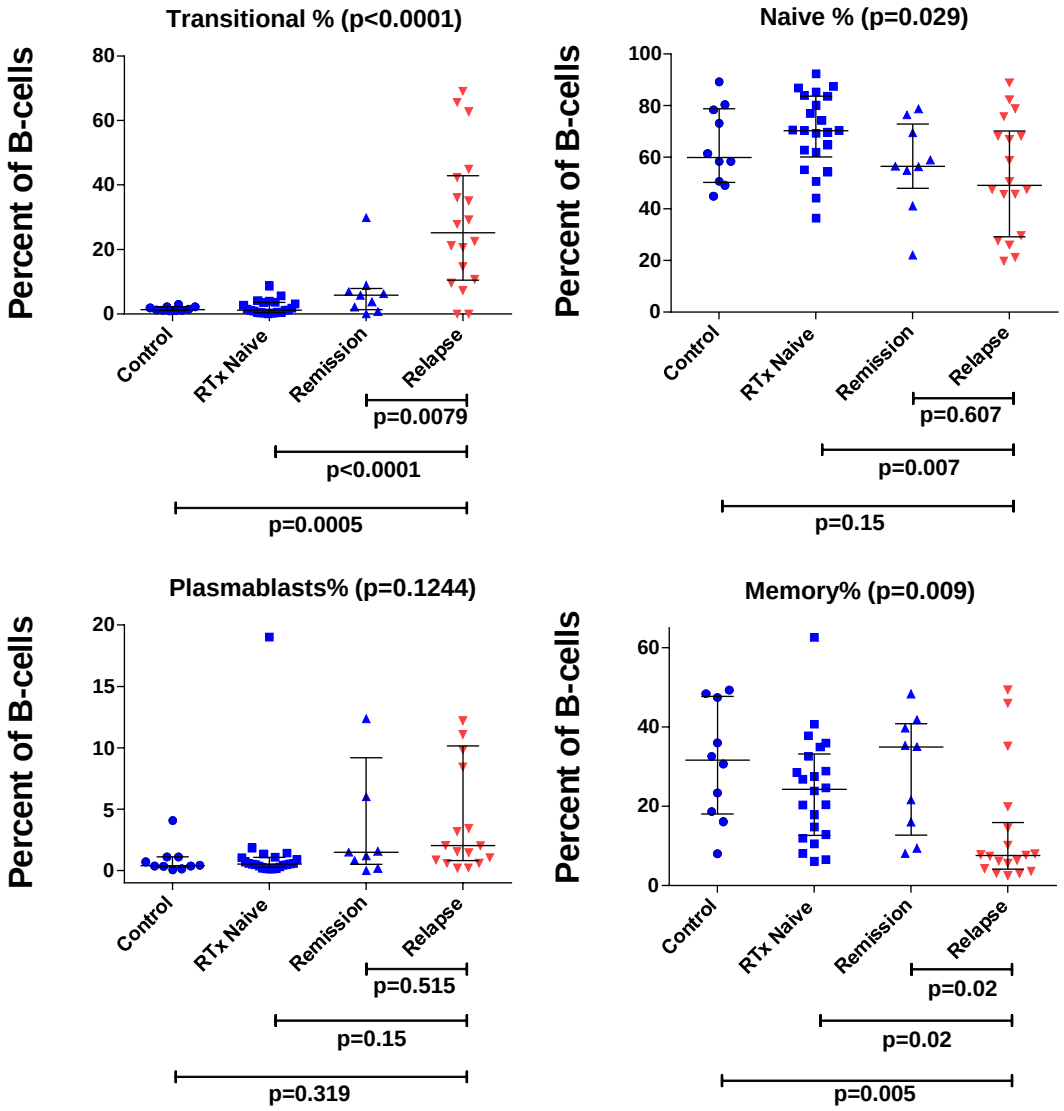

Figure 6.4-9 Proportion of Naïve, Memory, Transitional B-cells and Plasmablasts in different patient groups

The central line represents the median and the extreme lines represent the 25th and 75th quartiles. P value for comparison between multiple groups was calculated by 1way ANOVA and two-tailed t test was used to compare between two groups. Controls (n=10), Rituximab naïve active disease (n=22), Remission with biologic therapy (n=9) and Relapse post-rituximab (n=18). The proportion of memory (p=0.009) and naïve B-cells (p=0.029) were significantly reduced whereas the transitional B-cells (p<0.0001) was significantly elevated in patients relapsing post-rituximab directly due to the B-cell depletion. There was no difference in proportion of plasmablasts between patient groups (p=0.124). B-cells were classified into the subsets shown as per gating strategy described in Figure 5.2-5.

7.1.6 Skewing of the memory B-cell subset distribution is not appreciable by examining the absolute numbers due to the overall reduction in B-cell numbers due to rituximab therapy

Absolute count is a better marker of expansion of cell populations than percentages since percentage can be skewed by changes in the other subsets. However, patients who have been treated with rituximab tend to exhibit lower numbers of B-lineage cells for two to three years due to the delay in reconstitution. Therefore, evaluating the absolute numbers of the different subsets will show a universal reduction of all subsets in rituximab treated patients as shown below. Therefore, the relative proportion of the various subsets is a better index to identify potential pathogenic subsets in the clinical situations following B-cell depletion.

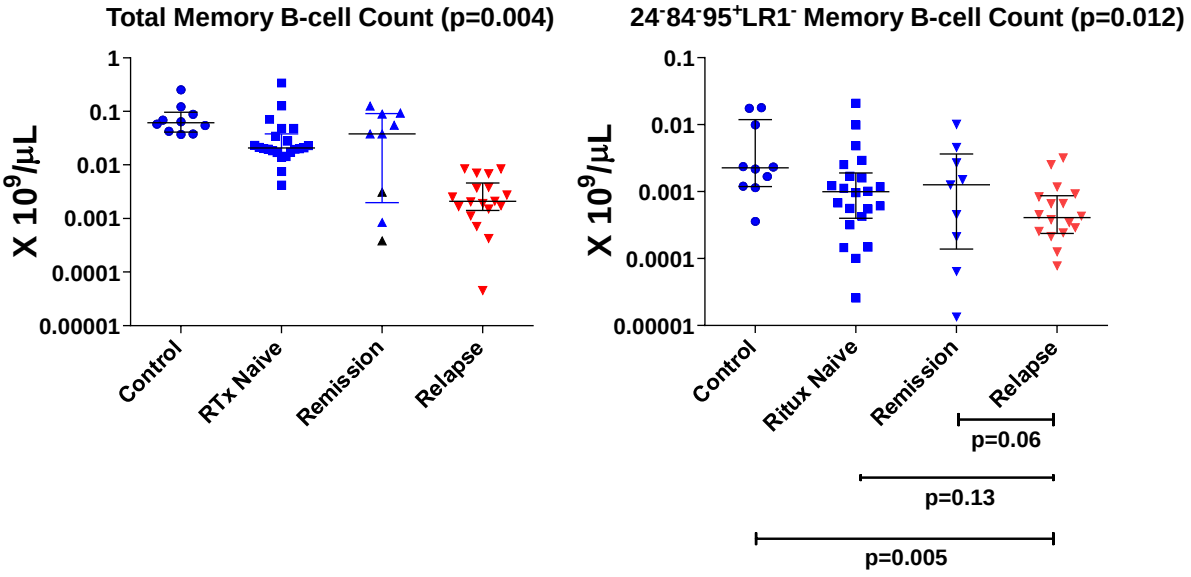

Figure 6.4-10 Absolute numbers of relapse associated memory B-cells and total B-cells

The spots represent individual patients, the central line is the median and the extreme lines represent 25th and 75th quartiles. The p-value (1way ANOVA) for comparison between 3 groups is given at the top and the 't test' value for comparison between individual groups at the bottom. The cell counts are shown on a logarithmic scale. Controls (n=10), Rituximab naïve active disease (n=22), Remission (n=9) and Relapse post-rituximab (n=18).

7.1.7 Memory B-cell subsets during remission following rituximab do not exhibit the skewing of their subset distribution like relapsing patients

The review of patients following rituximab therapy is set up such that they have an open clinic appointment and contact the clinic for review only when the disease flares. Therefore, it is difficult to obtain samples from patients who are in remission and the initial dataset contained only 3 patients in remission post rituximab. To assess in more detail whether the relapse-associated memory B-cell subset is different in patients who are relapsing or in remission post rituximab, samples were collected if the patients had a clinic visit after 3 months of last dose. In patients who were not due for clinical review, forms were given for a blood sample to be taken 6 months after the last dose. The rituximab patient registry was scanned and patients who had not had repeat therapy or presented to the clinic for more than 6 months were identified and request forms were posted to those patients for sample collection. Samples from a total of 44 RA patients were collected and analysed.

Out of the 44 patients, 7 showed total or near-total absence of memory B-cells due to delay in reconstitution or earlier sampling and therefore were excluded. The samples were collected at 5 months or later from all the 37 patients. Clinical notes from these patients were reviewed to subdivide the patients into 2 groups – relapse and remission. 24 patients had relapse of RA inflammatory symptoms around the time of the sample. The clinical data from the remaining 13 patients is shown in the table below.

Table 6.4-2 Clinical details and memory B-cell subsets in patients with no definitive evidence of RA flare-up

24-84-95+LR1- and 24+84+95-LR1+ memory B-cells (defined as shown in Figure 5.2-6) are expressed as a percentage of memory B-cells in 13 patients. The clinical details available for the patients at the time of sampling are provided in the last column. * denotes patients who were in remission with no intercurrent inflammatory or infective illness.

Patient	$24^{+}84^{+}$ $95^{-}LR1^{+}$ %	$24^{-}84^{-}$ $95^{+}LR1^{-}$ %	Clinical Scenario
H20269	22.5	4.9	L Knee effusion ?mechanical, skin rash - ?folliculitis
*****H20563	3.4	41.5	Severe flare-up within 2 months of sample
H20978	8.8	15.6	L knee injected with depomedrone for ruptured baker cyst 5 months before sample
*****H21746	30.4	2.2	VAS 10, DAS28-1.67, Remission
*****H21953	30.2	5.0	Clinically mild flare when reviewed a month later.
*****H24369	24.3	14.7	EMS 0. Vas - 10. Remission
H25421	0.0	28.6	Multiple COPD exacerbations
*H26453	12.9	12.9	In remission 6 weeks prior to sample
*****H26541	16.7	11.1	EMS-10mins, VAS-40, No tender/swollen joints. CRP-8. Prev 2 doses - half dose. So, premptive next dose
H26684	0.0	65.2	Known MGUS, Quantiferon positive TB treated 9 months ago
H301	3.4	25.2	Trochanteric bursitis. Injected with steroids
H552	9.4	21.9	3 months prior to sample - EMS 30mins, cervical pain.
H2770	6.5	16.9	Well 3 months prior to and severe flare up 6 months after sample. Unclear how long symptomatic. Prev Ca bowel. Ileorectal anastomosis. 2 A&E visits with chest infection

The above 13 patients could be considered in remission since there was no definitive signs or symptoms of RA flare up at the time of sampling. However on reviewing the clinical picture in more detail, the majority of the patients had some infective or inflammatory process such as chest infections or joint symptoms, which were not necessarily thought to be due to RA. Nevertheless, these symptoms required treatment with antibiotics or steroids respectively. When the patients with infective or inflammatory processes before sampling were excluded there were only 6 patients who were in remission at the time of sampling. Five out of the six patients had a lower proportion of $24^{-}84^{-}95^{+}LR1^{-}$ and a higher proportion of $24^{+}84^{+}95^{-}LR1^{+}$ memory B-cells similar to controls or pre-rituximab state. The remaining patient who did show the skewed phenotype presented with severe clinical symptoms within 2 months of the sampling. Therefore, skewing in the proportion of memory B-cell subsets during reconstitution is likely to indicate ongoing or recent inflammatory activity. While in some cases this may not be due to RA, it could be argued that detection of this skewing should initiate close follow up to monitor for signs of relapse.

7.1.8 The relapse associated memory B-cell subset is predominantly class-switched in RA patients and controls

ACPA measured in the clinical setting and known to be specific for RA is of the IgG isotype. Therefore the immunoglobulin isotype of relapse-associated memory B-cell subset was analysed for evidence of class-switching. Surface staining with antibodies against IgM and IgD was performed and the16 memory B-cell subsets were analysed individually for class-switching. The majority of the relapse-associated memory B-cell subset was class-switched in both the RA patients and controls. In contrast, the usual dominant memory B-cell subset was predominantly constituted by IgM+ memory B-cells. However, there was a lower proportion of class-switched memory B-cells within the usual dominant memory B-cell subset in RA patients compared to controls ($p<0.0001$). There was a lower proportion of class-switched memory B-cells in the relapse-associated subset in RA patients compared to controls, but this did not achieve statistical significance ($p=0.064$). In case of controls none of them had less than 75% class-switched memory B-cells within the relapse-associated subset.

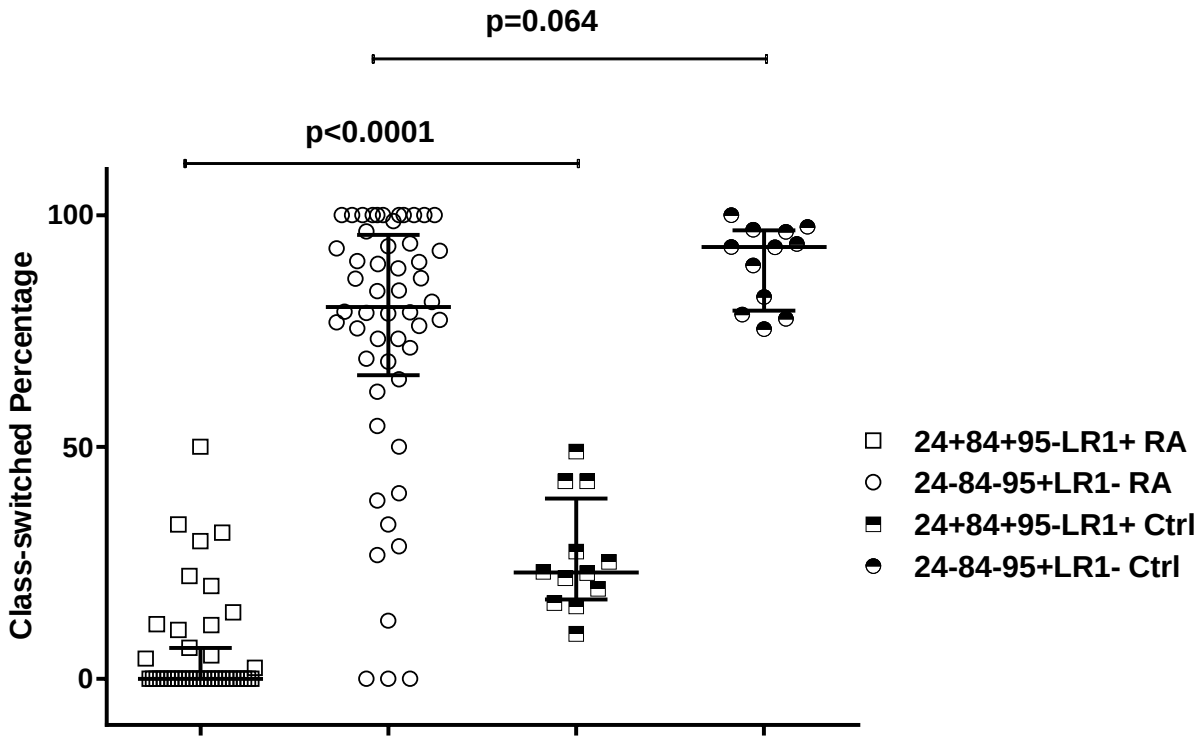

Figure 6.4-11 Proportion of class-switched cells within memory B-cell subsets in RA and controls

The proportion of class-switched memory B-cells within the two polar opposite memory B-cell subsets is shown for RA patients and healthy controls. The central line is the median and extreme lines represent 25th to 75th centiles. P-values from unpaired t test shown.

7.1.9 The relapse-associated memory B-cell subset surface phenotype in patients relapsing post-rituximab is reminiscent of plasmablasts

The surface expression profile for the surface markers used to classify memory B-cells were examined on plasmablasts since plasmablasts have been shown to be predictive of clinical response in RA. Plasmablasts generated in vitro from peripheral blood B-cells of a control (as described in Figure 5.4-1) and peripheral blood plasmablasts from a RA patient relapsing post-rituximab were evaluated. Plasmablasts were defined based on their scatter profile and $CD19^{+}CD20^{-}CD27^{Hi}CD38^{Hi}$. The surface expression pattern of CD24, CD84, CD95 and LAIR1 by in vitro generated plasmablasts and peripheral blood plasmablasts is similar to the relapse-associated memory B-cell subset. The surface expression profile of the relapse-associated subset is different to plasmablasts in terms of CD20 and CD38.

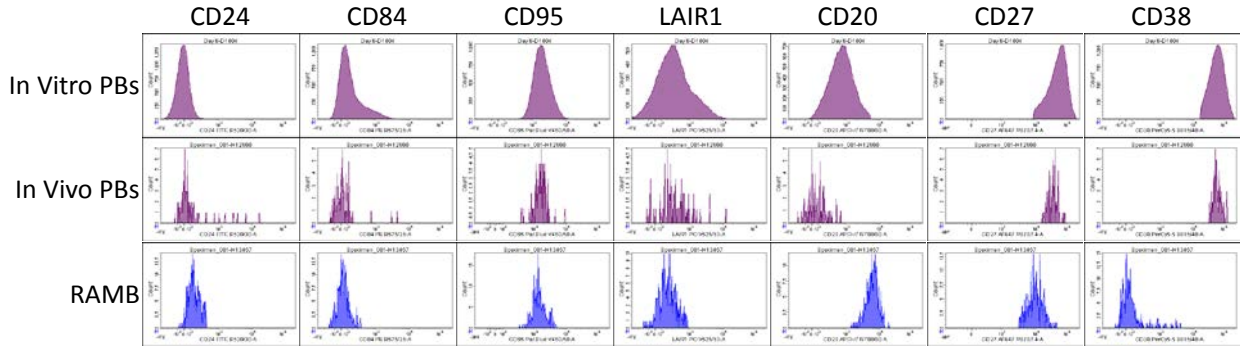

Figure 6.4-12 Comparison of relapse-associated memory B-cell subset with plasmablasts

The top two rows show the surface expression of the markers specified by plasmablasts generated by in vitro differentiation of normal B-cells and peripheral blood RA plasmablasts. Plasmablasts were defined based on their scatter profile and $CD19^{+}CD20^{-}CD27^{Hi}CD38^{Hi}$. The bottom row shows peripheral blood CD24-CD84-CD95+LAIR1- memory B-cells from a RA patient relapsing post-rituximab.

7.2 Summary and discussion

Memory B-cells defined as CD27 positive are a very heterogeneous population and can be sub-divided into 16 different subsets based on four carefully selected surface markers. Whilst all these subsets are unlikely to be functionally distinct, certain subsets might be. Once a subset is identified to be functionally distinct, in this case autoreactive, it could be further analysed. It can be argued that whether subsets need to be merged or a subset needs further subclassification depends on its sensitivity and specificity. Alternatively providing a mechanistic understanding of the factors governing phenotypic states and their relationship to transient or stable cell states, would provide a rationale for subset linkage or fractionation.

Further phenotypic subclassification would be possible by using additional markers which is mainly limited by available technology. Even though additional markers can be used by flow cytometry with extra lasers and additional channels available for the violet laser in particular (Brilliant Violet fluorochromes), the data analysis becomes complicated. Additional channels also add to the complexity due to compensation issues. The recent advance of mass cytometry (CyTOF) enables assessment in theory of up to 100 markers on a single cell with minimal signal overlap (89). The downstream analysis depends on complex clustering algorithms to deal with the vast amounts of multidimensional data generated (90). Furthermore the destructive nature of this technology means that reduction to a more restricted flow cytometry panel would ultimately be necessary to allow functional cellular analysis, gene expression profiling and sequencing the immunoglobulin gene to identify the antigen specificity.

On analysing the distribution of memory B-cell subsets in different patient groups, the RA patients relapsing post-rituximab showed a skewed distribution. A population of memory B-cells was identified which is of higher proportion in patients relapsing post-rituximab compared to controls, patients in remission and patients with active disease whose B-cells have never been depleted. The shift in proportions of cells with relapse could be due to two possible reasons – an increase in number of pro-inflammatory cells or decrease in number of regulatory cells. However, the clinical response to B-cell depletion makes the latter possibility less likely. The increased proportion of this subset is not reflected in the absolute cell numbers due to the general reduction in B-cells including memory B-cells following B-cell depletion by rituximab. The polar opposite CD24+CD84+CD95+LAIR1- memory B-cell subset is the dominant subset in

all other patient groups except during RA relapse post-rituximab when CD24-CD84-CD95+ LAIR1- subset is dominant. This skewing in the distribution of memory B-cells is unlikely to be a direct effect of depleting B-cells since it is not seen in other instances of therapeutic B-cell depletion for non-autoimmune conditions such as B-cell lymphomas treated with rituximab or campath therapy prior to renal transplantation. Therefore, this memory B-cell subset is likely to be linked to disease pathogenesis in RA and may contain the autoreactive B-cells.

The levels of the relapse associated subset can be elevated in some patients who have not had any evidence for clinical relapse of RA. However, these RA patients had other intercurrent infective or inflammatory processes requiring treatment with steroids or antibiotics post-rituximab and prior to sampling. This suggests that the increase in the memory B-cell subset is quite sensitive to inflammatory processes and may be not be a specific marker for RA disease process. There could also be a potential selection bias, since patients who are well during remission do not have the need to attend clinics and did not have any blood sampling. There was less than 50% response rate from patients invited by post to have samples taken at 6 months. Overall patients are more likely to respond if they had to seek medical help for flare up of RA or other reasons. This could have led to the pre-selection of patients who are relapsing or had other intercurrent illnesses. The RA patients are more prone to infections due to various factors (91) and also continue on immunosuppression post-rituximab compared to lymphoma patients in remission. This helps explain the difference in subset distribution pattern seen during remission in lymphoma and RA.

The lower proportion of class-switched memory B-cells noted in RA patients compared to controls could simply be the effect of B-cell depletion and the fact that reconstituted B-cells have not had sufficient antigen exposure to generate enough class-switched memory B-cells. However, it is interesting to note that the class-switched memory B-cells segregate to the 24-84-95+LR1-subset and non-class-switched cells segregate to the polar opposite 24+84+95-LR1+ subset in both controls and patients. The lack of surface IgM and IgD seen in the relapse associated subset could also represent B-cells with reduced levels of surface immunoglobulins prior to plasmablast differentiation. Although it raises the suspicion of lymphoma, such surface immunoglobulin negative B-cells have also been identified in lymph nodes with chronic inflammatory processes (92).

Higher plasmablast number at baseline (86) and persistence of plasmablasts(25) in the early stages following B-cell depletion predicts poor response to rituximab. The surface expression of the four markers namely CD24, CD84, CD95 and LAIR1 by the relapse-associated memory B-cell subset is similar to plasmablasts. Therefore, it is possible that this subset could be precursors of plasmablasts or on their way to plasmablast differentiation and have functional similarities to plasmablasts in terms of RA pathogenesis. Therefore, it is likely that this subset contains pathogenic cells.

To understand the functional role of this subset, it is essential to identify its antigen specificity particularly for citrullinated proteins. If antigen-specific (autoreactive) cells can be identified by an independent technique other than surface phenotyping, then those cells could be phenotyped using these markers to validate the technique. If this population does not contain autoreactive B-cells then its other functional characteristics could be important to pathogenesis, and the relationship of this phenotype to gene expression and Immunoglobulin gene somatic mutation status needs to be established.

8 Third Results Chapter: Functional characterisation of RA relapse associated B-cells

Altered B-cell subsets have been described in autoimmune disorders and attempts have been made to identify subsets that correlate with the clinical status. The results from previous chapter identified $CD24^{-}CD84^{-}CD95^{+}LAIR1^{-}$ memory B-cells were increased in proportion prior to relapse following rituximab therapy. This relapse associated subset has not been described in the literature before. These cells are likely to be involved in RA pathogenesis but also could be an epiphenomenon. To understand the role of these cells, the functional attributes of these cells need to be defined. The memory B-cell subsets of interest were flow sorted for further functional analysis and plasmablasts were also isolated at the same time to detect presence of ACPA secreting plasmablasts in the peripheral circulation. ACPA secretion was not detectable by ELISpot (Figure 8.1-1) which is likely to be due to technical issues with ELISpot but lack of ACPA secreting plasmablasts could not be confirmed due to lack of a positive control for ACPA secretion. The naïve B-cells isolated during the same flow-sort were differentiated to antibody secreting cells in vitro and tested for ACPA secretion by ELISpot. The naïve B-cells have class-switched during the in vitro differentiation as evidenced by the secretion of IgG but ACPA secretion was not detectable (Figure 8.1-2). One of the functional attributes of the B-cells is their antigen specificity. Since detection of citrullinated protein specific B-cells was quite challenging, other attributes were sought.

The functional role of B-cells could be inferred from the knowledge of the stage of B-cell life cycle the cell belongs to. The expression pattern of the four markers used to classify the memory B-cells resembled plasmablasts as shown previously (Figure 6.4-12). Therefore, it was hypothesized that this particular surface expression pattern was acquired following B-cell stimulation prior to plasmablast differentiation. Due to the difficulties in tracking human cell populations in vivo to determine the stage at which this phenotype is acquired, in vitro methods were sought. One such recently described protocol (60)which is able to generate plasmablasts and plasma cells from B-cells was utilized. The memory B-cells are heterogeneous in peripheral blood with them being predominantly CD24, CD84 and LAIR1 positive and CD95 negative. On stimulation, CD24 surface expression was lost and CD95 was gained quite early within the first

3 days. CD84 and LAIR1 expression were lost later closer to plasmablast stage. The closest stage in vitro to the relapse associated $CD24^{-}CD84^{-}CD95^{+}LAIR1^{-}$ memory B-cell subset was the activated B-cell stage (ABC) between days 3 to 4. Gene expression analysis at different stages of in vitro B-cell differentiation was performed by Cocco et al (60) and the previously published data was reanalysed. It was hypothesized that the relapse associated subset is directly involved in RA pathogenesis via generation of proinflammatory mediators. Therefore, the group of genes that increase in expression levels during the ABC stage were assessed for the enrichment of proinflammatory mediators by gene ontology analysis. The analysis revealed 60 genes that are involved in immune system processes were enriched during the ABC stage. This included mediators directly related to RA pathogenesis such as TNFα, lymphotoxin, AIF1 and MMP7 and multiple chemokines such as CXCL9, CXCL10, CCL2, CCL3, CCL17 and CCL22 (Figure 8.3-3 and Figure 8.3-4). To evaluate for the presence of protein expression accompanying transcriptional activity, TNFα was chosen which is well known to have a direct role in RA pathogenesis. Spontaneous secretion of TNFα on day 3 of in vitro differentiation by normal B-cells was demonstrable by ELISpot (Figure 8.3-6). The secretion of the other inflammatory mediators could be confirmed in future work by multiplex luminex assay of the supernatants or ELISpot. This supports the hypothesis that the relapse associated B-cells are involved in RA pathogenesis. However, TNF secretion by sorted $CD24^{-}CD84^{-}CD95^{+}LAIR1^{-}$ memory B-cells was not demonstrable by ELISpot (Figure 8.3-7). There were technical issues with the ELISpot assay due to low cell numbers and poor viability of the cells following the flow sorting. These issues can potentially be overcome by pooling samples from multiple patients to overcome the lower cell numbers and dialysing the antibodies used for flow sorting to exclude azide which can reduce cell viability. The secretion of pro-inflammatory mediators by relapse associated memory B-cells can also be evaluated by multiplex luminex assay of the supernatants and single cell gene expression analysis.

There remains the possibility that the relapse associated subset seen in relapsing RA patients is unrelated to the in vitro day 3 ABC. Irrespective of the ABC being similar to the relapse associated subset, it was an interesting observation that B-cells secrete proinflammatory mediators during the differentiation of B-cells to plasmablasts. Studies in the past have demonstrated cytokine secretion by B-cells with highly potent stimuli but the dataset generated by Cocco et al. (60) used an activation protocol mimicking a physiological stimulus capable of generating long-lived PCs. Cytokine secretion has mostly been demonstrated in the past from

culture supernatants and a phenotype for B-cells secreting the inflammatory mediators has not been described. If a surface marker can be identified specific for the in vitro ABC stage, this can be assessed on in vivo B-cells to be considered as a biomarker. The previously published gene expression data was re-analysed for surface molecules that are expressed only on activation and lost on PC differentiation corresponding to the ABC stage. Two such markers were chosen – CD30 and TIM3 (Figure 8.3-8). CD30 has been well studied in B-cell neoplasms and is known to be induced on B-cell activation. The role of TIM3 in B-lineage cells has not been studied before which were additional reasons for choosing these two markers.

The protein expression of the surface markers identified by the gene expression data was verified during in vitro differentiation of B-cells by flow cytometry. Surface expression of TIM3 was gained by ABC on day 3 of in vitro differentiation and lost on day 10 (Figure 8.3-9). TIM3 surface expression can be induced by CD40L and TLR stimuli as shown in Figure 8.3-10. The surface expression of CD30 followed a similar time course with earlier loss of expression by day 6 on differentiation to plasmablasts (Figure 8.3-11) in line with the gene expression data (Figure 8.3-8). To exclude non-specific binding as a cause for the detected staining by flow cytometry isotype controls were evaluated which confirmed the staining to be specific for the tested anti-TIM3 and anti-CD30 antibodies Figure 8.3-12. The expression of TIM3 could be further confirmed by real-time PCR for TIM3 and alternative techniques for protein detection such as western blot at different time points during in vitro B-cell differentiation. Alternatively, cell lines representing different stages of B-cell differentiation could also be used. To ensure that the detection of TIM3 is not an in vitro artefact, TIM3 expression should be demonstrable on in vivo B-lineage cells as well.

TIM3 has been extensively studied in T-cells and monocytes and is only expressed by a very low proportion of T-cells in peripheral blood. TIM3 is expressed on activation of T-cells. Therefore, different clinical situations such as an active inflammatory process or B-cells from lymphoid organs and sites which are likely to contain actively differentiating B-cells were evaluated. TIM3 was not detectable on surface of B-cells from healthy controls, patients with inflammatory disorders or lymph nodes, bone marrow and synovium (Figure 8.3-13 and Figure 8.3-14). Low levels of TIM3 expression was observed on B-cells from a spleen sample which was significantly weaker than the levels expressed in vivo. Since various B-cell neoplasms represent different stages of B-cell life cycle and TIM3 expression was transient in

vitro during B-cell differentiation, expression of TIM3 by B-cell neoplasms was assessed. Bone marrow samples from patients with follicular lymphoma, chronic lymphocytic leukaemia, mantle cell lymphoma, marginal zone lymphoma and plasma cell neoplasia were assessed and TIM3 expression was detectable only in patients with marginal zone lymphoma (Figure 8.3-15).

Since TIM3 has not been studied in B-cells so far, the role of TIM3 in B-cell biology and whether the detected TIM3 is functional is not known. Studying the effect of the ligand for TIM3 on B-cells would throw more light on its role and also prove the presence of functional TIM3. Therefore, the effect of TIM3 ligand galectin 9 was evaluated in vitro during B-cell differentiation. Galectin 9 adversely affected viability of the differentiating B-cells which was not blocked by anti-galectin 9 or anti-TIM3 antibodies. The TIM3 agonistic and blocking antibodies did not have any effect on B-cell differentiation or cell viability. Therefore, the role of TIM3 in B-cell biology remains unclear and the noted effect of Galectin 9 on cell viability is not likely to be mediated via TIM3. Interestingly, there is on-going debate in the literature whether galectin 9 is a ligand for TIM3 (93). Further functional evaluation of TIM3 would require obtaining galectin 9 from different sources for testing after further confirmation of TIM3 expression in vitro with western blot which will be the subject of a future project.

It is not known whether the relapse associated $CD24^{-}CD84^{-}CD95^{+}LAIR1^{-}$ memory B-cell subset is a static or dynamic population. Sequential evaluation the proportion of this subset during an immune response is likely to provide vital information on its functional role. Since the onset of immune response is not predictable an alternative instance where the immune response occurs in a controlled fashion was sought. The annual seasonal influenza vaccination offered to health care professionals provided one such opportunity. This revealed that in more than half of the volunteers the proportion of the $CD24^{-}CD84^{-}CD95^{+}LAIR1^{-}$ subset increased in a day following the vaccination without an accompanying increase in their absolute count. In most of the donors that showed this pattern, the absolute count of the polar opposite $CD24^{+}CD84^{+}CD95^{-}LAIR1^{+}$ subset decreased. Although it could be hypothesized that the increase in proportion of $CD24^{-}CD84^{-}CD95^{+}LAIR1^{-}$ subset could be due to recruitment of the other subsets into the secondary lymphoid organs, there could be alternative explanations such as increased cell death and decay in the other subsets which could not be ruled out.

In summary, in this chapter different strategies to identify the functional role of the relapse associated subset were employed including identification of autoreactivity, directly pathogenic

inflammatory mediator secretion, variations during a controlled immune response and the properties of in vitro equivalent cells.

8.1 Flow sorting of two extreme memory B-cell subsets and plasmablasts from RA patients

The key memory B-cell subsets need to be separated for further functional characterisation to understand their role in disease pathogenesis. The key role in pathogenesis could be secondary to autoreactivity or inflammatory cytokine secretion. 3ml of peripheral blood from 5 RA patients was stained with the same antibodies used for memory B-cell subset classification (Version 1 **Error! Reference source not found.**) after red blood cell lysis with ammonium chloride. The stained cells were flow sorted with a similar gating strategy used to classify the memory B-cell subsets as shown in Figure 5.6-2 using Influx cell sorter (BD Biosciences).Four patients were ACPA positive and the other patient was ACPA negative. Out of the four ACPA positive patients, two were rituximab naive and two were relapsing post-rituximab. All patients had clinically active disease at the time of sampling. Since density gradient centrifugation can remove plasmablasts, ammonium chloride lysis was used to exclude red cells. Cells were then stained with the same antibodies used for memory B-cell subset analysis. The number of cells for each subset obtained is shown below. Due to the low numbers of cells in each fraction post-sort, the cells from the 2 rituximab naïve patients were combined into a single sample. The 2 post-rituximab samples were combined as well.

Table 8.1-1 B-cell subsets obtained from flow sorting of 5 RA patients

All 5 patients had active clinical disease. The total number of cells obtained by the sorting process (Influx cell sorter, BD Biosciences) from 3ml peripheral blood using 8 surface markers as described in Figure 5.6-2 is shown.

	Naïve	Plasmablasts	24-84-95+LR-	24+84+95-LR+
Ritux naïve active 1	1600	4	11	3
Ritux naïve active 2	24806	40	159	21
CCP Neg	11126	25	104	9
Post-Ritux relapse 1	28776	42	641	11
Post-Ritux relapse 2	35072	45	137	8

8.1.1 ELISpot for ACPA secretion by RA peripheral blood plasmablasts

Plasmablasts were incubated for 8 hours in the ELISpot plates coated with anti-IgG or CCP as capture peptides. Due to the lack of binding of CCP peptides to the ELISpot plates as shown in Figure 6.3-3, streptavidin coat was used to capture the biotinylated peptides onto the plate. The secreted IgG that was bound to the plates was detected with biotinylated anti-IgG followed by streptavidin HRP. For the wells where streptavidin-biotinylated CCP was used for capture, HRP directly conjugated to anti-IgG was used. The spots were developed using the standard kit protocol as described in methods section 5.9.

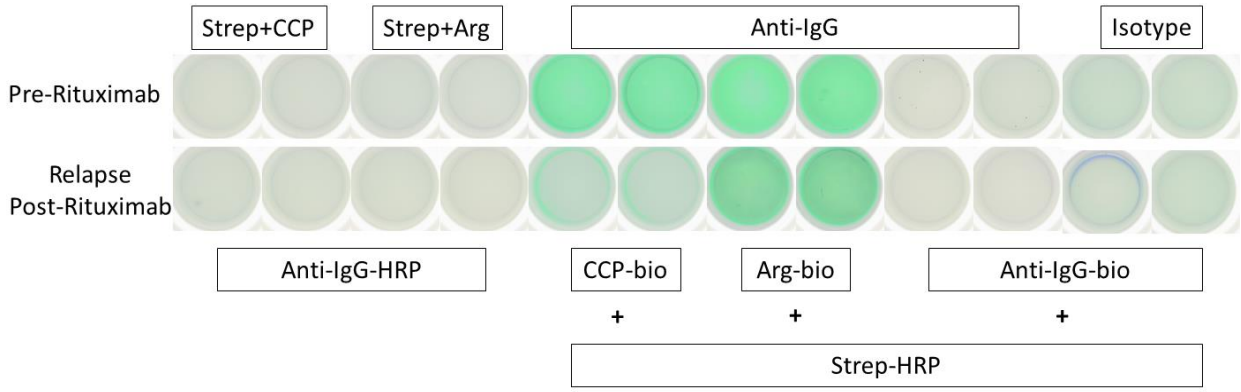

Figure 8.1-1 ELISpot for IgG and ACPA secretion by flow-sorted peripheral blood RA plasmablasts

Flow sorted plasmablasts (defined as $CD19^{+}CD20^{-}CD27^{Hi}CD38^{Hi}$) using the antibodies and gating strategy described in methods section 5.6.2 from 2 groups of patients with active disease – rituximab naïve and post-rituximab relapse (2 patients in each group) were incubated for 8 hours in wells coated with reagents shown in the top row. The reagents used for detection of the secreted antibodies bound to the plate are shown in the bottom row. The spots were developed using the standard kit protocol as described in methods section 5.9.

There was no detectable secretion of ACPA by the plasmablasts from the 2 different patient categories. There was no detectable secretion of IgG either and therefore the assay lacked a positive control. Out of the 8 different ELISpot experiments performed, IgG detection has been consistent and the same technique was applied to this experiment. Therefore, the lack of IgG secretion is likely to be due to the poor viability of the cells rather than a technical issue since IgG detection has never been a problem with ELISpot as shown in Figure 8.1-2.

8.1.2 ELISpot for ACPA secretion by plasmablasts generated in vitro from RA naïve B-cells

The naïve B-cells obtained during the flow sort were differentiated using CD40L/BCR/IL2/IL21 based protocol (Figure 5.4-1) up to day 6 to generate plasmablasts. The cells were incubated for 8 hours in ELISpot wells coated with anti-IgG, isotype antibody or streptavidin-tagged citrullinated and arginine versions of the peptide. The spots were developed as per standard kit protocol described in detail in the methods section 5.9. There was no detectable ACPA secretion by the in vitro generated plasmablasts derived from naïve B-cells. It was interesting to note that naïve B-cells from RA patients class-switched during the in vitro differentiation process and generated IgG secreting plasmablasts. In the bottom row, instead of cells, serum from ACPA positive and negative patients was used in alternative wells. The technique was not able to detect ACPA from the serum in an ELISA like fashion although it detected IgG as shown in the bottom row of Figure 8.1-2. Therefore, the presence of plate bound peptides at the time of detection could not be confirmed.

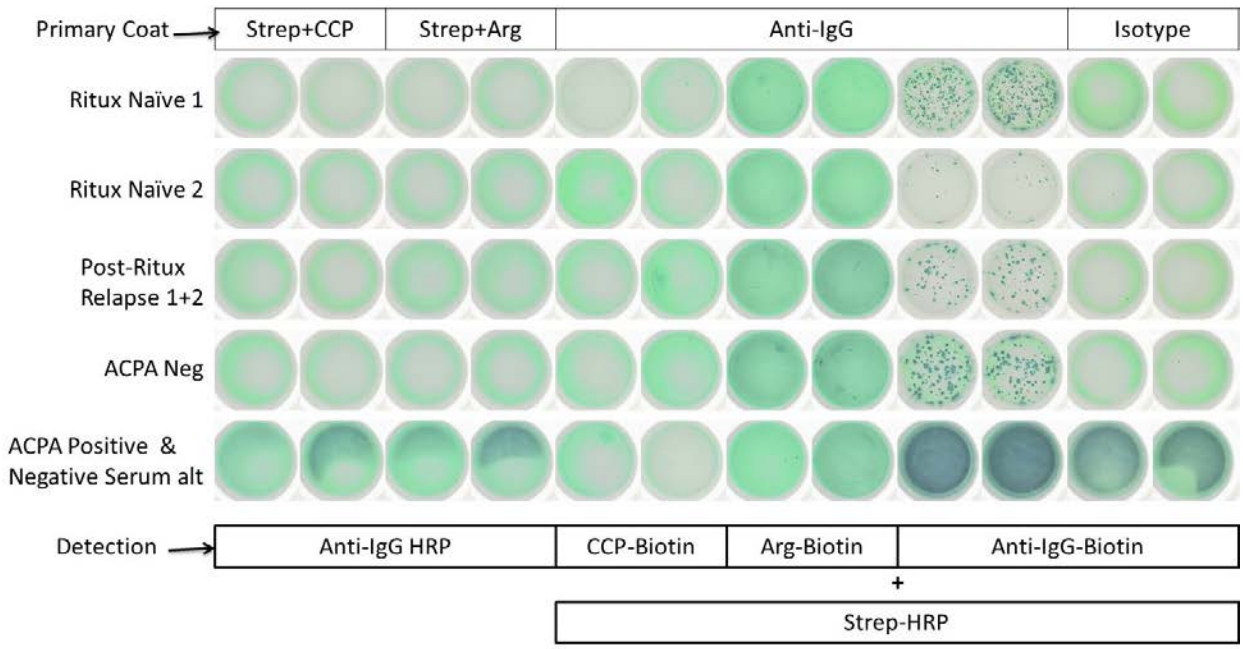

Figure 8.1-2 ELISpot for ACPA and IgG secretion by in vitro generated plasmablasts from flow-sorted naïve B-cells of RA patients

In vitro generated day 6 plasmablasts using CD40L/BCR/IL2/IL21 based protocol described in Figure 5.4-1 from flow-sorted naïve B-cells ($CD19^{+}CD20^{+}CD27^{-}$ - detailed gating strategy shown in Figure 5.6-2) of RA patients were incubated for 8 hours in wells coated with reagents shown at the top. The reagents used for detection of the secreted antibodies bound to the plate are shown in the bottom. The bottom row of wells was incubated with ACPA positive serum alternating with ACPA negative serum instead of cells. The spots were developed using the standard manufacturer's protocol described in detail in methods section 5.9.

The cell yield from flow sorting was poor and also affected the cell function and viability. ACPA detection was also limited by this factor and negative results were difficult to interpret in the absence of well-defined positive controls in the form of ACPA secreting PCs. Therefore other modes of functional evaluation were pursued.

8.2 Further functional characterisation of relapse associated B-cells.

To understand the functional and pathogenic role of relapse associated B-cells it is important to know what stage of the B-cell life cycle these cells represent. The 4 surface markers namely CD24, CD84, CD95 and LAIR1 used to classify memory B-cells and identify the relapse associated subset show a similar expression pattern in plasmablasts. It is not known at what stage during differentiation they acquire this surface marker profile. It is not feasible to follow the B-cells in vivo through their life cycle to ascertain the stage of differentiation of the relapse associated B-cell. Since this subset is present only as a minor proportion in peripheral blood, it is possible these cells are usually tissue resident or present at sites of activity like secondary lymphoid organs with some spill over into peripheral blood. Presence of only low numbers in peripheral blood makes it difficult to study these cells in more detail. Identifying a site which is rich in this subset or an in vitro correlate of this subset would enable better functional characterisation of this subset. The technical challenges with detection of ACPA-specific B-cells and flow sorted subsets make this even more vital.

8.2.1 Sequential changes in expression of CD24, CD84, CD95 and LAIR1 during B-cell differentiation

Using the in vitro differentiation system it is possible to study the change in the expression of these markers in a sequential fashion following B-cell stimulation as they mature to plasmablasts. It was reasoned that this might enable identification of a stage which is similar to the relapse associated subset. Negatively selected peripheral blood B-cells from a healthy control were stimulated with CD40L and BCR stimuli and IL2 till day 3. On day 3 the cells were removed from CD40L and cultured with IL2 and IL21 in a nutrient rich media (Figure 5.4-1). The cells at various stages of differentiation were stained with the same antibodies used for memory B-cell phenotyping (Antibody cocktail version 1 from Table 5.2-3). CD95 expression is acquired and CD24 expression is lost quite early following stimulation during the initial 3 days. Loss of CD84 and LAIR1 occurs later quite close to the time of maturation to plasmablasts. A minor proportion can continue to express LAIR1 even during the plasmablast stage, which can also be seen in peripheral blood plasmablasts. When plasmablasts mature into PCs LAIR1 expression is completely lost (94). Based on the expression of these 4 markers the relapse associated B-cells could be placed between days 3 to 5 of the differentiation, just before they differentiate into plasmablasts. However, the B-cells also start acquiring CD38 by this stage in vitro which is different to the relapse associated B-cells. These cells may still be identical in functional terms with the dissimilarities noted between the in vivo B-cell subset and the in vitro counterpart merely due to the different in vitro culture conditions and thus potentially not of functional relevance. Alternatively a distinct set of differentiation conditions may be required to promote the acquisition of this phenotype.

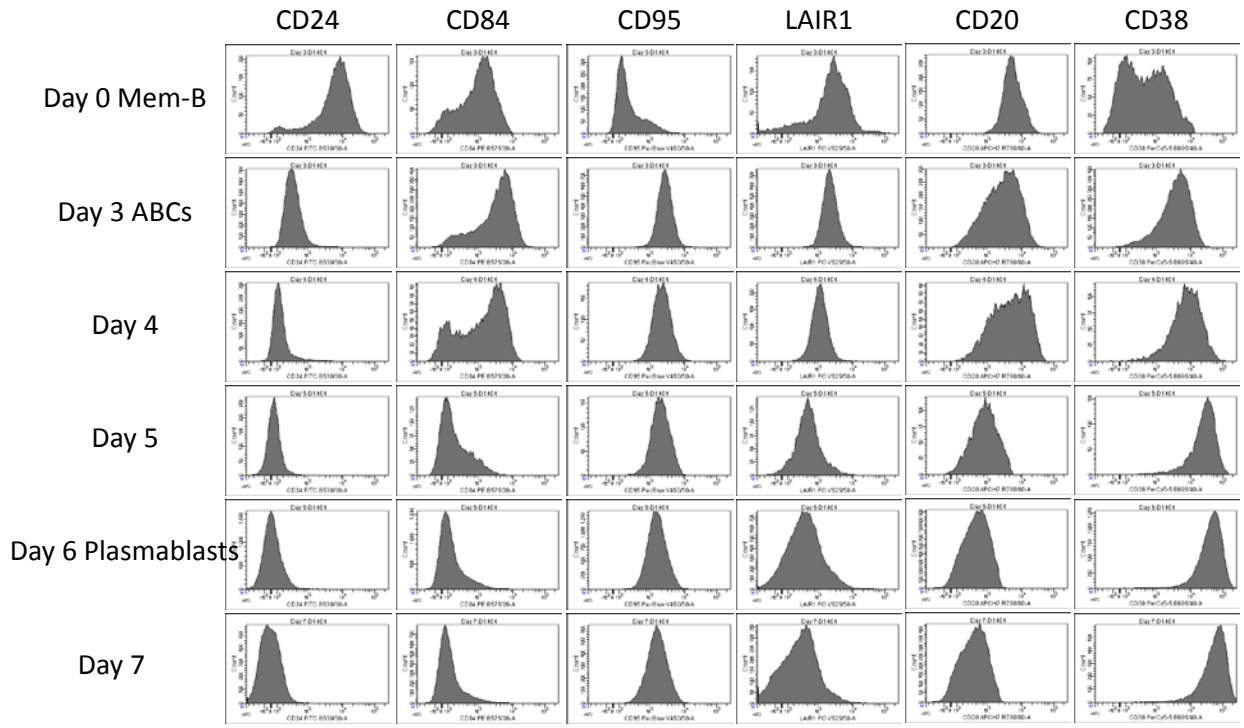

Figure 8.2-1 Sequential changes in surface expression of CD24, CD84, CD95 and LAIR1 during B-cell differentiation

Peripheral blood B-cells from a healthy control were stimulated with BCR and CD40L stimulus in the presence of IL2 till and day 3. On day 3 CD40L stimulus was withdrawn and cells were transferred to nutrient rich media with IL2 and IL21. CD24 expression was lost and CD95 was acquired quite early during B-cell differentiation whereas the loss of CD84 and LAIR1 occurred later. Data representative of 6 controls from 4 different experiments.

8.2.2 Identification of B-cells with closely-related phenotype to the relapse associated subset

Since the relapse associated subset was mainly seen in RA patients in high proportions, synovial fluid from various diseased states were evaluated. Synovial fluid collected in heparin from 3 patients with gout, one with lupus and 4 with RA who all had joint effusions were analysed. The sample was treated with ammonium chloride to lyse remnant RBCs and stained with the same antibodies used for memory B-cell phenotyping (Antibody cocktail version 1 from Table 5.2-3). In case of gout patients, the synovial fluid was predominantly neutrophilic and there was paucity of lymphocytes. In case of SLE and RA patients, the samples were mostly devoid of any cells except in one patient shown below. It is not clear whether the finding is typical for synovial fluid B-cells or occurs only in a proportion of patients due to lack of replicates. The day 4 activated B-cells generated by stimulation with CD40L and BCR stimuli and IL2 (Figure 5.4-1) are the closest to the relapse associated B-cells from the different stages of in vitro differentiation system. The synovial fluid B-cells had a similar expression profile except for CD84. However, from Figure 8.2-1 it is clear that CD84 expression could be lost in a quick fashion. Therefore, it is possible that CD84 is lost on egress to peripheral blood. The other interesting feature of the synovial fluid B-cells is that they can be divided into 2 populations based on their CD27 expression. CD27Neg cells are possibly at an earlier stage of their life cycle maturing into CD27Pos B-cells. It is also possible that this is the stage at which the bifurcation between memory B-cells and plasmablasts occurs in vivo but does not happen in vitro due to the lack of optimal conditions for generating memory B-cells.

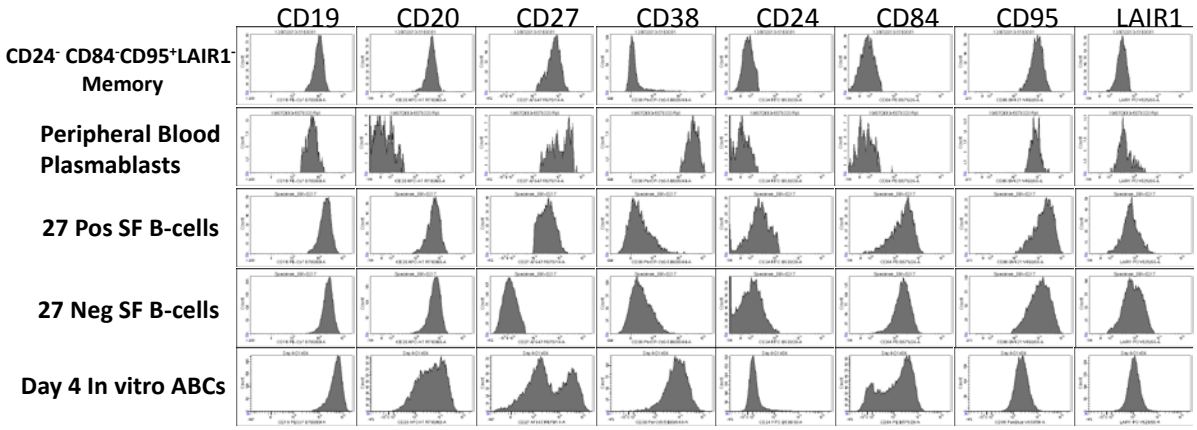

Figure 8.2-2 Comparison of the relapse associated B-cells with plasmablasts, synovial fluid B-cells and in vitro generated activated B-cells

Peripheral blood plasmablasts (defined as $CD19^{+}CD20^{-}CD27^{Hi}CD38^{Hi}$) show similar expression profile except for CD20 and CD38. CD27 positive and negative synovial fluid B-cells are identical in terms of other markers tested and closely resemble $24^{-}84^{-}95^{+}LAIR1^{-}$ subset except for CD84. Day 4 in vitro ABCs generated by CD40L and BCR stimuli and IL2 (Detailed protocol shown in Figure 5.4-1) are also related except for CD84 and CD38.

8.3 Functional profiling of the in vitro counterpart of relapse associated memory B-cell subset

The study of sequential changes in the markers used to classify the memory B-cell subsets during the course of in vitro B-cell differentiation from mature B-cells to plasmablasts revealed that the surface marker expression pattern was attained by the cells between day 3 and day 6.The gene expression changes occurring during this phase has been previously published by Cocco et al. and this pre-published data (60) was re-analysed for factors that were expressed at higher levels compared to the mature resting B-cells (Day 0). This reveals that B-cells during particular stages of their normal differentiation cycle can secrete inflammatory mediators. To identify this stage of B-cells in vivo additional surface markers that are present only during this stage of B-cell differentiation were sought which could then be evaluated in peripheral blood of RA patients to identify the pro-inflammatory B-cells. The mechanism by which the depletion of B-cells by rituximab leads to clinical remission remains unclear. The reduction in proinflammatory mediators secreted by the circulating B-cells or during their differentiation into plasmablasts might represent a mechanism contributing to drug effectiveness.

8.3.1 B-cells exhibit increased expression levels of proinflammatory mediators and chemoattractants during normal B-cell differentiation

Gene expression analysis was performed at various stages of B-cell differentiation to plasmablasts from negatively selected peripheral blood B-cells from 3 controls by Cocco et al. and the data was published previously(60). The gene expression was assessed on Illumina HumanHT-12 v4 arrays. The previously published data was reanalysed for the purpose of this study. From the published data 50 different clusters of genes with similar expression pattern were defined.

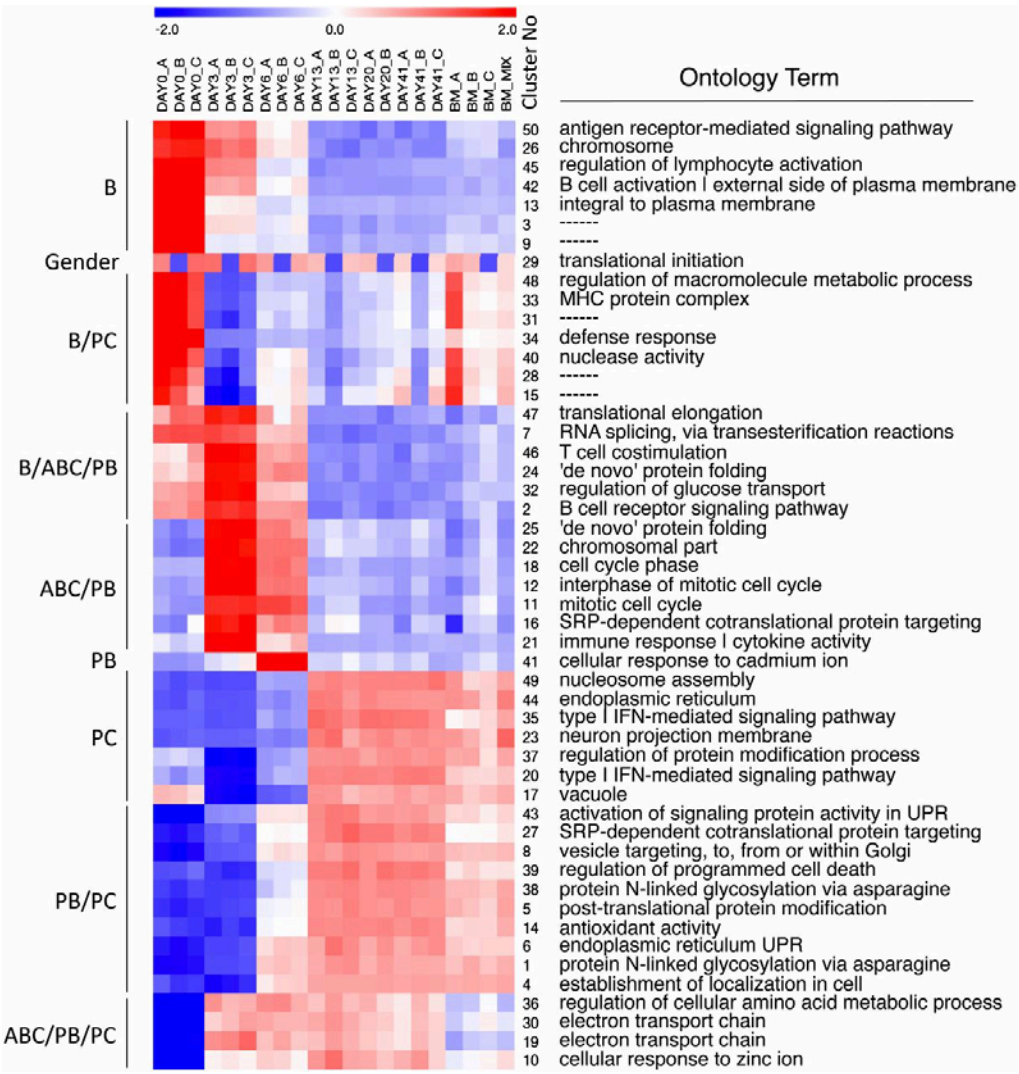

Reproduced with permission from Cocco et al.
The Journal of Immunology, 2012, vol. 189 no. 12 5773-5785

Figure 8.3-1 50 clusters of genes with similar patterns of expression during in vitro B-cell differentiation

Negatively-selected peripheral blood B-cells were differentiated to plasma cells in vitro and gene expression analysis at baseline, days 3, 6, 13, 20 and 41 were performed on Illumina HumanHT-12 v4 arrays by Cocco et al. 50 gene clusters with similar expression patterns were generated by k-means clustering. Z-score (-2 to +2) derived from median expression values of each cluster is shown as the expression values for the clusters in the heat map. The representative ontology term from GO enrichment analysis is provided on the right for each cluster. The sample time points are indicated at the top. One of the samples on day 20 failed quality control and was excluded. The RNA samples for days 13, 20 and 41 were obtained from sorted CD138 positive PCs. The categories were defined based on heat map distribution. B-cell (B), Activated B-cell (ABC), Plasmablast (PB), Plasma Cell (PC).

Since, the RAMB cells closely resemble the day 3 cells in the in vitro system, the activated B-cell stage (ABC) in the publication was chosen for further analysis. The ABC stage did not have a separate cluster and therefore ABC/PB stage was chosen which contained 7 clusters – 11, 12, 16, 18, 21, 22 and 25. When these clusters were examined 12, 16 and 25 contained genes that were highly expressed in plasma cells as well. The clusters 11, 18, 21 and 22 were chosen for further analysis. There were a total of 338 probes covering 261 genes in these 4 clusters. Since the RAMB were hypothesized to be involved in the inflammatory process in RA and closely resemble day 3 in vitro differentiated B-cells, the presence of pro-inflammatory genes in these 4 clusters were sought to provide a mechanistic explanation for the potential role of RAMB in RA.

Gene ontology enrichment analysis was performed to identify the genes which are involved in an immune response using g:profiler (Version: r1440_e81_eg28. Date analysed – 29/09/2015, Gene Ontology annotations: GO direct 22/07/2015, GO terms: releases – 05/09/2015). 209 GO terms were significantly enriched ($p<0.05$) when the list of 261 genes was assessed. The full list of enriched GO terms sorted on their significance levels is provided in the table below. The comprehensive list of genes associated with each of the significantly enriched GO terms is provided as a spreadsheet in the e-version of the thesis.

Table 8.3-1 Gene ontology terms enriched on assessment of genes expressed during activated B-cell stage of in vitro differentiation.

261 genes from the 4 ABC/PB clusters 11, 18, 21 and 22 shown in Figure 8.3-1 were assessed for GO enrichment (g:profiler Version: r1435_e80_eg27. Date analysed – 29/09/2015) and the GO terms that were enriched are presented in order of their significance.

p-value	Term ID	Term Name
1.79E-54	GO:0000278	mitotic cell cycle
4.27E-51	GO:1903047	mitotic cell cycle process
7.3E-49	GO:0022402	cell cycle process
1.3E-46	GO:0007049	cell cycle
3.53E-38	GO:0000280	nuclear division
4.14E-38	GO:0007067	mitotic nuclear division
1.72E-36	GO:0048285	organelle fission
8.91E-34	GO:0007059	chromosome segregation
1.36E-30	GO:0051301	cell division
1.76E-27	GO:0051276	chromosome organization
2.46E-25	GO:0098813	nuclear chromosome segregation
1.93E-23	GO:0006996	organelle organization
2E-21	GO:1902589	single-organism organelle organization
2.71E-21	GO:0000819	sister chromatid segregation
2.92E-19	GO:0044770	cell cycle phase transition
4.57E-19	GO:0044772	mitotic cell cycle phase transition
3.69E-18	GO:0000070	mitotic sister chromatid segregation
1.24E-17	GO:0000226	microtubule cytoskeleton organization
2.87E-17	GO:0071840	cellular component organization or biogenesis
1.68E-16	GO:0006260	DNA replication
2.13E-16	GO:0007017	microtubule-based process
3.7E-16	GO:0016043	cellular component organization
1.29E-15	GO:0006259	DNA metabolic process
2.39E-15	GO:0006261	DNA-dependent DNA replication
7.02E-15	GO:0010564	regulation of cell cycle process
1.12E-14	GO:0044763	single-organism cellular process
1.54E-14	GO:0007052	mitotic spindle organization
2.26E-14	GO:0051726	regulation of cell cycle
2.16E-13	GO:0044699	single-organism process
1.99E-12	GO:0007051	spindle organization
2.11E-12	GO:0071103	DNA conformation change
2.32E-12	GO:0007346	regulation of mitotic cell cycle
6.96E-11	GO:0006310	DNA recombination
1.02E-10	GO:0051302	regulation of cell division
1.71E-10	GO:0034508	centromere complex assembly

p-value	Term ID	Term Name
2.97E-10	GO:0006323	DNA packaging
3.03E-10	GO:0043933	macromolecular complex subunit organization
4.74E-10	GO:0031055	chromatin remodeling at centromere
5.55E-10	GO:0051983	regulation of chromosome segregation
8.55E-10	GO:0000075	cell cycle checkpoint
1.01E-09	GO:0000082	G1/S transition of mitotic cell cycle
1.48E-09	GO:0006270	DNA replication initiation
1.65E-09	GO:0007264	small GTPase mediated signal transduction
1.68E-09	GO:0071822	protein complex subunit organization
1.96E-09	GO:0044843	cell cycle G1/S phase transition
2E-09	GO:0007088	regulation of mitotic nuclear division
2.83E-09	GO:0051783	regulation of nuclear division
2.96E-09	GO:1902850	microtubule cytoskeleton organization involved in mitosis
8.7E-09	GO:0061641	CENP-A containing chromatin organization
8.7E-09	GO:0034080	CENP-A containing nucleosome assembly
1.04E-08	GO:0034724	DNA replication-independent nucleosome organization
1.04E-08	GO:0006336	DNA replication-independent nucleosome assembly
1.08E-08	GO:0070507	regulation of microtubule cytoskeleton organization
1.36E-08	GO:0007010	cytoskeleton organization
1.78E-08	GO:1901990	regulation of mitotic cell cycle phase transition
2.5E-08	GO:0032886	regulation of microtubule-based process
3.62E-08	GO:0006271	DNA strand elongation involved in DNA replication
4.81E-08	GO:0008608	attachment of spindle microtubules to kinetochore
6.62E-08	GO:1901987	regulation of cell cycle phase transition
9.29E-08	GO:0022616	DNA strand elongation
1.25E-07	GO:0033260	nuclear DNA replication
1.4E-07	GO:0050000	chromosome localization
1.4E-07	GO:0051303	establishment of chromosome localization
2.18E-07	GO:0043486	histone exchange
2.32E-07	GO:0009987	cellular process
3.13E-07	GO:0006974	cellular response to DNA damage stimulus
3.4E-07	GO:0090068	positive regulation of cell cycle process
4.42E-07	GO:0007080	mitotic metaphase plate congression
4.87E-07	GO:0033044	regulation of chromosome organization
6.78E-07	GO:0033043	regulation of organelle organization
9.74E-07	GO:0016568	chromatin modification
1.16E-06	GO:0051297	centrosome organization
1.23E-06	GO:0044786	cell cycle DNA replication
1.27E-06	GO:0008283	cell proliferation
1.59E-06	GO:0050896	response to stimulus
1.65E-06	GO:0006281	DNA repair

p-value	Term ID	Term Name
1.66E-06	GO:0031145	anaphase-promoting complex-dependent proteasomal
2.45E-06	GO:0045787	positive regulation of cell cycle
3.61E-06	GO:0031023	microtubule organizing center organization
4.73E-06	GO:0051321	meiotic cell cycle
5.4E-06	GO:0051310	metaphase plate congression
5.97E-06	GO:0007093	mitotic cell cycle checkpoint
8.12E-06	GO:0045930	negative regulation of mitotic cell cycle
8.6E-06	GO:0034453	microtubule anchoring
9.88E-06	GO:0065004	protein-DNA complex assembly
1.37E-05	GO:0006325	chromatin organization
1.66E-05	GO:0051304	chromosome separation
1.74E-05	GO:0090307	mitotic spindle assembly
1.81E-05	GO:0043044	ATP-dependent chromatin remodeling
2.94E-05	GO:0007098	centrosome cycle
3.44E-05	GO:0051225	spindle assembly
3.53E-05	GO:0051383	kinetochore organization
0.000037	GO:0051782	negative regulation of cell division
4.13E-05	GO:0006338	chromatin remodeling
4.48E-05	GO:0051716	cellular response to stimulus
4.49E-05	GO:0070271	protein complex biogenesis
4.49E-05	GO:0006461	protein complex assembly
4.66E-05	GO:0033554	cellular response to stress
4.98E-05	GO:0006950	response to stress
5.51E-05	GO:0031497	chromatin assembly
6.32E-05	GO:0031577	spindle checkpoint
7.94E-05	GO:0007126	meiotic nuclear division
8.22E-05	GO:0071824	protein-DNA complex subunit organization
8.54E-05	GO:0045786	negative regulation of cell cycle
0.000105	GO:0030071	regulation of mitotic metaphase/anaphase transition
0.000108	GO:0010948	negative regulation of cell cycle process
0.000109	GO:0000086	G2/M transition of mitotic cell cycle
0.00011	GO:0006334	nucleosome assembly
0.000112	GO:0065003	macromolecular complex assembly
0.000117	GO:1903046	meiotic cell cycle process
0.000124	GO:1902099	regulation of metaphase/anaphase transition of cell cycle
0.000125	GO:0044839	cell cycle G2/M phase transition
0.000146	GO:0007091	metaphase/anaphase transition of mitotic cell cycle
0.000171	GO:0044784	metaphase/anaphase transition of cell cycle
0.000252	GO:0010639	negative regulation of organelle organization
0.000268	GO:0010965	regulation of mitotic sister chromatid separation
0.00031	GO:0033045	regulation of sister chromatid segregation

p-value	Term ID	Term Name
0.00031	GO:0033047	regulation of mitotic sister chromatid segregation
0.000336	GO:0030261	chromosome condensation
0.000358	GO:0051306	mitotic sister chromatid separation
0.00044	GO:0006333	chromatin assembly or disassembly
0.000472	GO:0045132	meiotic chromosome segregation
0.000553	GO:0008150	biological_process
0.000713	GO:0044710	single-organism metabolic process
0.000723	GO:0048247	lymphocyte chemotaxis
0.000764	GO:0000910	cytokinesis
0.000897	GO:0035556	intracellular signal transduction
0.000906	GO:0051784	negative regulation of nuclear division
0.00101	GO:0034502	protein localization to chromosome
0.00105	GO:0034728	nucleosome organization
0.00116	GO:0007076	mitotic chromosome condensation
0.00117	GO:0045931	positive regulation of mitotic cell cycle
0.00123	GO:0046605	regulation of centrosome cycle
0.00147	GO:0072676	lymphocyte migration
0.00155	GO:0002548	monocyte chemotaxis
0.00178	GO:0000018	regulation of DNA recombination
0.00179	GO:0061640	cytoskeleton-dependent cytokinesis
0.0023	GO:0051640	organelle localization
0.00231	GO:0031109	microtubule polymerization or depolymerization
0.00235	GO:0006301	postreplication repair
0.00237	GO:0000083	regulation of transcription involved in G1/S transition of mitotic
0.00265	GO:2001251	negative regulation of chromosome organization
0.00269	GO:0045839	negative regulation of mitotic nuclear division
0.00337	GO:0051781	positive regulation of cell division
0.00359	GO:0007094	mitotic spindle assembly checkpoint
0.00404	GO:0006302	double-strand break repair
0.00422	GO:0071173	spindle assembly checkpoint
0.00482	GO:1903363	negative regulation of cellular protein catabolic process
0.00494	GO:0045841	negative regulation of mitotic metaphase/anaphase transition
0.00494	GO:0071174	mitotic spindle checkpoint
0.005	GO:0000022	mitotic spindle elongation
0.005	GO:0007100	mitotic centrosome separation
0.00511	GO:0051129	negative regulation of cellular component organization
0.00551	GO:0070925	organelle assembly
0.00576	GO:1902100	negative regulation of metaphase/anaphase transition of cell
0.00583	GO:0000281	mitotic cytokinesis
0.0062	GO:0031399	regulation of protein modification process
0.0062	GO:0071345	cellular response to cytokine stimulus

p-value	Term ID	Term Name
0.00633	GO:0031570	DNA integrity checkpoint
0.00647	GO:0048522	positive regulation of cellular process
0.00661	GO:0044711	single-organism biosynthetic process
0.00762	GO:1901991	negative regulation of mitotic cell cycle phase transition
0.00775	GO:0033046	negative regulation of sister chromatid segregation
0.00775	GO:0033048	negative regulation of mitotic sister chromatid segregation
0.00775	GO:2000816	negative regulation of mitotic sister chromatid separation
0.00782	GO:0002376	immune system process
0.00861	GO:0034097	response to cytokine
0.0089	GO:0051231	spindle elongation
0.0089	GO:0051299	centrosome separation
0.00904	GO:0032435	negative regulation of proteasomal ubiquitin-dependent protein
0.00937	GO:0019886	antigen processing and presentation of exogenous peptide
0.0103	GO:0051985	negative regulation of chromosome segregation
0.0124	GO:0051128	regulation of cellular component organization
0.0133	GO:0002495	antigen processing and presentation of peptide antigen via
0.0135	GO:0031110	regulation of microtubule polymerization or depolymerization
0.0139	GO:1901799	negative regulation of proteasomal protein catabolic process
0.014	GO:0009314	response to radiation
0.0142	GO:0051656	establishment of organelle localization
0.0145	GO:0032434	regulation of proteasomal ubiquitin-dependent protein
0.0146	GO:1901988	negative regulation of cell cycle phase transition
0.0147	GO:0006268	DNA unwinding involved in DNA replication
0.0151	GO:0031572	G2 DNA damage checkpoint
0.0161	GO:0051052	regulation of DNA metabolic process
0.0172	GO:0002504	antigen processing and presentation of peptide or
0.0173	GO:0000003	reproduction
0.0179	GO:0007019	microtubule depolymerization
0.0199	GO:0009628	response to abiotic stimulus
0.0202	GO:0044085	cellular component biogenesis
0.022	GO:0051439	regulation of ubiquitin-protein ligase activity involved in mitotic
0.0223	GO:0046602	regulation of mitotic centrosome separation
0.0223	GO:1901992	positive regulation of mitotic cell cycle phase transition
0.0223	GO:0043146	spindle stabilization
0.0256	GO:1903308	regulation of chromatin modification
0.027	GO:0044237	cellular metabolic process
0.0276	GO:1903051	negative regulation of proteolysis involved in cellular protein
0.0276	GO:0070098	chemokine-mediated signaling pathway
0.0317	GO:1901989	positive regulation of cell cycle phase transition
0.0317	GO:0032508	DNA duplex unwinding
0.0339	GO:0051382	kinetochore assembly

p-value	Term ID	Term Name
0.0339	GO:0051988	regulation of attachment of spindle microtubules to kinetochore
0.0339	GO:0071459	protein localization to chromosome, centromeric region
0.036	GO:1901360	organic cyclic compound metabolic process
0.0362	GO:0043241	protein complex disassembly
0.0379	GO:1902275	regulation of chromatin organization
0.0391	GO:0007062	sister chromatid cohesion
0.0419	GO:0032201	telomere maintenance via semi-conservative replication
0.0447	GO:0016310	phosphorylation
0.0467	GO:0031401	positive regulation of protein modification process
0.0484	GO:0016446	somatic hypermutation of immunoglobulin genes

The GO term “Immune system processes” (GO:0002376) was significantly enriched (p=0.0078) which contained 60 genes from the list of 261 genes. The change in expression levels of these genes during B-cell differentiation is shown in the figure below (Gene-E version 3.0.204). The genes were ordered by hierarchical clustering using average linkage and one minus Spearman correlation as the row distance metric. The GO term “Lymphocyte chemotaxis” (GO:0048247) was also significantly enriched (p=0.0007) and the term included 8 genes - CCL22, CCL17, CCL2, CXCL9, CXCL10, CCL4L2, CCL3L1 and CCL3.

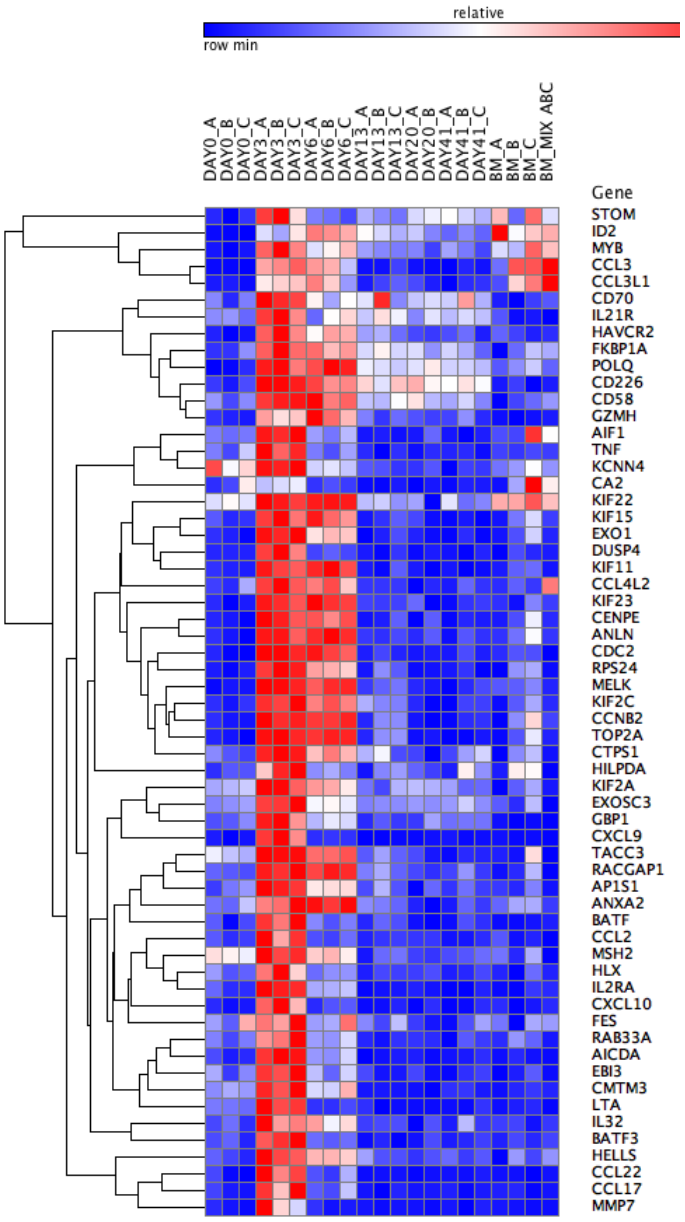

Figure 8.3-2 Expression levels of genes linked with immune system processes that are elevated during the activated B-cell stage of in vitro differentiation to PCs

261 genes from the 4 ABC/PB clusters were assessed for GO enrichment (g:profiler Version: r1435_e80_eg27. Date analysed – 29/09/2015) and 60 genes were linked with the GO term “immune system processes” (GO:0002376) (p=0.0078). The relative expression values over the time course of the differentiation series is provided for the 60 genes in the heat map. The genes were ordered by hierarchical clustering using average linkage and one minus Spearman correlation as the row distance metric.

To further illustrate the kinetics of gene expression, the expression values for 10 genes from the wider list of genes linked to “immune system process” and “lymphocyte chemotaxis” were illustrated as line graphs. This included 3 proinflammatory genes – Tumour Necrosis Factor (TNF-α), Allograft Inflammatory Factor 1 (AIF1), Lymphotoxin alpha (LTA) and the enzyme involved in extracellular matrix breakdown - Matrix Metalloproteinase-7 (MMP7) shown in Figure 8.3-3. It also included six chemokine ligands shown in Figure 8.3-4, which recruit other inflammatory cells including monocytes, T-cells and dendritic cells.

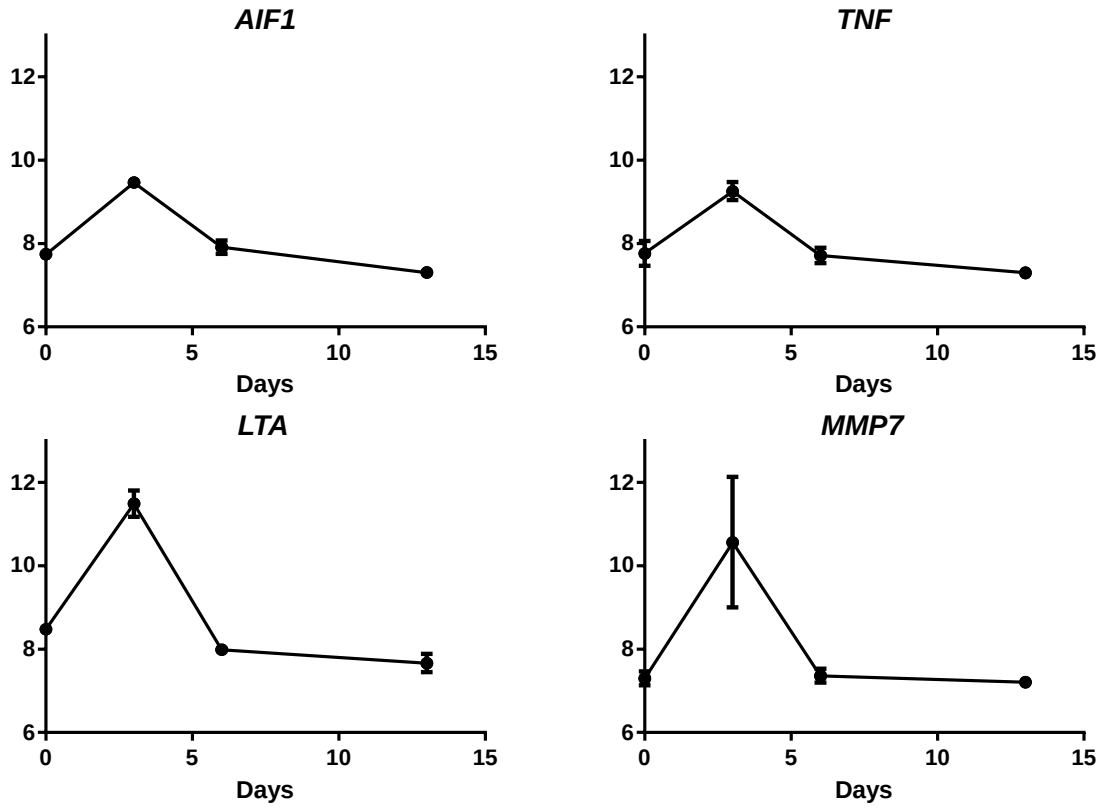

Figure 8.3-3 Gene expression levels of inflammatory mediators during normal B-cell differentiation

Gene expression was assessed at various stages of B-cell differentiation to plasmablasts from negatively selected peripheral blood B-cells from 3 controls using Illumina HumanHT-12 v4 arrays by Cocco et al. and the data was published previously (60). This graph was derived from reanalysis of previously published data. The absolute levels of gene expression by Illumina bead array at the time points indicated on the X axis from 3 controls. The dots represent the mean and the bars represent the standard deviation. Tumour Necrosis Factor (TNF), Allograft Inflammatory Factor 1(AIF1), Lymphotoxin alpha (LTA), Matrix Metalloproteinase-7 (MMP7)

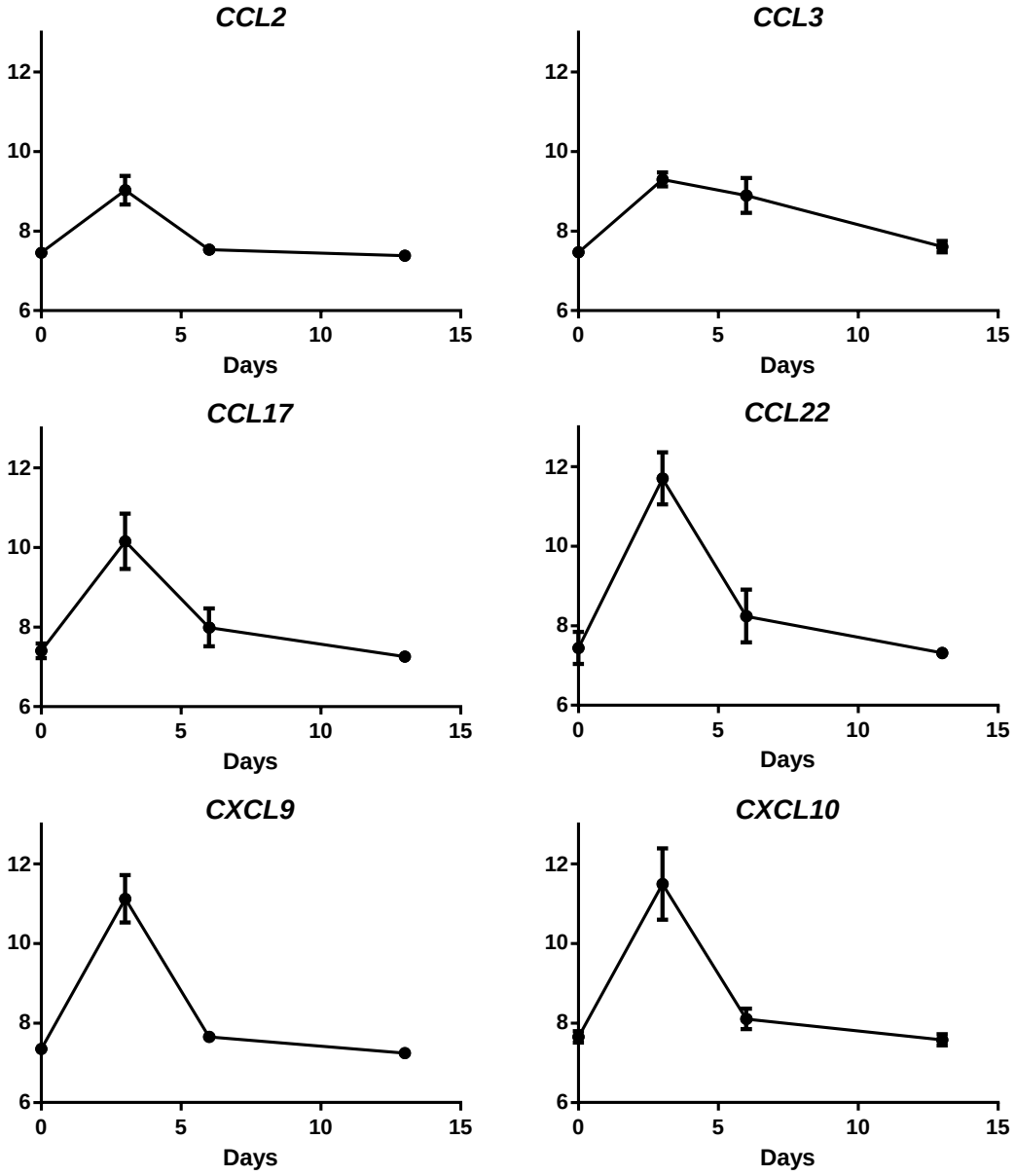

Figure 8.3-4 Gene expression levels of Chemoattractant proteins during normal B-cell differentiation

Gene expression was assessed at various stages of B-cell differentiation to plasmablasts from negatively selected peripheral blood B-cells from 3 controls using Illumina HumanHT-12 v4 arrays by Cocco et al. and the data was published previously (60). This graph was derived from reanalysis of previously published data. The absolute levels of gene expression by Illumina bead array at the time points indicated on the X axis from 3 controls. The dots represent the mean and the bars represent the standard deviation. CXCL – Chemokine (C-X-C motif) Ligand, CCL – Chemokine (C-C motif) Ligand.

Since anti-TNF therapy and B-cell depletion are both effective in RA, particular attention was given to TNF-α. The list surprisingly showed a multitude of pro-inflammatory and chemo-attractant proteins in addition to TNF. To ensure that this is not an isolated change in transcriptional activity without change in protein levels, the amount of TNF-α secreted by Day 3 B-cells was evaluated by ELISA of the culture supernatants. The cells were incubated at 37^0C for 4 hours. Media without cells was used as negative control and cells stimulated with a combination of PMA, Ionomycin and LPS was used as positive control. ELISA was performed according to standard manufacturer's protocol (Bethyl laboratories, USA) as described in methods section 5.8. The level of spontaneous secretion by day 3 B-cells is below the sensitivity of ELISA and therefore TNF-α secretion was detected only with stimulation (Figure 8.3-5). However secretion of TNF became apparent when using a technique with higher sensitivity, namely ELISpot (Figure 8.3-6). For ELISpot, wells with unstimulated B-cells without any primary coating were used as additional negative controls. The cells were incubated at 37^0C for 4 hours and developed using standard ELISpot kit protocol (Mabtech, Sweden) described in detail in methods section 5.9.

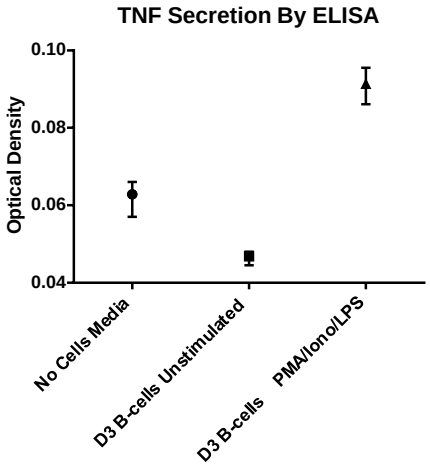

Figure 8.3-5 TNF secretion during day 3 of in vitro differentiation by B-cells detected by ELISA

The mean optical density of the triplicate samples are plotted as dots and the bars represent the range. Cells were incubated at 37^0C for 4 hours and supernatants were analysed. Media subjected to same conditions without the cells and stimulation with mixture of PMA (10 ng/ml), Ionomycin (1 μM) and LPS (1 μg/ml) were used as negative and positive controls respectively. ELISA was performed according to standard manufacturer's protocol as described in methods section 5.8.

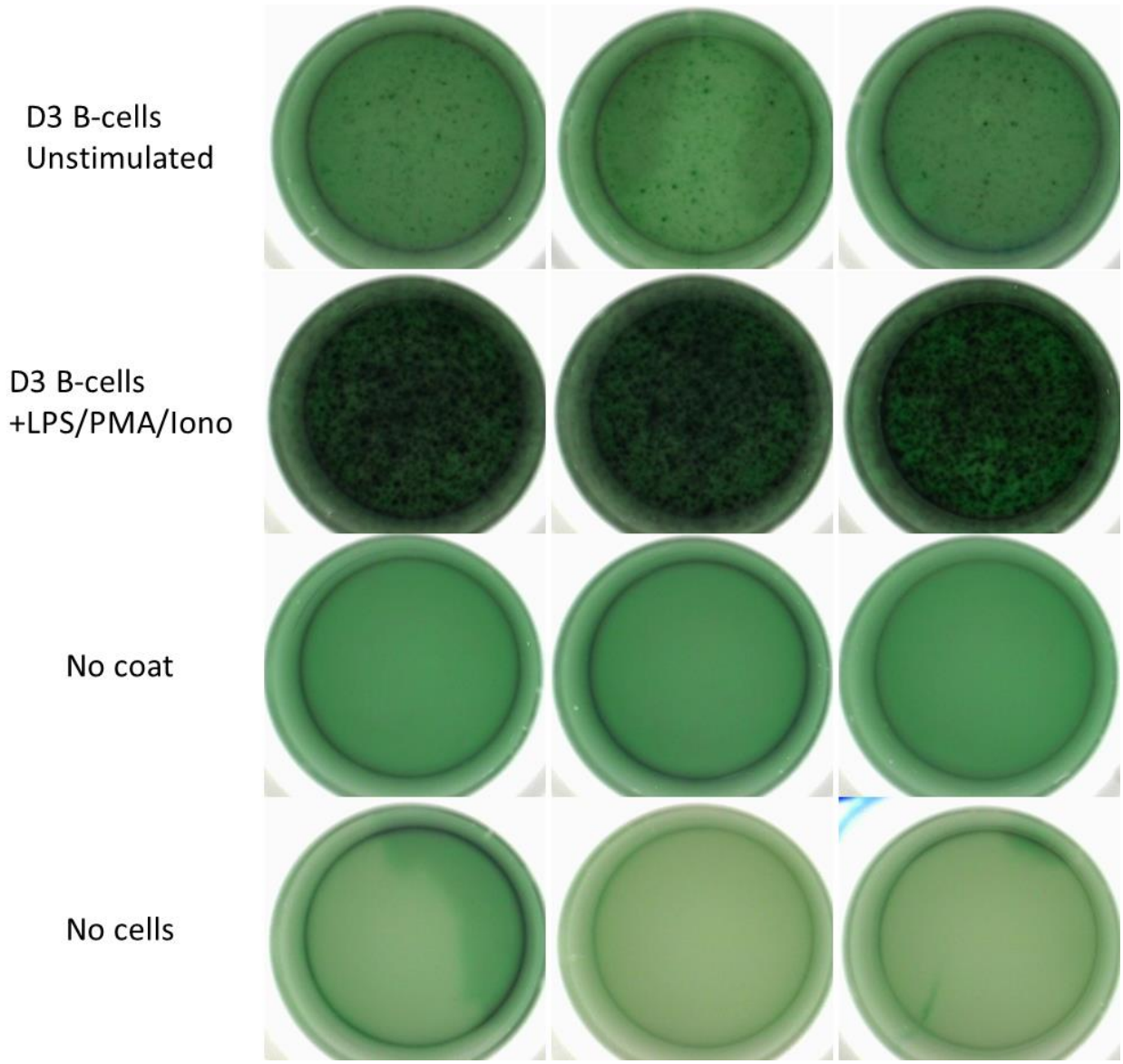

Figure 8.3-6 ELISpot for TNF secretion by B-cells during day 3 of in vitro differentiation

Day 3 B-cells at a density of 30000 cells per well were incubated in triplicates on wells coated with anti-TNF capture antibody. Uncoated wells with B-cells were used as negative controls. Media subjected to same conditions without the cells and cells stimulated with mixture of PMA (10 ng/ml), Ionomycin (1 µM) and LPS (1 µg/ml) were used as negative and positive controls respectively. The ELISpot plate was incubated at 37^0C for 4 hours. Biotinylated anti-TNF followed by streptavidin-HRP was used to detect the spots as described in methods section 5.9.

8.3.2 ELISpot for TNF secretion by memory B-cell subsets

The stage of in vitro differentiation that is closest to the relapse-associated memory B-cell subset is the stage when proinflammatory mediators are secreted. Therefore, TNF secretion by relapse-associated subset was evaluated. The flow sorted memory B-cell subsets as shown in Table 8.1-1 were seeded on to ELISpot plates coated with anti-TNF or anti-IgG capture antibodies whilst the antibody of same isotype but unrelated specificity served as negative control. Due to the very low cell numbers, cells from 2 patients who were rituximab naïve were combined. The 2 patients relapsing post-rituximab were combined into a single sample as well. The cells were incubated for 8 hours in cell culture media to allow for secretion. Anti-IgG or anti-TNF antibodies were used for detection. There was no detectable IgG or anti-TNF secretion from these cells, which could be due to the low cell numbers and viability as noted in case of plasmablasts in Figure 8.1-1.

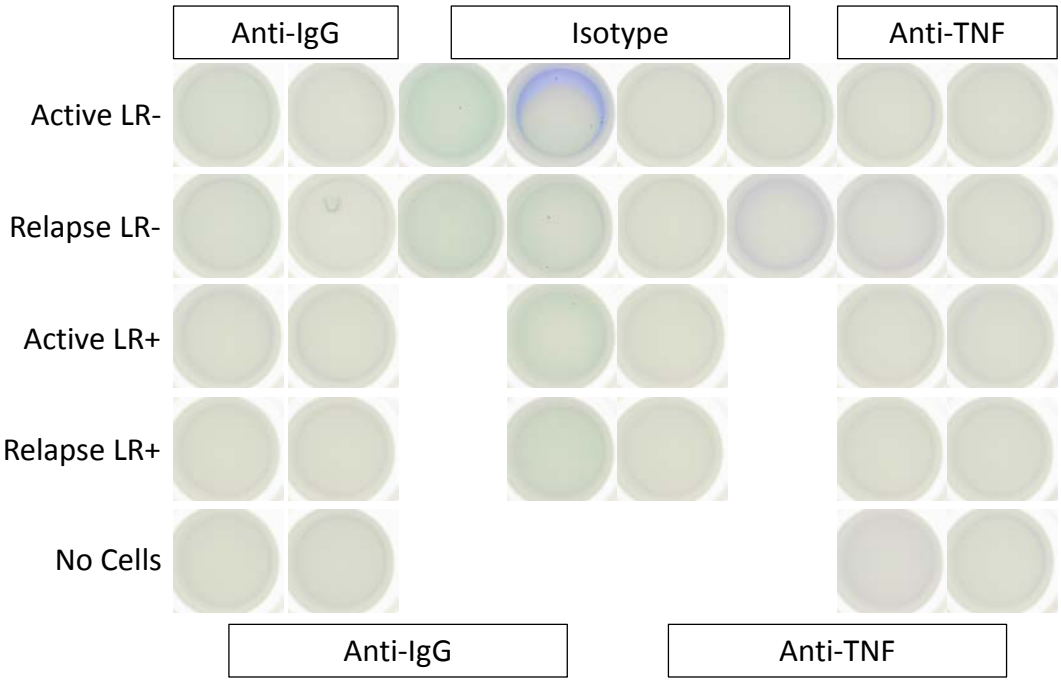

Figure 8.3-7 ELISpot for TNF secretion by sorted memory B-cell subsets

The 24-84-95+LR1- memory B-cell subset (LR-) and the opposite 24+84+95-LR1+ (LR+) subset from peripheral blood of 2 groups of RA patients with active disease – rituximab naïve and post-rituximab relapse (2 patients in each group) were incubated for 8 hours in wells coated with reagents shown in the top row. The spots were developed with biotinylated anti-IgG or anti-TNF as described in methods section 5.9.

8.3.3 Changes in surface markers that follow the pattern of inflammatory mediators

To identify the in vivo counterpart of the cells that secrete inflammatory mediators in vitro, the changes in expression of surface markers that coincide with the secretion of inflammatory mediators were sought. Surface markers detectable by flow cytometry are more reliable to be used as biomarkers rather than functional assays of protein secretion. The gene expression data generated by Cocco et al (60) was reanalysed for this purpose. TIM3 (T-cell Immunoglobulin domain and Mucin domain 3 official gene symbol *HAVCR2* – Hepatitis A Virus Cellular Receptor 2) and CD30 (TNFRSF8 – TNF Receptor Super Family) were identified which follow the similar pattern with peak around day 3 from baseline day 0 levels and start decreasing by day 6. A criteria of increase in absolute expression values by more than 1 between days 0 and 3 and decrease by more than 1 between days 3 and 6 was used to identify potential markers since the expression of proinflammatory genes follow this pattern.

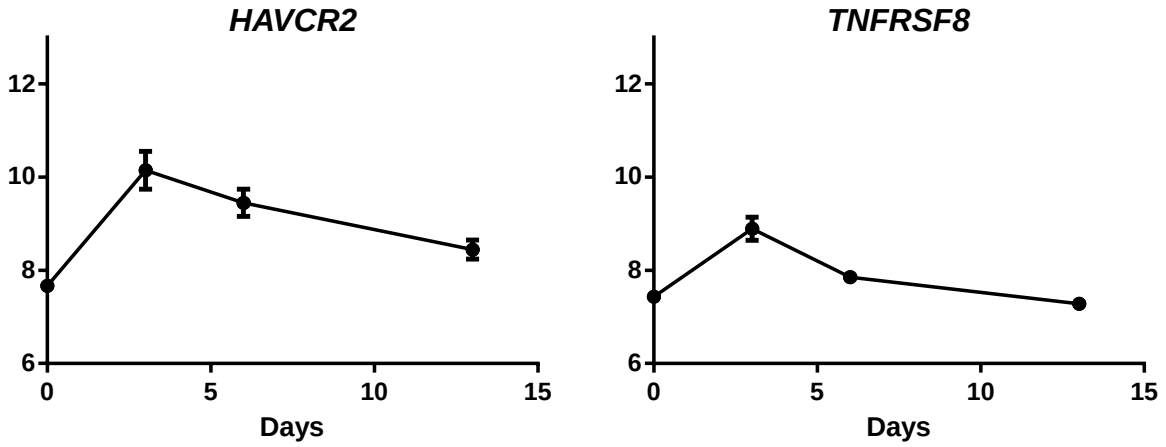

Figure 8.3-8 Gene expression levels of surface markers that are elevated during plasmablast differentiation.

Gene expression was assessed at various stages of B-cell differentiation to plasmablasts from negatively selected peripheral blood B-cells from 3 controls using Illumina HumanHT-12 v4 arrays by Cocco et al. and the data was published previously (60). This graph was derived from reanalysis of previously published data. Levels of absolute gene expression of TIM3 (*HAVCR2*) and CD30 (*TNFRSF8*) at the various time points during B-cell differentiation as indicated in 3 controls. The markers were chosen based on change in transcript levels that follow the inflammatory mediators.

8.3.4 Changes in surface expression of TIM3 during B-cell differentiation

The changes in TIM3 protein levels were examined sequentially in two controls during B-cell differentiation by flow cytometry to confirm the changes seen in gene expression. The cells were stained with CD24 FITC, TIM3 PE, CD4 PerCP-Cy5.5, CD38 PECy7, CD19 BV421, LAIR1 pacific orange, CD27 AF647 and CD20 APC-H7. Live cells were gated based on their scatter profile and CD4 was used as a negative marker. Peripheral blood B-cells did not express TIM3 and started expressing within two days of stimulation. The levels were at the highest on day 3 and gradually declined with only a tiny proportion positive on day 10 as shown in Figure 8.3-9. There is heterogeneity in TIM3 expression from day 3 to day 10 with at least a small proportion of cells negative throughout the course of differentiation. It is not clear whether it just reflects different subsets of B-cells such as naïve and memory B-cells changing the expression levels at varying rates or whether a certain subset does not upregulate TIM3 altogether.

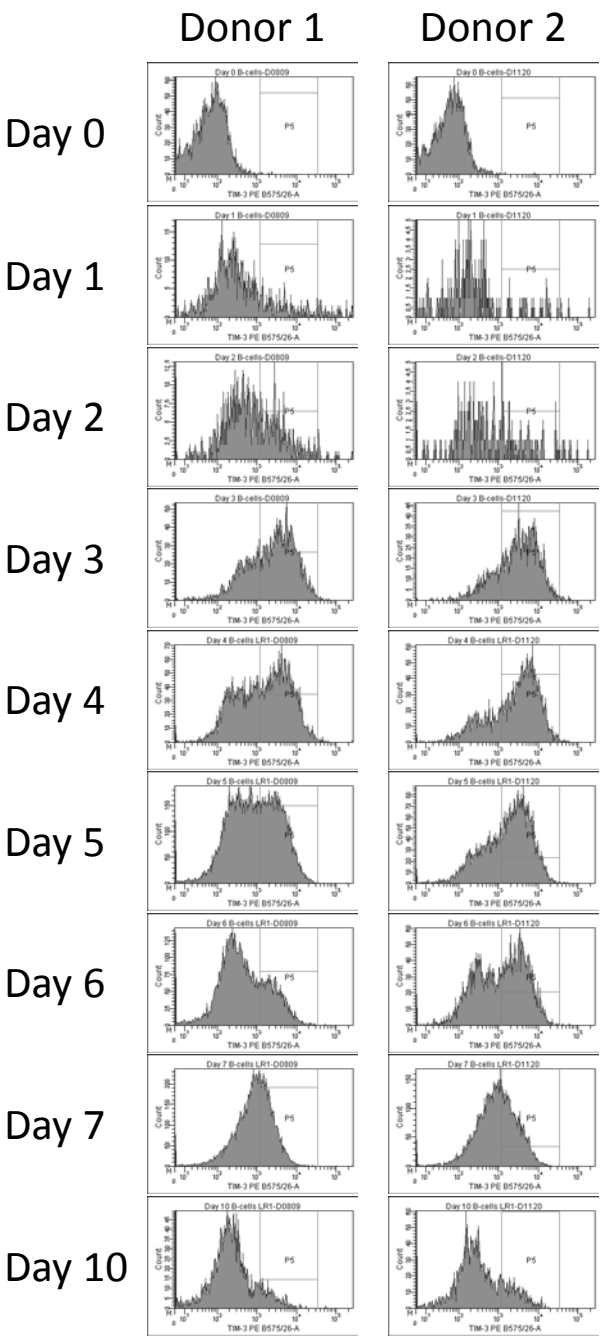

Figure 8.3-9 Changes in surface expression of TIM3 during B-cell differentiation

Negatively selected B-cells from two donors were differentiated using CD40L, BCR stimulus and IL2 based protocol (Figure 5.4-1) and their surface expression of TIM3 was examined every day during their course of differentiation. Histograms showing TIM3 expression levels (MFI) showing representative pattern of 5 different controls from 4 different experiments.

B-cells can be differentiated to PCs in vitro by using either CD40L or TLR ligand as co-stimulatory agents (detailed protocol given in methods section 5.4.4). It is not known whether upregulation of TIM3 during B-cell differentiation is dependent on CD40L co-stimulatory signals from T-cells. Therefore, B-cells stimulated with the TLR 7/8 agonist R848 (1 µg/ml) was monitored which showed that the surface expression of TIM3 was upregulated with both CD40L and R848 stimuli as shown in Figure 8.3-10. The cells were stained with CD24 FITC, TIM3 PE, CD4 PerCP-Cy5.5, CD38 PECy7, CD19 BV421, LAIR1 pacific orange, CD27 AF647 and CD20 APC-H7. Live cells were gated based on their scatter profile and CD4 was used as a negative marker.

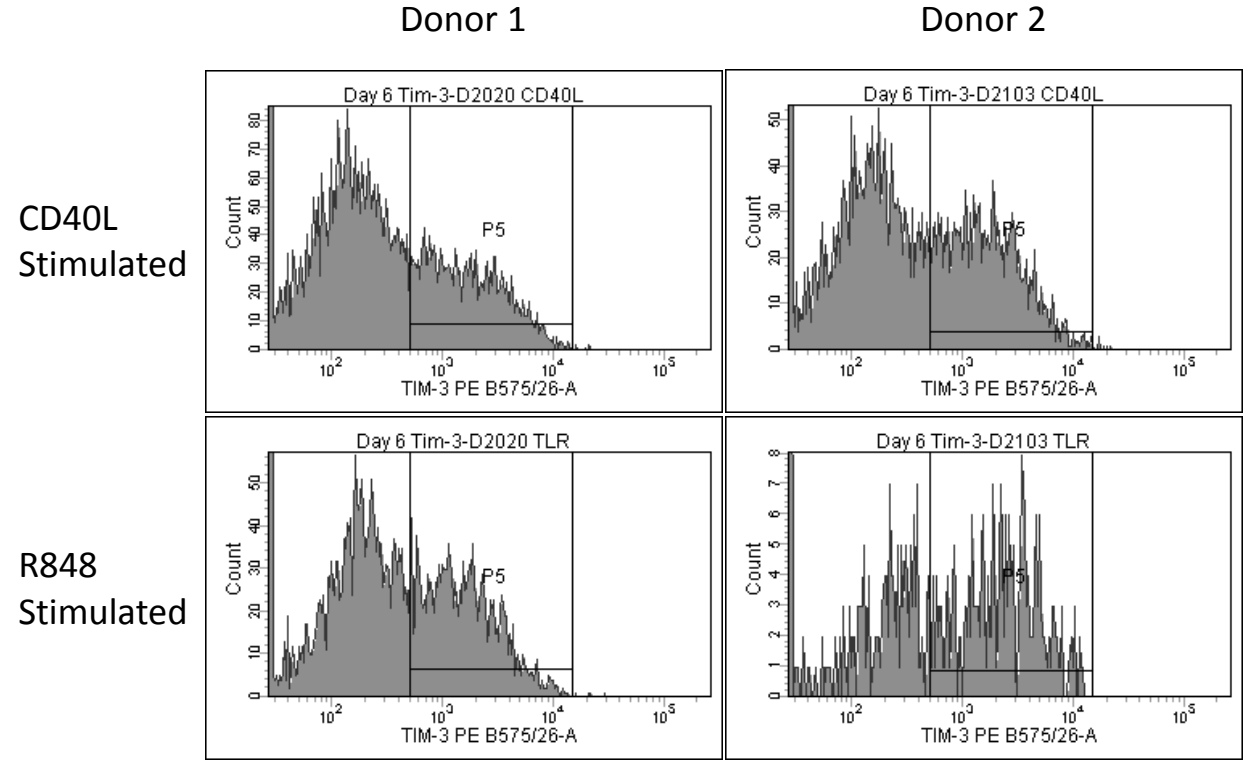

Figure 8.3-10 Upregulation of TIM3 expression on day 6 after B-cells were stimulated with CD40L or TLR agonist R848.

Histograms of TIM3 expression levels (MFI) on day 6 from 2 donors are shown whose B-cells were stimulated with either CD40L or the TLR agonist R848 (1 µg/ml). The detailed differentiation protocol is described in methods section 5.4.4. Data shown is from a single experiment.

8.3.5 Changes in surface expression of CD30 during B-cell differentiation

CD30 was the other surface marker that was upregulated based on gene expression analysis during the stage when proinflammatory mediators are secreted. The sequential change in levels of CD30 on cell surface was examined by flow cytometry to confirm the changes seen by gene expression. The cells were stained with CD24 FITC, CD30 PE, CD4 PerCP-Cy5.5, CD38 PECy7, CD19 BV421, LAIR1 pacific orange, CD27 AF647 and CD20 APC-H7. Live cells were gated based on their scatter profile and CD4 was used as a negative marker. Figure 8.3-11 shows representative changes in levels of CD30 from 6 different experiments. The expression reached peak levels between day 3 and day 4 and reduced to almost baseline levels by day 6. Staining with TIM3/CD30 antibodies showed consistently higher signal than the isotype antibody. Therefore, the changes in levels of TIM3 and CD30 are not due to non-specific binding of the antibodies during certain stages of B-cell differentiation.

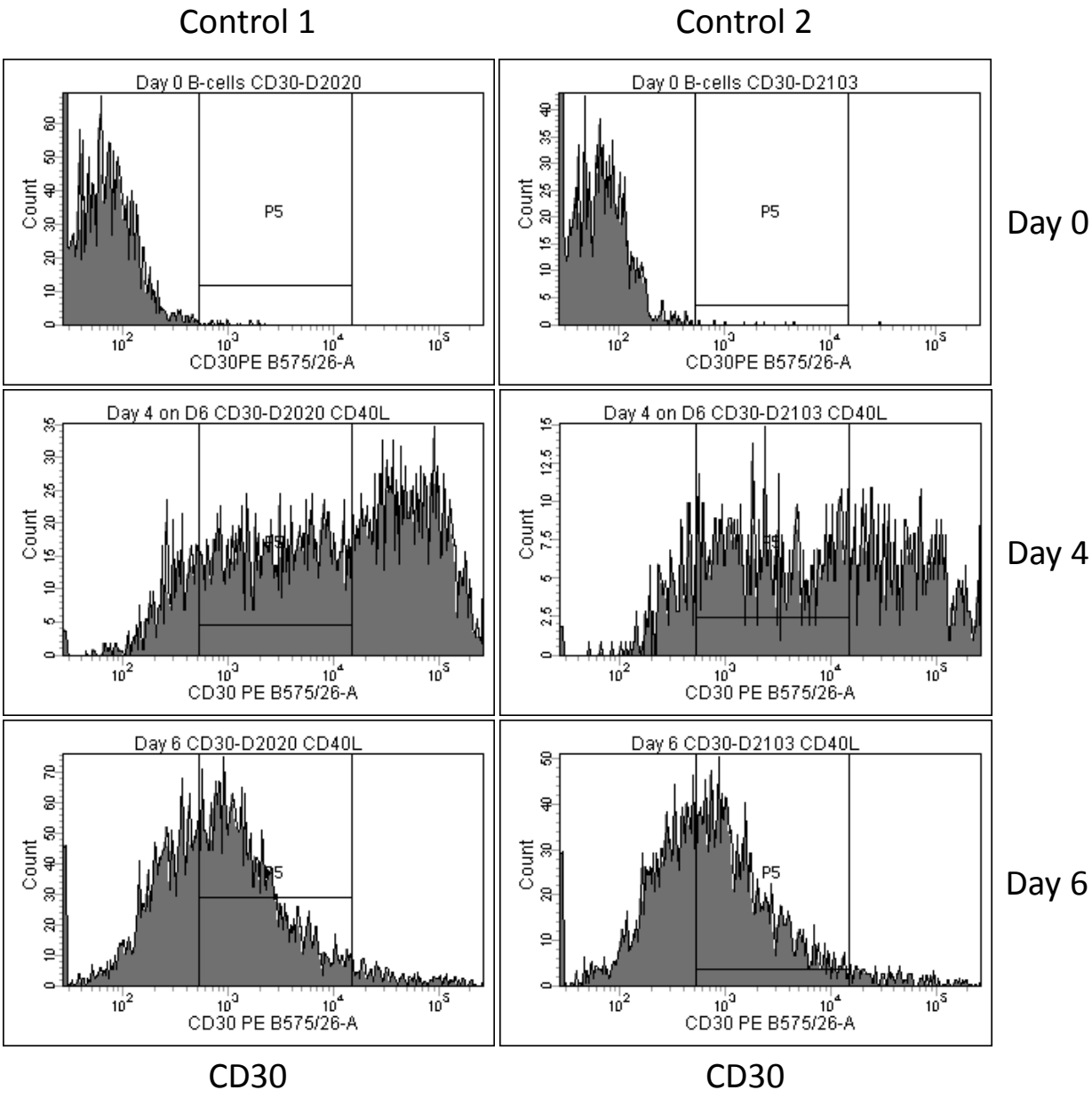

Figure 8.3-11 Transient upregulation in surface expression of CD30 during B-cell differentiation

Negatively selected B-cells from 2 donors were differentiated using CD40L, BCR stimulus and IL2 based protocol (Figure 5.4-1) and histograms of levels of CD30 surface expression (MFI) at baseline, day 4 and day 6 are shown. Live cells were gated based on their scatter profile and CD4 was used as a negative marker. This is representative of 6 experiments which all showed similar pattern of changes in CD30 expression.

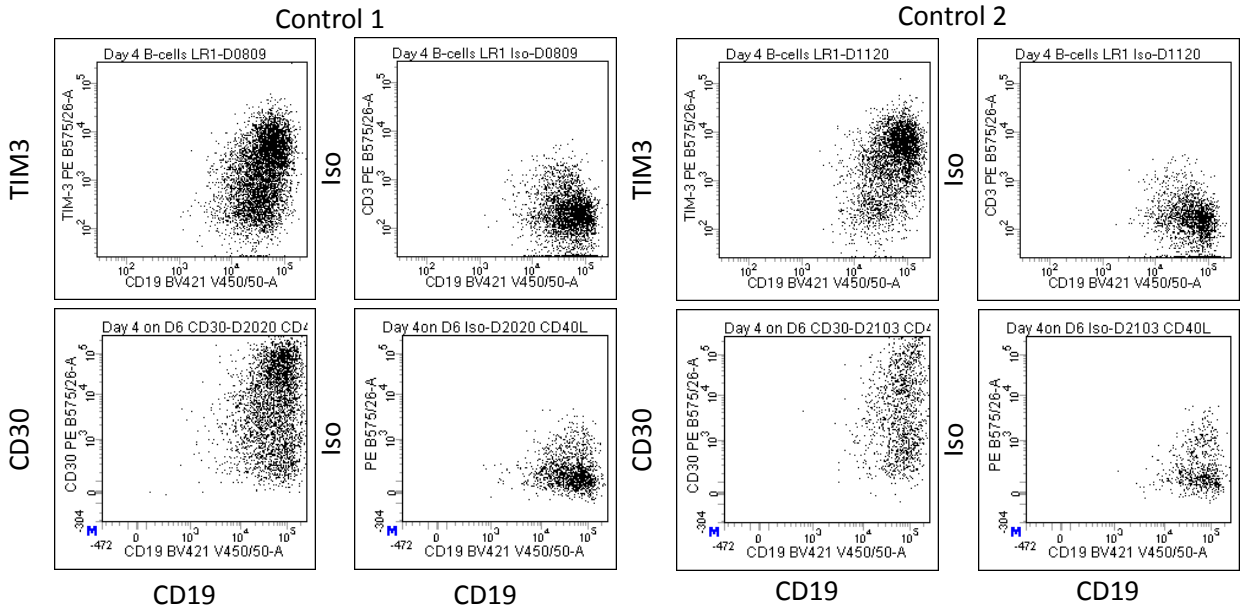

Figure 8.3-12 Changes in TIM3/CD30 expression is not due to non-specific binding

Cells from day 4 of B-cell differentiation (detailed differentiation protocol represented in Figure 5.4-1) when the levels of expression of TIM3 and CD30 are close to peak levels are shown. Cells were stained with anti-CD30, anti-TIM3 or isotype antibody and only live cells based on scatter profile were analysed. Dot plots showing CD19 on the x-axis and CD30/TIM3/Isotype along the y-axis.

8.3.6 Surface expression of TIM3 by B-lineage cells in vivo

TIM3 is not expressed by the peripheral blood B-cells as seen in Figure 8.3-9. The increase in TIM3 expression occurs following activation of B-cells in vitro and therefore peripheral blood from patients with ongoing inflammatory process was analysed. The peripheral blood B-cells from a diseased control showing a reactive picture and from an active RA/SLE overlap patient were analysed (Figure 8.3-13). A slightly modified antibody cocktail (version 1 from Table 5.2-3) used for memory B-cell phenotyping was used for staining the cells following RBC lysis with ammonium chloride. CD84 from the memory B-cell panel was replaced with TIM3. B-cells were defined based on their scatter profile and dual positivity for CD19 and CD20. This did not show TIM3 expression by any B-lineage cells.

Since the peripheral blood B-cells are likely to be resting and the changes in surface expression levels were seen during active differentiation, cells from other sites likely to contain activated B-cells were sought. B-cells from the synovial fluid from the knee joint with clinically active disease of a RA patient did not show any increased expression. Cells from secondary lymphoid organs like spleen, lymph node and bone marrow which are sites of B-cell differentiation were analysed. 4 lymph nodes which were affected by different pathologies including reactive, granulomatous inflammation, infiltration by follicular lymphoma and lung carcinoma did not show a distinct TIM3 positive B-cell population although sparse TIM3 positive cells could be observed. Representative lymph node TIM3 expression pattern is shown in Figure 8.3-13. B-cells from reactive bone marrow did not show any increased levels of TIM3 expression either. However in the spleen sample analysed, TIM3 expressing B-cells were identified all be it as a minor proportion of cells.

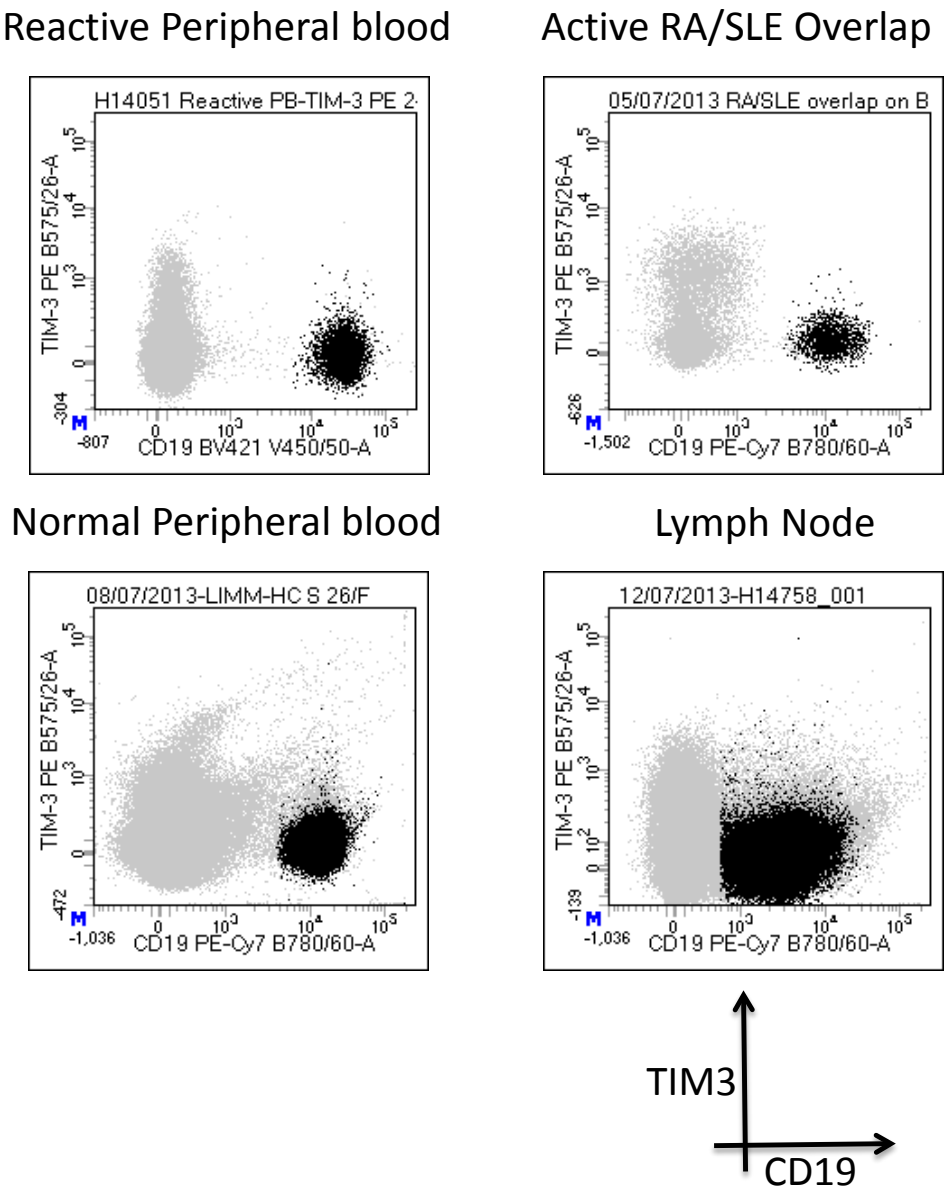

Figure 8.3-13 Lack of TIM3 surface expression on in vivo B-cells

Peripheral blood B-cells showing their surface levels of TIM3. Lymphocytes were gated based on their scatter profile are shown in grey and B-cells were gated based on their co-expression of CD19 and CD20. Expression pattern in a lymph node which is representative of the 4 lymph nodes analysed.

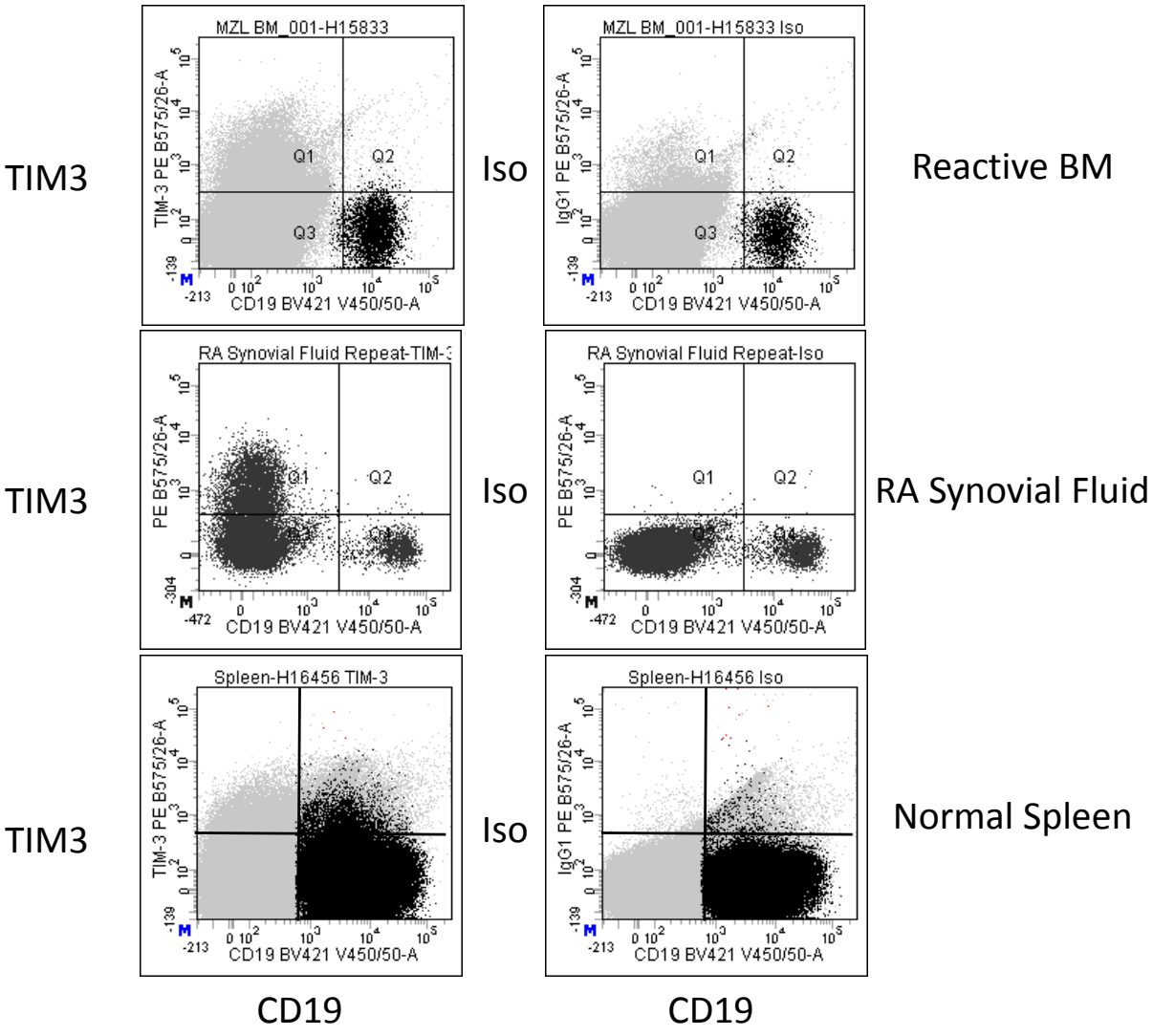

Figure 8.3-14 TIM3 expression by B-cells derived from various sites.

Lymphocytes are gated based on their scatter profile and B-cells were defined based on their co-expression of CD19 and CD20. Lymphocytes are denoted by grey colour and B-cells by black colour except row 2 where all lymphocytes are coloured black. Low levels of TIM3 expressing B-cells were detected in spleen but not in reactive bone marrow or RA synovial fluid.

The various B-cell neoplasms represent different stages in a B-cell life cycle. Therefore TIM3 expression by B-cell neoplasms was sought to identify the closest B-cell stage that expresses TIM3. 12 bone marrow samples from different B-cell neoplasms including follicular lymphoma, chronic lymphocytic leukaemia, mantle cell lymphoma, marginal zone lymphoma and plasma cell neoplasia were analysed. Other pathologies affecting the bone marrow like myelofibrosis and myelodysplastic syndromes were used as disease controls. The cells were stained with CD24 FITC, TIM3 PE, CD4 PerCP-Cy5.5, CD38 PECy7, CD19 BV421, CD27 BV605, LAIR1 AF647 and CD20 APC-H7 after RBC lysis with ammonium chloride. Live cells were gated based on their scatter profile and CD4 was used as a negative marker. Out of the B-cell neoplasms affecting the bone marrow only marginal zone lymphoma (MZL) showed positive TIM3 expression. The level of MZL cells in bone marrow did not correlate with TIM3 positivity as shown in Figure 8.3-15.

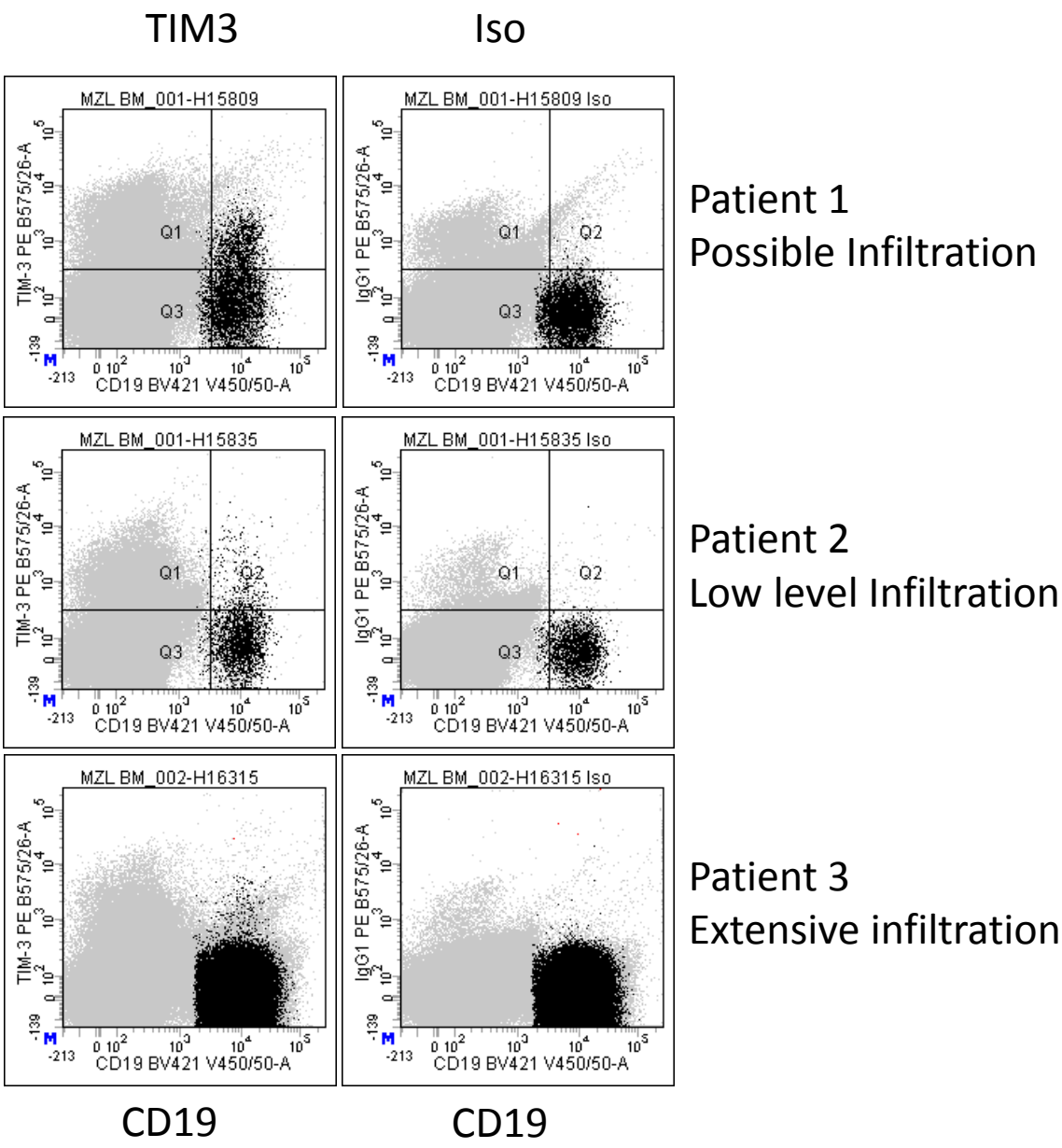

Figure 8.3-15 TIM3 expression on bone marrow marginal zone lymphoma B-cells

Bone marrow samples from 3 patients with varying levels of marginal zone lymphoma involvement of the bone marrow. Lymphocytes are gated based on their scatter profile and B-cells were defined based on their co-expression of CD19 and CD20. Lymphocytes are denoted by grey colour and B-cells by black colour

While these data suggested that TIM3 expression was not a common feature amongst reactive or neoplastic B-cells, this needs to be viewed in the context of the transient nature of the B-cell activation state at which TIM3 expression is maximally observed in vitro. CD30, the other marker co-expressed in activated B-cells, though readily detectable amongst a sub-population of large activated B-cells by immunohistochemistry is not readily identified in most reactive conditions tested by flow cytometry. Equally CD30 is only expressed by a subset of B-cell neoplasms in the context of diffuse large B-cell lymphomas and classical Hodgkin lymphoma. Thus a logical further extension of this work will be to examine a range of reactive lymph nodes and suitable neoplasms for TIM3 expression by immunohistochemistry.

8.3.7 Effect of TIM3 ligand galectin9 on B-cell differentiation

The effect of TIM3 has been extensively studied in T-cells. Stimulation of TIM3 on T-cells with galectin9 leads to apoptosis and cell death. However the role played by TIM3 on B-cell differentiation is not known. Since TIM3 is transiently expressed during B-cell activation and certain malignancies, targeting TIM3 might prove to be a therapeutic option in B-cell mediated autoimmune conditions and malignancies. Therefore, the in vitro effect of galectin9 on B-cell differentiation was studied.

Galectin-9 had a very narrow active to toxic window. Doses of 10-25 nM of recombinant human galectin-9 (R&D systems) had minimal to no effect on viability of cells whereas the 50 nM dose used to modulate T-cells killed the majority of cells. Cell counts were obtained by flow cytometry using countbright beads (Invitrogen) after excluding dead cells with propidium iodide stain. Blocking (Clone 2E2) or agonistic TIM3 antibody (Clone 5D12) on day 3 did not have any effect on viability at 24 hours. Galectin-9 at 50 nM dose was toxic to cells at 24 hours which was not blocked by Anti-Galectin9 or anti-TIM3 antibody. The effect of galectin-9 for 24 hours on viability of B-lineage cells was similar up to day 11 of B-cell differentiation. Most cells have differentiated to plasmablasts or plasma cells by day 10 which do not express TIM3. Therefore, the effect of galectin9 is likely to be non-specific toxicity and not mediated via TIM3. However it should be noted that there has been previous debate in the literature regarding the efficacy of the R&D Galectin-9 used (93), and an alternate source of Galectin-9 would need to be evaluated to address this question further.

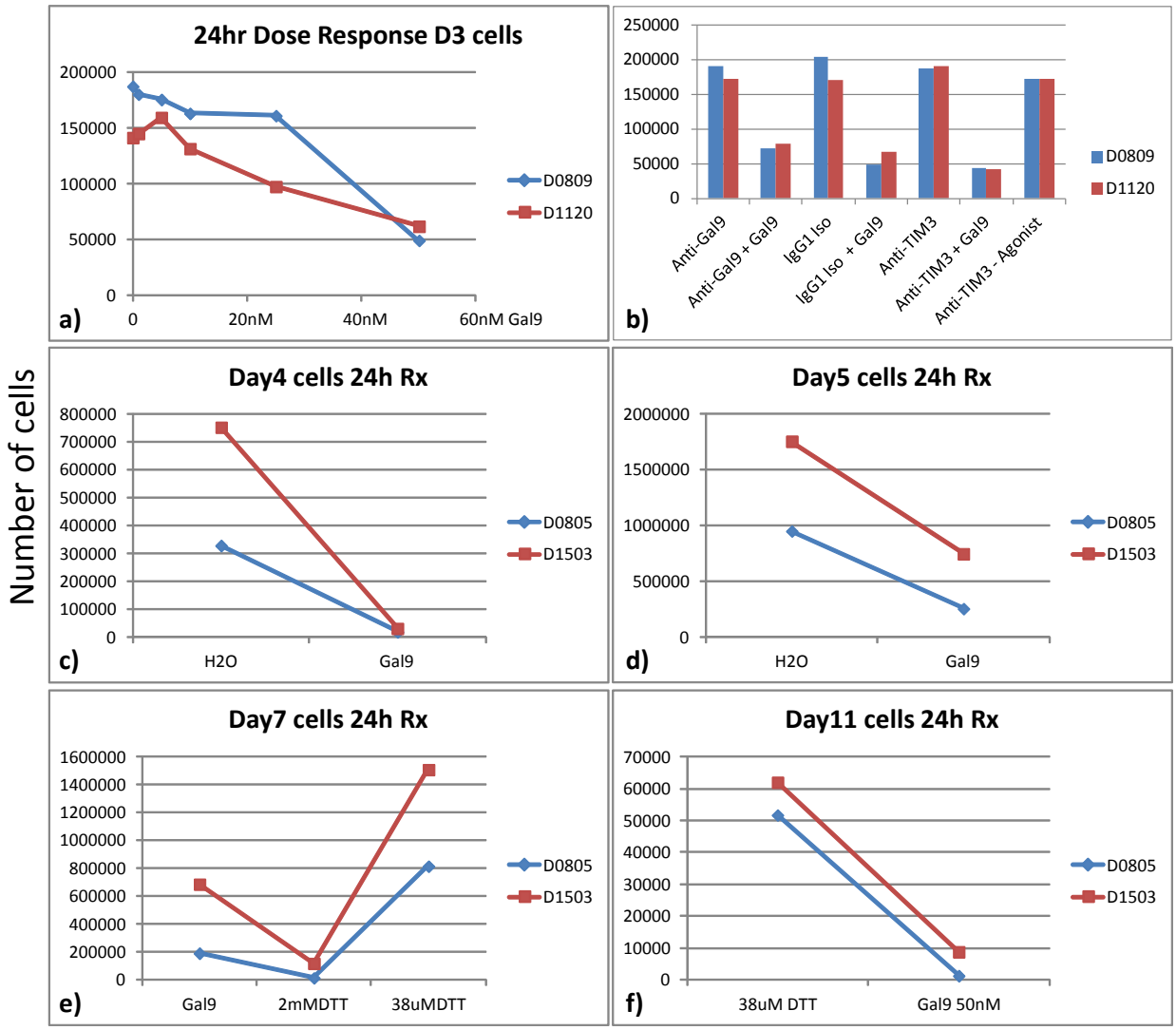

Figure 8.3-16 Effect of TIM3 ligand galectin9 on B-cells during various stages of B-cell differentiation

a) Effect of galectin-9 treatment for 24 hours on day 3 B-cells on viability at the concentrations indicated on the X-axis.

b) Effect of galectin-9 treatment for 24 hours on day 3 B-cells on viability in combination with anti-TIM3 or anti-Gal9 antibody as well as the antibodies without Gal9.

c-f) Effect of galectin-9 treatment for 24 hours on day 4, 5, 7 and 11 cells on viability. DTT – Dithiothreitol. Live cells were counted by flow cytometry using countbright beads (Invitrogen) and dead cells were excluded with propidium iodide staining.

8.4 Alterations in memory B-cell subsets during immune response to seasonal influenza vaccination

The memory B-cells are heterogeneous in steady state, while during in vitro differentiation the entire B-cell population changes as a whole. However, during an immune response in vivo whether there is predominance of certain subsets is not known. The changes in subset distribution pattern during an immune response can provide vital information regarding the functional relevance of the different subsets. The in vivo monitoring of relapse-associated memory B-cell subset seen in RA patients during relapse is challenging. The immune response can predate clinical symptoms and can be difficult to predict. Immune responses generated due to intercurrent infections and other inflammatory processes can also alter memory B-cell subsets. Immune responses to infections are also difficult to study due to the heterogeneity caused by varying levels of severity and different types of infections. Vaccination can induce an immune response in a controlled fashion, which should generate a similar immune response in the vacinees. Seasonal influenza vaccination is offered routinely to NHS staff and university staff in autumn in the UK. This opportunity was used to monitor the B-cell subsets in 6 controls in 2 different experiments.

8.4.1 Plasmablast response following influenza vaccination

The memory B-cell subsets were evaluated before and at serial time points following the vaccine. All the controls have had the flu vaccine the year before and therefore the immune response is likely to be a mixture of primary and secondary immune response. However the antigens in the flu vaccine are altered on a yearly basis and therefore likely to induce more of a primary immune response depending on the degree of change from the previous year. B-cells were analysed at baseline, days 1, 6 and 13. All of the vaccinated controls made an immune response to the vaccine as evidenced by the increase in absolute plasmablast count on day 6. 2 controls had a weak response (<2-fold increase in plasmablast count between day 0 and day 6). The other 4 controls had more than 7-fold increase in plasmablast count. The plasmablast response resolved to pre-vaccination levels in a week from the peak levels on day 6 in all except one control. If the absolute plasmablast count at day 6 is considered as the only criteria for response irrespective of the base line levels, the 6 controls segregate into 3 groups: Low (less than 4000 cells/mL), Moderate (4000-10000 cells/mL) and Good (>10000 cells/mL) responders.

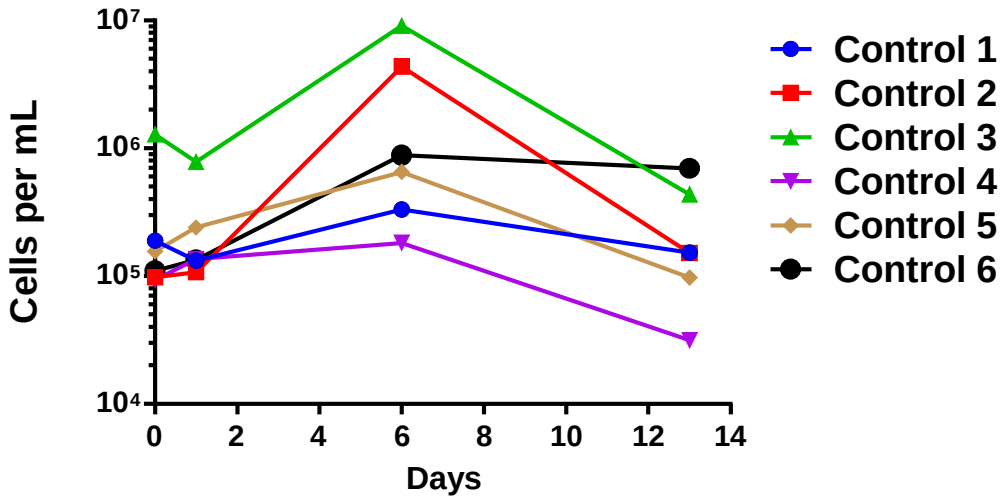

Figure 8.4-1 Plasmablast numbers peak on day 6 following influenza vaccination

Plasmablasts (defined as $CD19^{+}CD20^{-}CD27^{++}CD38^{++}$) in the 6 controls on the days specified on the X-axis following influenza vaccination. The absolute counts were derived using dual-platform methodology using the mononuclear cell counts by Sysmex haematology analyser.

8.4.2 Correlates of poor plasmablast response following influenza vaccination

The proportion of the 16 memory B-cell subsets as a percentage of memory B-cells and their absolute count was monitored sequentially following the vaccination of 6 healthy controls. Peripheral blood B-cells were stained with antibodies given in Table 5.2-3 (Version 2) after RBC lysis with ammonium chloride. Memory B-cells were defined as CD19, CD20 and CD27 positive and further sub-classified as per the gating strategy demonstrated in Figure 5.2-6. 4 out of 6 controls showed an increase in proportion of 24-84-95+LR1- subset after vaccination prior to plasmablast response but their absolute count remained stable. 3 out of 4 controls who showed this pattern of response had a decrease in the absolute count of the usually dominant 24+84+95-LR1+ subset. In control 2 the decrease in absolute count of 24-84-95+LR1- subset is accompanied by an increase in its relative proportion. This is likely to be due to the absolute counts of the other subsets decreasing much more than the 24-84-95+LR1- subset. This suggests that the increase noted in the proportion of relapse-associated memory B-cell subset post vaccination is due to the decrease in the numbers of usual dominant subset. This relative change in proportions was not universal since control 6 showed a mild decrease in proportion and absolute count of the 24-84-95+LR1- subset.

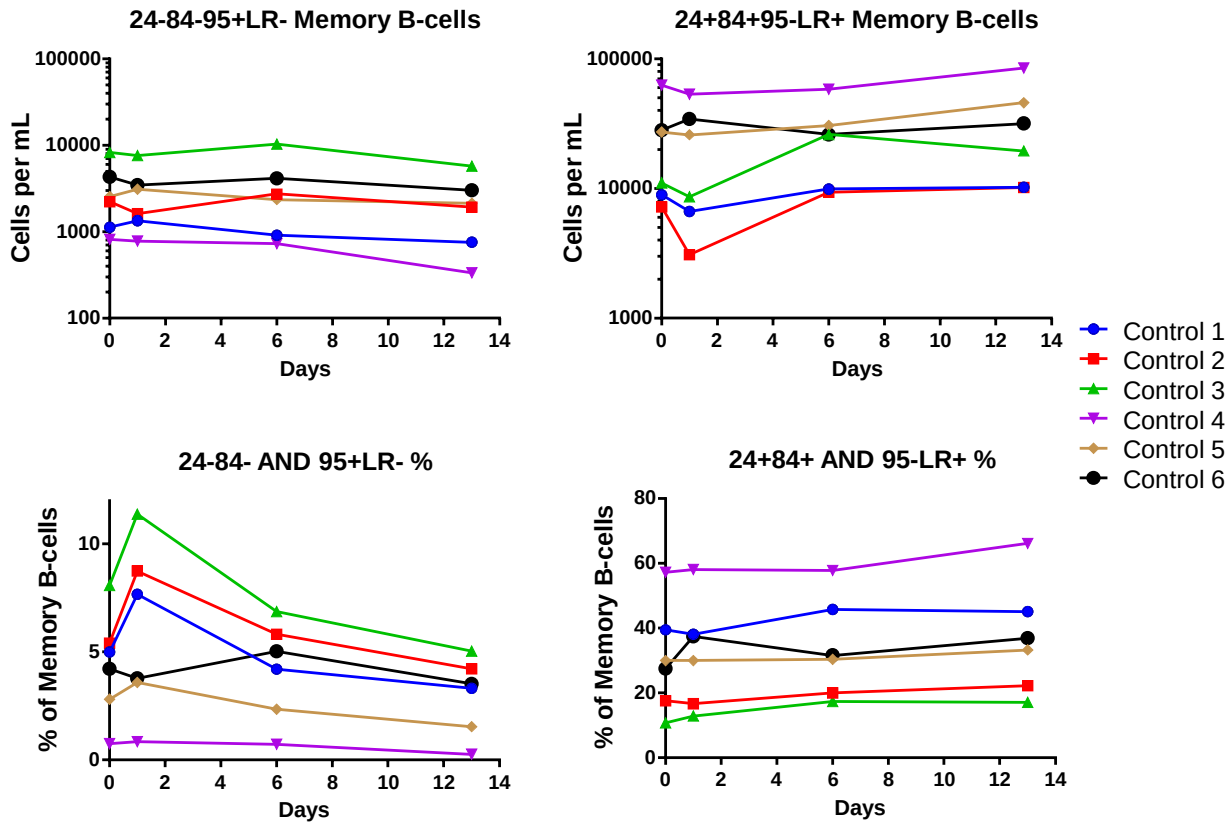

Figure 8.4-2 Sequential change in proportions and absolute numbers of the 2 key memory B-cell subsets during immune response to influenza vaccination

The sequential change in absolute cell counts (logarithmic scale) and percentages of 24-84-95+LR1- and 24+84+95-LR1+ memory B-cell subsets in 6 controls are shown. Memory B-cells were gated based on their lymphocyte scatter profile and $CD19^{Pos}CD20^{Pos}CD27^{Pos}$. The subsets were then defined based on the above markers. Detailed gating strategy is provided in Figure 5.2-6.

The sequential change in proportion of each of the 16 subsets was analysed and the results are shown in Table 8.4-1. To decide whether that particular subset is showing an increase or decrease prior to plasmablast response arbitrary criteria were used – half or more than half of the samples showing an increase or decrease of 2 fold or more.

Table 8.4-1 Changes in the proportion memory B-cell subsets during an immune response to seasonal influenza vaccination

The 16 memory B-cell subsets are classified into 3 groups based on whether their relative proportions increase, decrease or static before the plasmablast response. An arbitrary criteria of the change in proportion of more than 2 fold between base line and before plasmablast response in 3 or more samples was used to determine whether there was increase or decrease of that particular subset.

Increase in Percentage	Decrease in Percentage	No change in Percentage
24+84-95-LR-	24+84-95+LR-	24+84-95-LR+
24-84-95+LR-	24+84-95+LR+	24+84+95-LR-
24-84-95+LR+	24+84+95+LR-	24+84+95-LR+
24-84-95-LR-	24+84+95+LR+	24-84+95+LR-
24-84-95-LR+		
24-84+95+LR+		
24-84+95-LR-		
24-84+95-LR+		

Changes in the various subsets seen in the table suggest some of the subsets might have a similar propensity and can be consolidated into fewer subsets with similar changes in proportions post vaccination. All subsets with CD24 negative memory B-cells show an increase in proportion except one whereas the subsets with CD24 positive memory B-cells show a decrease or no change in proportion following vaccination before the plasmablast response. The proportion of CD24 and CD95 dual-positive memory B-cells decreases prior to plasmablast response.

The fold increase in plasmablast count between day 0 and day 6 has a positive correlation with the proportion (Spearman's correlation coefficient (r) =0.429, p=0.420) and absolute count (r=0.543, p=0.297) of relapse-associated memory B-cell subset at baseline which did not reach statistical significance. The baseline proportion (r=-0.771, p=0.103) and absolute count (r=-0.371, p=0.497) of usual dominant subset showed negative correlation, which was not

statistically significant. Lower relapse-associated memory B-cell count of less than 2000 cells/mL and higher usual dominant memory B-cell percentage of more than 30% was associated with a weak plasmablast response.

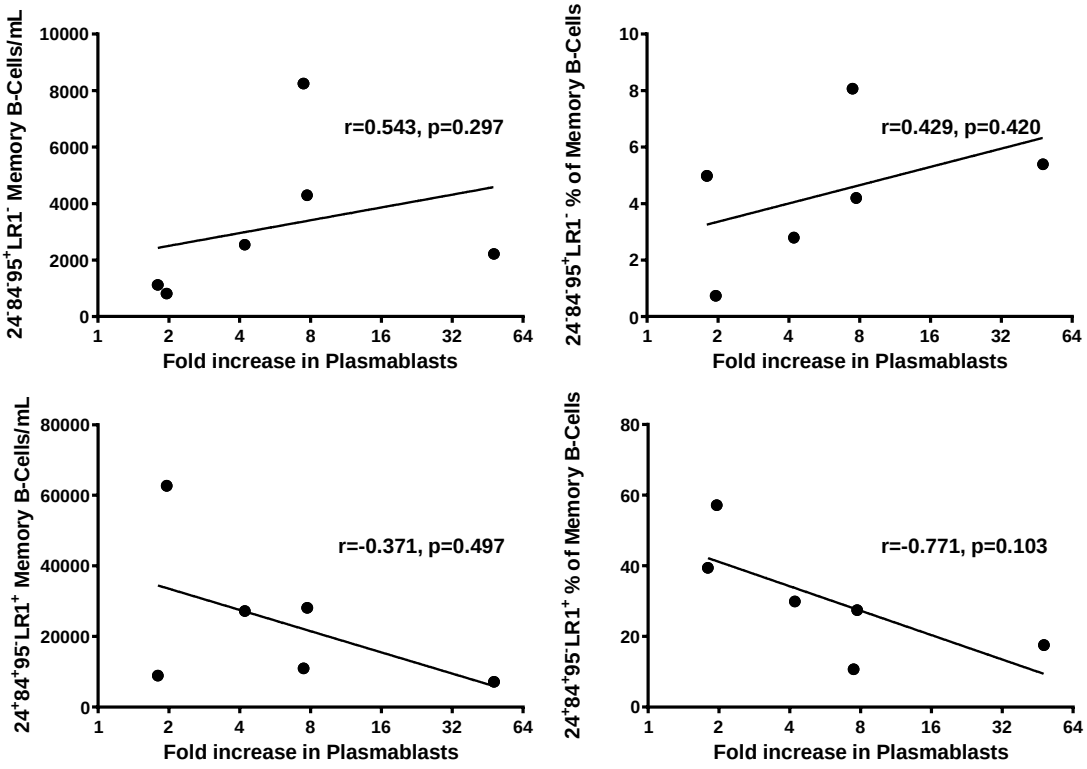

Figure 8.4-3 Correlation of baseline parameters with plasmablast response

Absolute counts (cells/mL) and proportion of the 2 key memory B-cell subsets (relapse associated and usual dominant subset) are represented on the Y-axis and the fold increase in plasmablast response between day 0 and day 6 represented on the X-axis. Plasmablasts were gated based on their scatter profile and $CD27^{High}CD38^{High}CD20^{Neg}CD19^{Pos}$. Fold increase in plasmablasts was calculated as ratio of absolute plasmablast count on day 6 / absolute plasmablast count on day 0. The Spearman's correlation coefficient (r) and p-value are given. There was a positive correlation with the proportion (r =0.429, p=0.420) and absolute count (r=0.543, p=0.297) of relapse-associated $24^-84^-95^+LAIR1^-$ memory B-cell subset at baseline which did not reach statistical significance. The baseline proportion (r=-0.771, p=0.103) and absolute count (r=-0.371, p=0.497) of usual dominant $24^+84^+95^-LAIR1^+$ subset showed negative correlation with plasmablast response which again did not reach statistical significance.

The analysis of correlation of the levels of the various memory B-cell subsets as well as the key B-cell subsets with the fold increase in plasmablast numbers between day 0 and day 6 is tabulated as below.

Table 8.4-2 Correlation of various baseline B-cell parameters with plasmablast response to influenza vaccination

Non-parametric spearman's test of correlation between the fold increase in plasmablasts between baseline and day 6 and the baseline parameters indicated in the first column.

	Spearman's Coefficient 'R'	P Value (two-tailed)
Transitional B-cell%	0.371	0.497
Naïve B-cell%	-0.429	0.419
Memory B-cell%	0.257	0.658
Plasmablasts %	0.029	> 0.999
Transitional B-cell Count	0.600	0.242
Naïve B-cell Count	-0.257	0.658
Memory B-cell Count	0.086	0.919
Plasmablasts Count	-0.200	0.714
24+84-95+LR- %	0.029	> 0.999
24+84-95+LR+ %	0.314	0.564
24+84-95-LR- %	0.371	0.497
24+84-95-LR+ %	-0.200	0.714
24+84+95+LR- %	0.200	0.714
24+84+95+LR+ %	0.200	0.714
24+84+95-LR- %	0.200	0.714
24+84+95-LR+ %	-0.771	0.103
24-84-95+LR- %	0.429	0.419
24-84-95+LR+ %	0.886	0.033
24-84-95-LR- %	0.886	0.033
24-84-95-LR+ %	0.714	0.136
24-84+95+LR- %	0.543	0.297
24-84+95+LR+ %	0.543	0.297
24-84+95-LR- %	0.714	0.136
24-84+95-LR+ %	-0.200	0.714

8.5 Summary and discussion

The purpose of this chapter was to investigate the function of the different memory B-cell subsets and plasmablasts in vitro and in vivo to better delineate potentially relevant autoreactive populations in RA.

ACPA secretion by flow sorted peripheral blood plasmablast was not detectable by ELISpot, the cause for which could be multifactorial. The cell numbers were too low and beyond the sensitivity of ELISpot. The functional ability of the cells might be impaired due to the sorting process and need time to recover or their viability has been affected. The potential reasons could be the mechanical stress experienced by the cells during the sorting process, stimulatory or inhibitory effects of the antibodies used for sorting and the azide content in the antibodies.

The problem with cell numbers could be overcome by pooling samples from multiple patients which is not ideal. Density centrifugation which removes granulocytes cannot be used when plasmablasts need to be preserved. The ammonium chloride lysed sample retains granulocytes which increase the cell count many fold and reduces the sort efficiency and prolongs the sort duration. The other option is to enrich the sample for B-cells by magnetic selection before flow sorting. However, this option is not suitable for plasmablasts due to weaker expression of CD19 and presence of exclusion markers in the negative selection kits. The mechanical stress to cells during sorting could be reduced by using a larger bore nozzle but it affects purity. The cells could be allowed to recover for a set period of time in vitro following the sorting process and then subject to functional assays. If the antigen specificity of the cell is the only parameter to be assayed, then the sorted cells could be expanded in vitro before further analysis. However culture techniques need to be validated and optimised for such low numbers of cells and the effects of flow sorting need to be accounted for as well.

ACPA secretion by plasmablasts generated in vitro from naïve B-cells of RA patients was not detectable by ELISpot. This could be due to the sensitivity of the assay or lower frequency of CCP-specific cells within the naïve B-cells. The lack of a positive control for ACPA secreting cells reduces the confidence in negative findings from this assay. The anti-IgG coated wells were able to detect IgG present in the serum in an ELISA like fashion but not able to detect ACPA which again raises the sensitivity issue for ACPA ELISpot. The IgG detection has a signal amplification step using biotinylated anti-IgG followed by strep-HRP. Since CCP is immobilised

to the plate with streptavidin, the ACPA detection uses directly HRP conjugated anti-IgG and therefore lacks the amplification.

The detected IgG secretion from in vitro generated plasmablasts derived from naïve B-cells is due to class-switching occurring in the in vitro differentiation system but is not clear whether this is confined only to RA patients since the experiment did not have any non-RA controls. The other possibility is that there are IgG positive B-cells within the sorted CD27 negative B-cells since RA patients are known to have increased proportion of 27^- IgD^- B-cells (70). In that study, other isotypes apart from IgD were not checked and might also include surface immunoglobulin negative B-cells. This could be further evaluated by surface phenotyping of the RA B-cells with antibodies against all immunoglobulin isotypes and CD79b.

B-cells have been shown to secrete proinflammatory and regulatory cytokines following stimulation (95). In the past non-physiologic mitogenic stimuli have been used which may not be a true reflection of the events in vivo. Cell lines have been used as well which again is not ideal. Further studies mimicking physiological stimuli with primary B-cells have shown secretion of TNF, LTA, IL6 and IL10 by activated B-cells (96). The cytokines were detected in the supernatant but the cells were not followed during their differentiation in those studies to assess at what stage the secretion starts and how long into their differentiation it continues. There were no definitive phenotypes identified for the B-cells that secreted these cytokines. Secretion of the chemokine receptor ligands by B-cells have not been studied in the past except for CCL2 (97), CCL3 (98).

TNF plays a key role in RA pathogenesis as evidenced by the good clinical response to anti-TNF therapy (99). The B-cell derived LTA and TNFA have been shown to be involved in development of B-cell follicles (100) and follicular dendritic cells (101). AIF1 has been shown to be elevated in RA synovial fluid compared to osteoarthritis and induces IL6 production by synovial fibroblasts and PBMCs (102). AIF1 gene polymorphisms have been shown to be associated with active form of RA (103). High levels of MMP7 expression has been shown in rheumatoid nodules and is associated with early onset disease (104). These published studies have shown evidence of secretion of inflammatory mediators such as AIF1 and MMP7 in the context of RA but interestingly findings from this chapter are consistent with these mediators generated during normal B-cell differentiation. Therefore, activation of B-cells in a specific or non-specific fashion could trigger a proinflammatory milieu. The secretion of proinflammatory

mediators is transient during the B-cell differentiation. Therefore treatment strategies targeting certain stages of differentiation rather than the whole B-cell compartment might be a better option for some patients particularly if the B-cells with regulatory properties could be preserved.

Multiple chemokine genes show an increase in expression levels during the stage of B-cell differentiation that is closest to the phenotype of relapse associated memory B-cell subset. Although gene expression does not always translate to protein, the chemokine ligands could contribute to the establishment of an inflammatory cell milieu within the joints in RA. CCR2, the receptor for the CCL2 secreted by B-cells is known to be elevated and more responsive in RA neutrophils (105). CCL3, also known as MIP1α (Macrophage Inflammatory Protein) is known to be elevated in RA synovial fluid (106) and is associated with susceptibility to RA based on genome-wide haplotype association analysis (107). CCL17, which is a potent chemoattractant of T-cells is elevated in synovial fluid of RA patients (108). CCL22 has been shown to be increased in plasma and synovial fluid of RA patients compared to controls (109). CXCL9 and CXCL10 are sensitive markers of disease activity (110) and CXCL10 polymorphism has been shown to be associated with extra-articular manifestations in RA (111).

The secretion of proinflammatory cytokines and chemokines is confined to certain stages during B-cell differentiation which has not been studied in detail before. Surface markers of this particular stage such as CD30 and TIM3 were identified by gene expression analysis and protein expression was detected by flow cytometry. However, the gene expression pattern for TIM3 obtained by the Illumina array needs to be confirmed further with real-time PCR. TIM3 protein expression needs to be confirmed with a different clone of antibody although the F38-2E2 clone used in this study has been used in published literature (112). The protein expression also needs to be confirmed by a different technique such as western blot. CD30, also known as TNFRSF8 is a member of the TNF-receptor superfamily and was originally described as a marker of Reed-Sternberg cells in Hodgkin's lymphoma. It is expressed by virus-infected lymphocytes, lymphoid neoplasms and subsets of activated B and T-cells (113). Stimulation or overexpression of CD30 can drive downstream NFκB activation through recruitment of TRAF2 and TRAF5 (114). If B-cells at the stage when they express CD30 play a key role in RA pathogenesis by secretion of proinflammatory mediators and chemoattractants, therapeutic strategies to target this stage is feasible with already available naked or conjugated monoclonal anti-CD30 antibodies which have been through clinical trials in Hodgkin's lymphoma (115).

There are 3 members of the TIM (T-cell Immunoglobulin domain Mucin domain) gene family in humans, TIM-1, TIM-3 and TIM-4 which have been linked with regulation of immune responses and disease processes such as autoimmunity and asthma (116). TIM3 was identified as a negative regulator of T-cell response in terminally differentiated T-cells. In humans, only 1-2% of CD8 T-cells and none of the CD4 T-cells express TIM3 in peripheral blood but activated T-cells in lymph nodes express TIM-3 albeit at low percentages which increases to 25% on stimulation (117). TIM-3 is predominantly expressed by TH1 and TH17 cells, and mediates regulation of cytokines such as IL2, IL6, IL17 and IFNγ at the transcriptional level. TIM-3 is also expressed by a variety of cells involved in the innate immune response including NK cells, monocytes, macrophages, dendritic cells, mast cells and endothelial cells, and mostly functions as an inhibitory receptor (118). However, in certain circumstances it can lead to activation of cells such as macrophages during mycobacterial infections (119).

Synovial tissue from RA patients express higher levels of TIM-3 mRNA compared to osteoarthritis, and lower levels of Gal-9 mRNA in the peripheral blood mononuclear cells compared to controls (120). The proportion of TIM-3 positive T-cells and NK cells correlates negatively with disease activity in RA (121). Therefore, TIM-3 has been proposed as a therapeutic target in RA. Most of the studies have concentrated on T-cells and TIM-3 expression B-cells has not been explored as it is not expressed by resting B-cells. However, TIM-3 can be detected following B-cell activation in vitro (Figure 8.3-9) and in other secondary lymphoid organs (Figure 8.3-14). Since, TIM-3 has both regulatory and stimulatory properties, its role in B-cells cannot be extrapolated from its role in T-cells without further evaluation.

TIM3 ligand galectin-9 has been shown to regulate murine T-cells by induction of apoptosis (122). Human CD4 T-cells are also susceptible to galectin-9 induced apoptosis at 50nM concentration and the susceptibility is reduced in RA (123). The galectin-9 induced apoptosis was not specific when tested as evidenced by the inability to block the effect with anti-TIM-3 or anti-Galectin-9 antibodies (Figure 8.3-16). The noted cell death is unlikely to be mediated through TIM-3 since the susceptibility continued even after loss of TIM-3 expression. The negative result is likely to be due to the differences in Galectin-9 sourced from R&D systems since another study performed with the same Galectin-9 found a similar lack of specificity in T-cells (93).The other studies used in-house recombinant proteins or Galectin-9 sourced from GalPharma. However, the role of TIM-3 in apoptosis in human T-cells remains unclear, since

TIM-3 antagonistic antibodies did not alter the proliferation or survival of human T-cells (117). In the same study, blockade of TIM-3 ligand interaction with TIM-3-Ig fusion protein did not increase cytokine secretion in human T-cells. A recently published study has shown that CEACAM1 expressed on activated T-cells forms a heterodimer with TIM-3 and is required for T-cell inhibition (124), which might explain the differential effects of galectin-9 and TIM-3 antibodies. To understand the role of TIM-3 in B-cells further detailed evaluation is required with alternative galectin-9 and TIM-3 antibodies in conjunction with CEACAM1.

Influenza vaccination provides an excellent opportunity to study the immune response in a controlled fashion. The immune response, particularly the response of the B-lineage cells can be compared with the immune response during RA relapse. All the six controls tested showed a plasmablast response to the seasonal influenza vaccine. However, there was heterogeneity in the degree of response between controls with 2 controls showing less than 2-fold increase and the rest had greater than 7-fold increase in their absolute count. This was not dependant on the baseline plasmablast levels. The alternative way to assess the immune response would be to compare the levels of specific antibodies against the vaccine strain of influenza at baseline and at 4 weeks post vaccination in the serum. The options would be to source the vaccine proteins (Sino Biological Inc.) or use the influenza vaccine itself as the antigen to coat the ELISA plates which needs evaluation and optimisation.

This plasmablast response positively correlated with the baseline proportion and absolute count of the RA relapse associated CD24-CD84-CD95+LAIR1- memory B-cell subset. Although this did not reach statistical significance a larger sample size may be needed to observe significance with this correlation. The baseline proportion and absolute count of the usually dominant CD24+CD84+CD95-LAIR1+ memory B-cell subset showed a negative correlation, which again did not reach statistical significance. The lack of statistical significance could be due to the low sample numbers. CD24-84- memory B-cells showed a positive correlation with plasmablast response irrespective of the CD95 and LAIR1 expression. Some of the other subsets showed a better correlation than the relapse associated subset. This suggests that different subsets could be recruited during an immune response to influenza vaccination compared to relapse in RA and there might be heterogeneity within the RA patients as well.

Memory B-cells as percentage of total B-cells or the absolute count at baseline were less predictive of the plasmablast response than the subsets. This suggests that the heterogeneity

noted within the memory B-cells based on the surface expression of CD24, CD84, CD95 and LAIR1 transfers to a functional level and different subsets have a distinct functional role as noted in the case of influenza vaccination.

There was an increase in the proportion of the RA relapse associated CD24-CD84-CD95+LAIR1- memory B-cell subset following influenza vaccination. However the increase in proportion is not accompanied by an increase in absolute counts, which raises the suspicion that the noted increase in proportion is due to decrease in absolute counts of the other subsets. Indeed, there was a decrease in the absolute count of the polar opposite CD24+CD84+CD95-LAIR1+ memory B-cell subset in the same time frame. This could be due to the recruitment of the usually dominant CD24+CD84+CD95-LAIR1+ memory B-cell subset into sites of immune response such as the secondary lymphoid tissues with vaccination, or the synovium in RA. This pattern of change in memory B-cell subsets needs to be confirmed in more subjects since it was not consistent in all donors. However, there are alternative explanations for the decrease such as increased cell death and decay. The way to address this would be to sample the lymphoid organs such as lymph nodes and bone marrow at baseline and post vaccination to assess the changes in proportion of the memory B-cells at these sites. It is interesting in the context of such a model to note that it is the baseline levels of CD24-CD84-CD95+LAIR1- subset that correlates with evidence of an active plasmablast response to vaccination.

The recruitment of autoreactive memory B-cell subsets into the secondary lymphoid structures accounting for the skewing of the subset distribution is supported by the presence of follicular structures resembling germinal centers in RA synovium. The ectopic lymphoid structures in the synovium are surrounded by ACPA secreting PCs (10). The skewing of memory B-cell subsets seen during RA relapse could be due to the recruitment of usual dominant subset into or egress of the relapse associated subset from the synovial lymphoid structures. The study of synovial fluid was unwieldy with most samples lacking B-cells. This could be addresses further by evaluation of B-cells from synovial biopsies rather than from the fluid.

In RA, it is difficult to monitor the changes in memory B-cell subsets due the unpredictable nature and lack of control over the immune response, which could also be altered by the concomitant use of corticosteroids and other immunosuppressants. Although it could be speculated that the increase in proportion of the CD24-CD84-CD95+LAIR1- subset in RA during relapse is due to the recruitment of CD24+CD84+CD95-LAIR1+ subset into the sites of

inflammation and secondary lymphoid tissues, whether the response of memory B-cells would be similar in case of vaccination and RA is questionable. However, this suggests that change in the proportion of memory B-cells is indicative of an ongoing inflammatory response. Therefore, in RA even if the CD24-CD84-CD95+LAIR1- subset does not contain the autoreactive or pathogenic B-cells, it is still a useful marker of disease activity and relapse.

Since, there are limitations in studying the immune response in vivo, optimisation of in vitro methods becomes crucial.

In summary, the memory B-cell subsets that are skewed during relapse post-rituximab in RA could contain the autoreactive B-cells and might also play a role in pathogenesis by secretion of proinflammatory mediators but needs further work to confirm this.

9 Fourth Results Chapter: Novel mode of B-cell regulation

The study of plasma cells in vivo requires bone marrow sampling which is of considerable morbidity to patients and controls. Therefore, in vitro methods of PC generation would allow their study in details and also allow their manipulation. One of the restrictions in studying the antigen-specific cells was their low frequency. This could potentially be overcome by expansion of the cells in vitro and the antigen specificity could be inferred from the antibodies secreted by the cells of interest on differentiation to PCs. Therefore, in vitro modalities of generating PCs are vital for this study.

Multiple B-cell abnormalities have been described in RA and the initial aim was to test whether there is a significant difference in generation of PCs from B-cells in RA and controls. When negatively selected B-cells from RA patients were differentiated in vitro, there was an unexpected 15 to 80-fold expansion of non-B lineage cells at the stage of plasmablast to PC transition (Figure 9.1-1). There were adaptations made to the standard differentiation protocol in terms of cell densities and plate size to enable the assay to be performed with reduced cell numbers and thereby reducing the amount of blood required from the patients and also enables assessment of patients with reduced B-cell count. Since this was noted only very rarely when the other researchers were performing the assay with healthy controls, it was not clear whether this phenomenon was specific to RA B-cells or due to alterations to the standard protocol. Although this could be an in vitro artefact it was imperative to understand the cause for this expansion to devise strategies to avoid the expansion of non-B lineage cells at later time points in the culture.

Albeit rare, as it was noted in healthy controls as well, initially the changes in the culture conditions were evaluated as a cause for the expansion. On day 3 of the differentiation process the cells are removed from CD40L (mouse fibroblasts transfected with CD40L) and transferred to wells with nutrients and cytokines. It was hypothesized that due to the low density of B-cells and smaller sized wells there is a possibility of increased carry over of the CD40L fibroblasts causing the expansion. There was greater expansion of the non-B lineage cells when a 48 well plate was used instead of 24 well plate and this expansion could not be recapitulated by spiking the culture with CD40L transfected fibroblasts on day 3 (Figure 9.1-2). This excluded carry-over

of CD40L as the cause for the non-B lineage cell expansion. Since the expansion occurs between days 6 and 13, the change in culture conditions on day 6 such as addition of IFNα, IL6, IL21 and exposure to mouse stromal cell line M210B4 were suspected as a cause for the noted expansion. However, when negatively selected B-cells containing non-B cells were subjected directly to day 6 conditions, there was no expansion of the non-B lineage cells (Figure 9.1-3).

Further attempts were directed at identifying the phenotype of expanding cells and it was predominantly constituted by NK cells (Figure 9.2-2). Given the very high degree of expansion of the cells there remained a suspicion whether the NK cells could be derived from the cell population that was CD19 on day 6. B-cells can lose their CD19 expression on differentiation to PCs and therefore other surface markers are required to distinguish the CD19 low to negative plasmablasts and PCs from the NK cells. To address both these questions four cell fractions were sorted flow cytometrically based on CD19 and CD27 surface expression on day 6. This revealed that the expanding NK cells were predominantly derived from the CD19 and CD27 double negative cells on day 6 and CD27 negativity is a better marker on day 6 to identify these cells. Therefore, flow sorting the cells on day 6 based on CD27 could be used as a method to avoid the NK cell expansion.

Sorting of the day 6 cells for every experiment is practically not feasible due to restrictions in availability of the sorter facility only during weekdays and patient samples could not always be timed with the availability of the sorter. Therefore, if there was a component of the in vitro system that could be identified as the cause for NK cell expansion, this could be altered to circumvent this issue. The in vitro differentiation protocol (Figure 5.4-1) uses allogenic cells (mouse derived) at two stages – CD40L transfected mouse fibroblasts on day 0 and the mouse stromal cell line M2-10B4 on day 6. The use of TLR agonist instead of CD40L did not prevent NK expansion (Figure 9.3-2). The complete exclusion of M2-10B4 from the culture did not prevent it either. Therefore, the NK expansion was not due to the presence of allogeneic cells in the culture (Figure 9.3-3). This rules out the use of strategies such as using human recombinant CD40L and conditioned media from M2-10B4 cells to prevent the NK expansion. Double-purified B-cells and NK cells mixed at a ratio of 9:1 on day 0 led to NK expansion on day 10 which confirms that the expanding NK cells are derived from the contaminating day 0 NK cells Figure 9.3-3.

The NK cell expansion also had adverse effect on plasmablasts and PCs in the culture with marked reduction in their numbers (Figure 9.3-4). Although it could be speculated to be due to direct killing by NK cells it will need further detailed assessment with NK cell cytotoxicity assays to determine the reason. Due to the adverse effect on the PCs it is essential to devise strategies to prevent NK expansion.

It was hypothesized that if the mode of interaction between the B-lineage cells and NK cells could be identified, a simple strategy based on using a monoclonal antibody to block the NK cells could be employed to prevent the expansion. The stage at which the key interaction occurs need to be identified as well to deploy the preventive strategies. Freshly purified NK cells from the same donor did not expand when added to day 6 plasmablasts (Figure 9.4-1). This reveals that NK cells need prior priming for the expansion to occur. To test whether the B-NK interaction is contact dependant, the NK cells were cultured in transwells with and without B-cell contact (Figure 9.4-3). NK cells which were not in contact did not expand and this suggests that the interaction is contact dependant.

Blocking the contact dependent B-NK interaction is an attractive option to prevent the NK cell expansion if it can be achieved with monoclonal antibodies that are readily available. This would avoid the multiple purification steps required at baseline and flow sorting on day 6. If this B-NK interaction can be demonstrated to occur in vivo, it opens up the option of therapeutic targeting. Two pathways involved in B-NK interaction were evaluated. Peripheral blood NK cells can be expanded up to 1000-fold by stimulation with CD137L. However, blocking NK cells on days 3 and 6 with anti-CD137 antibody did not prevent the expansion (Figure 9.5-1). B-cells are known to express CD58 during activation and NK cells express CD2 which is involved in stable interaction by nano-tube formation. Antibodies blocking CD2 and CD58 were not able to prevent the expansion either (Figure 9.5-3).

NK cells are key players in immunity against viruses and therefore the possibility of viral contamination in the cultures which was accessible to the NK cells only after differentiation past the plasmablast stage was considered. EBV is known to be a latent virus inhabiting B-cells and enters lytic phase on plasma cell differentiation. Therefore, sample from a healthy control whose cells consistently showed this expansion was tested for EBV DNA by PCR and was positive (Figure 9.6-1 and Figure 9.6-2). It is interesting to speculate that EBV containing B-lineage cells are directly targeted and killed by NK cells particularly with IFNα support. However it would

require a large body of work to detect the various EBV proteins in multiple samples and demonstrate evidence of direct killing by NK cells. It can be proven to be primarily due to EBV by performing the experiments in parallel with EBV positive and negative donors. This was beyond the scope of this study and therefore was not pursued further and will be addressed in a future project.

If the NK cell expansion is primarily due to presence of EBV, it will pose a significant problem whenever there are contaminating NK cells on day 0 since the prevalence of latent EBV in the general population is estimated to be about 90%. Alternative purification methods were sought due to the failure to detect a molecular pathway that is amenable to blockade to prevent the NK expansion. The purification strategies were re-visited to improve the efficiency by using the reagents in excess as shown in Figure 9.7-1. The required purity on day 0 was achievable by modifying the cell selection process and additional positive selection with CD20 beads was used if the purity was less than 95%.

9.1 Strict purification required for In vitro differentiation of RA B-cells

Using the recently reported novel assay for the generation of long-lived PCs in vitro (60), the plan was to assess the perturbation in function of B-lineage cells in RA beyond autoantibody production. This method could also be used to expand the antigen-specific cells which are at low frequency to generate PCs and then analyse antigen-specificity by ELISA of supernatants or ELISpot as complementary to the other methods of direct detection of antigen-specific B-cells. Therefore, it is essential to be able to perform this assay on RA B-cells consistently.

9.1.1 Differentiation of B-cells from RA patients led to expansion of non-B lineage cells between day 6 to day 10 of the differentiation process

B-cells purified from 10 ml of peripheral blood from 3 RA patients were differentiated under standard protocol using CD40L, IL2, IL21 and BCR stimulus (Figure 5.4-1). The initial seeding concentration on day 0 was reduced to 250000 cells/well (one-fifth of standard concentration) to minimise the amount of blood sample required from patients. As an additional measure, 48 well plates were used instead of the standard 24 well plate. There was an unexpected proliferation of

non-B lineage cells (defined as annexin V, 7-AAD, CD19, CD20, CD38 and CD138 negative) between day 6 and day 13. The significant increase in percentage of non-B cells is unlikely to be an artefact due to decrease in the number of B-lineage cells as shown by the absolute count (obtained using countbright beads as described in methods section 5.2.2) in Figure 9.1-1. There was a 15-80 fold increase in the number of non-B cells between day 6 and day 13.

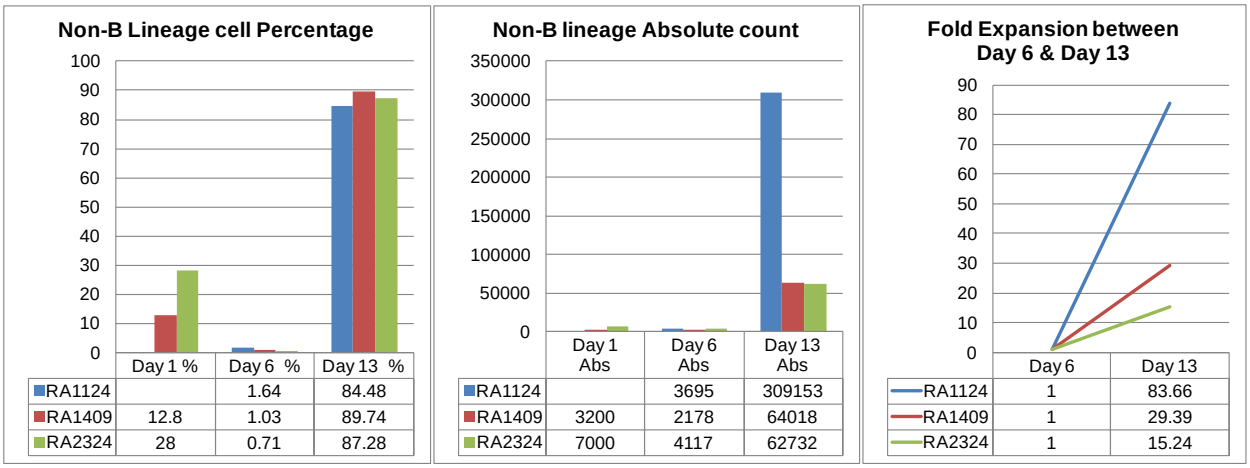

Figure 9.1-1 Expansion of non-B lineage cells between day 6 and day 13 of in vitro B-cell differentiation

The first graph shows the percentage of Non-B lineage cells (CD19 negative lymphocytes) within the cultures from 3 RA patients at different time points and the next graph shows their absolute numbers. The fold expansion was calculated as the number of non-B lineage cells at day 13 from a single well divided by the number of non-B lineage cells plated on to a single well on day 6. Live cells were identified based on negativity for annexin V and 7-AAD. The non-B lineage cells were identified as CD19 and CD20 dual negativity on day 0 and negative for CD19, CD20, CD38 and CD138 from day 6.

9.1.2 Expansion of non-B lineage cells is not due to carry over of CD40L cells from day 3

The contaminating cells (CD19 negative lymphocytes) observed in the RA derived B-cell differentiations limit the application of the assay and therefore attempts were made to resolve the issue. Of note similar expansions were observed on a sporadic basis in differentiations derived from healthy donors, with some bias to particular donors. Such expansion had also been observed occasionally by other researchers using the differentiation system, but were not a common event overall affecting in the region of 1/20 of all differentiations performed across multiple researchers in the same lab. Nonetheless given the observation in RA patients and the potential interest of the observation, this needed further investigation.

It was confirmed that the expansion of non-B lineage cells could be reproduced using media prepared by an independent experienced operator, excluding this as an explanation. The magnitude of expansion was higher with a 48-well plate compared to a 24-well plate and can be reduced by swapping from a 48 to a 24-well plate on day 6 (Supplementary Data Figure 14.1-4). Worsening of expansion with smaller sized wells is suggestive of an effect which is dependent on close contact. This could potentially be mediated by increased carryover of CD40L cells (plated on day 0) from smaller sized wells when cells are transferred to CD40L-free culture conditions on day 3.

Negatively selected peripheral blood B-cells from 2 controls were differentiated till day 3 according to the standard protocol in 24 or 48 well plates (Figure 5.4-1). To exclude carry over as a cause of the noted expansion, on day 3 the cells were plated on to wells coated with CD40L cells (mouse fibroblasts transfected with CD40L). 1%, 10% and 100% of the day 0 densities of CD40L cells were used. The starting proportion of non-B lineage cells (defined as annexin V, 7-AAD, CD19, CD20, CD38 and CD138 negative) on day 0 was 7.2% and 0.5% for D1503 and D2103 respectively. The absolute cell counts were assessed by flow cytometry using countbright beads (Figure 5.2-2). The expansion (measured as fold change from day 0 to day 10) seen with 48 well plate could not be recapitulated by using any of the 3 densities of CD40L cells between day 3 and day 6 in a 24 well plate. Therefore, the increased expansion of non-B lineage cells in a smaller sized well cannot be explained by interaction with CD40L cells between day 3 and day 6. The prolonged presence of CD40L also had a delaying effect on

differentiation of B-lineage cells like delay in upregulation of CD38 and persistence of CD30 (Data not shown).

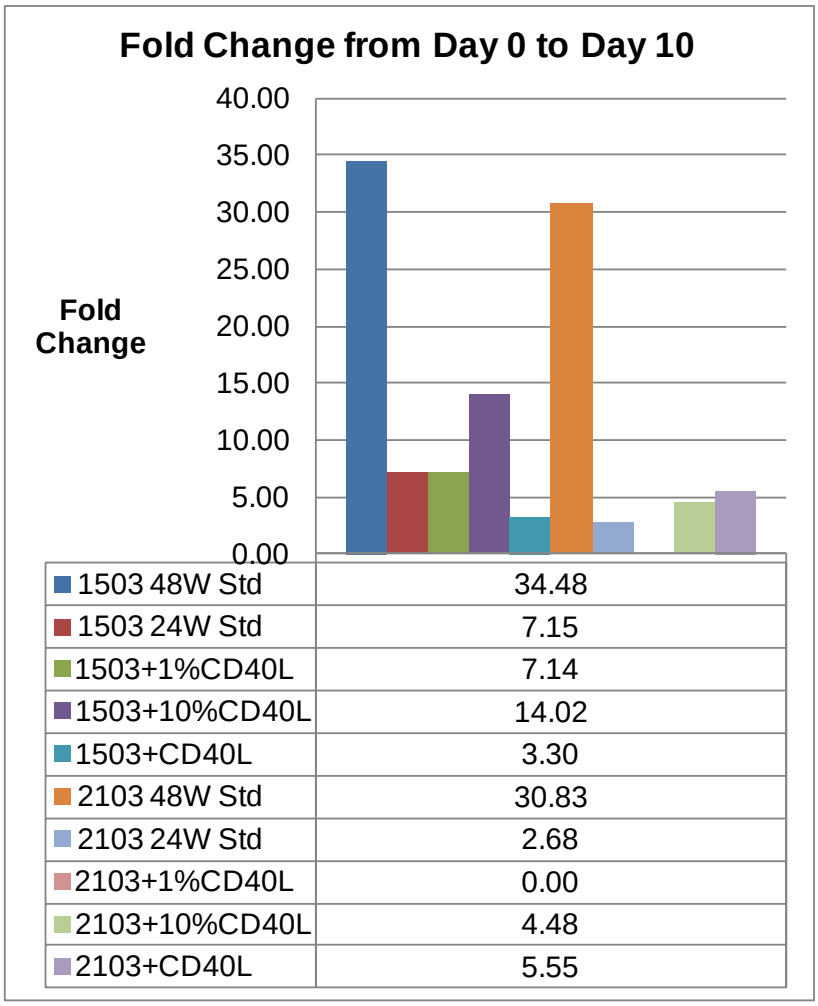

1503 48W Std	34.48
1503 24W Std	7.15
1503+1%CD40L	7.14
1503+10%CD40L	14.02
1503+CD40L	3.30
2103 48W Std	30.83
2103 24W Std	2.68
2103+1%CD40L	0.00
2103+10%CD40L	4.48
2103+CD40L	5.55

Figure 9.1-2 Effect of prolonged CD40L exposure on expansion of non-B lineage cells

Fold change in non-B lineage cells within the culture from 2 donors 1503 and 2103 shown which excludes prolonged CD40L exposure as a cause for non-B lineage cell expansion. 24W Std and 48W Std represent samples cultured throughout in 24 and 48 well respectively. +CD40L refers to addition of day 0 concentration of CD40L cells to the culture on day 3, and +1% and +10%CD40L represent addition of 1% and 10% of the day 0 concentrations. Fold change from day 0 to day 10 was calculated as (Number of cells on day 10 derived from a single day 0 well) **/** (Number of cells which started on day 0 in a single well). Live cells were identified based on negativity for annexin V and 7-AAD. The non-B lineage cells were identified as CD19 and CD20 dual negativity on day 0 and negative for CD19, CD20, CD38 and CD138 from day 6. The cell count was performed using countbright beads.

9.1.3 Non-B lineage cells do not expand when plated directly onto day 6 culture conditions

To assess whether the combination of cytokines, nutrients and the stromal cell layer used on day 6 can directly cause the expansion of non-B lineage cells, purified B-cells (with admixed non-B-cells) from 2 donors were plated directly on to day 6 culture conditions. The starting non-B cell percentage was 7.2% and 0.5% for D1503 & D2103 respectively. There was no expansion of non-B lineage cells which suggests the day 6 conditions such as IL6, IFNα, IL21 or the mouse stromal cells do not cause the observed expansion without prior activation.

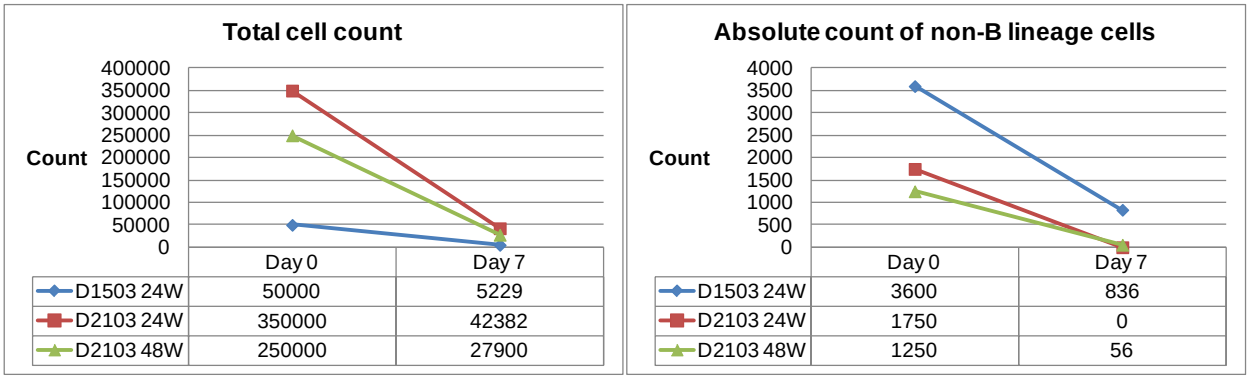

Figure 9.1-3 Culture of cells directly under day 6 conditions

Figures show the total cell counts and non-B lineage cell counts on day 0 and day 7 from a single well which were plated directly on to the day 6 conditions of the standard protocol (addition of IL6, IFNα, IL21 and the mouse stromal cells).

9.2 Identity of the contaminant population which expands between day 6 and day 10

When RA B cells were placed in the B differentiation assay that is known to generate PCs and maintain them in culture long-term, it was noted that the assay behaved in a different way to that seen with normal B cells. Specifically there was the emergence of predominant CD19 negative lymphocytes instead of B-lineage cells.

9.2.1 The contaminating cells were predominantly NK cells

Negatively selected peripheral blood B-cells from a healthy donor was differentiated using the standard protocol (Figure 5.4-1).The cultured cells were evaluated at baseline and at various stages of differentiation with a T-cell panel (CD45 APC-Cy7, CD16 PE, CD3 PE-Cy7, CD4 PerCP-Cy5.5, CD8 APC) used for routine diagnostic purposes at HMDS with additional CD19 Pacific Blue antibody to identify the expanding population as shown in Figure 9.2-1:

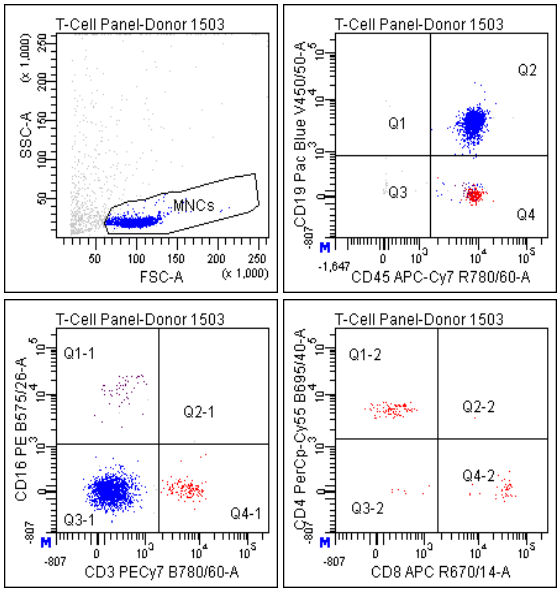

Figure 9.2-1 Gating strategy for analysing B-lineage, NK and T-cells

Mononuclear cells defined by their scatter profile were further sub-classified as below:

- B-lineage: CD19 +/wk, CD3- CD16- CD4- CD8-
- NK-cells: CD16+ CD3- $CD19^{Neg}$ CD4- CD8+/-
- T-cells: CD3+ $CD19^{Neg}$ CD16-

The cells expanding between day 6 and day 10 were predominantly constituted by NK cells and it was more than 90% of the expanding population in the experiment shown below.

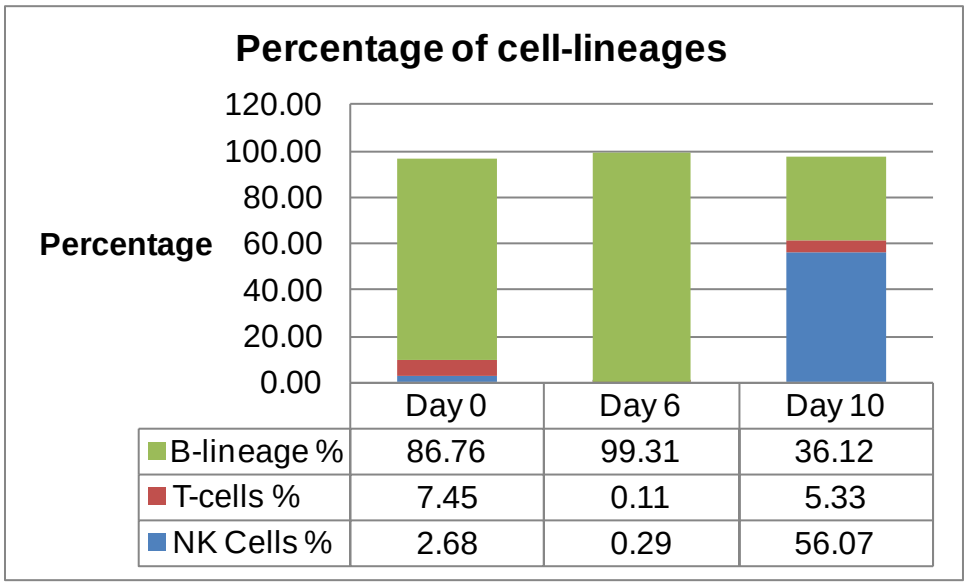

Figure 9.2-2 Identity of the expanding population between day 6 and day 10

Negatively selected B-cells from a healthy donor were differentiated using the standard protocol as shown in Figure 5.4-1. The proportion of various cell lineages identified using gating strategy described in Figure 9.2-1 at day 0, 6 and 10 of in vitro differentiation showing expansion of NK cells between day 6 and 10. The proportions provided for the different cell lineages are expressed as percentage of the live cells in the well. Green – B-lineage cells, Red – T-cells, Blue – NK cells.

Once the contaminating cells were identified to be predominantly NK cells, a specific antibody panel was developed which was used to identify the NK cells and other non-B lineage cell populations in future studies (Figure 5.2-7).

9.2.2 Sorting on CD27 expression at day 6 allows removal of contaminating non-B-cell populations.

There was a 50-100 fold expansion of non-B lineage cells between day 6 and day 13. Therefore, it was not clear whether the expanding CD19 negative population between day 6 and day 10 is derived from the cells that are CD19 positive or negative on day 6. Samples from two donors were stained with CD19PE and CD27 AF647 antibodies and flow-sorted into 4 populations based surface expression of CD19 and CD27 on day 6 on high speed Mo-Flo cell sorter as shown below.

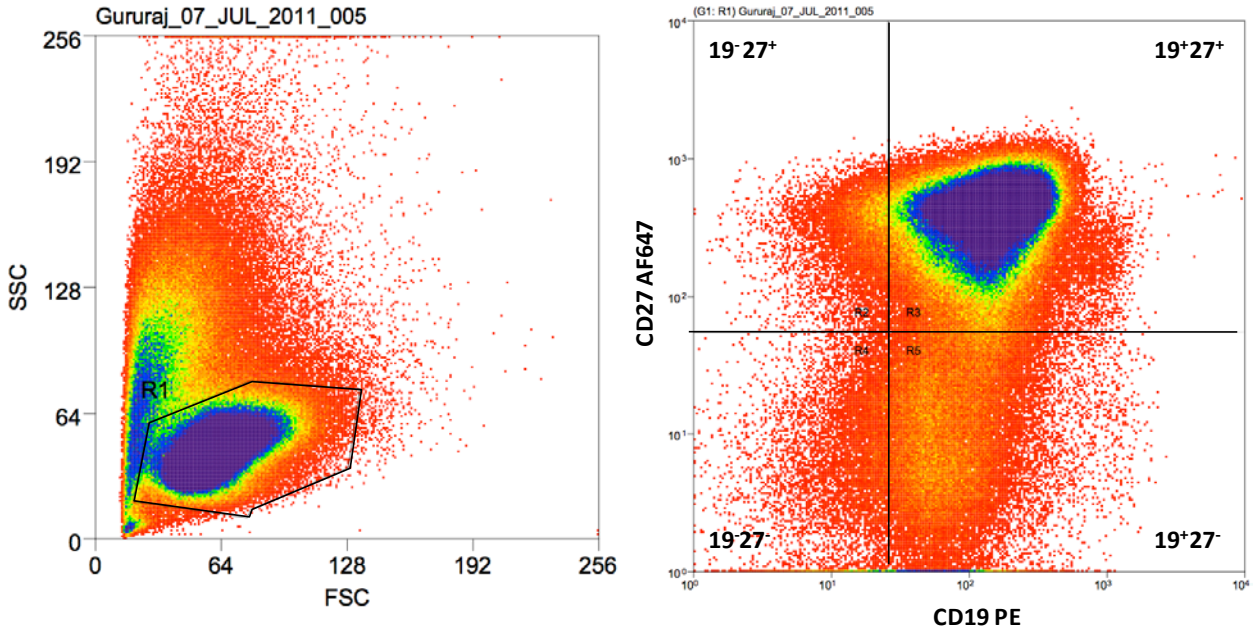

Figure 9.2-3 Flow-sort of in vitro differentiated day 6 cells based on CD19 and CD27

Scatter properties were used to gate live, nucleated cells and staining with CD19PE and CD27AF647 antibodies was used to sort the cells into 4 different populations on a Mo-Flo high speed cell sorter.

The sorted cells were re-suspended in media containing nutritional supplements, IL21, IFNα, IL6 and Stromal cell support as described in methods section 5.4.4. The antibody panel and detailed gating strategy for quantifying NK cells is shown in Table 5.2-4 and Figure 5.2-7 respectively. The NK cells were defined as CD16/CD56^{Pos} CD3^{Neg} CD19^{Neg} CD4^{Neg} CD27^{Neg}. The expanding NK cells on day 10 were predominantly derived from the cells that were CD19 and CD27 double negative on day 6. CD27 negativity provided a better marker to exclude the contaminant cells at day 6 rather than CD19 negativity due to the absence of any NK cells from the CD27 positive populations irrespective of their CD19 status. This could be due to a lower level of non-specific binding or better signal-to-noise ratio with the CD27 antibody. By sorting for CD27 positive cells on day 6, expansion of contaminating cells during further time points in the culture can be avoided. However, the effects of CD27 ligation on differentiation, proliferation and cell viability would need to be taken into account in subsequent analyses.

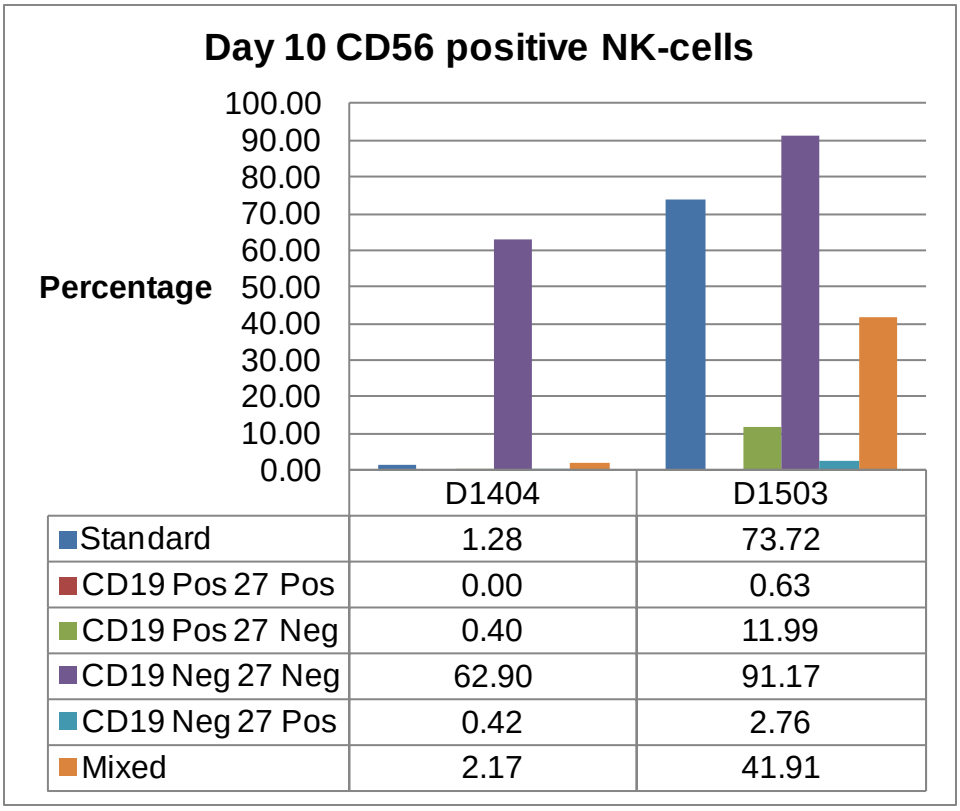

	D1404	D1503
Standard	1.28	73.72
CD19 Pos 27 Pos	0.00	0.63
CD19 Pos 27 Neg	0.40	11.99
CD19 Neg 27 Neg	62.90	91.17
CD19 Neg 27 Pos	0.42	2.76
Mixed	2.17	41.91

Figure 9.2-4 Proportion of CD56 positive NK cells on day 10 from the cells sorted on day 6

The 4 fractions obtained by flow sorting (Figure 9.2-3) on day 6 by differentiating B-cells in vitro were continued in culture as per standard protocol with IL21, IL6, IFNα and stromal cell support as described in methods section 5.4.4. The proportion of CD56 positive NK cells on day 10 from two donors D1404 (2% contamination on day 0) and D1503 (10% contamination on day 0) derived from day 6 sorted and unsorted cells. Standard – Unsorted cells. Mixed – Sorted cells with all the four fractions mixed together. The antibody panel and detailed gating strategy for quantifying NK cells is shown in Table 5.2-4 and Figure 5.2-7 respectively. The NK cells were defined as CD16/CD56^{Pos} CD3^{Neg} CD19^{Neg} CD4^{Neg} CD27^{Neg}.

9.3 Expansion of NK cells is not secondary to the presence of allogeneic cells in the culture system

Having observed that expansion of NK cells occurs in the in vitro system between days 6 to 10, there is a possibility the culture conditions that change on day 6 are influencing the expansion. One potential candidate is the mouse stromal cell layer M2-10B4, which could be sensed by human NK-cells as allogeneic and therefore needs excluding.

9.3.1 NK cell expansion is independent of the presence of mouse stromal cell layer M2-10B4 between Day 6 & Day 10 and direct addition/spiking of NK cells to highly pure B-cells, recapitulates inadvertent NK-cell expansion

B-cells purified by negative selection and positive selection (CD20 magnetic beads by Miltenyi) from selected donors were cultured in parallel using standard conditions (Figure 5.4-1). From day 6, the culture was continued in a transwell (no contact with M2-10B4) or in contact with M2-10B4 cells. NK cell numbers were calculated by flow cytometry using count bright beads and were defined as CD16/CD56^{Pos} CD3^{Neg} CD19^{Neg} CD4^{Neg} CD27^{Neg}. The antibody panel and detailed gating strategy for quantifying NK cells is given in Table 5.2-4 and Figure 5.2-7 respectively. There was a similar level of expansion of NK cells under both conditions.

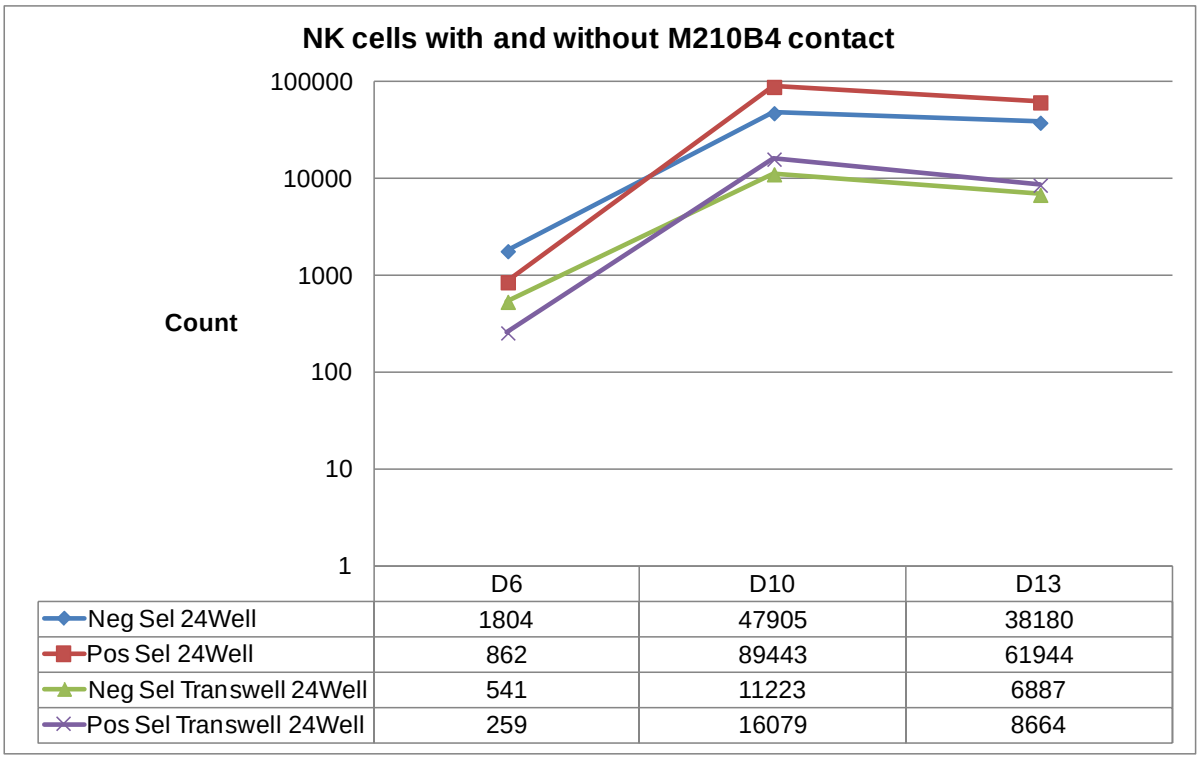

	D6	D10	D13
Neg Sel 24Well	1804	47905	38180
Pos Sel 24Well	862	89443	61944
Neg Sel Transwell 24Well	541	11223	6887
Pos Sel Transwell 24Well	259	16079	8664

Figure 9.3-1 NK cell expansion with and without M2-10B4 contact

B-cells isolated by negative selection (Neg sel) and CD20 positive selection (Pos sel) on day 0 were differentiated in vitro according to the standard protocol (Figure 5.4-1). From day 6 the cells were cultured with (24 Well) or without (Transwell 24 Well) M2-10B4 contact. NK cell numbers were calculated by flow cytometry using count bright beads and were defined as CD16/CD56^{Pos} CD3^{Neg} CD19^{Neg} CD4^{Neg} CD27^{Neg}. The counts are shown on a logarithmic scale from cells plated on to a single day 6 well on day 10 and day 13.

The other allogeneic cell present in the in vitro differentiation system is the CD40L transfected L-cells used on day 0 to stimulate the B-cells. Although the expansion occurs at least 4 to 5 days after the L-cells are removed, the possibility of their involvement in NK expansion cannot be ruled out. However, similar NK cell expansion was seen between days 6 and 10 when B-cells were stimulated with TLR 7/8 agonist R848 (1 µg/mL) on day 0 instead of CD40L.

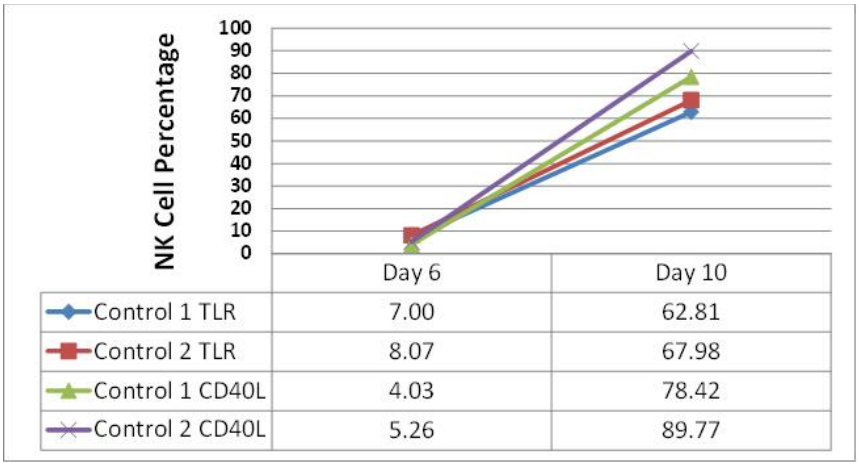

	Day 6	Day 10
Control 1 TLR	7.00	62.81
Control 2 TLR	8.07	67.98
Control 1 CD40L	4.03	78.42
Control 2 CD40L	5.26	89.77

Figure 9.3-2 NK cell expansion with CD40L and TLR stimuli on day 0

Peripheral blood B-cells from 2 controls were stimulated with CD40L transfected mouse fibroblasts (L-cells) or TLR7/8 agonist R848 on day 0 and the proportion of NK cells detected in the cultures on days 6 and 10 shown. NK cells were defined as CD16/CD56^{Pos} CD3^{Neg} CD19^{Neg} CD4^{Neg} CD27^{Neg}. Data shown is representative of 3 different experiments.

The simplest explanation for the results and the sporadic nature of the expansion was therefore that the degree of B-cell purity and the presence of contaminating NK cells at day 0 is the determinant. To address this, B-cells were double purified using sequential negative followed by positive selection with anti-CD20 beads, and cultured in parallel with and without addition of purified NK cells according to the standard protocol Figure 5.4-1. On day 6, cells from both conditions were plated with and without M2-10B4 to assess the effect of M2-10B4 on NK cell expansion. NK cell numbers were calculated by flow cytometry using count bright beads and were defined as CD16/CD56^{Pos} CD3^{Neg} CD19^{Neg} CD4^{Neg} CD27^{Neg}. Although there was a slight reduction in the proliferation without M2-10B4, there was still a significant expansion of NK cells without any M2-10B4. Thus an allogeneic signal from M2-10B4 cells is not necessary to drive expansion. Importantly this experiment also showed that differential purity of input B-cells is a critical factor and that the direct addition of NK cells at day 0 to highly pure B-cells can drive subsequent expansion between days 6 and 10.

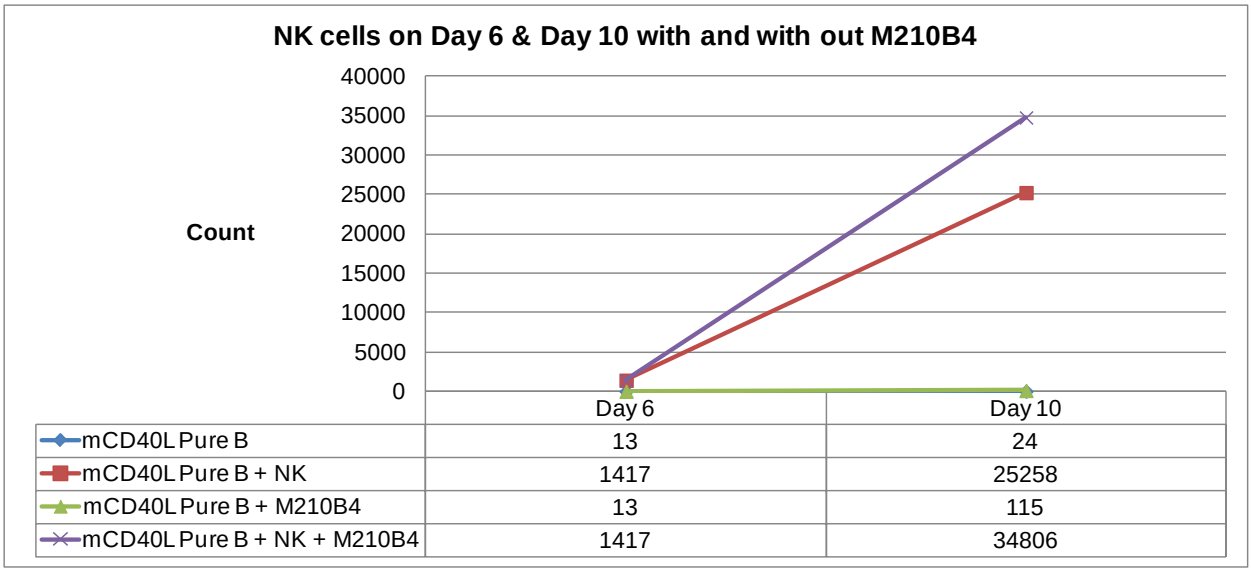

Figure 9.3-3 Effect of M2-10B4 on NK cell expansion

Double purified B-cells were differentiated with and without addition of purified NK cells using standard protocol up to day 6 (Figure 5.4-1). At day 6 the culture was continued with and without the mouse stromal cell M2-10B4 support. Figure shows the number of NK-cells on day 10 derived from a single day 6 well. NK cell numbers were calculated by flow cytometry using count bright beads and were defined as CD16/CD56^{Pos} CD3^{Neg} CD19^{Neg} CD4^{Neg} CD27^{Neg}.

Pure B= Double-purified B-cells on day 0 cultured without any M2-10B4 on day 6,

Pure B + NK = Double-purified B-cells on day 0 mixed with 10%NK cells on day 0 cultured without any M2-10B4 on day 6,

Pure B + M2-10B4 = Double-purified B-cells on day 0 cultured in contact with M2-10B4 on day 6,

Pure B + NK + M2-10B4 = Double-purified B-cells on day 0 mixed with 10%NK cells on day 0 cultured in contact with M2-10B4 on day 6

Transformation of CD19^{Pos} cells to NK cells and differentiation of NK cells from precursor stem cells are ruled out by this data and data from Figure 9.2-4.

9.3.2 Effect of NK cell expansion on antibody secreting cells

The effect of NK cell expansion between days 6 and 10 on plasmablasts when they differentiate into plasma cells was studied in the same experiment described in Figure 9.3-3. The number of plasma cells surviving on day 10 was markedly reduced due to NK expansion. This is unlikely to be due to a block in differentiation since there was higher number of plasma cells and slightly reduced number of plasmablasts on day 6 when NK cells were present in the culture suggestive of slightly accelerated differentiation. To account for the slightly decreased number of plasmablasts on day 6 when NK cells were present (242000 vs 175000), normalised counts are shown for plasmablasts in Figure 9.3-4. Plasmablasts and PCs showed equivalent survival with and without M2-10B4. Therefore, the plasmablast and plasma cell death is not due to killing of M2-10B4 by NK cells since the key role for M2-10B4 is to support long-term survival. The plasmablasts survival was also decreased by two- to three-fold which is suggestive of NK cell mediated cell death in plasmablasts and plasma cells. Although these data suggest that NK-cells have the capacity to curtail plasmablast/plasma cell responses at least in vitro, there could be other potential reasons for cell death such as lack of nutrient supply. To demonstrate direct NK mediated killing of the B-lineage cells further NK cell cytotoxicity assays are required which was beyond the scope of this project and therefore not pursued.

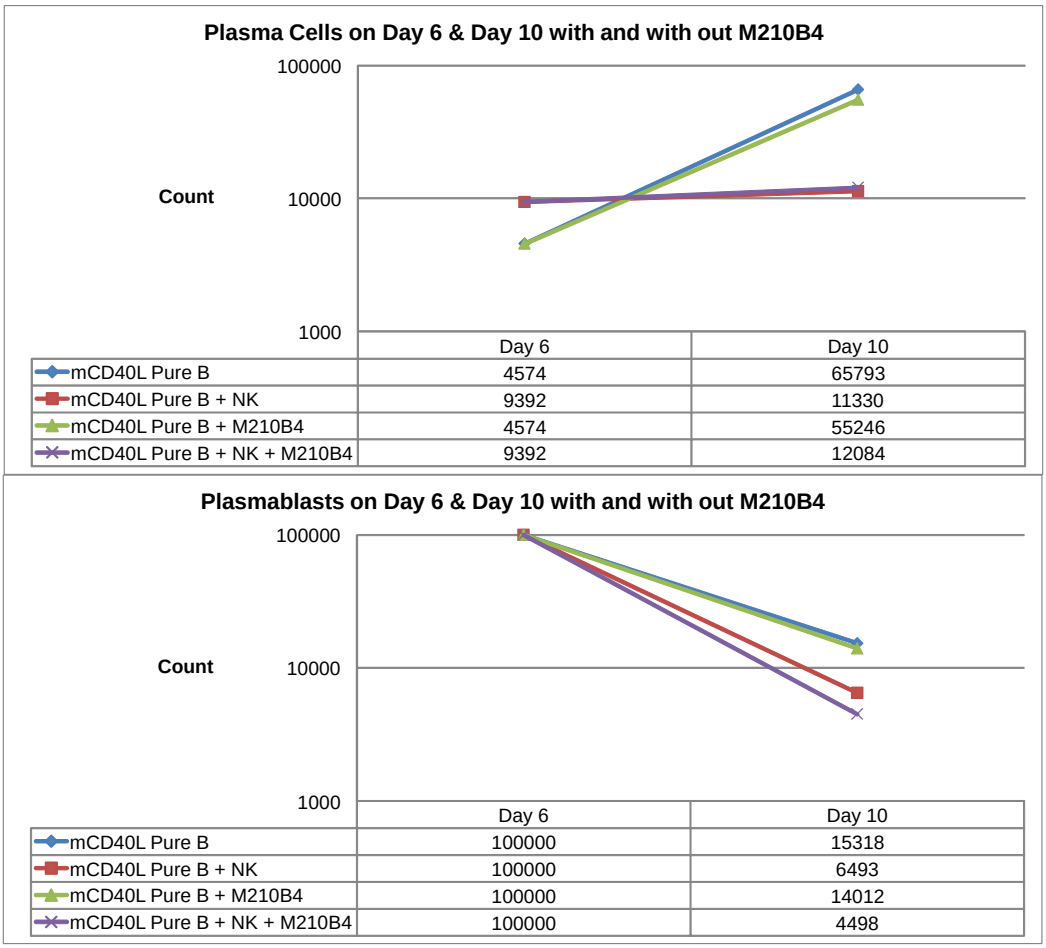

Figure 9.3-4 Effect of NK cell expansion on antibody secreting cells

Double purified B-cells were differentiated with and without addition of purified NK cells using standard protocol up to day 6 (Figure 5.4-1). At day 6 the culture was continued with and without the mouse stromal cell M2-10B4 support. The top figure shows the number of plasma cells defined as annexin V and 7-AAD negative, $CD20^{-}CD38^{Hi}CD138^{+}$ on days 6 and 10 derived from a single day 0 well (250000 B-cells). The bottom figure shows number of persisting plasmablasts defined as annexin V and 7-AAD negative, $CD20^{-}CD38^{Hi}CD138^{-}$ on day 10 from a normalised count of 100000 plasmablasts on day 6. The cell count is shown on a logarithmic scale.

Pure B = Double-purified B-cells on day 0 cultured without any M2-10B4 on day 6,

Pure B + NK = Double-purified B-cells on day 0 mixed with 10%NK cells on day 0 cultured without any M2-10B4 on day 6,

Pure B + M2-10B4 = Double-purified B-cells on day 0 cultured in contact with M2-10B4 on day 6,

Pure B + NK + M2-10B4 = Double-purified B-cells on day 0 mixed with 10%NK cells on day 0 cultured in contact with M2-10B4 on day 6

9.4 Potential contact-dependant interaction between B-lineage cells and NK cells

The expanding NK cells are derived from pre-existing NK cells in the culture. Having shown NK cell expansion is not dependant on sensitization by non-human cells and is not mediated solely by the combination of cytokines and nutrients on day 6, the next question was whether the interaction is contact dependant. This would allow simple strategies such as monoclonal antibodies to block this interaction in the culture. It is also critical to know at what stage during the B-cell differentiation this interaction occurs to understand the mechanism.

9.4.1 Plasmablasts are not directly able to induce NK cell expansion without prior priming

To identify the stage of B-cell differentiation which induced the NK cell expansion, plasmablasts were evaluated initially. Negatively selected B-cells were stimulated with IL2 CD40L and BCR stimuli as before (Figure 5.4-1) and differentiated to plasmablasts by day 6. NK cells from the same donor were freshly isolated on day 6 and co-cultured with the day 6 plasmablasts at 3 different concentrations. NK cells were cultured in transwells on their own or with B-cells but no contact or in contact with B-cells. NK cell concentrations were chosen to recreate the levels seen on day 6 in previous experiments. NK cell numbers were calculated by flow cytometry using count bright beads and were defined as CD16/CD56^{Pos} CD3^{Neg} CD19^{Neg} CD4^{Neg} CD27^{Neg}. The antibody panel and detailed gating strategy for quantifying NK cells is given in Table 5.2-4 and Figure 5.2-7 respectively. There was no expansion of NK cells cultured alone or in trans with Plasmablasts. There was one and a half to five-fold expansion when NK cells were in contact which is much less than what was observed in previous experiments.

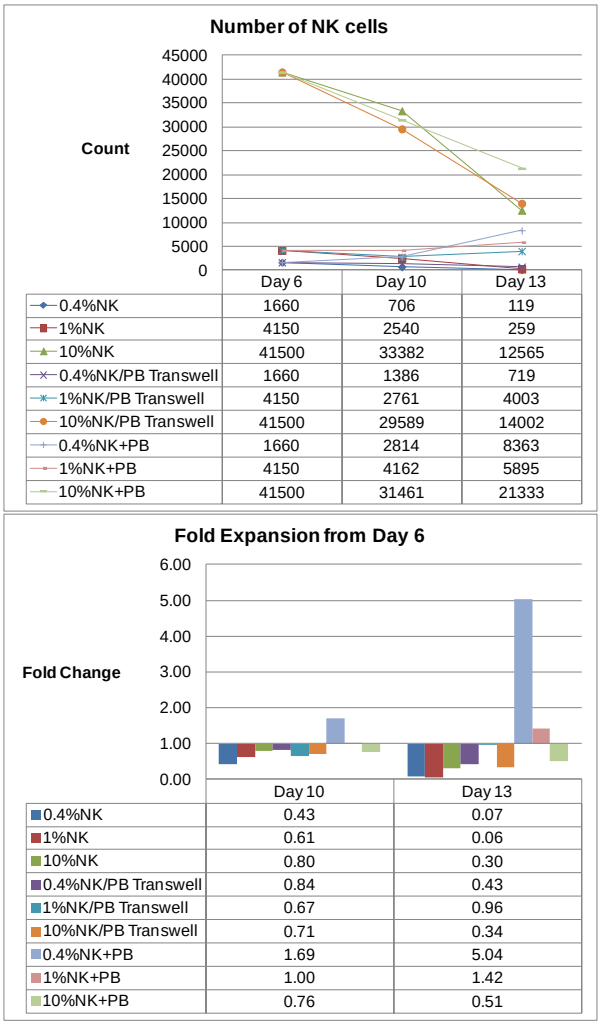

	Day 6	Day 10	Day 13
0.4%NK	1660	706	119
1%NK	4150	2540	259
10%NK	41500	33382	12565
0.4%NK/PB Transwell	1660	1386	719
1%NK/PB Transwell	4150	2761	4003
10%NK/PB Transwell	41500	29589	14002
0.4%NK+PB	1660	2814	8363
1%NK+PB	4150	4162	5895
10%NK+PB	41500	31461	21333

	Day 10	Day 13
0.4%NK	0.43	0.07
1%NK	0.61	0.06
10%NK	0.80	0.30
0.4%NK/PB Transwell	0.84	0.43
1%NK/PB Transwell	0.67	0.96
10%NK/PB Transwell	0.71	0.34
0.4%NK+PB	1.69	5.04
1%NK+PB	1.00	1.42
10%NK+PB	0.76	0.51

Figure 9.4-1 Freshly-isolated NK-cells on their own or co-cultured with Plasmablasts on day 6 do not expand without prior priming

Negatively selected peripheral blood B-cells were stimulated with IL2, CD40L and BCR stimuli to generate plasmablasts on day 6 as before (Figure 5.4-1). Freshly isolated NK cells were added on to the plasmablasts at the concentrations shown above. The top figure shows the number of NK cells on day 10 and day 13 derived from cells plated on to a single well on day 6. The bottom figure shows the fold expansion from day 6 on days 10 and 13 calculated as the number of cells on day 10 or day 13 divided by the number of cells plated on day 6 into a single well. Fold change of less than 1 represents a decrease in number. In conditions labelled NK+PB – cells were in contact and NK/PB – cells were not in contact. NK cell numbers were calculated by flow cytometry using count bright beads and were defined as CD16/CD56^{Pos} CD3^{Neg} CD19^{Neg} CD4^{Neg} CD27^{Neg}. In the data table below the figures the top 3 rows show NK cells cultured on their own at different concentrations, the middle 3 rows show NK cells cultured with plasmablasts without contact in a transwell and bottom 3 rows show NK cells mixed with plasmablasts.

9.4.2 The B-NK interaction is contact dependant

To establish whether the B-NK cell interaction is contact dependant or mediated by soluble mediators, purified NK cells and B-cells were cultured as shown in Figure 9.4-2.

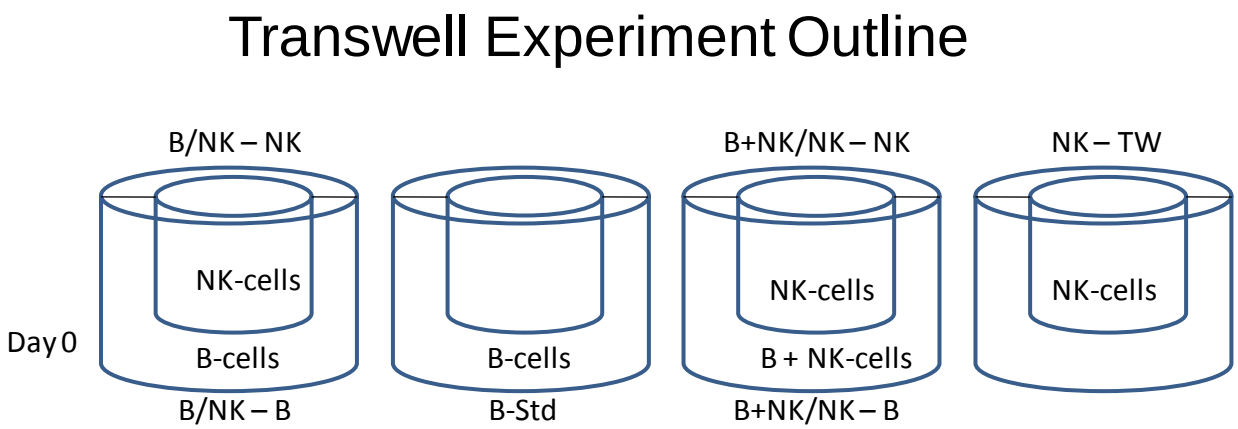

Figure 9.4-2 Outline of transwell experiment to establish nature of NK-B interaction

The figure shows the scheme of transwell experiments. Labels within the wells show what cells were seeded into the different compartments.

Negatively selected B-cells and NK cells on their own or with B-cells were stimulated with IL2 CD40L and BCR stimuli as before (Figure 5.4-1). The NK cells were cultured with B-cells on the same side as well as the opposite side of the transwell to assess the contact dependant nature of the interaction. The mouse stromal cell M2-10B4 was not used in this experiment between days 6 and 10. NK cell numbers were calculated by flow cytometry using count bright beads and were defined as CD16/CD56^{Pos} CD3^{Neg} CD19^{Neg} CD4^{Neg} CD27^{Neg}. The antibody panel and detailed gating strategy for quantifying NK cells is given in Table 5.2-4 and Figure 5.2-7 respectively. The purity of B-cells and NK cells were 99.5% was 98% respectively. NK cells which were not in contact with B-cells did not expand irrespective of the presence of soluble mediators from B-cells. The contact dependant nature of the interaction was reproducible in another similar experiment (data not shown).

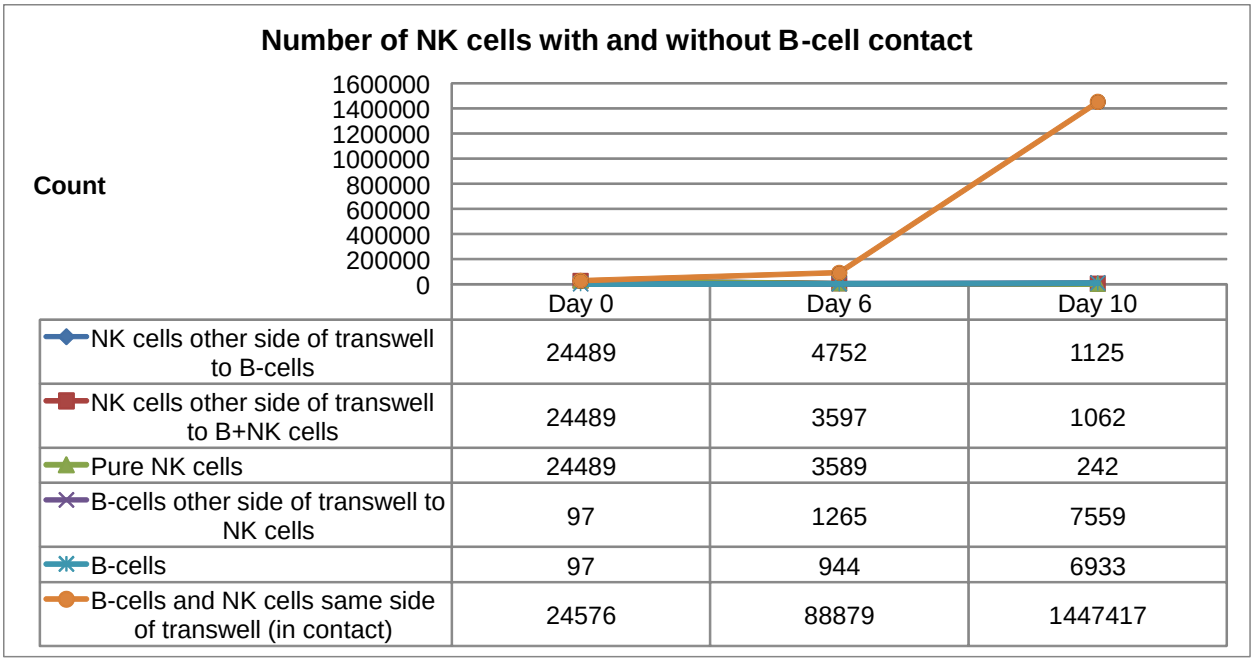

	Day 0	Day 6	Day 10
NK cells other side of transwell to B-cells	24489	4752	1125
NK cells other side of transwell to B+NK cells	24489	3597	1062
Pure NK cells	24489	3589	242
B-cells other side of transwell to NK cells	97	1265	7559
B-cells	97	944	6933
B-cells and NK cells same side of transwell (in contact)	24576	88879	1447417

Figure 9.4-3 NK cell expansion when grown in transwells with and without B-cell contact

The number of NK cells derived on day 6 and day 10 from a single day 0 well. The pure B-cell fraction on day 0 contained a small proportion of NK cells (0.5%). Data shown is representative of 2 different experiments.

The above experiment clearly shows the contact dependant nature of the NK-B interaction. NK cells within the transwell separated from a mixed culture of B-cells and NK-cells fail to expand, while the NK cells in the mixed culture on the outer side of the transwell in contact with B-cells expand dramatically. However, plasmablasts cannot directly induce NK cell expansion which needs prior priming or is dependent on interaction with B-lineage cells prior to the plasmablast stage, as shown in Figure 9.4-1.

The conclusion can be reached that NK cells if present at day 0 can be driven to expand dramatically on transfer into conditions that also promote plasma cell differentiation if cultured in contact with activated B-cells. Thus the contamination issue originally encountered can be avoided by using sequential negative followed by positive selection of B-cells on day 0 or excluding CD27Neg cells on day 6 by flow sort. Furthermore the expansion of NK-cells can be actively promoted by using a forced co-culture approach independent of the M2-10B4 stromal layer.

9.5 Evaluation of receptors and ligands involved in NK-B cell interaction

The cause for expansion of NK cells induced by the differentiating B-cells was shown to be contact dependent. The surface proteins involved in stimulation of NK cells by B-lineage cells is not known. The knowledge of the receptor-ligand interactions involved would aid in devising a strategy to prevent the expansion during in vitro culture. If this phenomenon of NK cell expansion occurs in vivo and is involved in disease pathogenesis, it opens up therapeutic options by blockade of this interaction.

9.5.1 NK-B cell interaction is not dependent on CD137

CD137/137L pathway is one of the co-stimulatory pathways involved in NK cell activation. Peripheral blood NK cells can be expanded 1000-fold in vitro in 3 weeks by combination of CD137L and IL15 (125). CD137L is known to be expressed by B-cells in lymphoid follicles and germinal centers (126) and therefore could be a potential mode of interaction in vitro which could be responsible for the noted NK cell expansion. This pathway and thereby the interaction should be amenable to inhibition by CD137 blocking antibody. B-cells and NK cells purified on day 0 were mixed at a ratio of 10:1 and differentiated following the standard B-cell differentiation protocol (Figure 5.4-1) and the proportion of NK cells was evaluated on day 10. NK cells were defined as CD16/CD56^{Pos} CD3^{Neg} CD19^{Neg} CD4^{Neg} CD27^{Neg} and the antibody panel and detailed gating strategy used for quantifying NK cells is given in Table 5.2-4 and Figure 5.2-7 respectively. The addition of 10 µg/ml of blocking anti-CD137 at various stages of differentiation did not block the expansion of NK cells as shown in Figure 9.5-1.

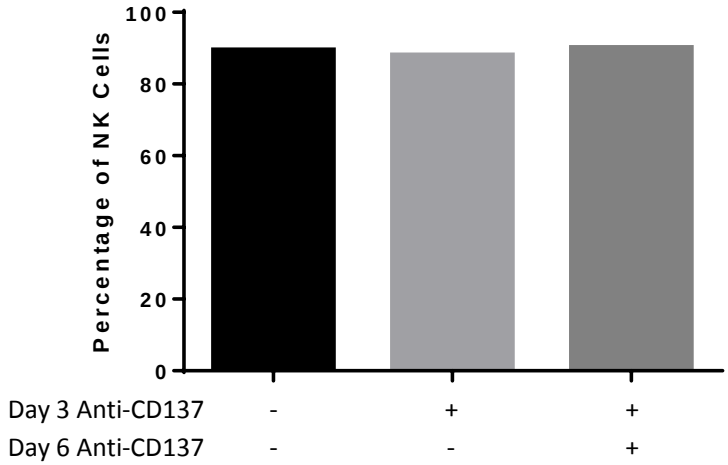

Figure 9.5-1 Effect of anti-CD137 on the percentage of NK cells on day 10 of culture

Purified peripheral blood B-cells and NK cells were mixed at a ratio of 10:1 on day 0 and simulated using IL2, CD40L and BCR stimuli and differentiated as before (Figure 5.4-1). Blocking anti-CD137 antibody was added at a concentration of 10µg/ml at the time points specified. NK cells were defined as CD16/CD56^{Pos} CD3^{Neg} CD19^{Neg} CD4^{Neg} CD27^{Neg} and expressed as percentage of live cells on day 10 of the culture.

9.5.2 NK-B cell interaction is not mediated via CD2/CD58 pathway

NK cell cytotoxicity requires stable interaction with target cells which is mediated by interaction of CD2 present on NK cell surface with CD58 by promoting nanotube formation (127). Initially B-cells from controls and RA patients were evaluated for surface expression of CD58. Peripheral blood containing an equivalent of 1 million white cells from patients and controls was treated with ammonium chloride to lyse the RBCs and then stained with CD48 FITC, CD58 PE, CD24 PE-CF594, CD16 PerCP-Cy5.5, CD2 PE-Cy7, CD19 BV421, CD3 V500, CD56 APC, CD27 AF700 and CD45 APC-H7. B-cells were defined based on their scatter profile and as CD19^{+}CD3^{-}CD56^{-}. The proportion of CD58 positive B-cells was not significantly different ($p = 0.48$, One-way ANOVA) between healthy controls (n=3), disease controls (n=3), rituximab naïve active RA patients (n=5) and RA patients relapsing post-rituximab (n=6). However, a proportion of the RA patients relapsing post-rituximab had higher levels of CD58 expressing B-cells (Figure 9.5-2). Since the CD2/CD58 pathway could also be potentially linked to RA pathogenesis, it was explored further.

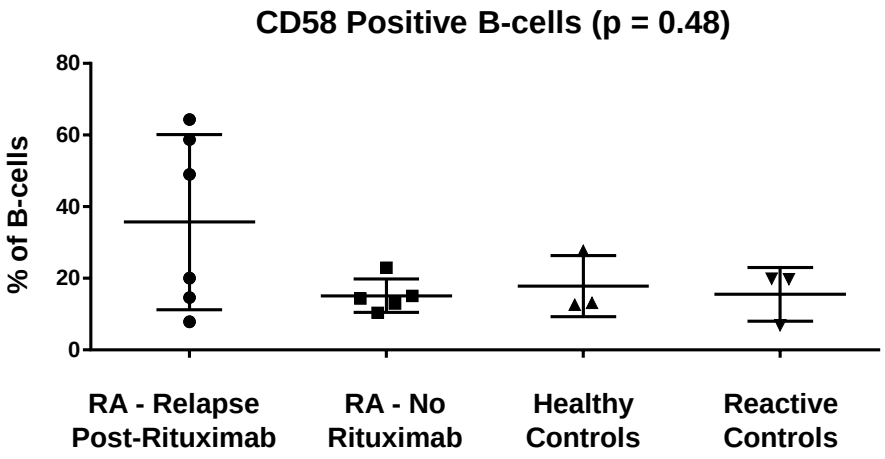

Figure 9.5-2 Expression of CD58 by peripheral blood B-cells by different patient groups

B-cells expressing CD58 on their surface expressed as a proportion of total B-cells in the different patient groups - healthy controls (n=3), disease controls (n=3), rituximab naïve active RA patients (n=5) and RA patients relapsing post-rituximab (n=6) shown. B-cells were defined based on their scatter profile and as $CD19^{+}CD3^{-}CD56^{-}$. The central lines represent the mean and the extreme lines represent the standard deviation. All the RA patients in this dataset had active disease at the time of sampling. The difference between the groups was not significant (p=0.48, One way ANOVA).

The gene expression data previously published by Cocco et al. (60) was reanalysed for the change in CD58 expression levels during the course of in vitro B-cell differentiation. CD58 was expressed on day 3 by differentiating B-cells and does not reach baseline levels till day 13 as seen in Figure 9.5-3 . The NK cell expansion occurs only after day 6 when the culture conditions change although CD58 is expressed from day 3. Therefore, the change in cytokine combinations or other culture conditions on day 6 is likely to be required as an additional trigger for the activation of the CD2/CD58 pathway. To evaluate this further the effect of CD2/CD58 blockade on NK cell expansion was studied. B-cells and NK cells purified on day 0 were mixed at a ratio of 10:1 and differentiated following the standard B-cell differentiation protocol (Figure 5.4-1) and the proportion of NK cells was evaluated on day 10. NK cells were defined as $CD16/CD56^{Pos}$ $CD3^{Neg}$ $CD19^{Neg}$ $CD4^{Neg}$ $CD27^{Neg}$ and the antibody panel and detailed gating strategy used for quantifying NK cells is given in Table 5.2-4 and Figure 5.2-7 respectively. The differentiating cells were treated with 10 µg/ml of tissue-culture grade anti-CD2 or anti-CD58 at baseline, day 3 and day 6. The addition of anti-CD2 or anti-CD58 at various time points during B-cell differentiation did not alter the NK cell expansion noted by day 10, as shown in Figure 9.5-3.

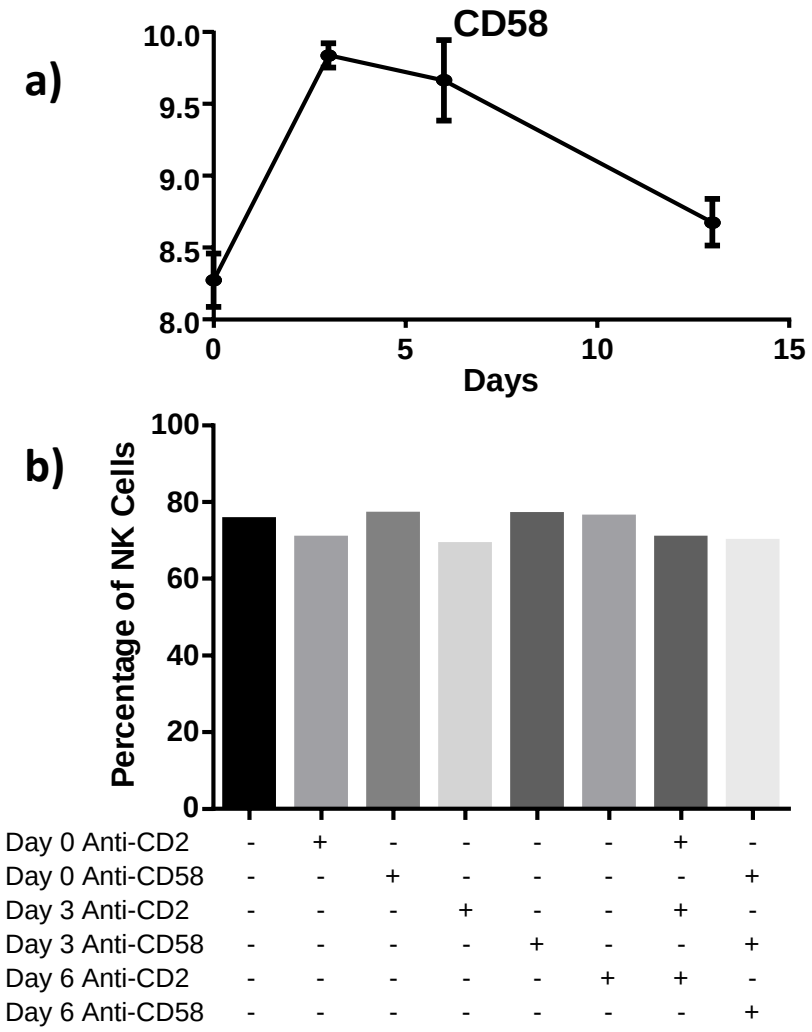

Figure 9.5-3 CD58 expression during B-cell differentiation and effect of CD2/CD58 blockade on NK expansion

a) Levels of absolute gene expression of CD58 at the various time points during B-cell differentiation as indicated in 3 controls. The data presented is reanalysis of data previously published by Cocco et al. (60). The dots represent the mean and the bars represent standard deviation.

b) Purified peripheral blood B-cells and NK cells were mixed at a ratio of 10:1 on day 0 and differentiated as per standard protocol (Figure 5.4-1). Blocking anti-CD2/anti-CD58 antibody was added at a concentration of 10µg/ml at the time points specified. NK cells were defined as CD16/CD56^{Pos} CD3^{Neg} CD19^{Neg} CD4^{Neg} CD27^{Neg} and expressed as percentage of live cells on day 10 of the culture. NK cell expansion was resistant to CD2 and CD58 blockade.

9.6 Further evaluation of cause for NK-B cell interaction

The mechanisms driving expansion of NK cells after day 6 remained unclear. During one of the experiments where cells from individual day 3 wells from the same donor were differentiated separately, it was noted that one of the wells did not show NK expansion on day 10 under same culture conditions. This could be due to the unequal distribution of the contaminating NK cells. However, this also raised the possibility of a subset of B-cells present in low frequency leading to expansion. EBV is present in B-cells in the latent phase. When B-cells undergo differentiation to plasmablasts, EBV enters lytic phase. This might be a key factor in triggering the NK cell expansion. Therefore evidence for the presence of EBV DNA was sought.

9.6.1 EBV DNA detected in the sample that consistently showed NK expansion

Plasmablasts generated in vitro on day 6 using standard IL2, CD40L and BCR stimuli based activation protocol (Figure 5.4-1) from a donor whose samples consistently led to NK cell expansion in the previous experiments, even with low level of NK-cell representation was analysed. The EBV DNA was detected using nested PCR which has been developed as a rapid method for diagnosing EBV infection in the context of non-Hodgkin's lymphoma (81) and the detailed protocol is described in the methods section 5.10. The first round of PCR reaction generated an 800bp fragment, which was then subjected to another round of PCR with primers designed to amplify both EBV type 1 and 2. Cell lines Raji and HeLa were used as positive and negative controls respectively. Annealing temperature of 60^0C and $MgCl_2$ concentration of 1.5mM was used. The band corresponding to the size of the second round PCR product was also detected by using the primary DNA sample directly in the second round PCR.

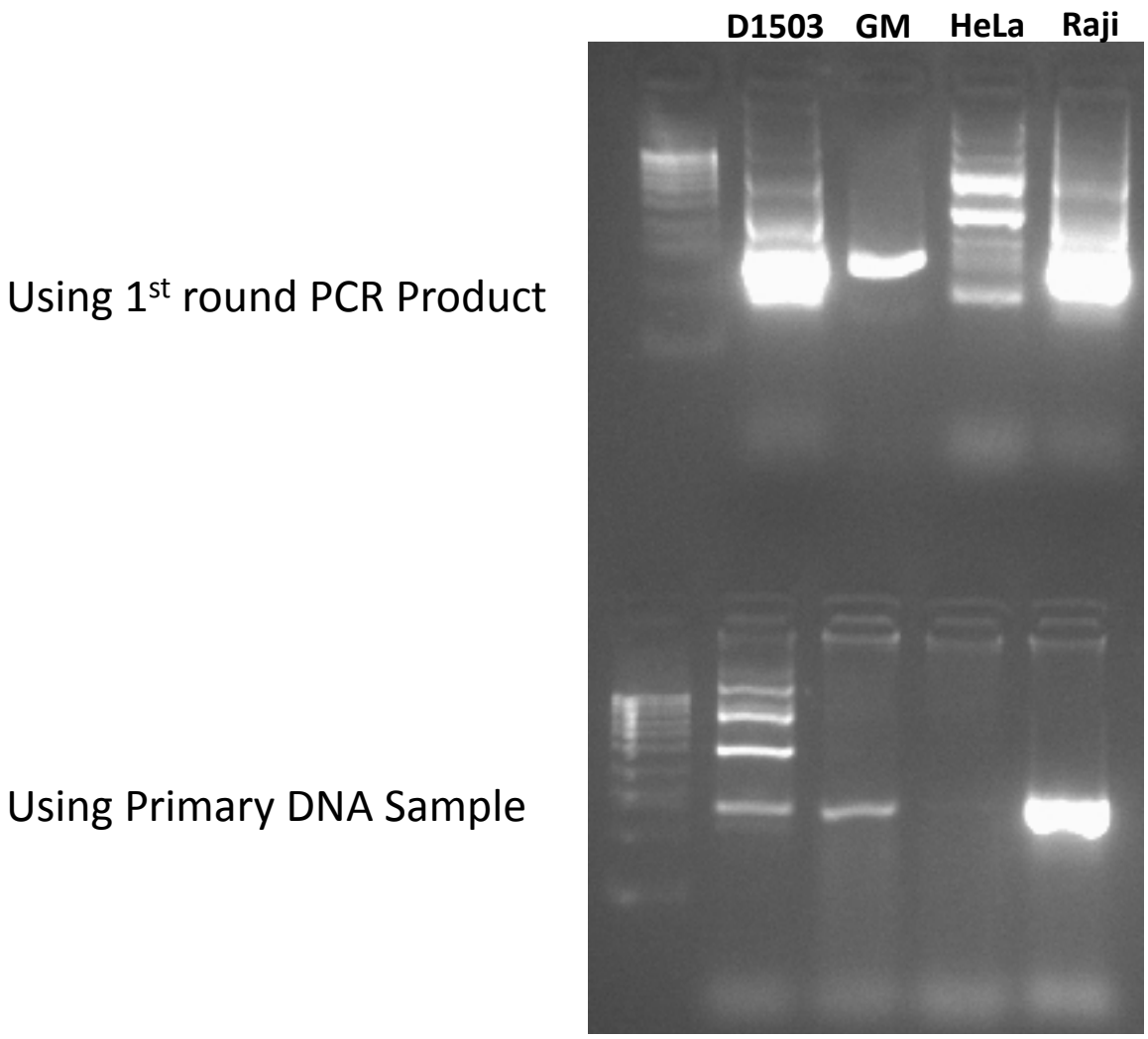

Figure 9.6-1 Electrophoresis of PCR products for detecting EBV DNA

Day 6 plasmablasts generated in vitro using standard IL2, CD40L and BCR stimuli based activation protocol (Figure 5.4-1)from a control (D1503) and 3 different cell lines – GM, HeLa and Raji were used. Annealing temperature of 60^0C and $MgCl_2$ concentration of 1.5mM was used. Products generated by the single PCR reaction are shown in the bottom row and the top row shows products of the two stage nested PCR.

The PCR product from the second reaction was size selected on agarose gel by electrophoresis and sequenced. The sequenced product showed 98% homology to human herpes virus 4 (EBV) genome. Although this confirms the presence of EBV DNA in the plasmablasts, it does not prove that EBV is the main cause for NK cell expansion. To prove EBV as the definitive cause for the NK cell expansion it will require substantial amount of work which is beyond the scope of this project but could be addressed in a future project.

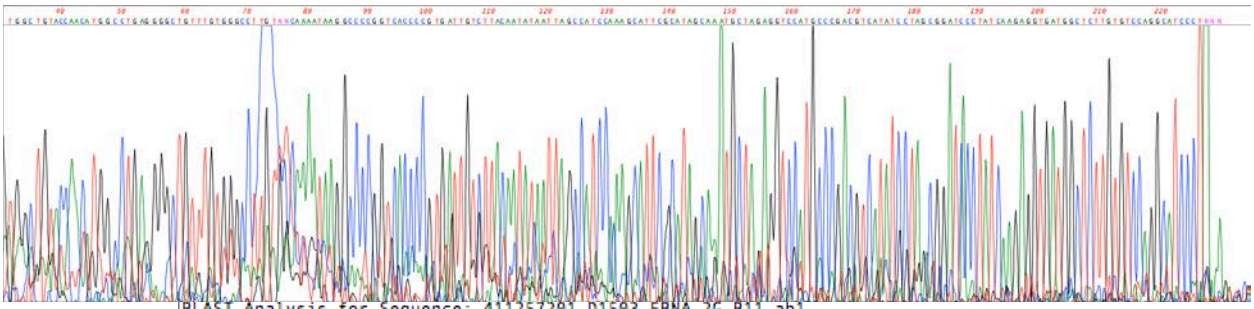

```
BLAST Analysis for Sequence: 411257201_D1503_EBNA_2G_B11.ab1
Search from 1 to 229                                  Program: blastn
Expect: 10          Low complexity filter: on         Matrix: n/a
Genetic Code: n/a                                     Gapped search: on
Open cost: 5        Extend cost: 2

Database: nr   (2,013,610,181 residues in 26,084,293 sequences)
Karlin-Altschul Statistics:
    Kappa = 0.41, Lambda = 0.625, Entropy = 0.78

  1. gi|428161017|gb|KC207813.1| Human herpesvirus 4 strain Akata, complete genome

     Length = 171323
     Score = 343.9 bits (380), Expect = 2.8e-91
     Identities = 194/197 (98%), Positives = 194/197 (98%), Gaps = 0/197 (0%)

       Query:       30 TGTGGCTGTACCAACATGGCCTGAGGGGCTGTTTGTGGGCCTTGTNNCAA
                       ||||||||||||||||||||||||||||||||||||||||||||  |||
       Subject:    36619 TGTGGCTGTACCAACATGGCCTGAGGGGCTGTTTGTGGGCCTTGTGGCAA

       Query:       80 AATAAGGCCCCGGTCACCCCGTGATTGTCTTACAATATAATTAGCCATCC
                       ||||||||||||||||||||||||||||||||||||||||||||||||||
       Subject:    36569 AATAAGGCCCCGGTCACCCCGTGATTGTCTTACAATATAATTAGCCATCC

       Query:      130 AAAGCATTCGCATAGCAAATGCTAGAGGTCCATGCCCGACGTCATATCCT
                       |||||||||||||||| ||||||||||||||||||||||||||||||||||
       Subject:    36519 AAAGCATTCGCATAGCAGATGCTAGAGGTCCATGCCCGACGTCATATCCT

       Query:      180 AGCGGATCCCTATCAAGAGGTGATGGCTCTTGTGTCCAGGCATCCCT
                       |||||||||||||||||||||||||||||||||||||||||||||||||||
       Subject:    36469 AGCGGATCCCTATCAAGAGGTGATGGCTCTTGTGTCCAGGCATCCCT
```

Figure 9.6-2 Sequencing of the EBV PCR product

The nested PCR product from the control was sequenced by Sanger sequencing. The obtained sequence had 98% homology to EBV genome.

9.7 Exploration of additional cell-selection strategies to improve B-cell purity

Differentiation of B-cells required high level of purity on day 0 to prevent expansion of non B-lineage cells post day 10. Therefore methods for improving the purity of the day 0 negative B-cell selection process were sought. The contaminating cells are mostly NK cells and T-cells. Methods of blocking the B-NK interaction and thereby the NK expansion with monoclonal antibodies is a much more viable strategy than multiple purification steps or flow cytometry based sorting and therefore pursued. However, due to the lack of positive findings from the pathways tested and the possibility of EBV being involved in the interaction, the cell selection strategies were re-visited. Monocytes have very high levels of Fc receptor and therefore can capture the depleting antibodies from the negative B-cell selection kit in a non-specific fashion. This can lead to reduction in the antibodies available to deplete the non-B cells. Indeed a likely explanation for differences between differentiations was whether column capacity was overloaded, while in the context of samples form inflammatory states the performance of column based purification appeared less reproducible. Therefore, the cell selection strategy was specifically modified to counteract these factors by using mixture anti-CD3/CD14/56 tagged magnetic beads to deplete T-cells, monocytes and majority of NK cells respectively.

9.7.1 B-cell negative selection purity improved with higher concentrations of reagents or additional purification steps

PBMCs obtained by density centrifugation was incubated with CD14 microbeads and depleted by passing through the magnetic column (detailed cell-selection protocol provided in methods section 5.3). Depleting the monocytes alone before negative B-cell selection did not achieve the necessary purity. It required an additional round of purification with anti-CD3/CD56 magnetic beads to improve the purity as shown in Figure 9.7-1. Therefore, monocytes are unlikely to be a key cause for the purification issues. Two step sequential selection using anti-CD3/CD56 magnetic beads either before or after the negative B-cell selection kit improved the purity to more than 99%. Using the reagents (biotinylated antibody cocktail and anti-biotin magnetic beads) in excess (10 times the manufacturer’s recommendation) also gave very high purity of 99%. This is suggestive of the fact that the antibodies may be consumed in a non-specific fashion by other cell types.

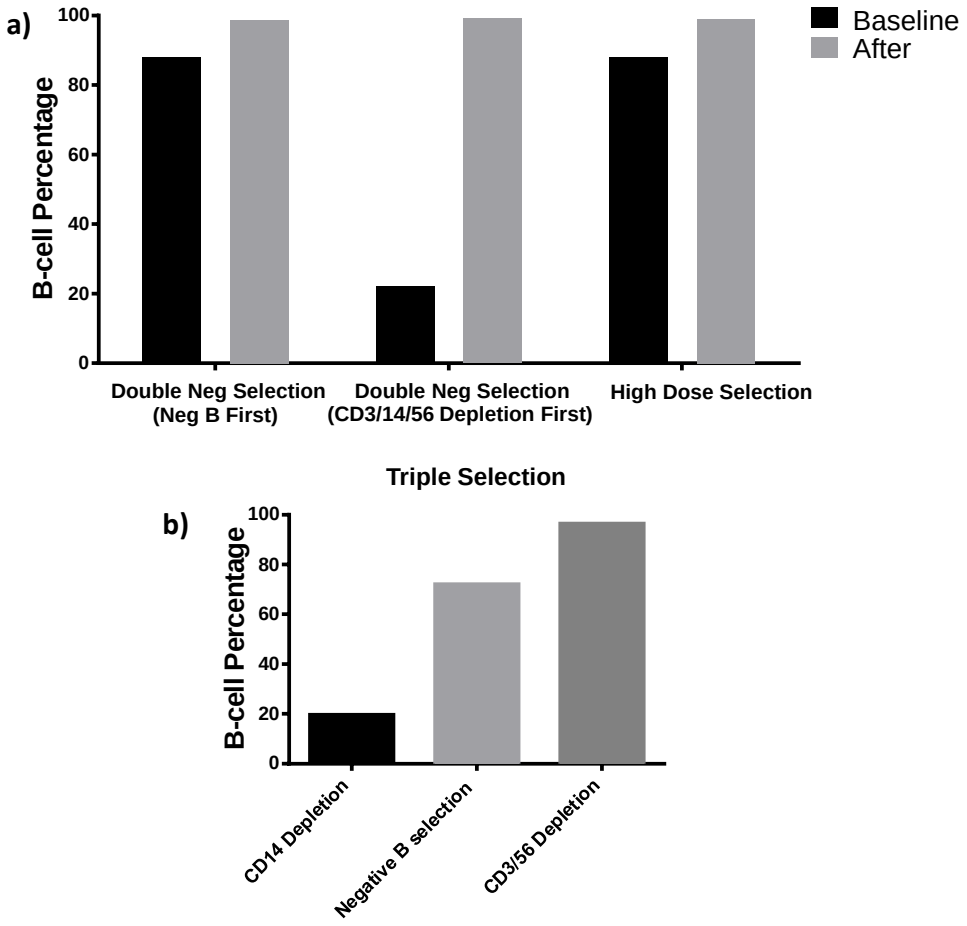

Figure 9.7-1 Additional cell-selection strategies to improve B-cell purity

B-cells were defined based on their scatter profile and CD19/CD20 dual-positivity. B-cells as a proportion of live cells is shown in the graph. PBMCs were isolated by density centrifugation and then subjected to the cell selection process as described in methods section 5.3.

a) Double negative selection refers to strategy of using negative B-cell selection kit and mixture of anti-CD3/14/56 beads sequentially. The purity after the first round of selection is denoted by black bars and the second round of selection is denoted by grey bars. With high dose selection, 10 times the recommended volume of biotinylated antibody cocktail and anti-biotin magnetic beads were used. The black bar denotes purity using the standard concentration and the grey bar denotes the high concentration.

b) Triple selection involves 3 rounds of successive negative selection with antiCD14 beads, negative B-cell selection kit and anti-CD3/CD56 beads. The purity from the 3 successive rounds of negative selection is depicted in the bar graph.

Reviewing the lymphoprep protocol to isolate mononuclear cells, it was noted that one of the wash steps specifically targets platelets. The protocol was modified to change the wash step to use ice-cold PBS rather than PBS at room temperature. This is likely to reduce platelet aggregation which could be the cause for consumption of the depleting antibodies. With the modified protocol and using twice the recommended amount of the antibody cocktail, acceptable levels of purity of >95% was achieved. The purity was checked following negative B-cell selection and the second stage of negative selection with anti-CD3/CD56 magnetic beads was used only if the purity was low.

9.8 Summary and discussion

In vitro differentiation of RA B-cells was attempted which led to the finding of non-B-cell expansion post day 6 of culture. This was also seen sporadically in some control samples but was worse in case of RA patients. The identity of the expanding non-B cells was established to be NK cells. NK cell activation is based on the balance of stimulatory and inhibitory signals received by the surface receptors and can be activated by allogenic cells. Therefore the cells of mouse-origin in the culture system were suspected to be the cause for expansion namely, CD40L transfected fibroblasts (L-cells) between days 0 and 3, and the mouse bone marrow stromal cells (M2-10B4) that support plasma cell survival after day 6. This was excluded by using recombinant soluble CD40L and the expansion occurred in the absence of M2-10B4. NK cells differentiated using the same protocol used for B-cells did not show such expansion. The cytokine cocktail used in the culture on day 6 was not sufficient to stimulate NK cell proliferation without prior priming. It is not clear whether they need to be primed along with B-cells or just the culture conditions would suffice.

The NK cell expansion was contact dependant since NK cells on the other side of a transwell did not proliferate. The molecules that can be involved in NK cell activation with corresponding ligands present in B-lineage cells were considered and two such pathways were assessed. The CD137 (41-BB, TNFRSF9) receptor/ligand system has been well studied in the context of T-cell co-stimulation (128). However, NK cells also express CD137 on activation (129) and B-cells express CD137L on activation (126). Majority of NK cells and T-cells express CD2 whose ligand is the adhesion molecule CD58 also known as LFA-3 (Lymphocyte Function Associated Antigen -3) (130). Although peripheral blood B-cells do not express CD58 (131), it can be induced on activation (Figure 9.5-3). The NK cell expansion was not inhibited by blocking antibodies anti-CD137, anti-CD2 or anti-CD58 and therefore is unlikely to be mediated via CD137/CD137L or CD2/CD58 pathway.

NK cells are lymphocytes of the innate immune system and are activated based on the balance of stimulatory and inhibitory signals provided by the target to the multitude of NK cell receptors. They play a key role in immunity against malignant cells and intracellular pathogens such as viruses (132). The B-cells during plasmablast transformation might be expressing unusual ligands in vitro, sensed by NK cells as something similar to a malignant cell which triggers their

expansion. The other possibility is the presence of viruses within the culture system. For the expansion to be mediated by a virus, it has to be present in the system from day 0 but invisible to NK cells until day 6. It is also possible that NK cells need additional IFNα added on day 6 for their proliferation. B-cells are known to harbour latent viruses such as EBV and EBV can survive long-term within resting memory B-cells without immune detection by shutting down expression of the viral proteins (133). However when the memory B-cells harbouring latent EBV undergo differentiation to plasmablasts, the virus enters a replicative phase irrespective of the mode of stimulation (134). During this replicative phase, the viral antigens and other cell danger molecules are expressed on the cell surface sensed by the NK cells. This along with IFNα induces an exuberant antiviral response with proliferation, cytokine secretion and cytotoxicity (135). Once the NK cells are activated, the immune response is not specific and targets both EBV positive and negative cells. This possibly leads to death of the B-lineage cells in the system as well as the mouse stromal cells. The other possible explanation for reduction in PC numbers with NK expansion is secondary to reduced cell survival due to lack of nutrients in the system and not direct killing. This will need further evaluation by NK cell functional assays. Presence of surface markers such as LAMP-1 would be suggestive of cytokine secretion and cytotoxicity. The specificity of killing by expanding NK cells can be established by isolating them from the culture and testing on cell lines and plasmablasts from a different donor.

The sample which had most consistently shown NK cell expansion in fact had detectable EBV DNA on day 6.EBV as the main cause for NK cell expansion could be further confirmed by detection of EBV mRNA. The definitive way of proving this would be to differentiate B-cells from an EBV-negative control which is ethically not feasible due to the requirement of pre-screening the donors for EBV and there is a high prevalence of latent EBV of >95% in the adult population. The other option is to sort the EBV positive and negative cells based on LMP2A which is expressed by EBV harbouring B-cells and check for NK expansion. However, none of the available antibodies are validated for flow cytometry to perform this experiment.

EBV also known as HHV-4 (Human Herpes Virus) has been linked with RA pathogenesis through multiple mechanisms (136). RA patients have higher frequency and levels of antibodies directed against EBV proteins and reduced cytotoxicity against EBV infected lymphocytes. Molecular mimicry due to similarity in sequences between EBV proteins and synovial tissue and human heat shock proteins has also been proposed (137). Higher proportion of RA patients

have EBV DNA/RNA detectable by PCR in the synovial tissue(138), and increased frequency of EBV specific T-cells have been demonstrated within the synovial fluid (139). Higher frequency of EBV-infected B-cells (140) and higher EBV viral load (141) were detected in peripheral blood of RA patients. Although these studies suggest a link between EBV and RA, no direct proof of pathogenesis has been established.

Antibodies directed against citrullinated proteins are specific for RA. Antibodies directed against citrullinated-EBV derived peptides were detected in 45% of RA patients and levels correlate with ACPA (142). These antibodies were shown to cross-react with citrullinated proteins specific for RA such as fillagrin (143). EBV present in the synovial tissue and synovial fluid possibly elicits a low level antigen-specific response. When the B-cells with latent EBV are activated in an antigen-specific or polyclonal fashion the EBV enters a replicative phase. This generates an explosive immune response by NK cells and T-cells similar to that seen above which recruits other inflammatory mediators and cells that can perpetuate inflammation and incite tissue damage. NK cells were also noted in synovial tissue of early RA patients and correlated with inflammatory markers in serum (144). NK cells from synovial fluid of RA patients exhibit an activated phenotype (145) and were also involved in triggering osteoclastogenesis and bone destruction (146). B-cells from tonsils can stimulate NK cells when they are activated and are differentiating to plasmablasts (147). This pattern of interaction between activated B-cells and NK cells was shown to be contact-dependant (148). Although not specifically tested, presence of latent EBV in the B-cells used in these previously published studies could not be ruled out. Thus EBV harbouring B-cells through activation of NK cells could play a key role in loss of tolerance and tissue damage in RA.

Large granular lymphocytic leukaemia (LGL) is a lymphoproliferative disorder characterised by clonal expansion of NK cells or more commonly, CD8 cytotoxic T-cells. 25% of LGL patients have a history of RA and LGL patients also have a higher frequency of HLADR4 haplotype (149). LGL is also associated with other autoimmune disorders such as Sjogren's syndrome and the underlying pathogenic process is chronic antigenic stimulation causing polyclonal expansion followed by clonal proliferation (150).EBV DNA has been detected in a proportion of NK-LGL patients and has been linked to pathogenesis (151). In some of the experiments in this chapter when T-cells were present in the contaminating population, there was expansion of T-cells but not to the same degree as NK cells (Data not shown). Therefore, the contact dependant B-NK

interaction observed in his chapter could be contributory to the development of LGL in RA patients.

Regulation of antibody production and thereby the immune response of B-cells is thought to be mainly mediated by competition for survival niches in the bone marrow. NK cells in addition to rapid immune response against infections and tumours also possess immunoregulatory properties. Regulation of T-cells by NK cells is mediated by multiple different mechanisms including perforin-mediated killing, cytokines such as IFNγ and IL10, and various NK receptor-ligand interactions such as NKG2A/D, NKp46 resulting in cell death (152). NK cells play a key role in termination of antibody responses in the context of vaccination (153) and respiratory syncytial virus infection (154). Therefore, irrespective of the presence of EBV, the NK cell proliferation during plasma cell differentiation could be a novel key mode of NK cell mediated regulation of B-cells that has not been appreciated or studied in detail.

10 Fifth Results Chapter: Phenotyping of long-lived plasma cells

Persistence of anti-microbial and autoantibodies after therapeutic B-cell depletion for various autoimmune disorders including RA is a clear proof of the presence of long-lived PCs. Clinical improvement or reduction in autoantibodies following B-cell depletion would be consistent with pathogenesis being mediated by short-lived PCs. The lack of clinical response after B-cell depletion would suggest pathogenesis that is at least in part mediated by long-lived PCs. The antibodies secreted by long and short-lived plasma cells could be of different clinical relevance in different pathological conditions. To understand this difference it is imperative to identify the long-lived plasma cells phenotypically for which until recently there were no known markers (155). ELISpot can be used to confirm the antigen specificity of PCs thereby their longevity depending on time since exposure to the antigen. However potential phenotypic markers need to be identified for testing by ELISpot.

Examination of the PCs from bone marrow of RA patients would be ideal to understand the behaviour of the short-lived and long-lived PCs in RA. However, it is difficult to recruit patients to have a bone marrow examination performed when it does not influence their clinical care directly due to the significant pain caused by the procedure. Although small, there is a definitive risk associated with the procedure including bleeding and infection and it also requires the expertise of the Haematologists. It will also require an additional hospital visit by the patients. The previous study attempting bone marrow examination failed to recruit more than 2 patients. Therefore, the surplus bone marrow samples from the diagnostic lab (HMDS) which were analysed and found not to have any disease involvement were used for analysis. This will allow deeper understanding of normal PC biology and specific questions in relation to RA such as antigen specificity if required can be addressed in future studies.

CD19 was identified based on historical work at the HMDS in monitoring marrow reconstitution following bone-marrow ablation, where $CD19^{Pos}$ PCs return earlier compared to $CD19^{Neg}$ PCs. Myeloma is characterised by presence of $CD19^{Neg}$ PCs in majority of the cases and the cell of origin for myeloma is thought to be the long-lived PCs. Therefore CD19 negativity was pursued as a marker of long-lived PCs. The aim of the study was not related to myeloma PCs. However, since CD19 negativity was pursued as a marker of long-lived PCs and majority of the myeloma

cases are characterised by $CD19^{Neg}$ PCs, it is essential to understand the difference between the normal $CD19^{Neg}$ and myeloma PCs. Since myeloma PCs are considered to be derived from long-lived PCs, comparison of the features that are different between CD19Pos and CD19Neg normal PCs with myeloma PCs might reveal clues regarding mechanisms contributing to longevity.

A significant proportion of $CD19^{Neg}$ PCs were present in bone marrow of controls which were polyclonal and therefore different to myeloma PCs (Figure 10.1-1). To test whether the $CD19^{Pos}$ and $CD19^{Neg}$ PCs are genuinely distinct populations, the differences in expression of other surface markers were evaluated and in particular enrichment for markers associated with PC longevity such as CD28 (156) was assessed. This revealed that there was further heterogeneity within PCs as noted for memory B-cells and 4 out of the 8 subsets identified based on expression of CD28/CD45/CD56 were differentially distributed between $CD19^{Pos}$ and $CD19^{Neg}$ PCs (Figure 10.1-2) and CD28 was predominantly expressed by $CD19^{Neg}$ PCs (Figure 10.1-3). Since myeloma PCs are understood to be derived from long-lived PCs, The expression levels of markers used to phenotype myeloma PCs were assessed to check whether the myeloma PCs are distinct from normal PCs which revealed that $CD19^{Pos}$ and $CD19^{Neg}$ PCs were different to myeloma PCs and similar to each other for majority of the markers tested. For those markers with differentially expressed markers, the profile of myeloma PCs followed an exaggerated pattern to that of normal $CD19^{Neg}$ PCs (Figure 10.1-4). Long-lived PCs are likely to express higher levels of anti-apoptotic molecules and lower levels of pro-apoptotic molecules and the expression of BCL2 and CD95 by $CD19^{Neg}$ PCs were consistent with this hypothesis (Figure 10.1-5).

The expression of molecules associated with survival in itself does not prove the longevity of the $CD19^{Neg}$ PCs. Therefore, evidence for a prolonged life-span for $CD19^{Neg}$ PCs in vivo was sought. Bone marrow ablation therapy depletes entire PC compartment and therefore both short and long-lived PCs and B-cell depletion is likely to deplete the short lived PCs from the marrow due to their constant requirement for replenishment from the B-cells. To test this further, reconstitution of PCs during remission following bone marrow ablation for myeloma and therapeutic depletion of B-cells with anti-CD52 therapy for CLL were studied. When both $CD19^{Pos}$ and $CD19^{Neg}$ PCs were depleted the $CD19^{Neg}$ PCs did not recover to normal levels even after 5 years following their depletion (Figure 10.2-1). However, on B-cell depletion, the

$CD19^{Pos}$ PCs were almost completely depleted but recovered within 2 years (Figure 10.2-2) whereas the $CD19^{Neg}$ PCs remained stable. These results are suggestive of distinct kinetics in generation of $CD19^{Pos}$ and $CD19^{Neg}$ PCs.

From data available so far and from the published literature, there still remains few unanswered questions. It is not known at what stage during the course of differentiation, the decision to become a $CD19^{Neg}$ PC is made and whether they are derived from $CD19^{Pos}$ PCs. Human and murine B-cell differentiation shows phenotypic divergence even for key antigens and murine models do not allow direct extrapolation of phenotypes linked to plasma cell longevity (157, 158). Direct in vivo assessment of plasma cell longevity in humans is challenging both technically and ethically, and in vitro approaches have been hampered by the lack of model systems allowing long-term human plasma cell maintenance in vitro. However, the recently developed assay previously described allows the maintenance of long-lived human plasma cells in vitro (60) and therefore the generation of $CD19^{Pos}$ and $CD19^{Neg}$ PCs was studied in vitro.

$CD19^{Neg}$ PCs can be generated by stimulation of B-cells with IL2, CD40L and BCR stimuli based protocol in vitro (Figure 5.4-1) and it was confirmed using 3 different CD19 antibody clones and fluorochromes (Figure 10.3-1).Long-lived PCs are likely to be under stricter control and therefore likely to be generated via a classical germinal centre reaction. It is not known whether CD40L stimulus is mandatory for generation of $CD19^{Neg}$ PCs. Therefore, stimulation with TLR agonist instead of CD40L was tested and $CD19^{Neg}$ PCs were generated with TLR stimulation. The $CD19^{Neg}$ PCs were generated quite early during in vitro differentiation of PCs with both CD40L and TLR stimuli. To test whether the $CD19^{Neg}$ PCs are generated early in vivo, the immune response to seasonal influenza vaccine was studied which is suggestive of early $CD19^{Neg}$ plasmablast generation (Figure 10.3-7) but requires further studies for confirmation.

The in vivo studies described above provide an indirect evidence for longer life span of $CD19^{Neg}$ PCs. When tested in vitro by long-term cultures, the change in the relative proportions of CD19Neg PCs and CD19Pos PCs was suggestive of a longer life span for $CD19^{Neg}$ PCs (Figure 10.3-8). One possible explanation for the delayed reconstitution of $CD19^{Neg}$ PCs shown in Figure 10.2-1 is that $CD19^{Neg}$ PCs are derived from $CD19^{Pos}$ PCs with time. To address this in vitro generated $CD19^{Pos}$ PCs were flow sorted and monitored for the development of $CD19^{Neg}$ PCs in vitro which did not reveal any evidence to support the hypothesis (Figure 10.3-9). The immunoglobulin repertoire of the bone marrow $CD19^{Pos}$ and $CD19^{Neg}$ PCs was analysed to

understand the similarities and differences between the two populations. A lower degree of overlap in the IGHV sequences between cell populations would be suggestive of their distinct nature and therefore the overlap between $CD19^{Neg}$ and $CD19^{Pos}$ PCs was assessed. Memory B-cells are known to have shorter CDR3 length compared to transitional and naïve B-cells (159). Therefore, differences in CDR3 length might be suggestive of their cell of origin and when it was analysed; $CD19^{Neg}$ PCs were noted to have shorter CDR3 length.

In summary, this chapter addresses various different properties of $CD19^{Pos}$ PCs and $CD19^{Neg}$ PCs in vivo and in vitro to identify the subset which is likely to contain the cells with potential for longevity.

10.1 Phenotyping and characterisation of bone marrow plasma cells

To phenotype PCs, an approach similar to that used for classification of memory B-cells was employed. Since CD19 negativity was pursued as a marker of long-lived PCs and myeloma PCs are known to be CD19 negative, normal PCs were initially checked for light chain restriction. The expression levels of pro-survival and apoptotic proteins were compared between the PC subsets. The surface markers used for routine phenotyping of myeloma PCs were compared and contrasted.

10.1.1 Polyclonal $CD19^{Neg}$ PCs can be detected in normal bone marrow and are a heterogeneous population

PCs were analysed from 23 bone marrow samples investigated for possible haematological malignancy but lacking evidence of disease involvement of the marrow. The surplus bone marrow samples were subjected to RBC lysis with ammonium chloride and stained with the antibodies in Table 5.2-2 for surface staining or Table 5.2-5 for intracellular staining. PCs were defined as $CD38^{Hi}CD138^{Hi}CD45^{int/wk}$ and based on their scatter profile as per the gating strategy shown in Figure 5.2-4. In all cases the majority of PCs co-expressed CD19 and CD45 but a minor population of $CD19^{Neg}45^{int}$ PCs were detected in all samples, representing a median 24% of total PCs (interquartile range 16-35%, range 1 – 52%). The malignant PCs seen in multiple myeloma and MGUS (Monoclonal gammapathy of uncertain significance) are mostly CD19 negative but are typically monoclonal. Analysis of cytoplasmic immunoglobulin light chain of the initial 11/23 cases demonstrated that the $CD19^{Neg}$ PCs were polytypic in all cases, with a median cytoplasmic kappa:lambda ratio of 1.7:1 (range 1 – 3.8:1). The $CD19^{Neg}$ PCs had a predilection for kappa light chain with a slightly higher kappa:lambda ratio with p-value of 0.002 (Wilcoxon matched-pairs signed rank test).

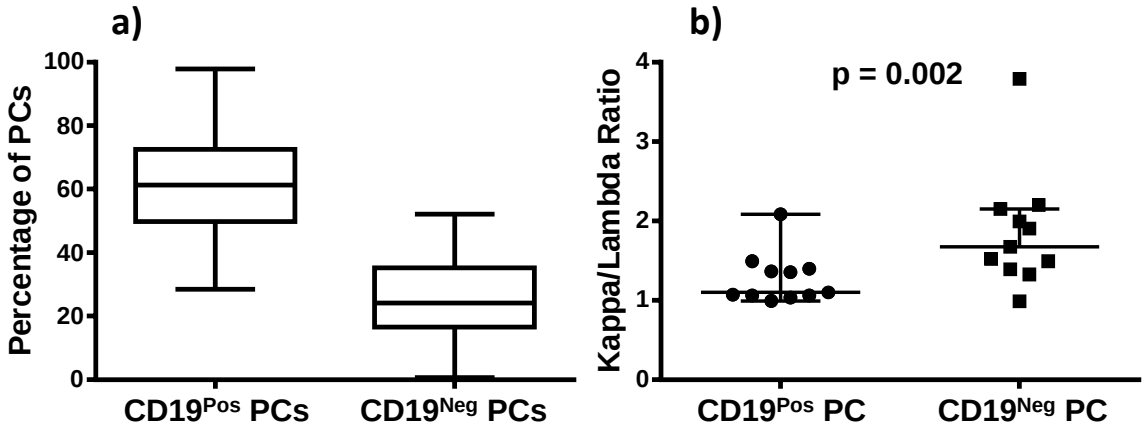

Figure 10.1-1 Proportion of $CD19^{Neg}$ PCs and analysis of light chain usage

Surplus bone marrow samples from 23 controls were investigated for various haematological conditions and reported to have a normal bone marrow were subjected to RBC lysis with ammonium chloride and stained with the antibodies in Table 5.2-2 or Table 5.2-5. PCs were defined as $CD38^{Hi}CD138^{Hi}CD45^{int/wk}$ and based on their scatter profile as per the gating strategy shown in Figure 5.2-4.

a) CD19 positive and negative PCs as a proportion of total PCs in disease free bone marrows from 23 controls are shown. The boxes represent the upper and lower quartiles and the whiskers represent the minimum and maximum values.

b) Kappa/Lambda ratio of $CD19^{Pos}$ and $CD19^{Neg}$ PCs from the first 11 controls in a) shown. The ratio is significantly different between the two PC subsets ($p = 0.002$, Wilcoxon matched-pairs signed rank test). The horizontal bars represent median with interquartile range.

10.1.2 The PC subset distribution pattern varies between CD19 positive and negative PCs

PCs were analysed from 12 bone marrow samples investigated for possible haematological malignancy but lacking evidence of disease involvement of the marrow. The surplus bone marrow samples were subjected to RBC lysis with ammonium chloride and stained with the antibodies in Table 5.2-2. PCs were defined as $CD38^{Hi}CD138^{Hi}CD45^{int/wk}$ and based on their scatter profile as per the gating strategy shown in Figure 5.2-4. Using the common markers used for phenotyping neoplastic PCs such as CD19, CD45, CD56 and CD28, PCs can be sub-divided into 16 different subsets as shown in Figure 10.1-2. This reveals a marked heterogeneity within the PC pool which is likely to be even greater with additional markers. The relative proportion of each subset within the $CD19^{Pos}$ and $CD19^{Neg}$ PCs was analysed. A higher proportion of $CD19^{Neg}$ PCs were CD56 positive, CD28 positive and CD45 weak compared to $CD19^{Pos}$ PCs (Figure 10.1-2). This pattern of cell surface expression is similar to myeloma PCs.

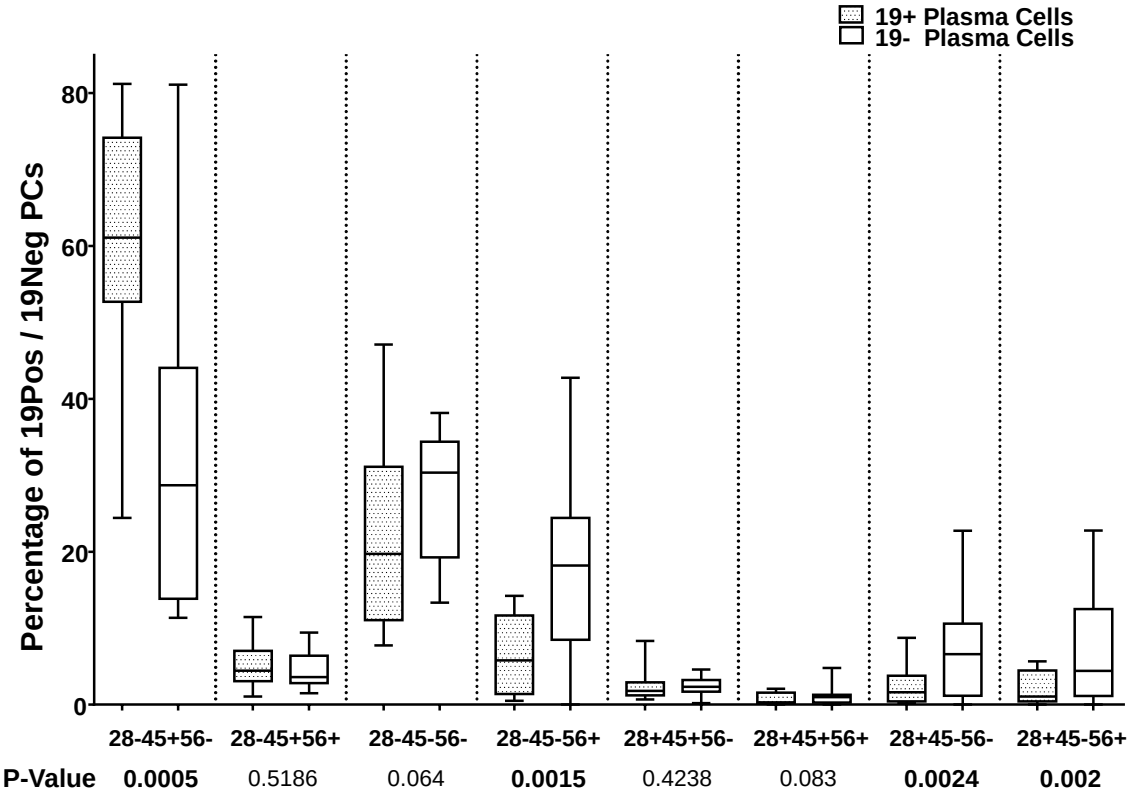

Figure 10.1-2 Differences in subset distribution of CD19^{Pos} and CD19^{Neg} PCs

Surplus bone marrow samples from 12 controls were investigated for various haematological conditions and reported to have a normal bone marrow were subjected to RBC lysis with ammonium chloride and stained with the antibodies in Table 5.2-2. PCs were defined as CD38^{Hi}CD138^{Hi}CD45$^{int/wk}$ and based on their scatter profile as per the gating strategy shown in Figure 5.2-4. PCs expressed as percentage of CD19^{Pos} or CD19^{Neg} PCs divided into 8 subsets each based on CD45/56/28 expression. The boxes represent the upper and lower quartiles and the whiskers represent the minimum and maximum values. Paired t-test (Wilcoxon signed-rank) 'p-value' shown with the significant values in bold. The boxes represent the upper and lower quartiles and the whiskers represent the minimum and maximum values. Dotted bars – Normal CD19^{Pos} PCs, Clear bars – Normal CD19^{Neg} PCs (n=12)

However, only CD28 has been mechanistically linked to PC longevity through downstream NFKB signalling (156). CD28 has also been shown to be a key pro-survival and apoptotic resistance mediator in myeloma PCs through the PI3K/Akt/FoxO3a/Bim pathway (160). CD28 expression is quite variable in normal human PCs and the common pattern is that the CD28^{Pos}PCs are mostly confined to the CD19^{Neg} PC subset. Occasionally there was the

presence of CD28^{Pos} PCs within the CD19^{Pos} PC subset or complete absence of CD28^{Pos} PCs (Figure 10.1-3). Further analysis of the CD28^{Pos} PCs revealed that the majority were CD19 negative and CD45 weak (p=0.001) (Figure 10.1-3).

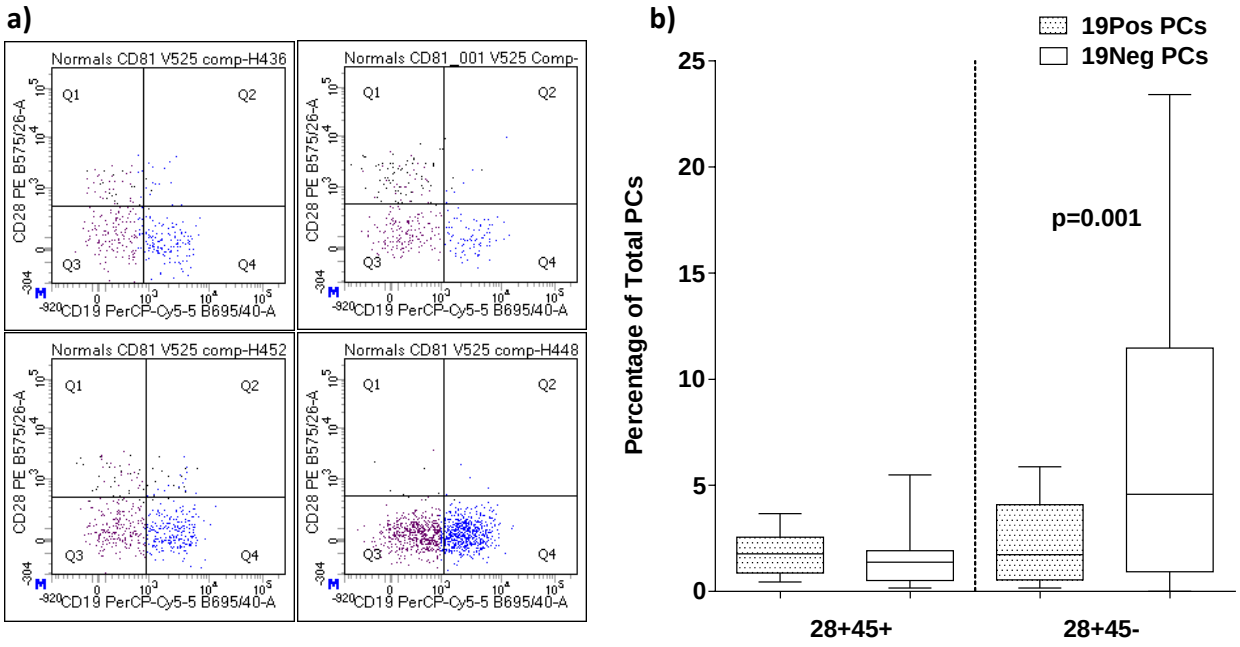

Figure 10.1-3 CD28 expression by normal CD19^{Pos} and CD19^{Neg} PCs

Surplus bone marrow samples from 12 controls were investigated for various haematological conditions and reported to have a normal bone marrow were subjected to RBC lysis with ammonium chloride and stained with the antibodies in Table 5.2-2. PCs were defined as CD38^{Hi}CD138^{Hi}CD45$^{int/wk}$ and based on their scatter profile as per the gating strategy shown in Figure 5.2-4.

a) Different expression patterns of CD19 and CD28 by PCs. CD19^{Pos} PCs are coded as blue and CD19^{Neg} PCs are purple.

b) CD28 positive PCs divided into subsets based on expression of CD19 & CD45 represented as percentage of total plasma cells. The boxes represent the upper and lower quartiles and the whiskers represent the minimum and maximum values. Paired t-test (Wilcoxon signed-rank) 'p-value' shown. (n=12)

10.1.3 Neoplastic myeloma PCs more closely resemble normal $CD19^{Neg}$ than $CD19^{Pos}$ PCs

In addition to the fraction of cell populations expressing antigen, the level of expression was assessed in the samples from the previous section along with 11 myeloma patients, and the analysis was extended to a wider range of antigens in the following groups: control $CD19^{Pos}$, control $CD19^{Neg}$ and myeloma PCs (all CD19 negative in this series). $CD19^{Pos}$ PCs from control bone marrow samples showed very few differences in protein expression to paired $CD19^{Neg}$ PCs except for CD45. CD56 expression identified a subset of normal $CD19^{Neg}$ PCs in the majority of control samples. As reported in several previous studies, CD56 is strongly expressed in approximately three quarters of myeloma cases and the level of expression by neoplastic PCs is typically more than ten-fold the level detected on normal $CD56^{Pos}CD19^{Neg}$ PCs. In addition to CD56, there were significant differences in levels of expression of CD27, CD81 and CD117 between neoplastic and normal $CD19^{Neg}$ PCs but there were no differences for these markers between normal $CD19^{Pos}$ and $CD19^{Neg}$ PCs (Figure 10.1-4).

Thus for the majority of markers, normal $CD19^{Pos}$ and $CD19^{Neg}$ PCs are phenotypically similar but for those markers with differential expression, namely CD45 and CD56, the profile on neoplastic PCs follows an exaggerated pattern of that seen on normal $CD19^{Neg}$ PCs.

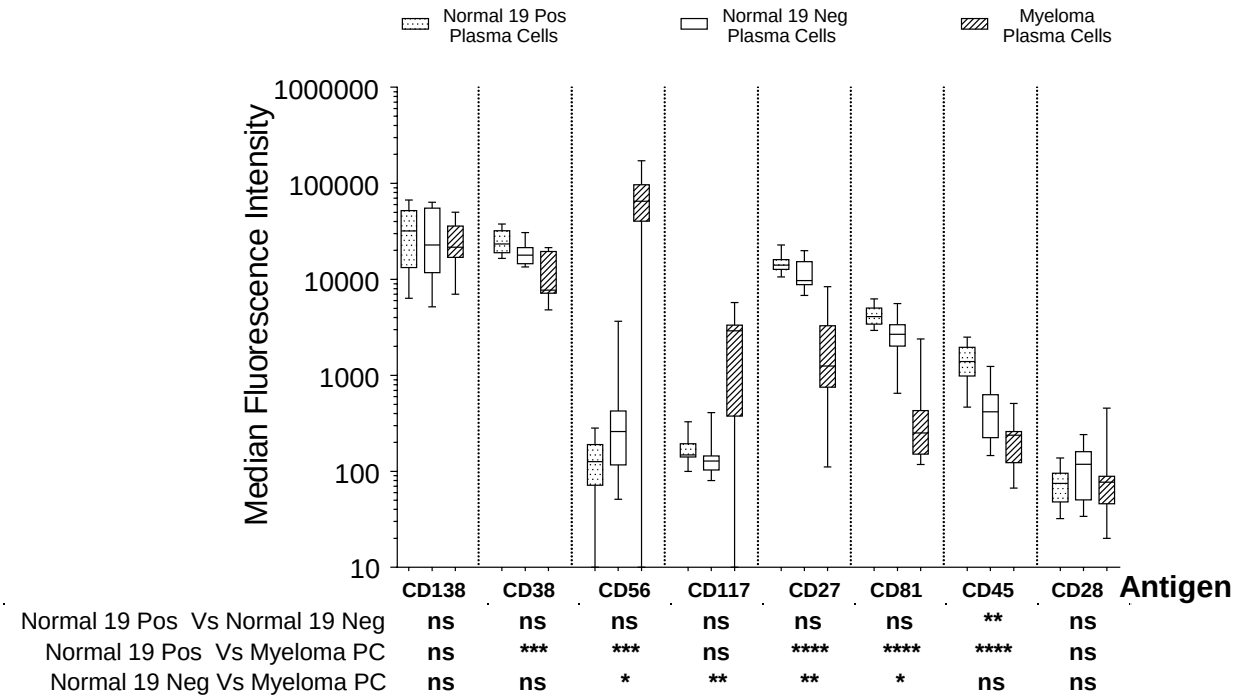

Figure 10.1-4 Comparison of antigen expression levels on normal CD19^{Pos}, normal CD19^{Neg} and myeloma plasma cells

Surplus bone marrow samples from 12 controls and 11 myeloma patients were subjected to RBC lysis with ammonium chloride and stained with the antibodies in Table 5.2-2. PCs were defined as CD38^{Hi}CD138^{Hi}CD45$^{int/wk}$ and based on their scatter profile as per the gating strategy shown in Figure 5.2-4. Surface expression levels (Median channel fluorescence) of the various antigens on normal plasma cells and myeloma plasma cells shown. Only samples with more than 20 events in each subset were included in the analysis. 'P values' (Kruskal-Wallis test with Dunn's multiple comparisons) for comparison of the MFIs between the different populations for the tested antigens is given in the table below. The boxes represent the upper and lower quartiles and the whiskers represent the minimum and maximum values. Dotted bars – Normal CD19^{Pos} PCs, Clear bars – Normal CD19^{Neg} PCs, Striped bars – Myeloma PCs. Plasma cells were gated based on their scatter profile and expression of CD138 and CD38. The level of CD19 expression on B-cells was used to guide the gating of the CD19 negative plasma cells. The CD19 levels on CD19^{Neg}plasma cells were lower than the lowest CD19 expressing B-cells.

10.1.4 Differential expression of pro- and anti-apoptotic markers in $CD19^{Pos}$ and $CD19^{Neg}$ PCs.

PC longevity is linked to resistance from apoptosis due to the differential expression of anti-apoptotic proteins of the BCL2 family such as Mcl-1, Bfl-1/A1 and the TNF receptor superfamily member BCMA (161-163), while the pro-apoptotic FAS receptor is upregulated during B-cell activation. Expression of FAS receptor CD95 and intracellular BCL2 were therefore evaluated in 11 control samples with only polyclonal PCs. Bone marrow samples from patients investigated for various haematological conditions but lacking evidence of disease involvement of the marrow were used. The surplus bone marrow samples were subjected to RBC lysis with ammonium chloride and intracellular staining was performed with the antibodies in Table 5.2-5. PCs were defined as $CD38^{Hi}CD138^{Hi}CD45^{int/wk}$ and based on their scatter profile as per the gating strategy shown in Figure 5.2-8. The expression of BCL2 was 28% higher in $CD19^{Neg}$ PCs (4-113%) compared to $CD19^{Pos}$ PCs from the same aspirate sample ($P<0.0001$). The expression of CD95 was 163% lower (79-284%) in $CD19^{Neg}$ PCs compared to paired $CD19^{Pos}$ PCs ($P<0.0001$) (Figure 10.1-5). The greater expression of BCL2 and lower expression of CD95 would be in keeping with pro-survival phenotype in $CD19^{Neg}$ PCs.

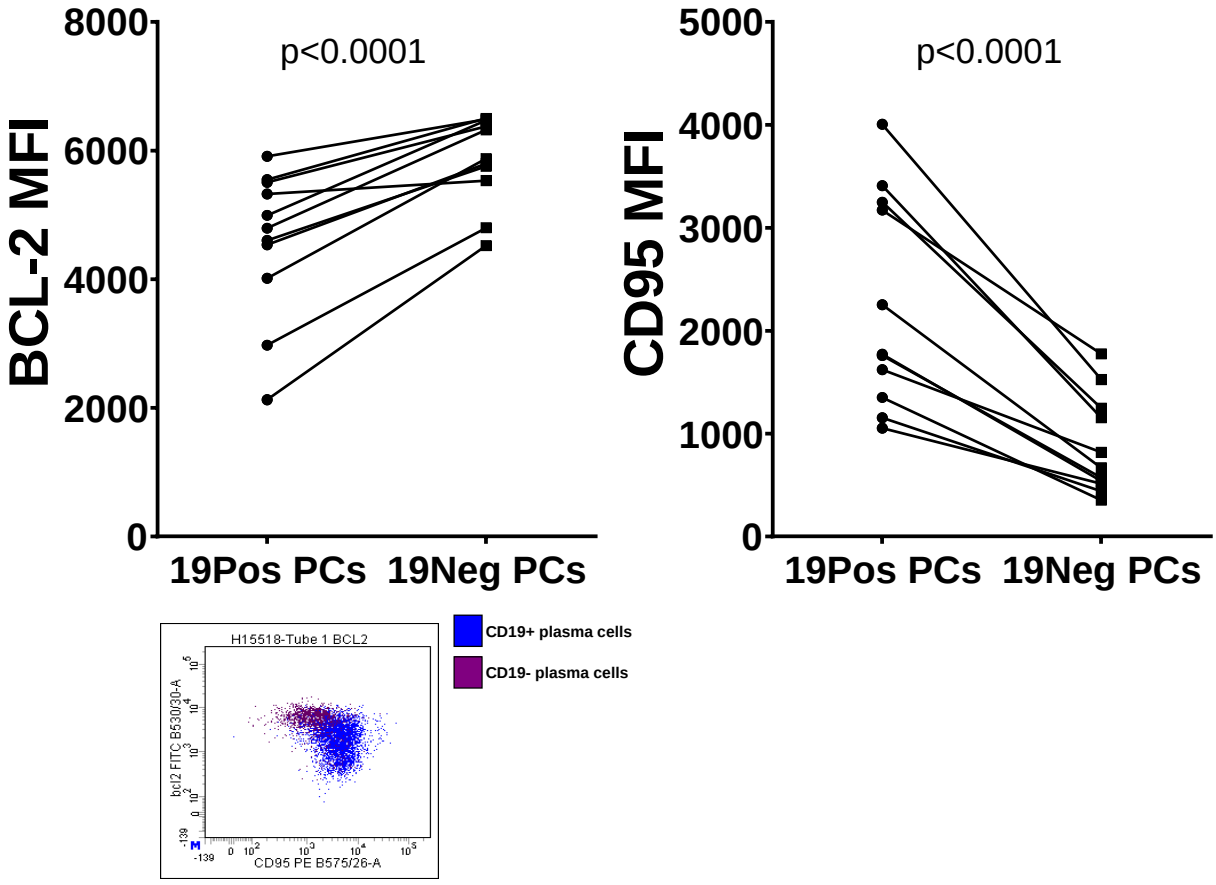

Figure 10.1-5 Expression levels of BCL2 and CD95 by normal polyclonal 19Positive and 19Negative PCs

Surplus bone marrow samples from 11 controls were subjected to RBC lysis with ammonium chloride and stained with the antibodies in Table 5.2-5. PCs were defined as $CD38^{Hi}CD138^{Hi}CD45^{int/wk}$ and based on their scatter profile as per the gating strategy shown in Figure 5.2-8. Intracellular and surface protein expression levels as measured by the median channel fluorescence intensity of BCL2 and CD95, by polyclonal $CD19^{Pos}$ and $CD19^{Neg}$ plasma cells. (n==11). Representative flow cytometry plot of expression levels of BCL2 & CD95 by $CD19^{Pos}$ (Blue) and $CD19^{Neg}$ (Purple) PCs shown.

10.2 Differential life span of human plasma cell subsets in vivo

It is challenging to track the life span of human PCs in vivo. Therefore, clinical situations where PCs or B-cells that generate the PCs are depleted were used to assess the life span of PCs in vivo.

10.2.1 Normal $CD19^{Neg}$PCs display markedly delayed recovery after myeloablative treatment relative to $CD19^{Pos}$PCs.

The depletion of normal bone marrow following high dose chemotherapy provides an opportunity to track the kinetics of bone marrow PC repopulation in humans. To ascertain whether the kinetics of $CD19^{Pos}$ and $CD19^{Neg}$ PC population recovery was similar or distinct, the data from thirty-one patients from the MRC Myeloma IX trial who had sequential bone marrow aspirate samples during remission after high-dose melphalan with autologous stem cell rescue was reviewed. Twenty-five patients were included, who fulfilled the criteria of having two or more samples in the seven years following therapy and remaining in remission. Normal $CD19^{Neg}$ PCs were defined based on weak CD45 and absence of aberrant CD56, CD27 or CD38 expression, according to established criteria (164). The primary diagnostic flow data was reanalysed for the presence of normal $CD19^{Pos}$ and $CD19^{Neg}$ PCs in the 80 total samples. Overall the complete absence of PCs was the exception (6/80). $CD19^{Pos}$ PCs recover rapidly after successful treatment in 74/80 samples, and represented more than 90% of PCs in the majority of remission samples. Whilst $CD19^{Neg}$PCs also recovered in most patients, the kinetics of recovery was distinct. In the 80 samples analysed, $CD19^{Neg}$ PCs were undetectable in 19 samples and remained at less than 1% of total PCs in 30/80 samples. Specifically, in samples taken within the first 3 years following myeloablation 26/48 had $CD19^{Neg}$ PCs represented at less than 1% of total PCs, while such low representation of $CD19^{Neg}$ PCs was significantly reduced in samples taken between year 4 and 7 (4/32 samples). Overall these results indicated a gradual increase in $CD19^{Neg}$ PCs with time (Figure 10.2-1). Bone marrow samples between 4 to 6 years showed significantly higher proportions of $CD19^{Neg}$ PCs compared to samples between 1 to 3 years ($p=0.0013$). The results demonstrate a major difference in the kinetics of $CD19^{Pos}$ and $CD19^{Neg}$ PCs recovery when both populations are depleted simultaneously. Linear regression analysis of this data predicts that if such rates of reconstitution were maintained it would take up to 50 years to reach normal levels of $CD19^{Neg}$ PCs ($p=0.006$, $R^2 = 9.33\%$).

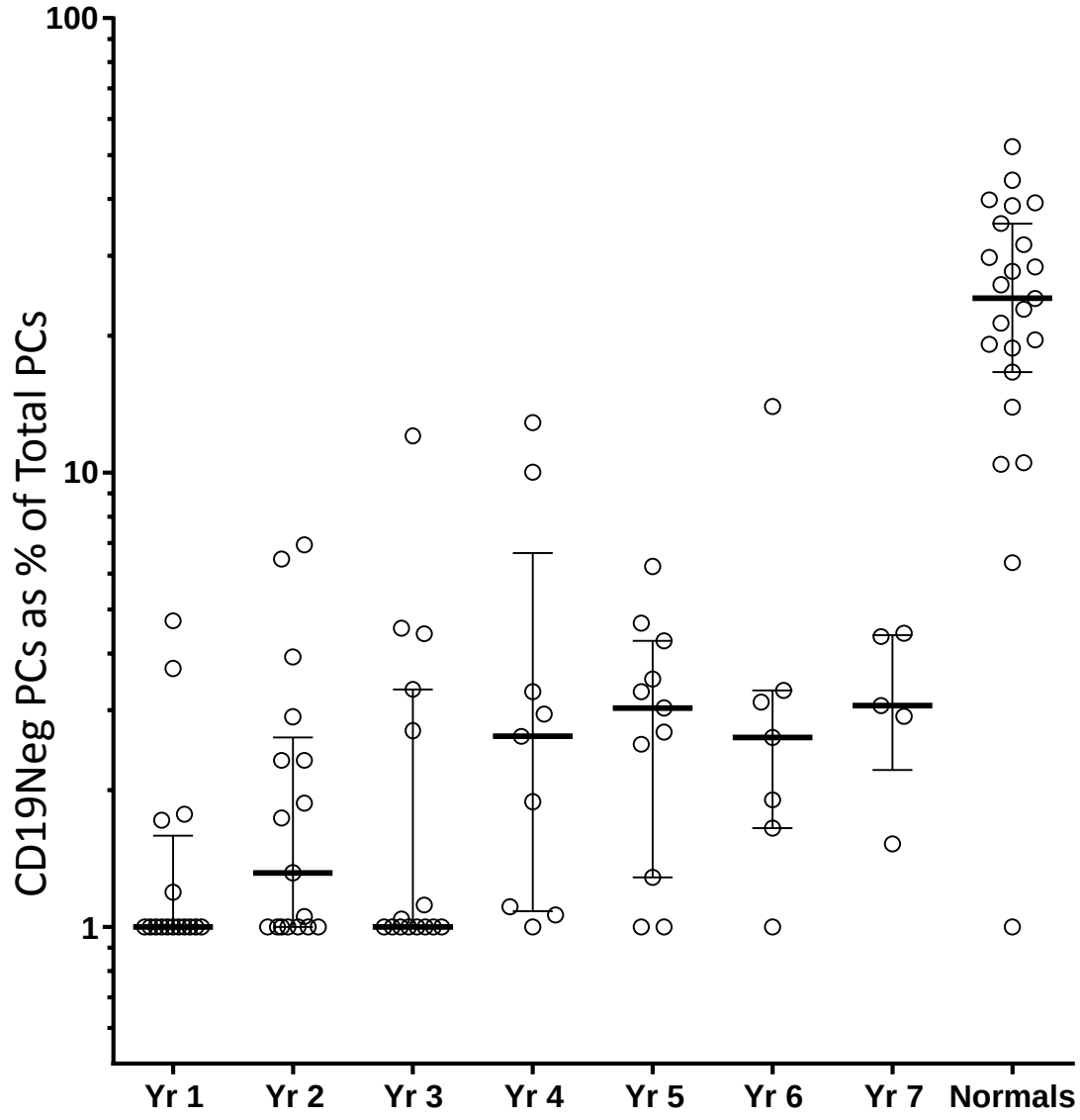

Figure 10.2-1 $CD19^{Pos}$ plasma cells recover rapidly after myeloablative treatment with stem cell rescue while $CD19^{Neg}$ plasma cells may take several years to regenerate

Scatterplot showing the 80 patient samples in the years following myeloablative therapy with autologous stem cell rescue for myeloma. The horizontal bars represent median and interquartile range. PCs were defined as $CD38^{Hi}CD138^{Hi}CD45^{int/wk}$ and based on their scatter profile as per the gating strategy shown in Figure 5.2-4. $CD19^{Neg}$ PCs are expressed as a percentage of total plasma cells. Figure shows progressive increase in the percentage of plasma cells that are $CD19^{Neg}$. The values below 1% have been rounded off to 1% for the purposes of the logarithmic scale in this figure.

10.2.2 B-cell depletion therapy results in loss of $CD19^{Pos}$ PCs within 3 months but $CD19^{Neg}$ PCs persist.

In order to determine whether there was any difference in the longevity of $CD19^{Pos}$ and $CD19^{Neg}$ PCs we reviewed bone marrow samples from CLL patients undergoing alemtuzumab therapy reported previously (74). Alemtuzumab targets CD52 and effectively depleted normal B-cells and GPI-expressing T-cells in the peripheral blood of all patients in the study, although there was differential depletion of CLL cells. Normal plasmablasts and PCs express at most low levels of CD52, similar to other populations that are resistant to alemtuzumab treatment. Depletion of normal B-cells may therefore be expected to result in reduced levels of short-lived PCs whilst having little or no effect on long-lived PCs. PCs from Campath trial were analysed retrospectively using markers from the panel designed for detection of residual CLL, comprising CD19 PE-Cy5 (FMC63, prepared in-house), CD5 APC (UCHT2, prepared in-house), CD20 FITC (B9E9, Coulter) and CD38 PE (HIT2, BD Biosciences). PCs were gated using CD38/CD20 and light scatter characteristics and the CD19 threshold was set using CD20-CD5+ lymphocytes as a negative control. The CLL patients in this study were extensively pre-treated and the PC proportion was low because of extensive marrow infiltration, but the relative proportions of $CD19^{Pos}$ and $CD19^{Neg}$ PCs changed significantly after exposure to alemtuzumab with almost complete depletion of the $CD19^{Pos}$ fraction. During treatment, the proportion of $CD19^{Neg}$ PCs remained low but stable. There was some recovery of $CD19^{Pos}$ PCs 1-3 months after cessation of alemtuzumab treatment, although pre-treatment equilibrium was not reached until 6-24 months after exposure to alemtuzumab (Figure 10.2-2). The results indicate that $CD19^{Pos}$ and $CD19^{Neg}$ PCs show distinct kinetics following therapeutic targeting of the immune system.

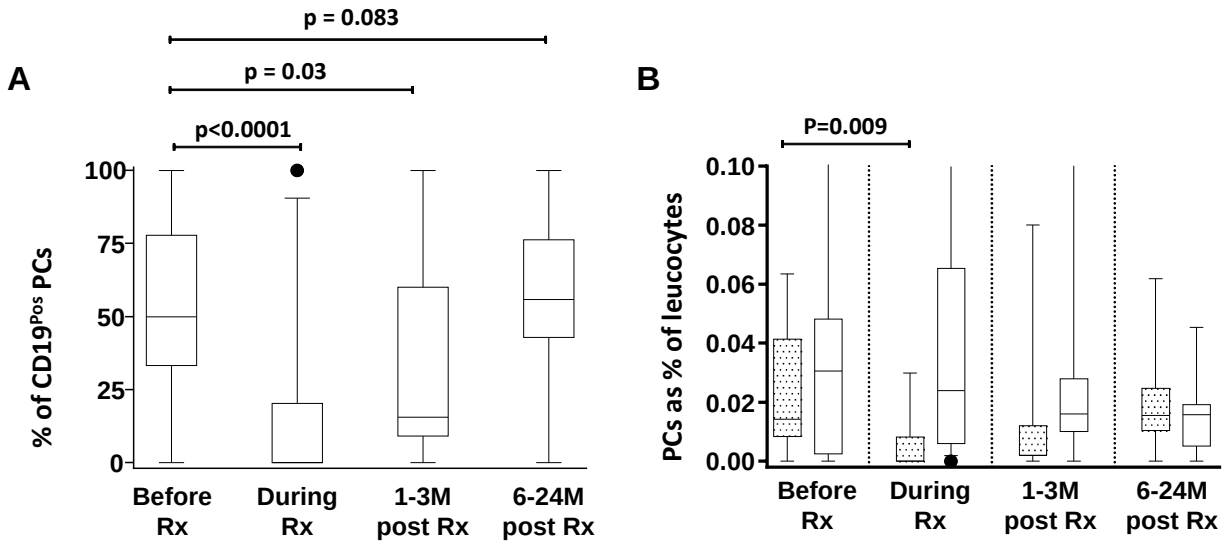

Figure 10.2-2 Recovery of PCs in CLL patients treated with Alemtuzumab

In CLL patients treated with alemtuzumab, total B-cell depletion results in a reduction in $CD19^{Pos}$ plasma cells but $CD19^{Neg}$ plasma cells persist. The $CD19^{Pos}$ PCs start recovering 1-3 months after treatment and reach normal levels by 2 years. The boxes represent the upper and lower quartiles and the whiskers represent the minimum and maximum values. Dotted bars – Normal $CD19^{Pos}$ PCs, Clear bars – Normal $CD19^{Neg}$ PCs. The different patient groups tested were - Before Rx (n=15), During Rx (n=38), 1-3 months post Rx (n=15), 6-24 months post Rx (n=18). Unpaired t test values given in figure A and paired t test value in figure B. PCs were gated using $CD38^{Hi}$ $CD20^{-}$ and light scatter characteristics and the CD19 threshold was set using $CD20^{-}CD5^{+}$ lymphocytes as a negative control.

The CD52 expression of normal PCs is 10-fold lower then alemtuzumab responsive cells and 5-fold lower than alemtuzumab resistant cells(165). However, some heterogeneity in the levels of CD52 expressed by PCs was also noted (165). Therefore CD52 expression was analysed specifically in CD19 positive and negative PC subsets. 5 surplus control bone marrow samples were subjected to RBC lysis with ammonium chloride and stained with CD52 FITC, CD28 PE, CD4 PerCP-Cy5.5, CD19 PE-Cy7, CD138 APC, CD38 AF700, CD45 APC-H7, CD56 BV421 and CD27 BV605. PCs were defined as $CD38^{Hi}CD138^{Hi}CD45^{int/wk}$ and based on their scatter profile as per the gating strategy shown in Figure 5.2-8. Although the levels of CD52 was slightly lower in $CD19^{Neg}$ PCs, the $CD19^{Pos}$ PC levels were significantly lower than B-progenitors ($p=0.04$) which are not depleted by alemtuzumab (Figure 10.2-3). Although the level of CD52 expression on both PC populations is significantly lower than alemtuzumab sensitive B-cells, the possibility of PCs being more sensitive cannot be ruled out. Therefore it cannot be excluded that

differential direct targeting of $CD19^{Neg}$ and $CD19^{Pos}$ PCs accounts for the preferential depletion of $CD19^{Pos}$ PCs. However, irrespective of the mode of depletion, the data demonstrate that in human bone marrow $CD19^{Neg}$ PCs are maintained independently of the $CD19^{Pos}$ PC population, and that $CD19^{Pos}$ PCs are reconstituted within 2 years which is much quicker than the reconstitution of $CD19^{Neg}$ PCs following myeloablation shown in Figure 10.2-1.

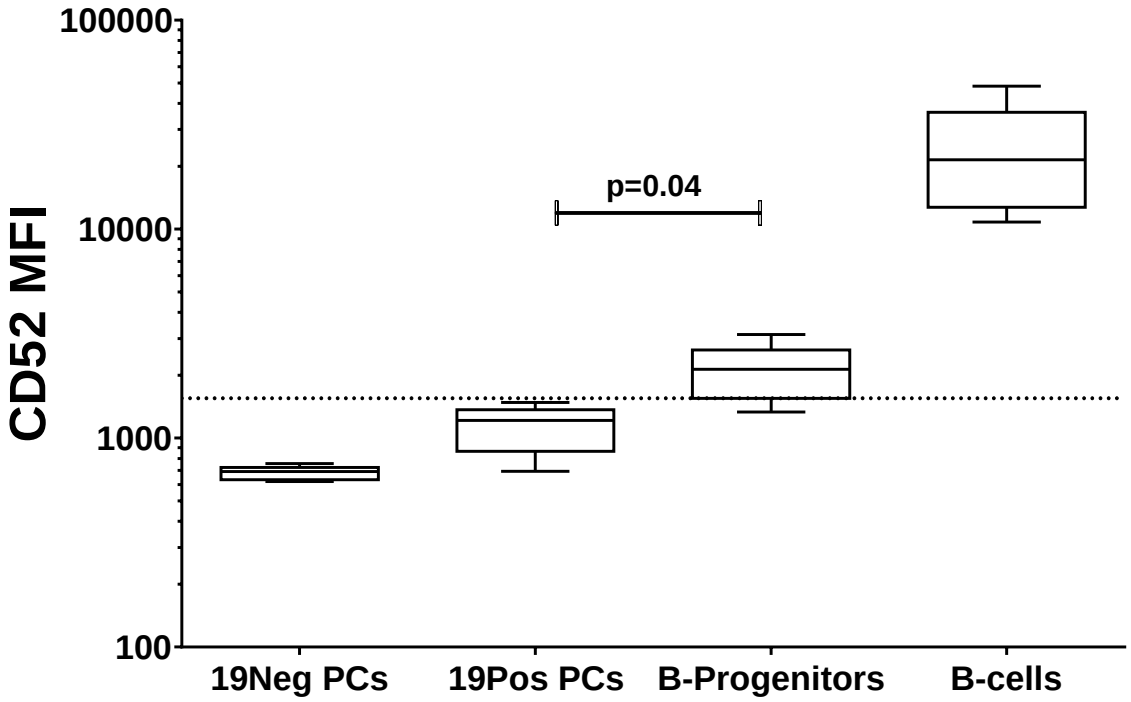

Figure 10.2-3 Levels of CD52 surface expression by B-lineage cell subsets

The median fluorescence intensity for CD52 surface expression by CD19 positive and negative PCs, B-progenitors and B-cells are shown (n=5). The CD19 positive PCs had significantly lower CD52 expression compared to B-progenitors which are not depleted by Alemtuzumab (p=0.04, paired t-test). PCs were defined as $CD38^{Hi}CD138^{Hi}CD45^{int/wk}$ and based on their scatter profile as per the gating strategy shown in Figure 5.2-4. B-cells were defined as $CD19^{+}CD45^{+}CD4^{-}$ and B-progenitors as $CD19^{+}CD45^{wk}CD38^{+}CD4^{-}$.

10.3 Generation and life span of in vitro derived $CD19^{Neg}$ plasma cells

Multiple models for in vitro generation of plasma cells exist (54-59, 166, 167). However these systems failed to generate long-lived PCs and it was not known whether $CD19^{Neg}$ plasma cells could be generated in vitro. Therefore, presence of $CD19^{Neg}$ PCs was analysed in the recently described in vitro differentiation system which was developed in-house and can generate long-lived PCs(60).

10.3.1 $CD19^{Neg}$ PCs can be generated in vitro

The origin and fate of human $CD19^{Neg}$ PCs is difficult to study due to requirement for sequential bone marrow sampling and lack of safe markers to track specific cell populations in vivo. Mouse models are not ideal due to the difference in surface phenotype of PCs compared to humans. Therefore, if $CD19^{Neg}$ PCs can be generated in vitro, they can provide an ideal model to study this subset.

In vitro generated PCs were heterogeneous for expression of CD19. There was variability in the pattern of CD19 heterogeneity displayed by PCs namely - distinct peaks or a continuum of expression levels from positive to negative as shown in Figure 10.3-1. To establish the cause for this variability, different clones and fluorochrome conjugates of the CD19 antibody were tested on PCs generated in vitro using the standard differentiation protocol (Figure 5.4-1). The PerCP-Cy5.5 and PE-Cy7 conjugated antibodies were of the same clone whereas the PE conjugated antibody was a different clone. Out of the three different fluorochromes tested, PerCP-Cy5.5 has the weakest signal. CD19 PE and CD19 PE-Cy7 had similar signal intensities but CD19 PE-Cy7 provided the best distinction between $CD19^{Pos}$ and $CD19^{Neg}$ PCs. However, since PE-Cy7 is a tandem conjugate which is prone to dissociation and compensation issues, CD19 PE was chosen. There is also an intrinsic variability between samples in the pattern of CD19 heterogeneity even when the same antibody was used.

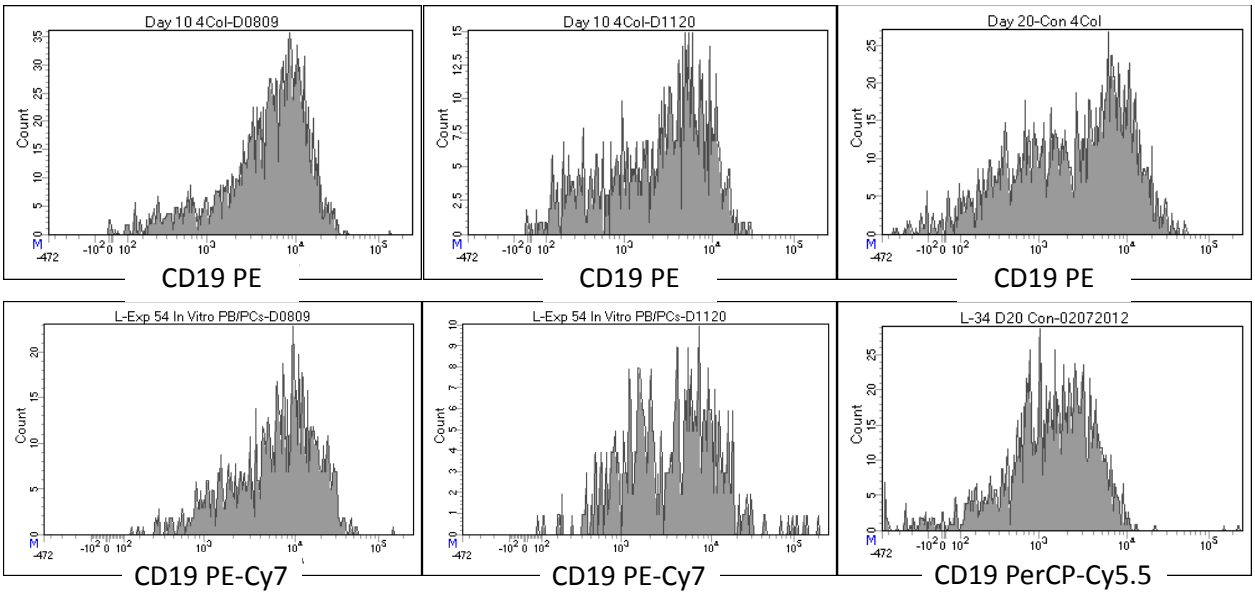

Figure 10.3-1 Different patterns of CD19 heterogeneity by in vitro generated PCs

CD19 expression by PCs defined as annexin/7AAD negative (Live), CD20 negative, CD38 & CD138 positive in the top row and CD38, CD27 & CD138 positive in the bottom row. Each column represents matched samples stained with different antibodies as indicated. The first two columns show day 10 PCs and the third column shows day 20 PCs generated in vitro using the standard protocol shown in Figure 5.4-1.

PCs from day 13 of the differentiation system were analysed for heterogeneity in surface expression of CD19. The CD19 expression levels (MFI) by flow cytometry was significantly different ($p<0.0001$) between the two subsets as shown in Figure 10.3-2. Some of the samples showed two peaks for the expression levels of CD19 and enabled easier segregation of subsets. In other samples there was no clear demarcation and in such cases the levels of baseline fluorescence seen with the isotype control was used as a guide to determine CD19 negativity as shown in Figure 10.3-2.

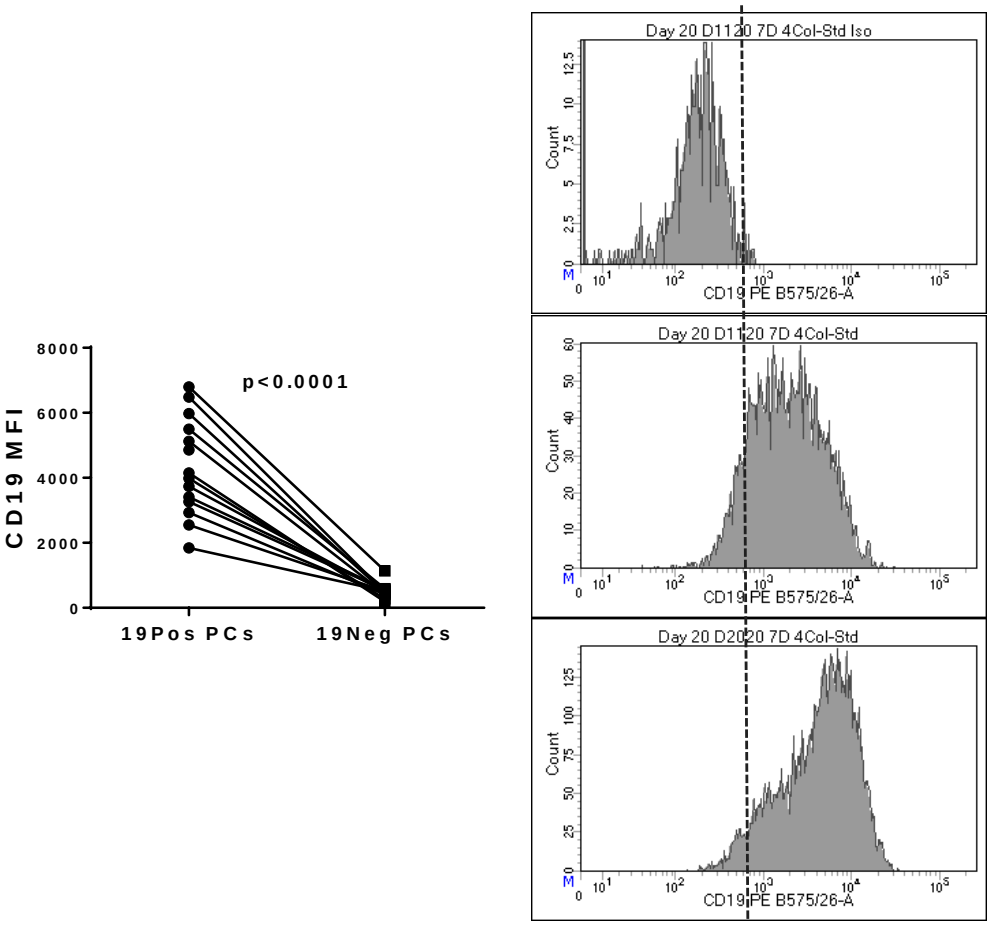

Figure 10.3-2 Evaluation of heterogeneity in surface expression of CD19 by PCs generated in vitro

Median Fluorescence Intensity (MFI) of CD19 on day 13 plasma cells generated using the standard protocol (Figure 5.4-1) defined as annexin/7AAD negative (Live), CD20 negative, CD38 & CD138 positive. This shows the presence of two distinct populations. Representative histograms of the types of samples which do not exhibit a clear demarcation between $CD19^{Pos}$ and $CD19^{Neg}$ cells shown. In such cases, CD19 negativity was determined based on the level of background fluorescence of the isotype control.

10.3.2 CD19 negativity is established early during PC differentiation

Negatively selected B-cells from controls were stimulated with IL2, CD40L and BCR stimuli and differentiated to PCs using the standard protocol (Figure 5.4-1). CD19 expression was sequentially analysed to determine at what stage during PC differentiation in vitro the CD19 negativity is established. The proportion of $CD19^{Neg}$ PCs increased with time during the course of plasma cell maturation. $CD19^{Neg}$ PCs were a very minor proportion or undetectable in most samples on day 6. There was a significant increase in the proportion of $CD19^{Neg}$ PCs for all the samples between day 6 and day 10 ($p<0.0001$). The increase in proportion continued till day 20 in most samples and it was significantly higher than day 10 ($p=0.004$). There was variability in the proportion of $CD19^{Neg}$ PCs generated by different samples. $CD19^{Neg}$ PCs are possibly generated from a distinct B-cell subset, the proportion of which is subject to biological variability within the same individual and/or between controls. Although the results are suggestive of $CD19^{Neg}$ PCs generated at the time of PC transition, it cannot be ruled out whether the $CD19^{Neg}$ PCs were $CD19^{Pos}$ before their transition in the short time frame between days 6 to 10. The in vivo data (Figure 10.2-1) would not support such quick evolution of $CD19^{Neg}$ PCs from $CD19^{Pos}$ PCs but cannot be ruled out in vitro. This can be addressed by sorting the $CD19^{Pos}$ PBs and PCs at multiple time points during the early stages of differentiation for generation of $CD19^{Neg}$ PCs. Alternatively if the cell of origin for $CD19^{Neg}$ PCs is identified, their PB to PC transition stage could be closely monitored in vitro.

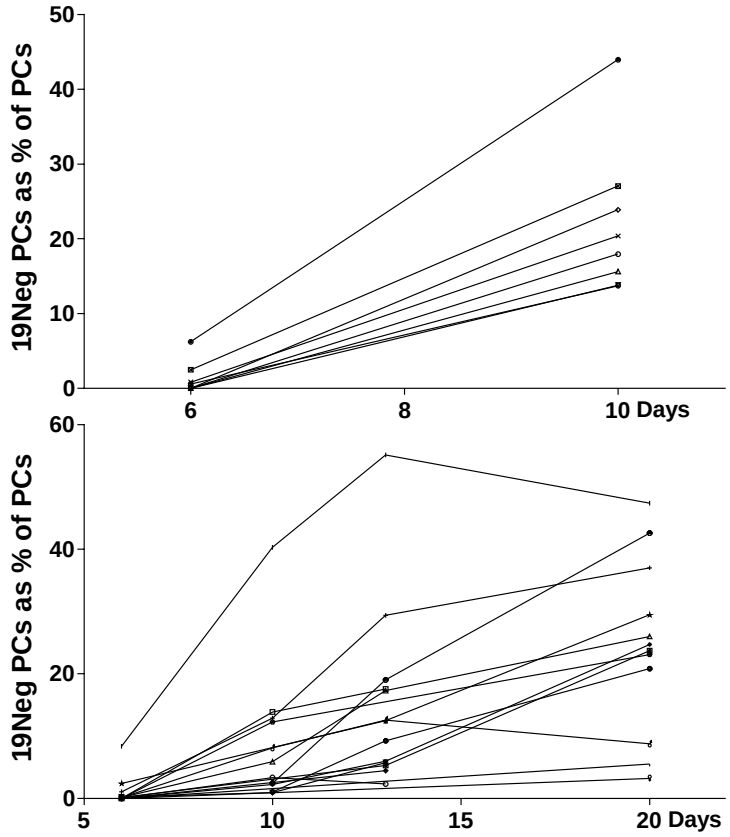

Figure 10.3-3Sequential change in proportion of CD19^{Neg} PCs during PC differentiation

Negatively selected B-cells were differentiated to PCs in vitro using the standard differentiation protocol Figure 5.4-1). Change in the proportion of CD19^{Neg} PCs (expressed as a percentage of total PCs) over short- and long-term in 8 and 16 controls respectively, acquired over 18 separate experiments.

10.3.3 CD19^{Neg} PCs can also be generated using TLR7/8 agonist R848 instead of CD40L for co-stimulation

The standard B-cell differentiation protocol (Figure 5.4-1) uses CD40L stimulus in the form of mouse fibroblasts transfected with human CD40L (L-cells). Whether the generation of CD19^{Neg} PCs is specifically linked to CD40L stimulation or other signals derived from L-cells is not known. Therefore, the TLR7/8 agonist - R848 was used to differentiate B-cells instead of L-cells. Viable PCs with phenotype similar to those generated with CD40L stimulus were generated and maintained the phenotype up to day 40 and possibly beyond as shown in Figure 10.3-4. The CD19 expression was also heterogeneous in PCs generated with both stimuli.

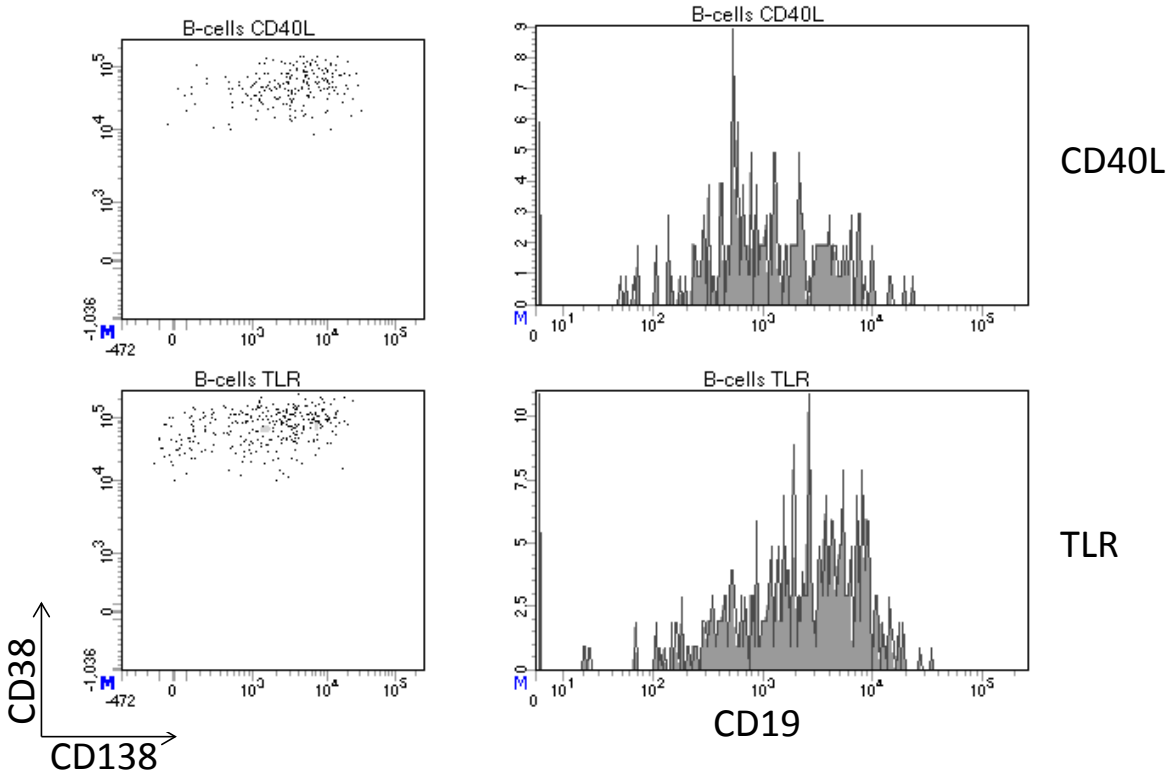

Figure 10.3-4 PCs generated with CD40 L or TRL7/8 agonist R848 exhibit similar phenotype

Negatively selected B-cells were differentiated to PCs in vitro using the standard protocol (Figure 5.4-1). Dot plots showing the presence of live (Annexin/7AAD negative) plasma cells (CD38 and CD138 positive) generated by CD40 ligand and TLR agonist R848 stimulation on day 42 of in vitro differentiation. Histograms for CD19 expression by PCs generated with CD40L stimulus (top row) and TLR stimulus (bottom row)

The sequential change in proportion of CD19^{Neg} PCs generated with different stimuli was compared in 3 controls. There was a trend towards higher proportions of CD19^{Neg} PCs generated with TLR stimulus when the sequential changes in proportion of CD19^{Neg} PCs during the early stages of PC maturation were plotted. However there was some variability during later stages (day 20) and when all the available time points were compared, the difference did not achieve statistical significance (p=0.084).

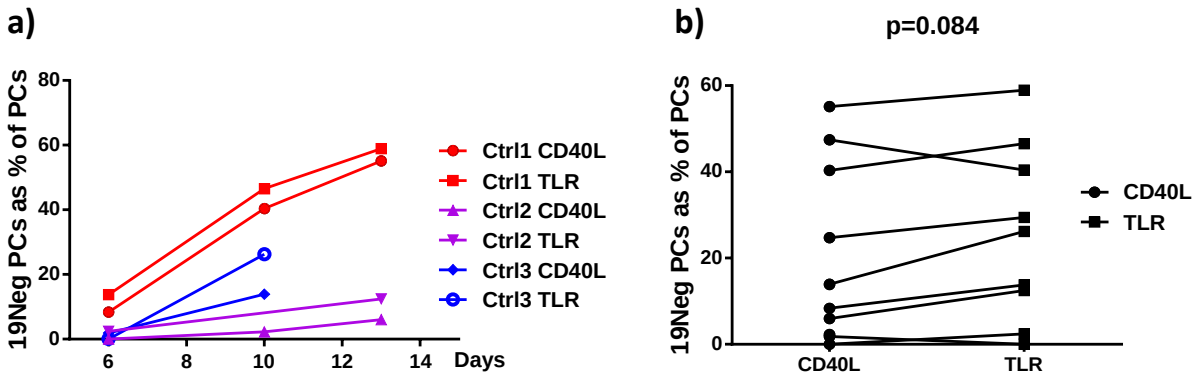

Figure 10.3-5 Comparison of proportion of CD19^{Neg} PCs generated with CD40L and TLR stimuli

Negatively selected B-cells were differentiated to PCs in vitro using the standard protocol (Figure 5.4-1).

a) CD19^{Neg} PCs expressed as a percentage of total PCs (defined as Annexin/7AAD negative, CD38 and CD138 positive) generated by 3 controls in 3 different experiments at the specified time points.

b) Comparison of the proportion of CD19^{Neg} PCs generated with CD40L or TLR stimulus at identical time points in 3 controls shown. The time points are from 3 different experiments and vary between day 6 and day 42. 'P value' for the significance of the difference between the 9 pairs by paired t-test shown.

10.3.4 $CD19^{Neg}$ plasmablasts were generated early during immune response to seasonal influenza vaccination

$CD19^{Neg}$ PCs develop quite early during in vitro differentiation. It is not clear whether $CD19^{Neg}$ PCs can be detected early in vivo during an immune response. Peripheral blood B-lineage cells from 6 healthy controls were sequentially sampled to monitor the immune response to seasonal influenza vaccination. The transcription factor interferon regulatory factor 4 (IRF4) induces the transition from a germinal center gene expression program to that of a PC via BLIMP1 induction (168, 169). The presence of $CD19^{Neg}$ plasmablasts was confirmed with intracellular IRF4 staining after surface staining with the other 10 markers used in the memory B-cell panel which identified the relapse associated memory B-cell subset. IRF4 was tested in 3 controls at 2 different points. Plasmablasts had the highest level of IRF4 expression of all the cells in the sample. The plasmablasts are $CD20^{-}CD38^{++}CD27^{++}CD24^{-}CD84^{-}CD95^{+}IgD^{-}IgM^{-}LAIR1^{+/-}$. This expression profile of plasmablasts is known from the memory B-cell panels and also was confirmed with IRF4 staining. The $CD19^{Neg}$ plasmablasts had identical expression of all these above markers as well as similar scatter profile as $CD19^{Pos}$ plasmablasts as shown in Figure 10.3-6.

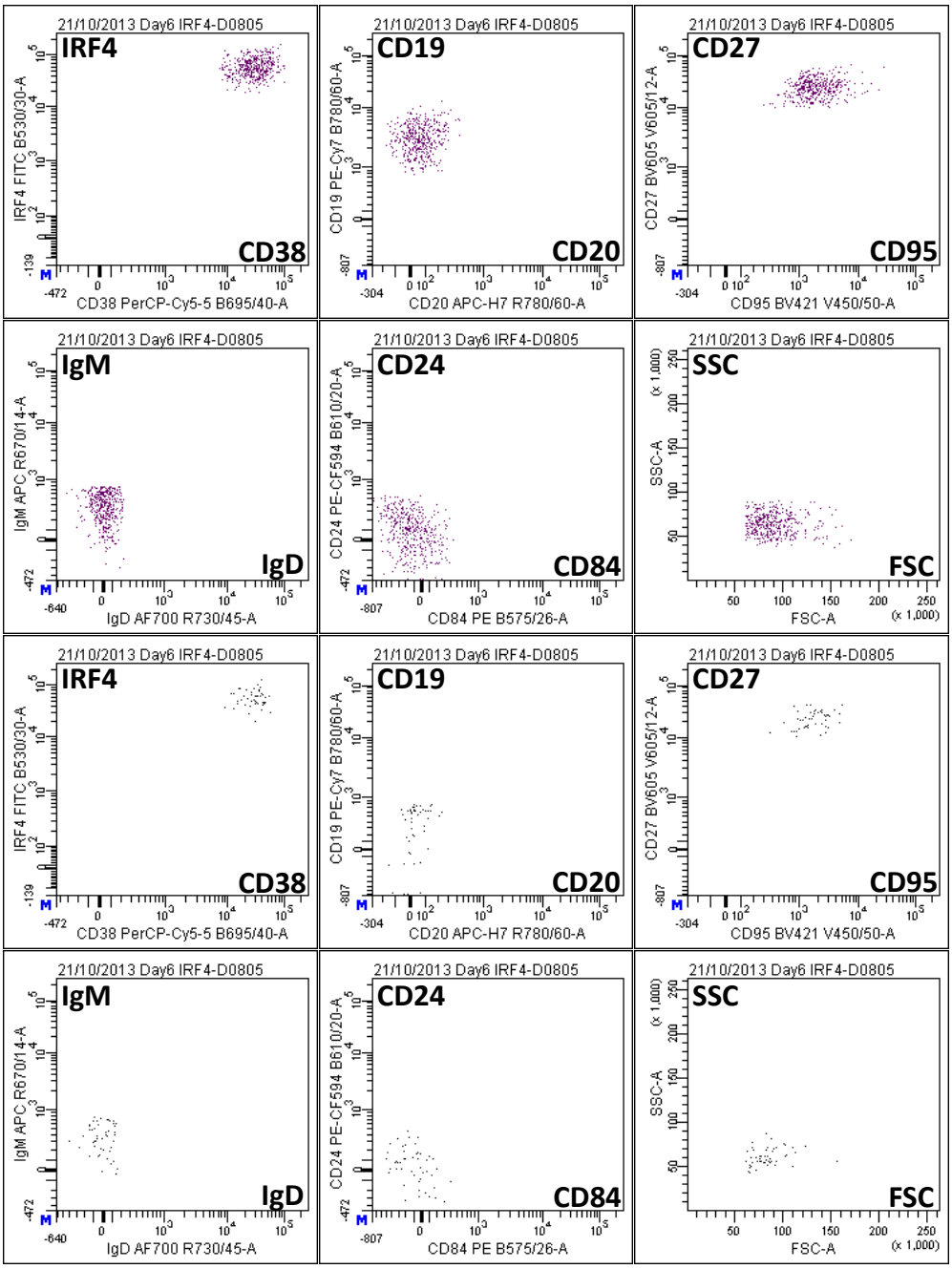

Figure 10.3-6 IRF4 and surface marker expression profile of CD19 positive and negative plasmablasts

The scatter profile and surface expression of 9 different surface markers and intracellular IRF4 (transcription factor that heralds PC differentiation) by peripheral blood $CD19^{Pos}$ and $CD19^{Neg}$ plasmablasts 6 days post seasonal influenza vaccination. Representative of 3 donors tested at 2 different time points (Pre vaccination and day 6). $CD19^{Pos}$ plasmablasts are denoted by purple colour and $CD19^{Neg}$ plasmablasts are shown in black.

The peak plasmablast response (increase in number of plasmablasts) is around day 6 which starts to resolve by day 14 in all the healthy controls and reaches normal levels by day 20. Controls 1 and 4 exhibited a weaker plasmablast response compared to the other controls. The disappearance of circulating $CD19^{Neg}$ plasmablasts was slightly delayed in some controls compared to $CD19^{Pos}$ plasmablasts. $CD19^{Neg}$ plasmablasts were detected at baseline although at very low numbers. There was a significant increase in $CD19^{Neg}$ plasmablast numbers on day 6 compared to baseline ($p=0.04$). There was a trend towards a decrease in proportion of $CD19^{Neg}$ plasmablasts on day 6 which was not statistically significant ($p=0.12$). Control 6 showed no change in the $CD19^{Neg}$ plasmablast proportion and control 1 showed an increase on day 6. Based on this data it could be hypothesized that $CD19^{Neg}$ plasmablasts could be generated as a part of immune response to influenza vaccination but needs further confirmation by establishing their antigen specificity by ELISpot or expressing their immunoglobulin sequence in vitro.

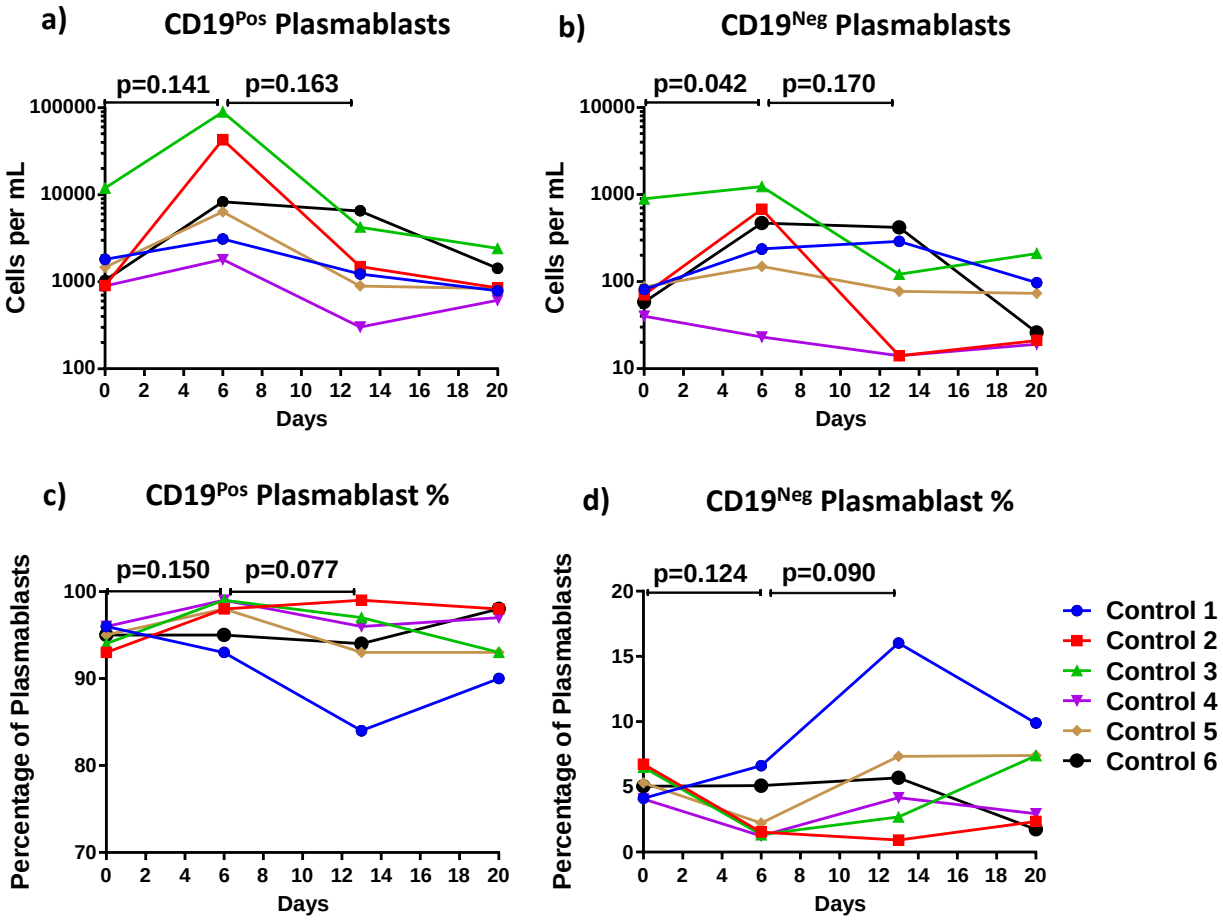

Figure 10.3-7 Plasmablast response following seasonal influenza vaccination

Absolute counts (Dual-platform methodology) and percentage of $CD19^{Neg}$ and $CD19^{Pos}$ plasmablasts (expressed as % of total plasmablasts) in the peripheral blood on the specified days since seasonal influenza vaccination. Plasmablasts were gated as $CD27^{High}CD38^{High}CD20^{Neg}$ within the lymphocyte scatter profile. The cell counts are shown on a logarithmic scale and percentages on a linear scale. Data shown from 2 different experiments with 3 controls each. The number of $CD19^{Neg}$ plasmablasts increased between baseline and day 6 in 5 out of 6 controls but their relative proportion did not increase in 5 out of 6 controls. P-values from paired t-test given.

10.3.5 $CD19^{Neg}$ PCs increase in proportion with time and can be maintained in culture for more than 100 days

It was not clear whether the $CD19^{Neg}$ PCs generated in vitro are a transient population or capable of longevity like the in vivo $CD19^{Neg}$ PCs. To address this, long-term feeding experiments were undertaken in transwells on PCs generated in vitro from negatively selected peripheral blood B-cells as described in detail in methods section 5.4.4. It was possible to maintain live $CD19^{Neg}$ PCs and were detectable after 100days of culture and can survive possibly longer (Figure 10.3-8).

The cell of origin for $CD19^{Neg}$ PCs is not known. $CD19^{Neg}$ PCs could possibly be generated by a distinct B-cell subset or CD19 negativity is determined stochastically during the process of B-cell differentiation. There was heterogeneity in expression of CD27 on day 6 plasmablasts. The plasmablasts that were lagging in CD27 expression gained CD27 to similar levels by day 20. To examine whether CD27 expression at the plasmablast stage was associated with the loss of CD19 in PCs, the plasmablasts were sorted into CD27 positive and negative fractions on day 6 and continued in culture. The proportion of $CD19^{Neg}$ PCs generated was similar between the two sorted fractions as was the unsorted control.

There is wide fluctuation in the cell numbers particularly that of the $CD19^{Pos}$ PCs during the initial plasmablast to PC transition. When cells numbers were normalised on day 30 there was similar rate of decline in $CD19^{Pos}$ and $CD19^{Neg}$ PCs with the rate slightly slower in case of 19Neg PCs. There was a significant drop in CD19 MFI for the $CD19^{Pos}$ PCs which stabilised by day 30 whereas the $CD19^{Neg}$ PCs remained stable throughout. Although the levels of CD19 expression dropped for $CD19^{Pos}$ PCs, they never reached the levels of $CD19^{Neg}$ PCs. For the experiment where CD27 positive fraction was sorted, data from the unsorted cells was used till day 20 since the CD27 expression equilibrated between the two fractions by day 20 and cells were CD27 positive by then. The noted increase in CD19 MFI in the sorted cells could be due to the residual staining from the antibodies used for the flow sorting.

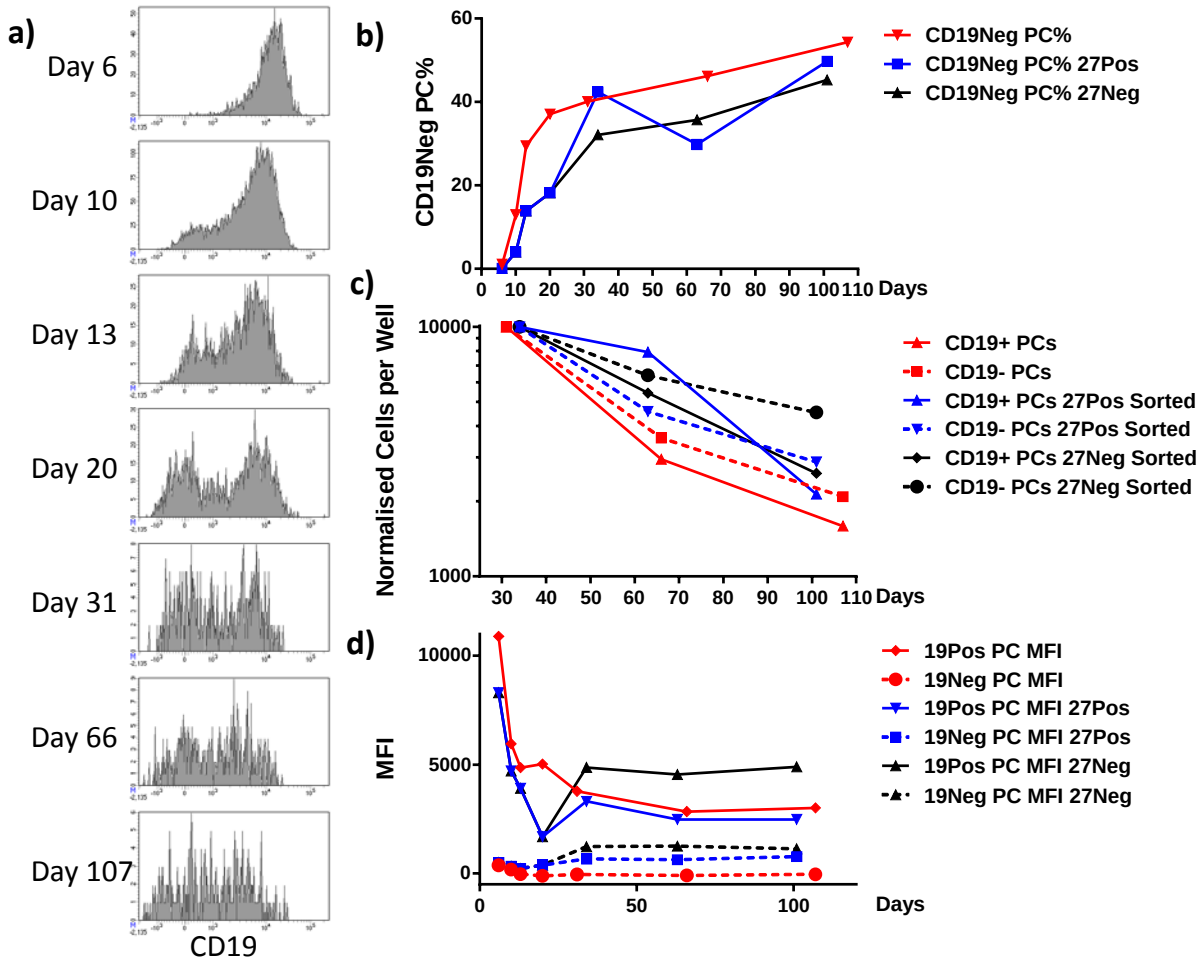

Figure 10.3-8 Changes in PC characteristics during long-term culture

a) Histogram of CD19 expression by in vitro generated PCs (defined as Annexin/7AAD negative, CD38 and CD138 positive) generated using standard protocol (Figure 5.4-1) at specified time points. Data shown representative of 3 samples over 2 different experiments.

b) Data shown from 2 experiments. In one of the experiments $CD19^{Pos}$ plasmablasts on day 6 were sorted into CD27Pos and CD27Neg fractions. Proportion of $CD19^{Neg}$ PCs generated from 3 samples shown which demonstrates relative increase or slower decay of $CD19^{Neg}$ PCs. Data from the unsorted cells is shown up to day 20 for CD27Pos and CD27Neg fractions.

c) The changes in absolute counts of $CD19^{Neg}$ and $CD19^{Pos}$ PCs normalized to the cell numbers on day 30 in 3 samples shown.

d) Sequential change in CD19 MFI of $CD19^{Neg}$ and $CD19^{Pos}$ PCs shown for 3 samples. Data from the unsorted cells is shown up to day 20 for CD27Pos and CD27Neg fractions

10.3.6 CD19 expression changes in sorted $CD19^{Neg}$ and $CD19^{Pos}$ PCs

It is not known whether the $CD19^{Neg}$ PCs are generated from the $CD19^{Pos}$ PCs or determined at the time of plasmablast to PC transition. To address this issue, PCs were sorted based on their CD19 expression after day 10 when the $CD19^{Neg}$ PC proportion reached 20-30%. Until this point the standard differentiation protocol was followed as described in detail in methods section 5.4.4. Live (7-AAD negative) CD138 positive were sorted into CD19 positive and negative fractions on BD Influx cell sorter. One of the samples was sorted on day 10 and the other two on day 16. The sorted cells were maintained in transwells with stromal cell support and re-fed twice per week with fresh nutrients and cytokines. The sorted PCs were monitored for 10-20 days for changes in phenotype.

The CD19 negative fraction of the sort was of very good purity close to 100% but the CD19 positive fraction was of much lower purity – 60 to 75%. The proportion of 25 – 40% of $CD19^{Neg}$ PCs present in the CD19 positive fraction was maintained at the same level in all samples. Interestingly, $CD19^{Pos}$ PCs were generated from $CD19^{Neg}$ PCs in all the samples suggesting a degree of plasticity in PCs, at least in vitro. The CD19 MFI of the $CD19^{Pos}$ PCs generated from $CD19^{Neg}$ PCs never attained the same levels as that of the native $CD19^{Pos}$ PCs. This suggests that CD19 expression could be dynamically regulated in PCs and interconversion between $CD19^{Pos}$ and $CD19^{Neg}$ PCs can occur. It is not known whether PCs in vivo maintain equilibrium between $CD19^{Pos}$ and $CD19^{Neg}$ subsets similar to seen in vitro due to survival or functional constraints. The other possibility is CD19 protein could be circulated between the surface and intracellular compartments without any changes in gene expression. The data from monitoring bone marrow PCs treated with myeloablative therapy and alemtuzumab is not suggestive of such recirculation of the CD19 protein in vivo. However such a process happening in vitro cannot be ruled out. Therefore, this will need further investigations for confirmation such as continuous monitoring of the CD19 protein in the live in vitro generated PCs by using time-lapse confocal microscopy and testing of cytoplasmic and membrane fractions of sorted CD19Neg PCs for CD19 protein by western blot.

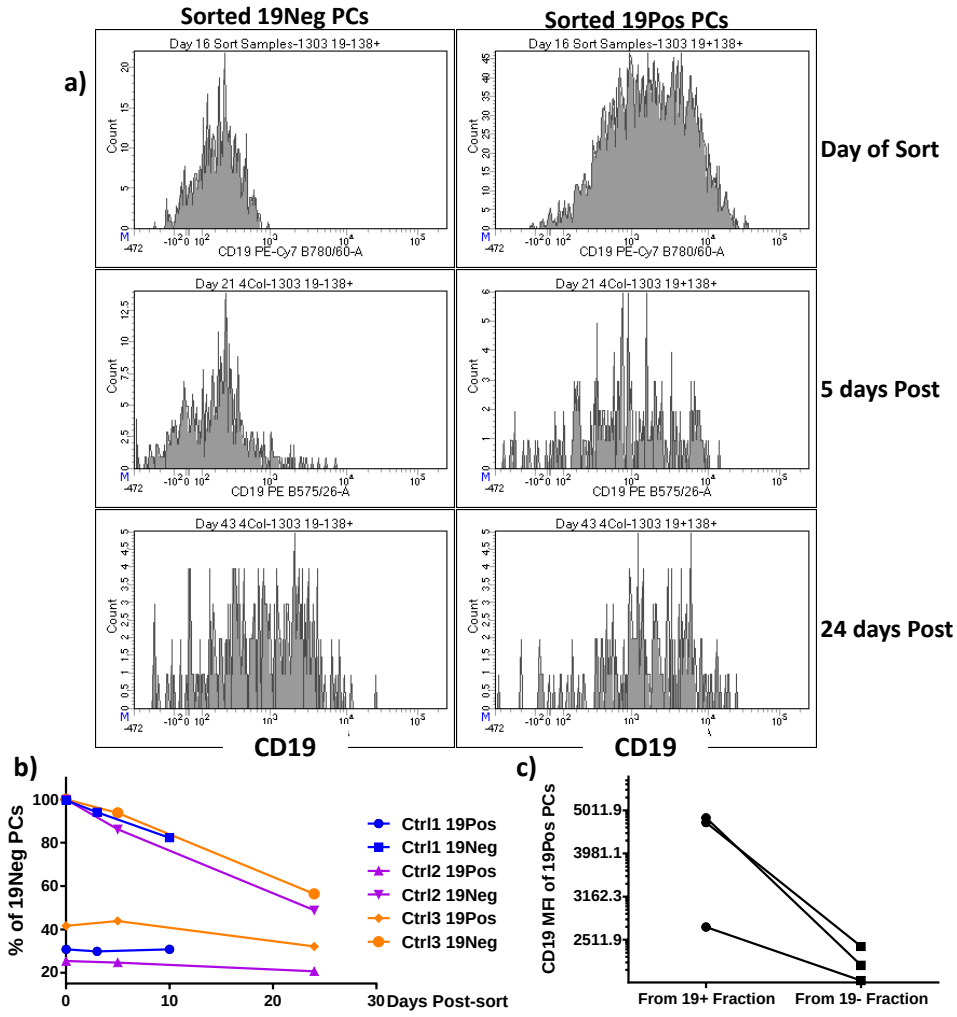

Figure 10.3-9 Phenotypic changes of flow sorted in vitro generated CD19^{Pos} and CD19^{Neg} PCs

a) Histograms of sequential changes in CD19 expression by sorted PCs representative of 3 controls from 2 different experiments. The live 7-AAD negative CD138 positive PCs were sorted into CD19 positive and negative fractions on BD Influx cell sorter between days 10 to 16 of B-cell differentiation when more than 20% CD19^{Neg} PCs were present. The sorted cells were maintained in vitro for 10 to 24 days in transwells with re-feeding.

b) CD19^{Neg} PCs expressed as percentage of total PCs defined as Annexin/7AAD negative, CD20 negative, CD38 and CD138 positive. This showed that CD19^{Pos} PCs can be generated from the sorted CD19^{Neg} fraction.

c) CD19 MFI of the CD19^{Pos} PCs generated from the sorted CD19^{Pos} and CD19^{Neg} fractions showed that the CD19^{Pos} PCs generated from the CD19^{Neg} fraction did not attain the levels of CD19 expression as the CD19^{Pos} fraction.

10.4 Analysis of the immunoglobulin repertoire of bone marrow plasma cells

It is not known whether the development of CD19 negativity is dependent on the antigen specificity of the plasma cell and thereby the immunoglobulin sequence. It is also not clear whether one of the subsets is generated from the other subset in vivo or is determined at the time of plasma cell differentiation. Analysis of the immunoglobulin sequence is likely to reveal the relationships between the two subsets and might provide clues to their B-cell of origin.

10.4.1 Normal $CD19^{Pos}$ and $CD19^{Neg}$ PCs have a largely discrete immunoglobulin repertoire.

The data from bone marrow PCs indicate that $CD19^{Pos}$ and $CD19^{Neg}$ PCs show extended phenotypic differences and have different kinetics of in vivo response following therapeutic bone marrow perturbation. These features suggest distinct origin and behaviour, but this conclusion would be contradicted if extensive overlap in IGHV repertoire usage could be observed. To address this RNA from FACS sorted $CD19^{Neg}$ and $CD19^{Pos}$ plasma cells from bone marrow of 4 controls pre-enriched with CD138 magnetic beads was extracted by alcohol-chloroform method. RNA was reverse transcribed and IGHV region was sequenced from cDNA by next generation sequencing on Roche 454 GS Junior platform. Clinical details of the samples and number of cells in each fraction obtained from flow sort are given in Table 10.4-1.

Table 10.4-1 Details of samples used for IGHV sequencing

Sample	Clinical History	No. of CD19 Pos PCs	No. of CD19 Neg PCs
H3627	Reactive Marrow	35000	25000
H3739	Leucopenia	10600	9612
BM12	Hip replacement	4774	4937
BM15	Hip replacement	1171	1282

IGHV@ was amplified and sequenced with between 2535 and 8048 sequences corresponding to functional IGHV rearrangements identified in each case. More than 97% of the sequences were mutated (cut-off >2% difference from germ line) and the proportion of mutated sequences were similar between $CD19^{Pos}$ and $CD19^{Neg}$ PCs. There was little overlap between the immunoglobulin heavy chain repertoire with only 2.1 to 3.7% of unique IGHV rearrangements shared between the $CD19^{Pos}$ and $CD19^{Neg}$ fractions (Figure 10.4-1). Only a very low proportion

of sequences were present twice or more in both subsets (<2%) and <1% of sequences were present more than 5 times in both subsets (Denoted as frequent sequences in Figure 10.4-1).

Unique Sequences	BM12	BM15	H3627	H3739
CD19Pos Sequences	1494	702	1840	1106
CD19Neg Sequences	1109	598	2422	1023
Overlapping Sequences	93	37	88	46
Overlap %	3.71	2.93	2.11	2.21
More than once in both fractions%	1.88	1.64	1.09	1.43
Frequent in both fractions %	0.50	0.78	0.19	0.66
More than once in 19+ as % of 19+	60.04	68.66	48.64	64.83
Frequent in 19+ as % of 19+	22.09	46.72	11.03	38.16
More than once in 19- as % of 19-	48.96	66.39	56.65	66.08
Frequent in 19- as % of 19-	10.73	40.80	21.10	30.69
More than once in either fraction %	55.94	68.01	53.57	65.53
Frequent in either fraction %	18.05	45.13	17.37	34.81

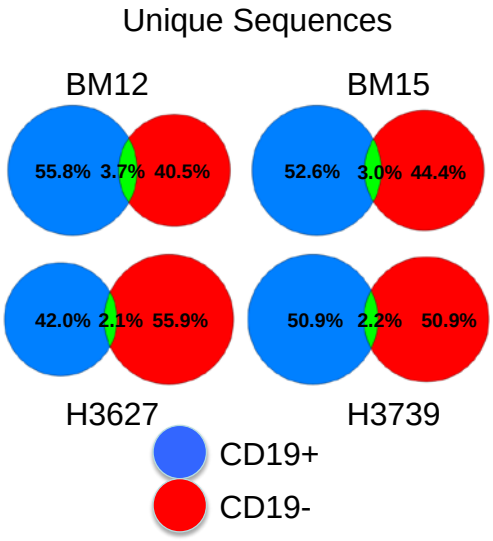

Figure 10.4-1 Low degree of IGHV sequence overlap between CD19^{Pos} & CD19^{Neg} PCs

Venn diagram overlap depicts the percentage of identical amino acid sequences between the CD19^{Neg} and CD19^{Pos} plasma cell compartments. Sequences occurring 5 times or more are labeled as frequent.

The amino acid length was slightly skewed towards shorter CDR3 in the $CD19^{Neg}$ fraction compared to the $CD19^{Pos}$ fraction but was not consistent in all samples ($p<0.0001$ in 3 out of 4 samples). The mutation load was significantly higher in CD19Pos PCs compared to CD19Neg PCs ($p<0.0001$).

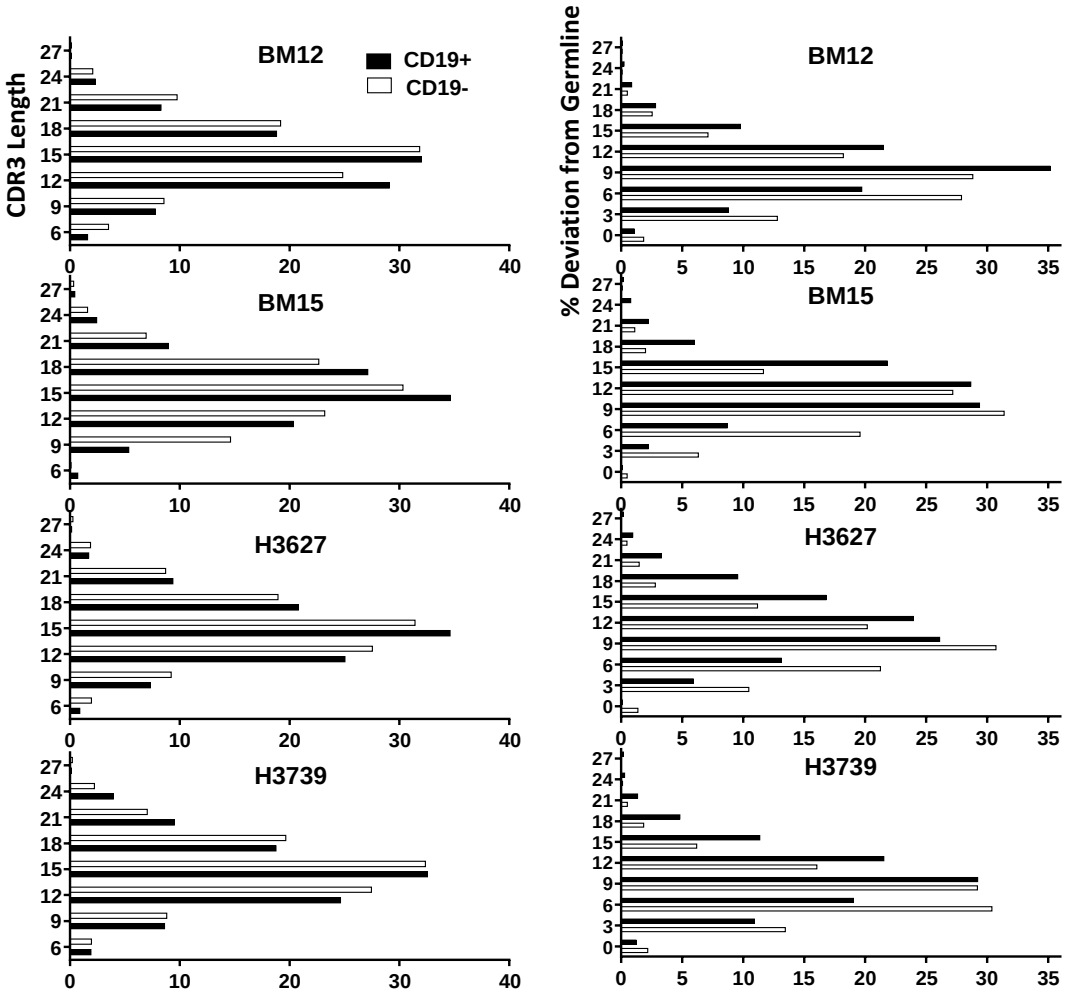

Figure 10.4-2 CDR3 length and mutation load in $CD19^{Pos}$ and $CD19^{Neg}$ PCs

The amino acid length of the CDR3 region from 4 controls shown. The X-axis represents the relative proportion of each CDR3 length (bin size of 3) with in the $CD19^{Pos}$ PCs or $CD19^{Neg}$ PCs. The mutation load is calculated as percentage deviation from the germline sequence. The X-axis represents the relative proportion of each mutation load (bin size of 3) with in the $CD19^{Pos}$ PCs or $CD19^{Neg}$ PCs. The $CD19^{Pos}$ PCs are represented by black bars and $CD19^{Neg}$ Pcs by clear bars.

The IGHV family usage showed no difference in preference between $CD19^{Pos}$ and $CD19^{Neg}$ PCs (Figure 10.4-3).

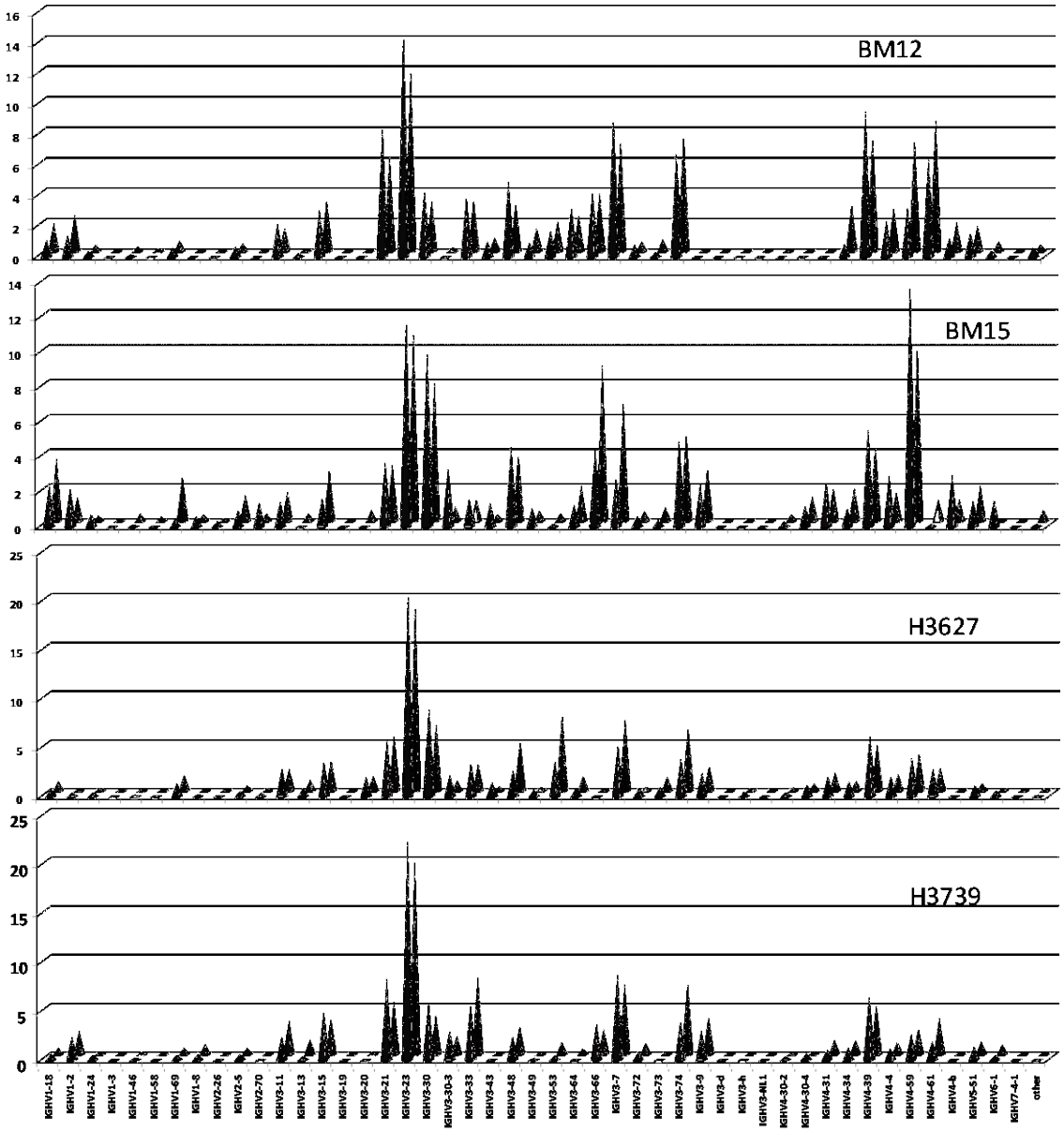

Figure 10.4-3 : IGHV gene family usage by 19Pos and 19Neg PCs

The relative proportion of sequences from each IGHV family (labelled along the X-axis) expressed as percentage of $CD19^{Pos}$ or $CD19^{Neg}$ PCs. Black cones – $CD19^{Pos}$ PCs, Light grey cones – $CD19^{Neg}$ PCs

10.5 Summary and discussion

A definitive fraction of $CD19^{Neg}$ PCs exists in the normal bone marrow. Although this heterogeneity of the normal PC pool has been known for a long time, detailed studies of $CD19^{Neg}$ PCs have just begun to emerge (155). There remains uncertainty regarding the similarities between $CD19^{Neg}$ and $CD19^{Pos}$ PCs in terms of function, life span, mode of generation, in vivo kinetics and response to various immunomodulatory therapies. The analysis presented here confirms that division into $CD19^{Pos}$ and $CD19^{Neg}$ PCs is linked to extended differences in terms of phenotype and function between these populations. This extends recent data presented by Mei et al (155). While the similarity between the normal PC populations is greater than the similarity between either of these and neoplastic PCs, a number of antigens in particular CD45 and CD56 follow a similar trend in $CD19^{Neg}$ PCs to that observed in a more exaggerated version in neoplastic PCs of myeloma. Therefore, if a normal counterpart of neoplastic PCs exists, it is likely to reside within the $CD19^{Neg}$ PC fraction. Whether the additional differences in expression of CD56, CD45 and CD28 observed in this population represent distinct subpopulations, response to niche factors, or exaggerated stochastic variation remains uncertain.

Tracking in vivo cellular populations in human is challenging. Therapeutically perturbed bone marrow samples have been taken advantage of to determine differences in response characteristics of $CD19^{Neg}$ and $CD19^{Pos}$ PCs populations. During the initial few years following bone marrow ablation therapy, the proportion of $CD19^{Neg}$ PCs was significantly lower compared to controls; this is consistent with a more restricted control over $CD19^{Neg}$ PC generation as might be expected for long-lived PCs. Although it cannot be excluded that a preferential loss of a specific niche essential of $CD19^{Neg}$ PC maintenance accounts for this difference, this seems a less likely explanation given the reconstitution of otherwise functional bone marrow in such patients. Long-lived antibody responses are generated from germinal center B-cells and potentially also from post-GC memory B-cells (170). Therefore depletion of memory B-cells due to prior therapy and the gradual re-encounter of antigens eliciting appropriate GC responses could in part explain the kinetics of recovery. Memory B-cells are known to have a shorter CDR3 length compared to naïve B-cells (159). Thus the shorter CDR3 length noted in $CD19^{Neg}$ PCs would be consistent with origin either directly from a memory B-cell or from a common precursor of both memory B-cells and long-lived PCs such as a germinal center B-cell. Overlap of 1.1% in

amino acid sequences of CDR3 region has been noted in peripheral blood samples from the same individual for an estimated total B-cell repertoire size of 1.5 million which is constituted by tens of thousands of activated B-cells and millions of naïve B-cells (171). Although no definitive data for PC repertoire size exists, due to selective pressures during selection into the PC pool, it is likely to be much smaller than the total B-cell repertoire size. A smaller repertoire size would be expected to show a higher degree of overlap, thus a high degree of overlap in IGHV sequences between $CD19^{Neg}$ & $CD19^{Pos}$ PCs would have supported the conclusion that the two subsets represent a phenotypic continuum of a single population. In contrast the low degree of overlap observed supports predominantly independent derivation of the two populations. The alternate explanation is that $CD19^{Neg}$ PCs derived from $CD19^{Pos}$ PCs with gradual loss of expression of CD19 over time, while the IGHV@ repertoire differences could be explained by origin from distinct temporal waves of immune response this is not supported by the significant difference in CDR3 length and mutational load.

While differential effects of alemtuzumab on PC populations or their niche components cannot be entirely excluded, the reciprocal persistence of $CD19^{Neg}$ PCs following B-cell depletion is again empiric data supportive of greater life span in this PCs population relative to $CD19^{Pos}$ PCs. This is supported by another recent study by Mei et al., where similar findings were noted following B-cell depletion with rituximab (155). Furthermore the data indicate that over the time course examined the $CD19^{Neg}$ population can be maintained in a fashion independent of variation in the $CD19^{Pos}$ PCs.

Longevity of plasma cells is supported by extrinsic factors supplied by microenvironmental survival niches (51). However the stability of antigen specific immune responses in human supports an element of lifespan programming, determined by the nature of inciting immune response. A unifying theory would be that factors intrinsic to PCs, which are established during initial PC differentiation, determine subsequent affinity for survival niches, which in turn promote PCs survival. The presence of higher levels of anti-apoptotic factor BCL2 and lower levels of the death receptor CD95 in $CD19^{Neg}$ PCs could reflect an intrinsic survival advantage to this PC population. Indeed in mouse expression of BCL2 family member MCL1 is essential for the generation of long-lived PCs (161). Of the surface markers identified as differentially expressed between $CD19^{Pos}$ and $CD19^{Neg}$ PCs, only CD28 has been mechanistically linked to PC longevity (156). CD28 has also been shown to be a pro-survival and apoptotic resistance mediator in

myeloma PCs through the PI3K/AKT/FOXO3a/BIM pathway (160), but CD28 is expressed in only one-third of myeloma patients (172). CD28 has been identified as a potential factor contributing to the longevity of murine PCs (173). However contradictory evidence has also been provided in other mouse models, in which deficiency of CD28 was found to lead to both increased plasma cell numbers and increased antibody production (174). Although detected only at low level in this analysis, normal CD28+ PCs were predominantly $CD19^{Neg}$, potentially supporting an association between CD28 expression and longevity. However, CD28 was heterogeneous both in relation to CD19 and within the $CD19^{Neg}$ PC population. Furthermore in some bone marrow aspirate samples, in which PCs in general were well represented, CD28 expressing PCs were undetectable. Thus the detailed analysis of PC phenotypes suggests a highly selective role for CD28 in human bone marrow PC, but would not lend support to the argument that CD28 provides a general determinant of normal bone marrow PC survival or function in human. Further studies are necessary to determine the factors contributing to the heterogeneity of CD28 expression on normal human PC populations.

In the context of in vitro model systems of human PC differentiation, $CD19^{Neg}CD138^{Pos}$ PCs are predominantly generated early during initial maturation from the $CD19^{Pos}CD38^{Pos}$ PB state, and are not generated substantially as a sequential process through loss of CD19 from $CD19^{Pos}CD138^{Pos}$ PCs. $CD19^{Neg}CD138^{Pos}$ PCs generated early can persist in this state and can be maintained independently of the bulk $CD19^{Pos}$ PC population for substantial periods of time. The identification of $CD19^{Neg}$ PBs in the peripheral blood at steady state and during active in vivo immune responses supports such an early divergence of $CD19^{Pos}$ and $CD19^{Neg}$ cell states as a feature of antibody secreting cells generated during in vivo immune responses. This complements the previous work which showed the presence of $CD19^{Neg}$ PBs in the bone marrow and peripheral blood (175), and the identification of $CD19^{Neg}$ PCs amongst inflammatory infiltrates (155).

Several lines of evidence point to the possibility that $CD19^{Neg}$ PCs include the long-lived bone marrow PC populations in human. Consistent with such a proposal $CD19^{Neg}$ PCs increase with time amongst in vitro long-lived PCs and can be maintained independently of the $CD19^{Pos}$ PC pool, consistent with a greater potential for longevity. However $CD19^{Neg}$ PCs are generated within 3-4 days of the PB state in vitro, and $CD19^{Neg}$ PBs exist as an identifiable population in the peripheral blood at steady state and post vaccination in vivo although it needs further

confirmation with determining antigen specificity of the $CD19^{Neg}$ PBs. Thus absence of CD19 alone in a PC population should not be taken as *prima facie* evidence of PC "age" but instead may reflect a greater potential for extended life-span.

The data presented here, and that of Mei et al. (155), indicate that bone marrow PCs are not a uniform population but include subsets with differential protein expression and generation kinetics, different longevity after B-cell depletion, and with a non-overlapping immunoglobulin repertoire. Although neoplastic PCs are readily distinguishable from normal PC subsets, they share more features in common with normal $CD19^{Neg}$ PCs than with normal $CD19^{Pos}$ PCs. $CD19^{Neg}$ PCs can be generated early in vitro and also identified during immune response to vaccination. Identifying the developmental pathway of normal $CD19^{Neg}$ PCs is therefore likely to improve our understanding both of autoimmune B-cell disorders and the oncogenic process in myeloma and other neoplastic processes, as well as greatly enhancing understanding of the development of long-lived humoral immunity.

11 Discussion

The role of B-cells in RA pathogenesis is a fundamental question in RA biology. The purpose of this work was to address aspects of this question, concentrating on the relationship between phenotypic memory B-cell sub-populations, autoantigen specificity and prediction of response to and relapse following BCDT. This has been facilitated in Leeds by the availability of a combination of clinical samples from one of the largest RA cohorts in Europe, a novel in vitro B-cell differentiation assay to explore B-cell function and flow cytometry expertise. There are two major strands to the line of investigations. First, given that ACPA antibodies are strongly associated with RA, a major aim is to determine whether ACPA specific populations in memory B cells, plasmablasts and plasma cells may be associated with disease expression and relapse. Second, phenotypic markers for long-lived PCs were sought since short and long-lived PCs are differentially involved in RA and other autoimmune disease pathogenesis, and with the eventual future aim of testing whether ACPA secretion would be correlated with a distinct phenotypic subset

11.1.1 Markers used for flow cytometric phenotyping of memory B-cell subsets

Flow cytometric phenotyping for surface molecule expression and utilising expression profiles to identify novel B-cell subsets are techniques that have been successfully used in the past in autoimmunity to identify markers of disease response. In this study I found CD24, CD95, CD84 and LAIR1 to be of particular value in fractionating peripheral blood memory B-cells into phenotypic subsets. To my knowledge the co-ordinated regulation of these surface proteins has not been previously studied, but their common association with signal transduction pathways would be in keeping with a potential for differential response within linked B-cell sub populations.

CD24, a glycophasphatidylinositol (GPI)-anchored membrane sialoglycoprotein is considered to be a redundant costimulatory molecule in lymphoid tissues. It is overexpressed by multiple solid organ tumours and is a marker for diagnosis and poor prognosis (176). CD24 has been

considered as a genetic checkpoint in T-cell homeostasis and a SNP has been shown to be of increased frequency in RA patients (177).

CD95 (Fas) is a death receptor expressed by B-cells on activation and plays an important role in elimination of non-specific and autoreactive cells in the GC (178). CD95 mediated death signal can be overcome by antigen-dependant (BCR) and antigen-independent (IL4) survival signals and defective function of CD95 has been described in RA (179).

CD84 is a member of the CD2 subset of Ig superfamily and interacts in a homotypic fashion. The cytoplasmic tail contains tyrosine motifs which when phosphorylated interact with SHP2 and SH2D1A, and are known to enhance IFN secretion in T-cells (180). It has also been shown to downregulate FcRε1 mediated signalling in mast cells independent of SH2D1A and SAP binding and therefore speculated to play a role in allergy and autoimmunity (181).

LAIR1 is another Ig superfamily member expressed by most cells of the immune system with two ITIMs (Immunoreceptor tyrosine-based inhibitory motif) in its cytoplasmic tails. LAIR1 cross-linking leads to downregulation of BCR mediated calcium flux and Ig and cytokine secretion (182). Reduced expression of LAIR1 described on lupus B-cells is suggestive of a role in autoimmune process (68).

Memory B-cells are understood to be a markedly heterogeneous population (183). Previous studies have in particular identified FCRL4 (Fc Receptor-like 4) expressing subset of memory B-cells (184). However these studies used in-house generated antibodies and it was not detectable when tested (data not shown) with the commercially available antibody (Biolegend), thus the relationship to this population could not be defined. However the FCRL4 subset is predominantly CD27 negative and therefore unlikely to be related to the CD27 positive memory B-cell populations that were observed in this study.

11.1.2 Skewing of memory B-cell subsets regulatory or inflammatory

With detailed phenotyping of B-cells post-rituximab therapy, patients were found to show a skewed distribution of memory B-cell subsets prior to relapse. In controls and RA patients who have not been exposed to rituximab the dominant memory B-cell subset is $CD24^{+}84^{+}95^{-}LAIR1^{+}$ whereas in patients relapsing post-rituximab mediated B-cell depletion the inverse subset $CD24^{-}84^{-}95^{+}LAIR1^{-}$ was dominant. This skewing was unlikely to be a direct effect of depleting B-cells or specific to rituximab as it was not seen in patients treated with campath prior to renal transplant or rituximab for B-cell neoplasms. Therefore, a direct link with the underlying autoimmune process is most likely.

Given that rituximab is likely to be acting via direct depletion of B-cells, and the skewing of the subset distributions was linked to RA relapse, a direct pathogenetic role for these B-cell subsets is a possibility. This would suggest that, either the usual dominant memory B-cell subset that is reduced during relapse is regulatory or the relapse-associated memory B-cell subset which is raised contains pathogenic cells. It would be unusual for BCDT to have such a good clinical response, if reduced regulatory B-cells played a key role in RA pathogenesis. Although a key role for regulatory B-cells has been proven in various models of autoimmunity in mice, the same has not been possible in humans (185). The lack of increased autoimmunity in patients with a primary antibody deficiency due to total absence of B-cells, X-linked agammaglobulinaemia (XLA) and the presence of autoimmune complications in more than one-third of patients with the other variant of primary antibody deficiency where B-cells are present – common variable immunodeficiency (CVID) (186) further questions the central role of regulatory functions dependent on B-cells in human autoimmunity. Indeed the closest stage of in vitro differentiation that matches the RA relapse associated subset is the day 4-5 activated B-cells. During this stage the B-cells are capable of secreting multiple proinflammatory mediators, which would favour a more direct pathogenic role.

Sequential monitoring of the memory B-cell subsets following influenza vaccine revealed an increase in proportion of the relapse associated memory B-cell subset similar to that seen during relapse following rituximab in RA. However, the absolute count of the relapse associated subset did not increase but the count of the polar opposite, usual dominant subset decreased. This would suggest that the rise in the proportion of the RA relapse associated subset reflects a decrease in numbers of the other memory B-cell subsets, and the most likely explanation for

this given the short timeframes in the post vaccination follow up would be differential recruitment to the secondary lymphoid organs. Whether this applies to RA relapse is not clear, but differential homing and tissue localisation could certainly provide a plausible explanation for differences in peripheral blood representation.

Functional analysis of the memory B-cell subsets was rendered technically challenging due to their very low absolute numbers in the peripheral blood of relapsing RA patients. The process of flow sorting was also limiting due to the poor yield and poor viability and function of the cells post sorting, the cause for which could be physical stress from the sort or the multiple antibodies used. While in the timeframe of this study it was not possible to extend to a functional analysis of the different B-cell subsets, this would certainly be the logical extension to further delineate the functional significance of these subsets. A combination of gene expression analysis, IGHV@ sequence analysis and functional studies with ELISpot could be envisaged to further address this issue.

11.1.3 BCDT – Therapeutic experiment for enriching pathogenic B-cells

From vaccine studies, the frequency of antigen-specific memory B-cells has been estimated to be 1 in 10000 B-cells, which has been shown to be protective (50). This proves that memory B-cells are effective even at low absolute numbers in the peripheral blood, although these cells may be present in antigen rich tissues and secondary lymphoid organs which cannot be quantified. The lack of expansion in proportion of the relapse-associated memory B-cell subset in rituximab naïve RA patients could be due to the masking effect of various memory B-cell specificities accrued through decades of immune responses populating the memory B-cell compartment. During relapse post-BCDT, the expanding memory B-cells are most likely derived from an ongoing/recent immune response which in the case of relapsing patients are likely to be related to RA and thus more likely to be pathogenic given the ongoing exposure to inciting autoantigens.

11.1.4 Relapse associated memory B-cells – destiny

The work reported here in defined a novel memory B-cell subset which was explored further in patients and the in vitro model system. Similar surface expression profiles for the four markers – CD24, CD84, CD95 and LAIR1- characterising the relapse associated memory B-cell subset

has been seen during in vitro differentiation of B-cells to plasmablasts and also on in vivo derived plasmablasts. Hence the relapse associated memory B-cell could also be considered as plasmablast-like but the plasmablasts express high levels of CD38 and lose CD20 expression whereas relapse associated memory B-cells do not. At present it is unclear whether this phenotype represents a dynamic intermediate state, or alternatively is a stably maintained phenotype linked to specific functional properties.

Interestingly, if these cells are pre-plasmablasts, this profile was not captured during in vitro differentiation suggesting that if these are genuine pre-plasmablasts they derive from a set of in vivo conditions not mimicked in the in vitro system. Alternatively this subset may represent early post-GC B-cells destined to be memory B-cells and not seen in vitro due to lack of memory B-cell differentiation in the in vitro system.

The link between the surface expression profile and the autoimmune process can be speculated based on the fact that CD95, which is expressed by the relapse-associated memory B-cell subset, is an activation marker and CD84 and LAIR1 which are down-regulated are known to have regulatory properties. This would be consistent with a predicted phenotype for autoreactive cells during relapse, with increased expression of activation markers and down regulation of regulatory receptors. This subset could be similar to $CD38^{Neg}$ antibody secreting cells described in human tonsils as precursors of $CD38^{Pos}$ PCs (187) or short-lived $CD38^{Neg}$ PCs generated using a CD40L based in vitro differentiation system (188). If this subset is a precursor of short-lived PCs which are pathogenic, this could be the key population targeted by BCDT and would explain the effectiveness of BCDT. The identification of antigen specificity of this population would support this hypothesis. Nonetheless the inability to functionally isolate these cells, and to perform precursor-product relationship studies to assess transitions into alternate phenotypic states, currently precludes firm conclusions. Again these questions could be addressed in downstream investigations.

Whilst it is thought that the earliest events in RA may take place in the lymphoid organs, there is little doubt that the synovial environment in RA can sustain or exacerbate autoimmunity as shown by the presence of secondary lymphoid structures and ACPA secreting cells in the synovium (10). Therefore, the definition of the memory B-cells that are recruited and generated from these secondary lymphoid structures in the synovium is likely to provide further insights into role of B-lineage cells in pathogenesis and thereby identify potential biomarkers. The

phenotypic definition of the long lived PCs on the other hand would allow the analysis of the nature of ACPA secreting PCs generated from the synovial lymphoid structures and resident in the bone marrow which might have different roles in RA pathogenesis.

11.1.5 Detection of citrullinated protein-specific B-lineage cells has been challenging

The principle antigen specificity that would have allowed a firm conclusion relating to a pathogenic role for distinct B-cell subsets would have to be demonstration of specificity to citrullinated proteins. This was the target of significant but ultimately unsuccessful experimentation. Although ELISA of culture supernatants of purified peripheral blood B-cells from RA patients positive for ACPA proves the presence of ACPA-specific B-cells in the periphery. However ELISpot failed to detect the ACPA secreting cells due to a technical issue in that the CCP did not bind to the ELISpot plate as shown in Figure 6.3-3. To resolve this issue the options were to pre-coat with Streptavidin and attach biotinylated-CCP to the plate or use the biotinylated-CCP as a probe. Streptavidin binding will also increase the affinity due to tetramerisation of the peptide. However the ELISpot assays were further hampered by the lack of positive controls in the form of ACPA secreting cells.

Lack of detection of citrullinated protein-specific cells by flow cytometry is likely to be due to the low frequency of these cells (50), low-affinity to the monomeric peptide (189) and non-specific binding hampering the detection. Pre-enrichment for B-cells has been used to improve the sensitivity and dual fluorochrome tagging of a non-specific peptide and excluding cells positive for both fluorochromes has been shown to be an elegant and effective solution to exclude non-specific binding (82). Tetramerisation of the peptide has the additional benefit of improving the affinity of the BCR for the peptide.

The technical difficulties in identifying citrullinated protein-specific B-cells are reflected by the paucity of published literature. The only published method for detecting citrullinated protein-specific B-cells in peripheral blood uses in vitro culture of RA B-cells and analysing the supernatants (85). However, this study required two rounds of strong stimuli, two-week culture and five-fold concentration of the supernatant for ACPA to be detected and as a consequence a high proportion of control samples were positive for ACPA secretion. In relation to this, the data

obtained in this study suggests an enhanced ability to detect ACPA secretion in vitro since a shorter stimulation and no supernatant concentration was required for detection.

11.1.6 Role of B-NK cell interaction in RA pathogenesis

The contact dependent B-cell driven NK cell expansion demonstrated in this study could be secondary to latent EBV entering lytic phase during plasmablast differentiation or a mode of B-cell regulation by NK cells. EBV, which is known to be present at higher levels in RA peripheral blood and synovium could thus play a key role in breakdown of tolerance to citrullinated proteins and also perpetuate joint inflammation. LGL has been known to be triggered by chronic stimulation of NK cells and CD8 T-cells which could possibly be mediated by EBV containing B-cells. Thus the NK cell stimulation and expansion driven by EBV containing B-cells in the synovium could play a key role in joint damage and might also have a role in the pathogenesis of LGL.

11.1.7 Phenotype of Long-lived PCs and their role in RA pathogenesis

Since, ACPA levels do not generally deplete with rituximab, the assumption is that ACPA is predominantly secreted by long-lived PCs. Substantial interest has focused on defining phenotypic characteristics that may allow identification of long-lived PCs. The analysis presented here demonstrates that normal bone marrow PCs are not a uniform population but comprise at least two subsets with differential protein expression and generation kinetics, different longevity after B-cell depletion, and with a non-overlapping immunoglobulin repertoire. This is also mirrored in recent work published by Mei et al. which reached similar conclusions.

CD19 negativity identifies a subset of plasma cells that have a propensity for longer life span but does not necessarily represent aged PCs. $CD19^{Neg}$PCs are observed quite early in the in vitro differentiation system. Therefore, it is possible that CD19 negativity is determined quite early during the differentiation process, which could be linked to the strength of BCR signalling or the B-cell subset from which the PC was derived. The observed lower rate of decay in cell numbers of $CD19^{Neg}$ PCs compared to $CD19^{Pos}$ PCs in the in vitro long term culture is suggestive that the half-life of $CD19^{Neg}$ PCs is longer. Sequential monitoring of the sorted in vitro generated $CD19^{Pos}$ PCs does not support the hypothesis that $CD19^{Pos}$ PCs mature into $CD19^{Neg}$ PCs with time albeit in the limited time frame studied. However it does not exclude the possibility that $CD19^{Pos}$ PCs could mature into $CD19^{Neg}$ PCs with time in vivo. The controversy regarding

determinant of longevity of PCs is not resolved conclusively although in this in vitro system where all cells are provided equivalent support, the longevity is not determined by competition for niches.

While ACPA secretion may derive predominantly from long-lived, and presumably $CD19^{Neg}$ PCs, change in ACPA levels does not correlate with clinical response. This argues against a direct role in pathogenesis. In contrast, the level of rheumatoid factor decreases with B-cell depletion and rises during relapse (39). A unifying model would be that ACPA secreted by long-lived PCs are weakly pathogenic on their own and is markedly enhanced with cross-linking by rheumatoid factor secreted by short-lived PCs.

12 Conclusions and Future directions

The initial aim of identifying the citrullinated protein-specific B-cells was achievable by ELISA from culture supernatants but other strategies such as ELISpot and direct identification by flow cytometry which has potential to be used as a biomarker turned out to be far more challenging. This can be further pursued by

- Using citrullinated protein or peptide tetramers (82) for detection and their confirmation by single cell sorting and sequencing the immunoglobulin gene to be expressed in a hybridoma.
- Investigating for the presence of citrullinated protein specific B-cells in the synovium and lymphoid organs such as bone marrow which is likely to overcome the issue of their low frequency in the peripheral blood.
- EBV transformation of B-cells from RA patients to generate clones that secrete ACPA which can be used as a positive control.

A novel $CD24^{-}CD84^{-}CD95^{+}LAIR1^{-}$ memory B-cell subset was identified to be relatively expanded in RA patients relapsing post-rituximab which was not seen in other instances of B-cell depletion for non-autoimmune conditions suggestive of a direct role in RA pathogenesis. This exact phenotype was not detected in vitro or other lymphoid organs or sites of inflammation. The functional significance of this expanded memory B-cell subset prior to relapse still remains incompletely understood. This can be evaluated further by:

- Clinical samples collected longitudinally from patients undergoing BCDT to validate the data obtained from the initial dataset.
- Secretion of IgG, TNFα and ACPA by this subset by ELISpot with improved flow sorting techniques and availability of positive control for ACPA secreting cells.
- Gene expression profiling of relapse-associated memory B-cells, the usual dominant memory B-cells and plasmablasts.
- Evaluation of RA synovial B-cells obtained by synovial biopsy during relapse and remission to understand whether the skewing of memory B-cell subsets is due to spill over from or recruitment into the synovium.

The performance of gene expression profiling could be limited by the low frequency of these cells in peripheral blood. This can be circumvented by using highly sensitive amplification base methods, as used for single cells, or if required, by pooling of samples from clinically similar RA patients. Since this subset is also seen in healthy volunteers, using leukapheresis samples from blood donors would allow conclusions relating to the general functional properties of these cells if not their inflammatory associations.

The closest phenotype in vitro to this relapse associated subset was the activated B-cell stage during which the cells secrete pro-inflammatory mediators and are in the process of differentiating to plasmablasts and the synovial fluid B-cells also exhibit similar expression levels for most of the markers. The secretion of proinflammatory mediators could be studied further by multiplex analysis of the supernatants from RA B-cell cultures from different clinical groups and controls.

TIM3 was expressed in vitro during the stage of B-cell differentiation when they secrete inflammatory mediators. The assays to delineate the functional role of TIM3 in B-cells were largely unsuccessful. TIM3 has not been studied on B-lineage cells so far and this could be of potential relevance to RA, other B-cell mediated autoimmune disorders, B-cell neoplasms and normal B-cell biology. This can be addressed by:

- Confirming the presence of TIM3 protein with different antibody clones and different techniques such as western blot, and RNA by real-time PCR.
- Confirming the presence of TIM3 expression on B-lineage cells in vivo by immunohistochemistry.
- Repeat evaluation of the role of galectin-9 by sourcing the protein from different labs on B-cell life span and differentiation in vitro.

Long-lived plasma cells are likely to be $CD19^{Neg}$ as shown by delay in reconstitution in vivo and slower decay of $CD19^{Neg}$ PCs during long-term in vitro culture. The in vitro findings were suggestive of the $CD19^{Neg}$ PCs being generated early and independent of $CD19^{Pos}$ PCs and there was also some evidence that $CD19^{Neg}$ PBs could be generated early in vivo during a controlled immune response. It would be important to extend these studies to:

- Prove the longevity of $CD19^{Neg}$ PCs by detecting vaccine-specific cells within this subset by ELISpot.

- Confirm the generation of $CD19^{Neg}$ PBs early during an immune response by assessing their antigen specificity and also assessing for their presence in lymphoid organs.
- Gene expression profiling of $CD19^{Neg}$ and $CD19^{Pos}$ PCs to identify differential expression of survival factors and possible targets on short and long-lived PCs.
- Confirm the lack of CD19 in the in vitro $CD19^{Neg}$ PCs by time-lapse confocal microscopy and western blot of cytoplasmic and membrane fractions.

There was an unexpected finding of B-cell mediated contact-dependant upregulation of NK cells that has not been studied in detail before. Although this was beyond the scope of the project, it has potential relevance in various fields including cancer biology, autoimmunity, immunodeficiency and basic B&NK-cell biology. There was also a suggestion of NK cell mediated death of B-lineage cells which needs further confirmation with functional NK cell cytotoxicity assays. There is a potential role for EBV in this interaction which could be studied further by preselecting EBV negative B-cells for differentiation with NK cells. This interesting topic can be further evaluated by

- Analysis of NK cell activation markers and markers of degranulation such as LAMP1 as well as supernatants for the presence of NK cell secreted cytokines such as IFNγ and TNFα.
- Evaluation of the cytotoxicity of the in vitro expanding NK cells on B-cell lines.
- Confirmation of the presence of EBV RNA by real-time PCR and proteins by western blot.

13 References

1. Aletaha D, Neogi T, Silman AJ, Funovits J, Felson DT, Bingham CO, 3rd, et al. 2010 Rheumatoid arthritis classification criteria: an American College of Rheumatology/European League Against Rheumatism collaborative initiative. Arthritis Rheum. 2010 Sep;62(9):2569-81. PubMed PMID: 20872595. Epub 2010/09/28. eng.
2. Alamanos Y, Drosos AA. Epidemiology of adult rheumatoid arthritis. Autoimmun Rev. 2005 Mar;4(3):130-6. PubMed PMID: 15823498. Epub 2005/04/13. eng.
3. Padyukov L, Silva C, Stolt P, Alfredsson L, Klareskog L. A gene-environment interaction between smoking and shared epitope genes in HLA-DR provides a high risk of seropositive rheumatoid arthritis. Arthritis Rheum. 2004 Oct;50(10):3085-92. PubMed PMID: 15476204. Epub 2004/10/12. eng.
4. Symmons D, Turner G, Webb R, Asten P, Barrett E, Lunt M, et al. The prevalence of rheumatoid arthritis in the United Kingdom: new estimates for a new century. Rheumatology (Oxford). 2002 Jul;41(7):793-800. PubMed PMID: 12096230. Epub 2002/07/04. eng.
5. The economic burden of Rheumatoid Arthritis(2010).
6. Minaur NJ, Jacoby RK, Cosh JA, Taylor G, Rasker JJ. Outcome after 40 years with rheumatoid arthritis: a prospective study of function, disease activity, and mortality. J Rheumatol Suppl. 2004 Mar;69:3-8. PubMed PMID: 15053445. Epub 2004/04/01. eng.
7. Gregersen PK, Silver J, Winchester RJ. The shared epitope hypothesis. An approach to understanding the molecular genetics of susceptibility to rheumatoid arthritis. Arthritis Rheum. 1987 Nov;30(11):1205-13. PubMed PMID: 2446635. Epub 1987/11/01. eng.
8. Klareskog L, Ronnelid J, Lundberg K, Padyukov L, Alfredsson L. Immunity to citrullinated proteins in rheumatoid arthritis. Annu Rev Immunol. 2008;26:651-75. PubMed PMID: 18173373. Epub 2008/01/05. eng.
9. McInnes IB, Schett G. The pathogenesis of rheumatoid arthritis. N Engl J Med. 2011 Dec 8;365(23):2205-19. PubMed PMID: 22150039. Epub 2011/12/14. eng.
10. Humby F, Bombardieri M, Manzo A, Kelly S, Blades MC, Kirkham B, et al. Ectopic lymphoid structures support ongoing production of class-switched autoantibodies in rheumatoid synovium. PLoS Med. 2009 Jan 13;6(1):e1. PubMed PMID: 19143467. Pubmed Central PMCID: 2621263. Epub 2009/01/16. eng.
11. McInnes IB, Schett G. Cytokines in the pathogenesis of rheumatoid arthritis. Nat Rev Immunol. 2007 Jun;7(6):429-42. PubMed PMID: 17525752. Epub 2007/05/26. eng.
12. Waaler E. On the occurrence of a factor in human serum activating the specific agglutintion of sheep blood corpuscles. 1939. APMIS : acta pathologica, microbiologica, et immunologica Scandinavica. 2007 May;115(5):422-38; discussion 39. PubMed PMID: 17504400.
13. Rose HM, Ragan C, et al. Differential agglutination of normal and sensitized sheep erythrocytes by sera of patients with rheumatoid arthritis. Proceedings of the Society for Experimental Biology and Medicine Society for Experimental Biology and Medicine. 1948 May;68(1):1-6. PubMed PMID: 18863659.

14. van Boekel MA, Vossenaar ER, van den Hoogen FH, van Venrooij WJ. Autoantibody systems in rheumatoid arthritis: specificity, sensitivity and diagnostic value. Arthritis Res. 2002;4(2):87-93. PubMed PMID: 11879544. Pubmed Central PMCID: 128920. Epub 2002/03/07. eng.
15. Shmerling RH, Delbanco TL. The rheumatoid factor: an analysis of clinical utility. Am J Med. 1991 Nov;91(5):528-34. PubMed PMID: 1951415. Epub 1991/11/01. eng.
16. Schellekens GA, Visser H, de Jong BA, van den Hoogen FH, Hazes JM, Breedveld FC, et al. The diagnostic properties of rheumatoid arthritis antibodies recognizing a cyclic citrullinated peptide. Arthritis Rheum. 2000 Jan;43(1):155-63. PubMed PMID: 10643712. Epub 2000/01/22. eng.
17. Nielen MM, van Schaardenburg D, Reesink HW, van de Stadt RJ, van der Horst-Bruinsma IE, de Koning MH, et al. Specific autoantibodies precede the symptoms of rheumatoid arthritis: a study of serial measurements in blood donors. Arthritis Rheum. 2004 Feb;50(2):380-6. PubMed PMID: 14872479. Epub 2004/02/12. eng.
18. Aggarwal R, Liao K, Nair R, Ringold S, Costenbader KH. Anti-citrullinated peptide antibody assays and their role in the diagnosis of rheumatoid arthritis. Arthritis Rheum. 2009 Nov 15;61(11):1472-83. PubMed PMID: 19877103. Pubmed Central PMCID: 2859449. Epub 2009/10/31. eng.
19. Ronnelid J, Wick MC, Lampa J, Lindblad S, Nordmark B, Klareskog L, et al. Longitudinal analysis of citrullinated protein/peptide antibodies (anti-CP) during 5 year follow up in early rheumatoid arthritis: anti-CP status predicts worse disease activity and greater radiological progression. Ann Rheum Dis. 2005 Dec;64(12):1744-9. PubMed PMID: 15843452. Pubmed Central PMCID: 1755292. Epub 2005/04/22. eng.
20. Kuhn KA, Kulik L, Tomooka B, Braschler KJ, Arend WP, Robinson WH, et al. Antibodies against citrullinated proteins enhance tissue injury in experimental autoimmune arthritis. J Clin Invest. 2006 Apr;116(4):961-73. PubMed PMID: 16585962. Pubmed Central PMCID: 1421345. Epub 2006/04/06. eng.
21. Singh JA, Christensen R, Wells GA, Suarez-Almazor ME, Buchbinder R, Lopez-Olivo MA, et al. Biologics for rheumatoid arthritis: an overview of Cochrane reviews. Sao Paulo Med J. 2010;128(5):309-10. PubMed PMID: 21181074. Epub 2010/12/25. eng.
22. Bugatti S, Codullo V, Caporali R, Montecucco C. B cells in rheumatoid arthritis. Autoimmun Rev. 2007 Dec;7(2):137-42. PubMed PMID: 18035324. Epub 2007/11/24. eng.
23. Boross P, Leusen JH. Mechanisms of action of CD20 antibodies. Am J Cancer Res. 2012;2(6):676-90. PubMed PMID: 23226614. Pubmed Central PMCID: 3512181. Epub 2012/12/12. eng.
24. Cambridge G, Leandro MJ, Edwards JC, Ehrenstein MR, Salden M, Bodman-Smith M, et al. Serologic changes following B lymphocyte depletion therapy for rheumatoid arthritis. Arthritis Rheum. 2003 Aug;48(8):2146-54. PubMed PMID: 12905467. Epub 2003/08/09. eng.
25. Dass S, Rawstron AC, Vital EM, Henshaw K, McGonagle D, Emery P. Highly sensitive B cell analysis predicts response to rituximab therapy in rheumatoid arthritis. Arthritis Rheum. 2008 Oct;58(10):2993-9. PubMed PMID: 18821683. Epub 2008/09/30. eng.
26. Patel AM, Moreland LW. Interleukin-6 inhibition for treatment of rheumatoid arthritis: a review of tocilizumab therapy. Drug Des Devel Ther. 2010;4:263-78. PubMed PMID: 21116333. Pubmed Central PMCID: 2990387. Epub 2010/12/01. eng.
27. Roll P, Muhammad K, Schumann M, Kleinert S, Einsele H, Dorner T, et al. In vivo effects of the anti-interleukin-6 receptor inhibitor tocilizumab on the B cell compartment. Arthritis Rheum. 2011 May;63(5):1255-64. PubMed PMID: 21305508. Epub 2011/02/10. eng.
28. Weinblatt ME, Kavanaugh A, Genovese MC, Musser TK, Grossbard EB, Magilavy DB. An oral spleen tyrosine kinase (Syk) inhibitor for rheumatoid arthritis. N Engl J Med. 2010 Sep 30;363(14):1303-12. PubMed PMID: 20879879.

29. van Vollenhoven RF, Fleischmann R, Cohen S, Lee EB, Garcia Meijide JA, Wagner S, et al. Tofacitinib or adalimumab versus placebo in rheumatoid arthritis. N Engl J Med. 2012 Aug 9;367(6):508-19. PubMed PMID: 22873531.
30. Barr TA, Shen P, Brown S, Lampropoulou V, Roch T, Lawrie S, et al. B cell depletion therapy ameliorates autoimmune disease through ablation of IL-6-producing B cells. J Exp Med. 2012 May 7;209(5):1001-10. PubMed PMID: 22547654. Pubmed Central PMCID: 3348102. Epub 2012/05/02. eng.
31. Huang H, Benoist C, Mathis D. Rituximab specifically depletes short-lived autoreactive plasma cells in a mouse model of inflammatory arthritis. Proceedings of the National Academy of Sciences of the United States of America. 2010 Mar 9;107(10):4658-63. PubMed PMID: 20176942. Pubmed Central PMCID: 2842072. Epub 2010/02/24. eng.
32. Wilk E, Witte T, Marquardt N, Horvath T, Kalippke K, Scholz K, et al. Depletion of functionally active CD20+ T cells by rituximab treatment. Arthritis Rheum. 2009 Dec;60(12):3563-71. PubMed PMID: 19950291. Epub 2009/12/02. eng.
33. Smolen JS, Landewe R, Breedveld FC, Dougados M, Emery P, Gaujoux-Viala C, et al. EULAR recommendations for the management of rheumatoid arthritis with synthetic and biological disease-modifying antirheumatic drugs. Ann Rheum Dis. 2010 Jun;69(6):964-75. PubMed PMID: 20444750. Pubmed Central PMCID: 2935329. Epub 2010/05/07. eng.
34. Nam JL, Winthrop KL, van Vollenhoven RF, Pavelka K, Valesini G, Hensor EM, et al. Current evidence for the management of rheumatoid arthritis with biological disease-modifying antirheumatic drugs: a systematic literature review informing the EULAR recommendations for the management of RA. Ann Rheum Dis. 2010 Jun;69(6):976-86. PubMed PMID: 20447957. Epub 2010/05/08. eng.
35. Chatzidionysiou K, Lie E, Nasonov E, Lukina G, Hetland ML, Tarp U, et al. Highest clinical effectiveness of rituximab in autoantibody-positive patients with rheumatoid arthritis and in those for whom no more than one previous TNF antagonist has failed: pooled data from 10 European registries. Ann Rheum Dis. 2011 Sep;70(9):1575-80. PubMed PMID: 21571731. Epub 2011/05/17. eng.
36. Marston B, Palanichamy A, Anolik JH. B cells in the pathogenesis and treatment of rheumatoid arthritis. Curr Opin Rheumatol. 2010 May;22(3):307-15. PubMed PMID: 20090526. Pubmed Central PMCID: 2947313. Epub 2010/01/22. eng.
37. Rosengren S, Wei N, Kalunian KC, Kavanaugh A, Boyle DL. CXCL13: a novel biomarker of B-cell return following rituximab treatment and synovitis in patients with rheumatoid arthritis. Rheumatology (Oxford). 2011 Mar;50(3):603-10. PubMed PMID: 21098574.
38. Duroux-Richard I, Pers YM, Fabre S, Ammari M, Baeten D, Cartron G, et al. Circulating miRNA-125b is a potential biomarker predicting response to rituximab in rheumatoid arthritis. Mediators of inflammation. 2014;2014:342524. PubMed PMID: 24778468. Pubmed Central PMCID: 3980876.
39. Cambridge G, Perry HC, Nogueira L, Serre G, Parsons HM, De La Torre I, et al. The effect of B-cell depletion therapy on serological evidence of B-cell and plasmablast activation in patients with rheumatoid arthritis over multiple cycles of rituximab treatment. J Autoimmun. 2014 May;50:67-76. PubMed PMID: 24365380.
40. Teng YK, Tekstra J, Breedveld FC, Lafeber F, Bijlsma JW, van Laar JM. Rituximab fixed retreatment versus on-demand retreatment in refractory rheumatoid arthritis: comparison of two B cell depleting treatment strategies. Ann Rheum Dis. 2009 Jun;68(6):1075-7. PubMed PMID: 19435725. Epub 2009/05/14. eng.
41. Chung JB, Silverman M, Monroe JG. Transitional B cells: step by step towards immune competence. Trends in immunology. 2003 Jun;24(6):343-9. PubMed PMID: 12810111.

42. MacLennan IC, Toellner KM, Cunningham AF, Serre K, Sze DM, Zuniga E, et al. Extrafollicular antibody responses. Immunol Rev. 2003 Aug;194:8-18. PubMed PMID: 12846803.
43. Toyama H, Okada S, Hatano M, Takahashi Y, Takeda N, Ichii H, et al. Memory B cells without somatic hypermutation are generated from Bcl6-deficient B cells. Immunity. 2002 Sep;17(3):329-39. PubMed PMID: 12354385.
44. Liu YJ, Malisan F, de Bouteiller O, Guret C, Lebecque S, Banchereau J, et al. Within germinal centers, isotype switching of immunoglobulin genes occurs after the onset of somatic mutation. Immunity. 1996 Mar;4(3):241-50. PubMed PMID: 8624814.
45. Perez-Andres M, Paiva B, Nieto WG, Caraux A, Schmitz A, Almeida J, et al. Human peripheral blood B-cell compartments: a crossroad in B-cell traffic. Cytometry B Clin Cytom. 2010;78 Suppl 1:S47-60. PubMed PMID: 20839338. Epub 2010/09/21. eng.
46. Ahuja A, Anderson SM, Khalil A, Shlomchik MJ. Maintenance of the plasma cell pool is independent of memory B cells. Proceedings of the National Academy of Sciences of the United States of America. 2008 Mar 25;105(12):4802-7. PubMed PMID: 18339801. Pubmed Central PMCID: 2290811.
47. Slifka MK, Antia R, Whitmire JK, Ahmed R. Humoral immunity due to long-lived plasma cells. Immunity. 1998 Mar;8(3):363-72. PubMed PMID: 9529153.
48. Manz RA, Lohning M, Cassese G, Thiel A, Radbruch A. Survival of long-lived plasma cells is independent of antigen. Int Immunol. 1998 Nov;10(11):1703-11. PubMed PMID: 9846699.
49. Hammarlund E, Lewis MW, Hansen SG, Strelow LI, Nelson JA, Sexton GJ, et al. Duration of antiviral immunity after smallpox vaccination. Nature medicine. 2003 Sep;9(9):1131-7. PubMed PMID: 12925846.
50. Amanna IJ, Carlson NE, Slifka MK. Duration of humoral immunity to common viral and vaccine antigens. N Engl J Med. 2007 Nov 8;357(19):1903-15. PubMed PMID: 17989383. Epub 2007/11/09. eng.
51. Radbruch A, Muehlinghaus G, Luger EO, Inamine A, Smith KG, Dorner T, et al. Competence and competition: the challenge of becoming a long-lived plasma cell. Nat Rev Immunol. 2006 Oct;6(10):741-50. PubMed PMID: 16977339. Epub 2006/09/16. eng.
52. Winter O, Dame C, Jundt F, Hiepe F. Pathogenic long-lived plasma cells and their survival niches in autoimmunity, malignancy, and allergy. J Immunol. 2012 Dec 1;189(11):5105-11. PubMed PMID: 23169863.
53. Tassone P, Neri P, Burger R, Di Martino MT, Leone E, Amodio N, et al. Mouse models as a translational platform for the development of new therapeutic agents in multiple myeloma. Current cancer drug targets. 2012 Sep;12(7):814-22. PubMed PMID: 22671927. Pubmed Central PMCID: 3587184.
54. Arpin C, Dechanet J, Van Kooten C, Merville P, Grouard G, Briere F, et al. Generation of memory B cells and plasma cells in vitro. Science. 1995 May 5;268(5211):720-2. PubMed PMID: 7537388.
55. Minges Wols HA, Underhill GH, Kansas GS, Witte PL. The role of bone marrow-derived stromal cells in the maintenance of plasma cell longevity. J Immunol. 2002 Oct 15;169(8):4213-21. PubMed PMID: 12370351.
56. Jego G, Palucka AK, Blanck JP, Chalouni C, Pascual V, Banchereau J. Plasmacytoid dendritic cells induce plasma cell differentiation through type I interferon and interleukin 6. Immunity. 2003 Aug;19(2):225-34. PubMed PMID: 12932356.
57. Ettinger R, Sims GP, Fairhurst AM, Robbins R, da Silva YS, Spolski R, et al. IL-21 induces differentiation of human naive and memory B cells into antibody-secreting plasma cells. J Immunol. 2005 Dec 15;175(12):7867-79. PubMed PMID: 16339522.

58. Huggins J, Pellegrin T, Felgar RE, Wei C, Brown M, Zheng B, et al. CpG DNA activation and plasma-cell differentiation of CD27- naive human B cells. Blood. 2007 Feb 15;109(4):1611-9. PubMed PMID: 17032927. Pubmed Central PMCID: 1794051.
59. Jourdan M, Caraux A, De Vos J, Fiol G, Larroque M, Cognot C, et al. An in vitro model of differentiation of memory B cells into plasmablasts and plasma cells including detailed phenotypic and molecular characterization. Blood. 2009 Dec 10;114(25):5173-81. PubMed PMID: 19846886. Pubmed Central PMCID: 2834398.
60. Cocco M, Stephenson S, Care MA, Newton D, Barnes NA, Davison A, et al. In Vitro Generation of Long-lived Human Plasma Cells. J Immunol. 2012 Dec 15;189(12):5773-85. PubMed PMID: 23162129. Epub 2012/11/20. eng.
61. Bergsagel PL, Smith AM, Szczepek A, Mant MJ, Belch AR, Pilarski LM. In multiple myeloma, clonotypic B lymphocytes are detectable among CD19+ peripheral blood cells expressing CD38, CD56, and monotypic Ig light chain. Blood. 1995 Jan 15;85(2):436-47. PubMed PMID: 7529064.
62. Yaccoby S, Epstein J. The proliferative potential of myeloma plasma cells manifest in the SCID-hu host. Blood. 1999 Nov 15;94(10):3576-82. PubMed PMID: 10552969.
63. Cocco M, Stephenson S, Care MA, Newton D, Barnes NA, Davison A, et al. In Vitro Generation of Long-lived Human Plasma Cells. Journal of Immunology. 2012 Dec;189(12):5773-85. PubMed PMID: WOS:000311995800033. English.
64. Kuehl WM, Bergsagel PL. Multiple myeloma: evolving genetic events and host interactions. Nature reviews Cancer. 2002 Mar;2(3):175-87. PubMed PMID: 11990854.
65. Robillard N, Wuilleme S, Moreau P, Bene MC. Immunophenotype of normal and myelomatous plasma-cell subsets. Frontiers in immunology. 2014;5:137. PubMed PMID: 24744760. Pubmed Central PMCID: 3978250.
66. Erdei A, Isaak A, Torok K, Sandor N, Kremlitzka M, Prechl J, et al. Expression and role of CR1 and CR2 on B and T lymphocytes under physiological and autoimmune conditions. Mol Immunol. 2009 Sep;46(14):2767-73. PubMed PMID: 19559484. Epub 2009/06/30. eng.
67. Nicholas MW, Dooley MA, Hogan SL, Anolik J, Looney J, Sanz I, et al. A novel subset of memory B cells is enriched in autoreactivity and correlates with adverse outcomes in SLE. Clin Immunol. 2008 Feb;126(2):189-201. PubMed PMID: 18077220. Pubmed Central PMCID: 2812414. Epub 2007/12/14. eng.
68. Colombo BM, Canevali P, Magnani O, Rossi E, Puppo F, Zocchi MR, et al. Defective expression and function of the leukocyte associated Ig-like receptor 1 in B lymphocytes from systemic lupus erythematosus patients. PLoS One. 2012;7(2):e31903. PubMed PMID: 22355402. Pubmed Central PMCID: 3280211. Epub 2012/02/23. eng.
69. Palanichamy A, Barnard J, Zheng B, Owen T, Quach T, Wei C, et al. Novel human transitional B cell populations revealed by B cell depletion therapy. J Immunol. 2009 May 15;182(10):5982-93. PubMed PMID: 19414749. Pubmed Central PMCID: 2746373. Epub 2009/05/06. eng.
70. Brezinschek HP, Rainer F, Brickmann K, Graninger WB. B lymphocyte-typing for prediction of clinical response to rituximab. Arthritis Res Ther. 2012;14(4):R161. PubMed PMID: 22770118. Pubmed Central PMCID: 3580553.
71. Amanna IJ, Slifka MK. Quantitation of rare memory B cell populations by two independent and complementary approaches. J Immunol Methods. 2006 Dec 20;317(1-2):175-85. PubMed PMID: 17055526. Epub 2006/10/24. eng.
72. Khaled Amara JS, Fiona Murray, Henner Morbach, Blanca Fernandez-Rodriguez, Vijay Balasingh, Marianne Engstro¨m, Omri Snir, Lena Israelsson, Anca. I. Catrina, Hedda Wardemann, Davide Corti, Eric

Meffre Sr., Lars Klareskog and Vivianne Malmstro¨m. Monoclonal IgG Antibodies (ACPAs) From Synovial Fluid B Cells of Rheumatoid Arthritis Patients – Antigen-Driven Affinity Maturation and Cross Reactivity. Arthritis & Rheumatism. 2011 2011;63(S10):S1091.
73. Rawstron AC, Child JA, de Tute RM, Davies FE, Gregory WM, Bell SE, et al. Minimal residual disease assessed by multiparameter flow cytometry in multiple myeloma: impact on outcome in the Medical Research Council Myeloma IX Study. Journal of clinical oncology : official journal of the American Society of Clinical Oncology. 2013 Jul 10;31(20):2540-7. PubMed PMID: 23733781.
74. Kennedy B, Rawstron A, Carter C, Ryan M, Speed K, Lucas G, et al. Campath-1H and fludarabine in combination are highly active in refractory chronic lymphocytic leukemia. Blood. 2002 Mar 15;99(6):2245-7. PubMed PMID: 11877305.
75. Rawstron AC, Kennedy B, Moreton P, Dickinson AJ, Cullen MJ, Richards SJ, et al. Early prediction of outcome and response to alemtuzumab therapy in chronic lymphocytic leukemia. Blood. 2004 Mar 15;103(6):2027-31. PubMed PMID: 14630811.
76. Moreton P, Kennedy B, Lucas G, Leach M, Rassam SM, Haynes A, et al. Eradication of minimal residual disease in B-cell chronic lymphocytic leukemia after alemtuzumab therapy is associated with prolonged survival. Journal of clinical oncology : official journal of the American Society of Clinical Oncology. 2005 May 1;23(13):2971-9. PubMed PMID: 15738539.
77. Bagwell CB, Adams EG. Fluorescence spectral overlap compensation for any number of flow cytometry parameters. Ann N Y Acad Sci. 1993 Mar 20;677:167-84. PubMed PMID: 8494206.
78. Perez ML, Gomara MJ, Ercilla G, Sanmarti R, Haro I. Antibodies to citrullinated human fibrinogen synthetic peptides in diagnosing rheumatoid arthritis. J Med Chem. 2007 Jul 26;50(15):3573-84. PubMed PMID: 17585853. Epub 2007/06/26. eng.
79. van Dongen JJ, Langerak AW, Bruggemann M, Evans PA, Hummel M, Lavender FL, et al. Design and standardization of PCR primers and protocols for detection of clonal immunoglobulin and T-cell receptor gene recombinations in suspect lymphoproliferations: report of the BIOMED-2 Concerted Action BMH4-CT98-3936. Leukemia. 2003 Dec;17(12):2257-317. PubMed PMID: 14671650. Epub 2003/12/13. eng.
80. Brochet X, Lefranc MP, Giudicelli V. IMGT/V-QUEST: the highly customized and integrated system for IG and TR standardized V-J and V-D-J sequence analysis. Nucleic Acids Res. 2008 Jul 1;36(Web Server issue):W503-8. PubMed PMID: 18503082. Pubmed Central PMCID: 2447746. Epub 2008/05/27. eng.
81. Hassan R, White LR, Stefanoff CG, de Oliveira DE, Felisbino FE, Klumb CE, et al. Epstein-Barr virus (EBV) detection and typing by PCR: a contribution to diagnostic screening of EBV-positive Burkitt's lymphoma. Diagnostic pathology. 2006;1:17. PubMed PMID: 16893464. Pubmed Central PMCID: 1559641.
82. Taylor JJ, Martinez RJ, Titcombe PJ, Barsness LO, Thomas SR, Zhang N, et al. Deletion and anergy of polyclonal B cells specific for ubiquitous membrane-bound self-antigen. J Exp Med. 2012 Oct 22;209(11):2065-77. PubMed PMID: 23071255. Pubmed Central PMCID: 3478923. Epub 2012/10/17. eng.
83. Robinson WH. Sequencing the functional antibody repertoire-diagnostic and therapeutic discovery. Nat Rev Rheumatol. 2015 Mar;11(3):171-82. PubMed PMID: 25536486. Pubmed Central PMCID: 4382308.
84. Son KJ, Shin DS, Kwa T, You J, Gao Y, Revzin A. A microsystem integrating photodegradable hydrogel microstructures and reconfigurable microfluidics for single-cell analysis and retrieval. Lab on a chip. 2015 Feb 7;15(3):637-41. PubMed PMID: 25421651.

85. Bellatin MF, Han M, Fallena M, Fan L, Xia D, Olsen N, et al. Production of autoantibodies against citrullinated antigens/peptides by human B cells. J Immunol. 2012 Apr 1;188(7):3542-50. PubMed PMID: 22345652. Epub 2012/02/22. eng.
86. Vital EM, Dass S, Rawstron AC, Buch MH, Goeb V, Henshaw K, et al. Management of nonresponse to rituximab in rheumatoid arthritis: predictors and outcome of re-treatment. Arthritis Rheum. 2010 May;62(5):1273-9. PubMed PMID: 20131284. Epub 2010/02/05. eng.
87. Ghielmini M, Rufibach K, Salles G, Leoncini-Franscini L, Leger-Falandry C, Cogliatti S, et al. Single agent rituximab in patients with follicular or mantle cell lymphoma: clinical and biological factors that are predictive of response and event-free survival as well as the effect of rituximab on the immune system: a study of the Swiss Group for Clinical Cancer Research (SAKK). Annals of oncology : official journal of the European Society for Medical Oncology / ESMO. 2005 Oct;16(10):1675-82. PubMed PMID: 16030029.
88. Thompson SA, Jones JL, Cox AL, Compston DA, Coles AJ. B-cell reconstitution and BAFF after alemtuzumab (Campath-1H) treatment of multiple sclerosis. J Clin Immunol. 2010 Jan;30(1):99-105. PubMed PMID: 19763798.
89. Ornatsky O, Bandura D, Baranov V, Nitz M, Winnik MA, Tanner S. Highly multiparametric analysis by mass cytometry. J Immunol Methods. 2010 Sep 30;361(1-2):1-20. PubMed PMID: 20655312.
90. Bendall SC, Simonds EF, Qiu P, Amir el AD, Krutzik PO, Finck R, et al. Single-cell mass cytometry of differential immune and drug responses across a human hematopoietic continuum. Science. 2011 May 6;332(6030):687-96. PubMed PMID: 21551058. Pubmed Central PMCID: 3273988.
91. Doran MF, Crowson CS, Pond GR, O'Fallon WM, Gabriel SE. Frequency of infection in patients with rheumatoid arthritis compared with controls: a population-based study. Arthritis Rheum. 2002 Sep;46(9):2287-93. PubMed PMID: 12355475.
92. Zhao XF, Cherian S, Sargent R, Seethala R, Bonner H, Greenberg B, et al. Expanded populations of surface membrane immunoglobulin light chain-negative B cells in lymph nodes are not always indicative of B-cell lymphoma. American journal of clinical pathology. 2005 Jul;124(1):143-50. PubMed PMID: 15923170.
93. Leitner J, Rieger A, Pickl WF, Zlabinger G, Grabmeier-Pfistershammer K, Steinberger P. TIM-3 does not act as a receptor for galectin-9. PLoS pathogens. 2013 Mar;9(3):e1003253. PubMed PMID: 23555261. Pubmed Central PMCID: 3605152.
94. van der Vuurst de Vries AR, Clevers H, Logtenberg T, Meyaard L. Leukocyte-associated immunoglobulin-like receptor-1 (LAIR-1) is differentially expressed during human B cell differentiation and inhibits B cell receptor-mediated signaling. Eur J Immunol. 1999 Oct;29(10):3160-7. PubMed PMID: 10540327. Epub 1999/10/30. eng.
95. Pistoia V. Production of cytokines by human B cells in health and disease. Immunology today. 1997 Jul;18(7):343-50. PubMed PMID: 9238838.
96. Duddy ME, Alter A, Bar-Or A. Distinct profiles of human B cell effector cytokines: a role in immune regulation? J Immunol. 2004 Mar 15;172(6):3422-7. PubMed PMID: 15004141.
97. Francois A, Chatelus E, Wachsmann D, Sibilia J, Bahram S, Alsaleh G, et al. B lymphocytes and B-cell activating factor promote collagen and profibrotic markers expression by dermal fibroblasts in systemic sclerosis. Arthritis Res Ther. 2013;15(5):R168. PubMed PMID: 24289101. Pubmed Central PMCID: 3978899.
98. Teleshova N, Kenney J, Williams V, Van Nest G, Marshall J, Lifson JD, et al. CpG-C ISS-ODN activation of blood-derived B cells from healthy and chronic immunodeficiency virus-infected macaques. J Leukoc Biol. 2006 Feb;79(2):257-67. PubMed PMID: 16443827.

99. Chen YF, Jobanputra P, Barton P, Jowett S, Bryan S, Clark W, et al. A systematic review of the effectiveness of adalimumab, etanercept and infliximab for the treatment of rheumatoid arthritis in adults and an economic evaluation of their cost-effectiveness. Health technology assessment. 2006 Nov;10(42):iii-iv, xi-xiii, 1-229. PubMed PMID: 17049139.
100. Gonzalez M, Mackay F, Browning JL, Kosco-Vilbois MH, Noelle RJ. The sequential role of lymphotoxin and B cells in the development of splenic follicles. J Exp Med. 1998 Apr 6;187(7):997-1007. PubMed PMID: 9529316. Pubmed Central PMCID: 2212214.
101. Endres R, Alimzhanov MB, Plitz T, Futterer A, Kosco-Vilbois MH, Nedospasov SA, et al. Mature follicular dendritic cell networks depend on expression of lymphotoxin beta receptor by radioresistant stromal cells and of lymphotoxin beta and tumor necrosis factor by B cells. J Exp Med. 1999 Jan 4;189(1):159-68. PubMed PMID: 9874572. Pubmed Central PMCID: 1887694.
102. Kimura M, Kawahito Y, Obayashi H, Ohta M, Hara H, Adachi T, et al. A critical role for allograft inflammatory factor-1 in the pathogenesis of rheumatoid arthritis. J Immunol. 2007 Mar 1;178(5):3316-22. PubMed PMID: 17312183.
103. Pawlik A, Kurzawski M, Dziedziejko V, Safranow K, Paczkowska E, Maslinski W, et al. Allograft inflammatory factor-1 gene polymorphisms in patients with rheumatoid arthritis. Genetic testing and molecular biomarkers. 2012 May;16(5):341-5. PubMed PMID: 22106834.
104. Kazantseva MG, Hung NA, Highton J, Hessian PA. MMP expression in rheumatoid inflammation: the rs11568818 polymorphism is associated with MMP-7 expression at an extra-articular site. Genes and immunity. 2013 Apr;14(3):162-9. PubMed PMID: 23343931.
105. Talbot J, Bianchini FJ, Nascimento DC, Oliveira RD, Souto FO, Pinto LG, et al. CCR2 expression in neutrophils plays a critical role in their migration into joints in rheumatoid arthritis. Arthritis & rheumatology. 2015 Mar 16. PubMed PMID: 25779331.
106. Koch AE, Kunkel SL, Harlow LA, Mazarakis DD, Haines GK, Burdick MD, et al. Macrophage inflammatory protein-1 alpha. A novel chemotactic cytokine for macrophages in rheumatoid arthritis. J Clin Invest. 1994 Mar;93(3):921-8. PubMed PMID: 8132778. Pubmed Central PMCID: 293992.
107. Zhang R, Sun P, Jiang Y, Chen Z, Huang C, Zhang X, et al. Genome-wide haplotype association analysis and gene prioritization identify CCL3 as a risk locus for rheumatoid arthritis. International journal of immunogenetics. 2010 Aug;37(4):273-8. PubMed PMID: 20518837.
108. Radstake TR, van der Voort R, ten Brummelhuis M, de Waal Malefijt M, Looman M, Figdor CG, et al. Increased expression of CCL18, CCL19, and CCL17 by dendritic cells from patients with rheumatoid arthritis, and regulation by Fc gamma receptors. Ann Rheum Dis. 2005 Mar;64(3):359-67. PubMed PMID: 15331393. Pubmed Central PMCID: 1755402.
109. Flytlie HA, Hvid M, Lindgreen E, Kofod-Olsen E, Petersen EL, Jorgensen A, et al. Expression of MDC/CCL22 and its receptor CCR4 in rheumatoid arthritis, psoriatic arthritis and osteoarthritis. Cytokine. 2010 Jan;49(1):24-9. PubMed PMID: 19942450.
110. Kuan WP, Tam LS, Wong CK, Ko FW, Li T, Zhu T, et al. CXCL 9 and CXCL 10 as Sensitive markers of disease activity in patients with rheumatoid arthritis. J Rheumatol. 2010 Feb;37(2):257-64. PubMed PMID: 20032101.
111. Kotrych D, Dziedziejko V, Safranow K, Drozdzik M, Pawlik A. CXCL9 and CXCL10 gene polymorphisms in patients with rheumatoid arthritis. Rheumatology international. 2015 Feb 22. PubMed PMID: 25702175.
112. Zhang Y, Ma CJ, Wang JM, Ji XJ, Wu XY, Moorman JP, et al. Tim-3 regulates pro- and anti-inflammatory cytokine expression in human CD14+ monocytes. J Leukoc Biol. 2012 Feb;91(2):189-96. PubMed PMID: 21844165. Pubmed Central PMCID: 3290426.

113. Horie R, Watanabe T. CD30: expression and function in health and disease. Seminars in immunology. 1998 Dec;10(6):457-70. PubMed PMID: 9826579.
114. Horie R, Watanabe T, Morishita Y, Ito K, Ishida T, Kanegae Y, et al. Ligand-independent signaling by overexpressed CD30 drives NF-kappaB activation in Hodgkin-Reed-Sternberg cells. Oncogene. 2002 Apr 11;21(16):2493-503. PubMed PMID: 11971184.
115. Kim W. Utilizing CD30 expression as a rational target for therapy of lymphoma %U http://www.jhoonline.org/content/5/S1/A2. Journal of Hematology & Oncology. 2012;5 %@ 1756-8722(Suppl 1 %M doi:10.1186/1756-8722-5-S1-A2):A2.
116. Kuchroo VK, Meyers JH, Umetsu DT, DeKruyff RH. TIM family of genes in immunity and tolerance. Advances in immunology. 2006;91:227-49. PubMed PMID: 16938542.
117. Hastings WD, Anderson DE, Kassam N, Koguchi K, Greenfield EA, Kent SC, et al. TIM-3 is expressed on activated human CD4+ T cells and regulates Th1 and Th17 cytokines. Eur J Immunol. 2009 Sep;39(9):2492-501. PubMed PMID: 19676072. Pubmed Central PMCID: 2759376.
118. Han G, Chen G, Shen B, Li Y. Tim-3: an activation marker and activation limiter of innate immune cells. Frontiers in immunology. 2013;4:449. PubMed PMID: 24339828. Pubmed Central PMCID: 3857553.
119. Sada-Ovalle I, Chavez-Galan L, Torre-Bouscoulet L, Nava-Gamino L, Barrera L, Jayaraman P, et al. The Tim3-galectin 9 pathway induces antibacterial activity in human macrophages infected with Mycobacterium tuberculosis. J Immunol. 2012 Dec 15;189(12):5896-902. PubMed PMID: 23180819. Pubmed Central PMCID: 3516679.
120. Lee J, Oh JM, Hwang JW, Ahn JK, Bae EK, Won J, et al. Expression of human TIM-3 and its correlation with disease activity in rheumatoid arthritis. Scandinavian journal of rheumatology. 2011;40(5):334-40. PubMed PMID: 21446887.
121. Liu Y, Shu Q, Gao L, Hou N, Zhao D, Liu X, et al. Increased Tim-3 expression on peripheral lymphocytes from patients with rheumatoid arthritis negatively correlates with disease activity. Clin Immunol. 2010 Nov;137(2):288-95. PubMed PMID: 20805041.
122. Zhu C, Anderson AC, Schubart A, Xiong H, Imitola J, Khoury SJ, et al. The Tim-3 ligand galectin-9 negatively regulates T helper type 1 immunity. Nat Immunol. 2005 Dec;6(12):1245-52. PubMed PMID: 16286920.
123. Lee J, Park EJ, Noh JW, Hwang JW, Bae EK, Ahn JK, et al. Underexpression of TIM-3 and blunted galectin-9-induced apoptosis of CD4+ T cells in rheumatoid arthritis. Inflammation. 2012 Apr;35(2):633-7. PubMed PMID: 21717191.
124. Huang YH, Zhu C, Kondo Y, Anderson AC, Gandhi A, Russell A, et al. CEACAM1 regulates TIM-3-mediated tolerance and exhaustion. Nature. 2015 Jan 15;517(7534):386-90. PubMed PMID: 25363763. Pubmed Central PMCID: 4297519.
125. Zhang H, Cui Y, Voong N, Sabatino M, Stroncek DF, Morisot S, et al. Activating signals dominate inhibitory signals in CD137L/IL-15 activated natural killer cells. Journal of immunotherapy. 2011 Mar;34(2):187-95. PubMed PMID: 21304401. Pubmed Central PMCID: 3128544.
126. Zhao S, Zhang H, Xing Y, Natkunam Y. CD137 ligand is expressed in primary and secondary lymphoid follicles and in B-cell lymphomas: diagnostic and therapeutic implications. The American journal of surgical pathology. 2013 Feb;37(2):250-8. PubMed PMID: 23095505.
127. Comerci CJ, Mace EM, Banerjee PP, Orange JS. CD2 promotes human natural killer cell membrane nanotube formation. PLoS One. 2012;7(10):e47664. PubMed PMID: 23112830. Pubmed Central PMCID: 3480409.
128. Watts TH. TNF/TNFR family members in costimulation of T cell responses. Annu Rev Immunol. 2005;23:23-68. PubMed PMID: 15771565.

129. Wilcox RA, Tamada K, Strome SE, Chen L. Signaling through NK cell-associated CD137 promotes both helper function for CD8+ cytolytic T cells and responsiveness to IL-2 but not cytolytic activity. J Immunol. 2002 Oct 15;169(8):4230-6. PubMed PMID: 12370353.
130. Tangye SG, Phillips JH, Lanier LL. The CD2-subset of the Ig superfamily of cell surface molecules: receptor-ligand pairs expressed by NK cells and other immune cells. Seminars in immunology. 2000 Apr;12(2):149-57. PubMed PMID: 10764623.
131. Lee RV, Braylan RC, Rimsza LM. CD58 expression decreases as nonmalignant B cells mature in bone marrow and is frequently overexpressed in adult and pediatric precursor B-cell acute lymphoblastic leukemia. American journal of clinical pathology. 2005 Jan;123(1):119-24. PubMed PMID: 15762287.
132. Orange JS, Ballas ZK. Natural killer cells in human health and disease. Clin Immunol. 2006 Jan;118(1):1-10. PubMed PMID: 16337194.
133. Thorley-Lawson DA. Epstein-Barr virus: exploiting the immune system. Nat Rev Immunol. 2001 Oct;1(1):75-82. PubMed PMID: 11905817.
134. Laichalk LL, Thorley-Lawson DA. Terminal differentiation into plasma cells initiates the replicative cycle of Epstein-Barr virus in vivo. Journal of virology. 2005 Jan;79(2):1296-307. PubMed PMID: 15613356. Pubmed Central PMCID: 538585.
135. Biron CA, Nguyen KB, Pien GC, Cousens LP, Salazar-Mather TP. Natural killer cells in antiviral defense: function and regulation by innate cytokines. Annu Rev Immunol. 1999;17:189-220. PubMed PMID: 10358757.
136. Balandraud N, Roudier J, Roudier C. Epstein-Barr virus and rheumatoid arthritis. Autoimmun Rev. 2004 Jul;3(5):362-7. PubMed PMID: 15288002.
137. Fox RI, Luppi M, Pisa P, Kang HI. Potential role of Epstein-Barr virus in Sjogren's syndrome and rheumatoid arthritis. J Rheumatol Suppl. 1992 Jan;32:18-24. PubMed PMID: 1319486.
138. Saal JG, Krimmel M, Steidle M, Gerneth F, Wagner S, Fritz P, et al. Synovial Epstein-Barr virus infection increases the risk of rheumatoid arthritis in individuals with the shared HLA-DR4 epitope. Arthritis Rheum. 1999 Jul;42(7):1485-96. PubMed PMID: 10403278.
139. Scotet E, David-Ameline J, Peyrat MA, Moreau-Aubry A, Pinczon D, Lim A, et al. T cell response to Epstein-Barr virus transactivators in chronic rheumatoid arthritis. J Exp Med. 1996 Nov 1;184(5):1791-800. PubMed PMID: 8920867. Pubmed Central PMCID: 2192863.
140. Tosato G, Steinberg AD, Yarchoan R, Heilman CA, Pike SE, De Seau V, et al. Abnormally elevated frequency of Epstein-Barr virus-infected B cells in the blood of patients with rheumatoid arthritis. J Clin Invest. 1984 Jun;73(6):1789-95. PubMed PMID: 6327772. Pubmed Central PMCID: 437092.
141. Alvarez-Lafuente R, Fernandez-Gutierrez B, de Miguel S, Jover JA, Rollin R, Loza E, et al. Potential relationship between herpes viruses and rheumatoid arthritis: analysis with quantitative real time polymerase chain reaction. Ann Rheum Dis. 2005 Sep;64(9):1357-9. PubMed PMID: 16100341. Pubmed Central PMCID: 1755640.
142. Anzilotti C, Merlini G, Pratesi F, Tommasi C, Chimenti D, Migliorini P. Antibodies to viral citrullinated peptide in rheumatoid arthritis. J Rheumatol. 2006 Apr;33(4):647-51. PubMed PMID: 16511941.
143. Pratesi F, Tommasi C, Anzilotti C, Chimenti D, Migliorini P. Deiminated Epstein-Barr virus nuclear antigen 1 is a target of anti-citrullinated protein antibodies in rheumatoid arthritis. Arthritis Rheum. 2006 Mar;54(3):733-41. PubMed PMID: 16508937.

144. Tak PP, Kummer JA, Hack CE, Daha MR, Smeets TJ, Erkelens GW, et al. Granzyme-positive cytotoxic cells are specifically increased in early rheumatoid synovial tissue. Arthritis Rheum. 1994 Dec;37(12):1735-43. PubMed PMID: 7986219.
145. de Matos CT, Berg L, Michaelsson J, Fellander-Tsai L, Karre K, Soderstrom K. Activating and inhibitory receptors on synovial fluid natural killer cells of arthritis patients: role of CD94/NKG2A in control of cytokine secretion. Immunology. 2007 Oct;122(2):291-301. PubMed PMID: 17521371. Pubmed Central PMCID: 2266001.
146. Soderstrom K, Stein E, Colmenero P, Purath U, Muller-Ladner U, de Matos CT, et al. Natural killer cells trigger osteoclastogenesis and bone destruction in arthritis. Proceedings of the National Academy of Sciences of the United States of America. 2010 Jul 20;107(29):13028-33. PubMed PMID: 20615964. Pubmed Central PMCID: 2919936.
147. Wyatt RM, Dawson JR. Characterization of a subset of human B lymphocytes interacting with natural killer cells. J Immunol. 1991 Nov 15;147(10):3381-8. PubMed PMID: 1940341.
148. Gao N, Schwartzberg P, Wilder JA, Blazar BR, Yuan D. B cell induction of IL-13 expression in NK cells: role of CD244 and SLAM-associated protein. J Immunol. 2006 Mar 1;176(5):2758-64. PubMed PMID: 16493031.
149. Zambello R, Semenzato G. Large granular lymphocyte disorders: new etiopathogenetic clues as a rationale for innovative therapeutic approaches. Haematologica. 2009 Oct;94(10):1341-5. PubMed PMID: 19794080. Pubmed Central PMCID: 2754948.
150. Friedman J, Schattner A, Shvidel L, Berrebi A. Characterization of T-cell large granular lymphocyte leukemia associated with Sjogren's syndrome-an important but under-recognized association. Seminars in arthritis and rheumatism. 2006 Apr;35(5):306-11. PubMed PMID: 16616153.
151. Kawa-Ha K, Ishihara S, Ninomiya T, Yumura-Yagi K, Hara J, Murayama F, et al. CD3-negative lymphoproliferative disease of granular lymphocytes containing Epstein-Barr viral DNA. J Clin Invest. 1989 Jul;84(1):51-5. PubMed PMID: 2544630. Pubmed Central PMCID: 303951.
152. Crome SQ, Lang PA, Lang KS, Ohashi PS. Natural killer cells regulate diverse T cell responses. Trends in immunology. 2013 Jul;34(7):342-9. PubMed PMID: 23601842.
153. Abruzzo LV, Rowley DA. Homeostasis of the antibody response: immunoregulation by NK cells. Science. 1983 Nov 11;222(4624):581-5. PubMed PMID: 6685343.
154. Tregoning JS, Wang BL, McDonald JU, Yamaguchi Y, Harker JA, Goritzka M, et al. Neonatal antibody responses are attenuated by interferon-gamma produced by NK and T cells during RSV infection. Proceedings of the National Academy of Sciences of the United States of America. 2013 Apr 2;110(14):5576-81. PubMed PMID: 23509276. Pubmed Central PMCID: 3619373.
155. Mei HE, Wirries I, Frolich D, Brisslert M, Giesecke C, Grun JR, et al. A unique population of IgG-expressing plasma cells lacking CD19 is enriched in human bone marrow. Blood. 2015 Mar 12;125(11):1739-48. PubMed PMID: 25573986.
156. Rozanski CH, Utley A, Carlson LM, Farren MR, Murray M, Russell LM, et al. CD28 Promotes Plasma Cell Survival, Sustained Antibody Responses, and BLIMP-1 Upregulation through Its Distal PYAP Proline Motif. J Immunol. 2015 Apr 1. PubMed PMID: 25833397.
157. Mestas J, Hughes CC. Of mice and not men: differences between mouse and human immunology. J Immunol. 2004 Mar 1;172(5):2731-8. PubMed PMID: 14978070.
158. Gordon CJ, Grafton G, Wood PM, Larche M, Armitage RJ. Modelling the human immune response: can mice be trusted? Commentary. Current opinion in pharmacology. 2001 Aug;1(4):431-5. PubMed PMID: 11710744.

159. Wu YC, Kipling D, Leong HS, Martin V, Ademokun AA, Dunn-Walters DK. High-throughput immunoglobulin repertoire analysis distinguishes between human IgM memory and switched memory B-cell populations. Blood. 2010 Aug 19;116(7):1070-8. PubMed PMID: 20457872. Pubmed Central PMCID: 2938129.
160. Murray ME, Gavile CM, Nair JR, Koorella C, Carlson LM, Buac D, et al. CD28-mediated pro-survival signaling induces chemotherapeutic resistance in multiple myeloma. Blood. 2014 Jun 12;123(24):3770-9. PubMed PMID: 24782505. Pubmed Central PMCID: 4055924.
161. Peperzak V, Vikstrom I, Walker J, Glaser SP, LePage M, Coquery CM, et al. Mcl-1 is essential for the survival of plasma cells. Nat Immunol. 2013 Mar;14(3):290-7. PubMed PMID: 23377201. Pubmed Central PMCID: 4041127.
162. O'Connor BP, Raman VS, Erickson LD, Cook WJ, Weaver LK, Ahonen C, et al. BCMA is essential for the survival of long-lived bone marrow plasma cells. J Exp Med. 2004 Jan 5;199(1):91-8. PubMed PMID: 14707116. Pubmed Central PMCID: 1887725.
163. Tarte K, Jourdan M, Veyrune JL, Berberich I, Fiol G, Redal N, et al. The Bcl-2 family member Bfl-1/A1 is strongly repressed in normal and malignant plasma cells but is a potent anti-apoptotic factor for myeloma cells. British journal of haematology. 2004 May;125(3):373-82. PubMed PMID: 15086420. Pubmed Central PMCID: 2685897.
164. Rawstron AC, Orfao A, Beksac M, Bezdickova L, Brooimans RA, Bumbea H, et al. Report of the European Myeloma Network on multiparametric flow cytometry in multiple myeloma and related disorders. Haematologica. 2008 Mar;93(3):431-8. PubMed PMID: 18268286.
165. Rawstron AC, Laycock-Brown G, Hale G, Davies FE, Morgan GJ, Child JA, et al. CD52 expression patterns in myeloma and the applicability of alemtuzumab therapy. Haematologica. 2006 Nov;91(11):1577-8. PubMed PMID: 17043027.
166. Geffroy-Luseau A, Jego G, Bataille R, Campion L, Pellat-Deceunynck C. Osteoclasts support the survival of human plasma cells in vitro. Int Immunol. 2008 Jun;20(6):775-82. PubMed PMID: 18397910.
167. Jourdan M, Cren M, Robert N, Bollore K, Fest T, Duperray C, et al. IL-6 supports the generation of human long-lived plasma cells in combination with either APRIL or stromal cell-soluble factors. Leukemia. 2014 Aug;28(8):1647-56. PubMed PMID: 24504026.
168. Sciammas R, Shaffer AL, Schatz JH, Zhao H, Staudt LM, Singh H. Graded expression of interferon regulatory factor-4 coordinates isotype switching with plasma cell differentiation. Immunity. 2006 Aug;25(2):225-36. PubMed PMID: 16919487.
169. Nutt SL, Hodgkin PD, Tarlinton DM, Corcoran LM. The generation of antibody-secreting plasma cells. Nat Rev Immunol. 2015 Mar;15(3):160-71. PubMed PMID: 25698678.
170. Oracki SA, Walker JA, Hibbs ML, Corcoran LM, Tarlinton DM. Plasma cell development and survival. Immunol Rev. 2010 Sep;237(1):140-59. PubMed PMID: 20727034. Epub 2010/08/24. eng.
171. Vollmers C, Sit RV, Weinstein JA, Dekker CL, Quake SR. Genetic measurement of memory B-cell recall using antibody repertoire sequencing. Proceedings of the National Academy of Sciences of the United States of America. 2013 Aug 13;110(33):13463-8. PubMed PMID: 23898164. Pubmed Central PMCID: 3746854.
172. Mateo G, Montalban MA, Vidriales MB, Lahuerta JJ, Mateos MV, Gutierrez N, et al. Prognostic value of immunophenotyping in multiple myeloma: a study by the PETHEMA/GEM cooperative study groups on patients uniformly treated with high-dose therapy. Journal of clinical oncology : official journal of the American Society of Clinical Oncology. 2008 Jun 1;26(16):2737-44. PubMed PMID: 18443352.

173. Rozanski CH, Arens R, Carlson LM, Nair J, Boise LH, Chanan-Khan AA, et al. Sustained antibody responses depend on CD28 function in bone marrow-resident plasma cells. J Exp Med. 2011 Jul 4;208(7):1435-46. PubMed PMID: 21690252. Pubmed Central PMCID: 3135367.
174. Njau MN, Kim JH, Chappell CP, Ravindran R, Thomas L, Pulendran B, et al. CD28-B7 interaction modulates short- and long-lived plasma cell function. J Immunol. 2012 Sep 15;189(6):2758-67. PubMed PMID: 22908331.
175. Chaidos A, Barnes CP, Cowan G, May PC, Melo V, Hatjiharissi E, et al. Clinical drug resistance linked to interconvertible phenotypic and functional states of tumor-propagating cells in multiple myeloma. Blood. 2013 Jan 10;121(2):318-28. PubMed PMID: 23169779.
176. Fang X, Zheng P, Tang J, Liu Y. CD24: from A to Z. Cellular & molecular immunology. 2010 Mar;7(2):100-3. PubMed PMID: 20154703. Epub 2010/02/16. eng.
177. Sanchez E, Fernandez-Gutierrez B, Gonzalez-Gay MA, Balsa A, Garcia A, Rodriguez L, et al. Investigating the role of CD24 gene polymorphisms in rheumatoid arthritis. Ann Rheum Dis. 2008 Aug;67(8):1197-8. PubMed PMID: 18621973. Epub 2008/07/16. eng.
178. Koncz G, Hueber AO. The Fas/CD95 Receptor Regulates the Death of Autoreactive B Cells and the Selection of Antigen-Specific B Cells. Frontiers in immunology. 2012;3:207. PubMed PMID: 22848207. Pubmed Central PMCID: 3404404. Epub 2012/08/01. eng.
179. Rodriguez-Bayona B, Perez-Venegas JJ, Rodriguez C, Brieva JA. CD95-Mediated control of anti-citrullinated protein/peptides antibodies (ACPA)-producing plasma cells occurring in rheumatoid arthritis inflamed joints. Rheumatology (Oxford). 2007 Apr;46(4):612-6. PubMed PMID: 17132692. Epub 2006/11/30. eng.
180. Martin M, Romero X, de la Fuente MA, Tovar V, Zapater N, Esplugues E, et al. CD84 functions as a homophilic adhesion molecule and enhances IFN-gamma secretion: adhesion is mediated by Ig-like domain 1. J Immunol. 2001 Oct 1;167(7):3668-76. PubMed PMID: 11564780. Epub 2001/09/21. eng.
181. Oliver-Vila I, Saborit-Villarroya I, Engel P, Martin M. The leukocyte receptor CD84 inhibits Fc epsilon RI-mediated signaling through homophilic interaction in transfected RBL-2H3 cells. Mol Immunol. 2008 Apr;45(8):2138-49. PubMed PMID: 18243321. Epub 2008/02/05. eng.
182. Meyaard L. The inhibitory collagen receptor LAIR-1 (CD305). J Leukoc Biol. 2008 Apr;83(4):799-803. PubMed PMID: 18063695. Epub 2007/12/08. eng.
183. Tarlinton D, Good-Jacobson K. Diversity among memory B cells: origin, consequences, and utility. Science. 2013 Sep 13;341(6151):1205-11. PubMed PMID: 24031013.
184. Ehrhardt GR, Hsu JT, Gartland L, Leu CM, Zhang S, Davis RS, et al. Expression of the immunoregulatory molecule FcRH4 defines a distinctive tissue-based population of memory B cells. J Exp Med. 2005 Sep 19;202(6):783-91. PubMed PMID: 16157685. Pubmed Central PMCID: 2212938.
185. Bouaziz JD, Yanaba K, Tedder TF. Regulatory B cells as inhibitors of immune responses and inflammation. Immunol Rev. 2008 Aug;224:201-14. PubMed PMID: 18759928. Epub 2008/09/02. eng.
186. Chapel H, Lucas M, Lee M, Bjorkander J, Webster D, Grimbacher B, et al. Common variable immunodeficiency disorders: division into distinct clinical phenotypes. Blood. 2008 Jul 15;112(2):277-86. PubMed PMID: 18319398. Epub 2008/03/06. eng.
187. Arce S, Luger E, Muehlinghaus G, Cassese G, Hauser A, Horst A, et al. CD38 low IgG-secreting cells are precursors of various CD38 high-expressing plasma cell populations. J Leukoc Biol. 2004 Jun;75(6):1022-8. PubMed PMID: 15020647. Epub 2004/03/17. eng.
188. Tangye SG, Avery DT, Hodgkin PD. A division-linked mechanism for the rapid generation of Ig-secreting cells from human memory B cells. J Immunol. 2003 Jan 1;170(1):261-9. PubMed PMID: 12496408. Epub 2002/12/24. eng.

189. Franz B, May KF, Jr., Dranoff G, Wucherpfennig K. Ex vivo characterization and isolation of rare memory B cells with antigen tetramers. Blood. 2011 Jul 14;118(2):348-57. PubMed PMID: 21551230. Pubmed Central PMCID: 3138687. Epub 2011/05/10. eng.

14 Appendices

14.1 Supplementary Data

14.1.1 Expansion of non-B lineage cells is operator independent

The culture conditions are changed on day 6 which includes adding 3 different cytokines at specific concentrations and 3 different nutrients on top of a stromal cell layer. To exclude the possibility of operator dependent variability causing the expansion, on day 6 the cells were cultured with media made by self and media prepared by an independent experienced operator. There was a similar expansion with both sets of media with the non-B lineage cells expanding from less than half a percent on day 6 to more than 40 percent in both cases by day 13.

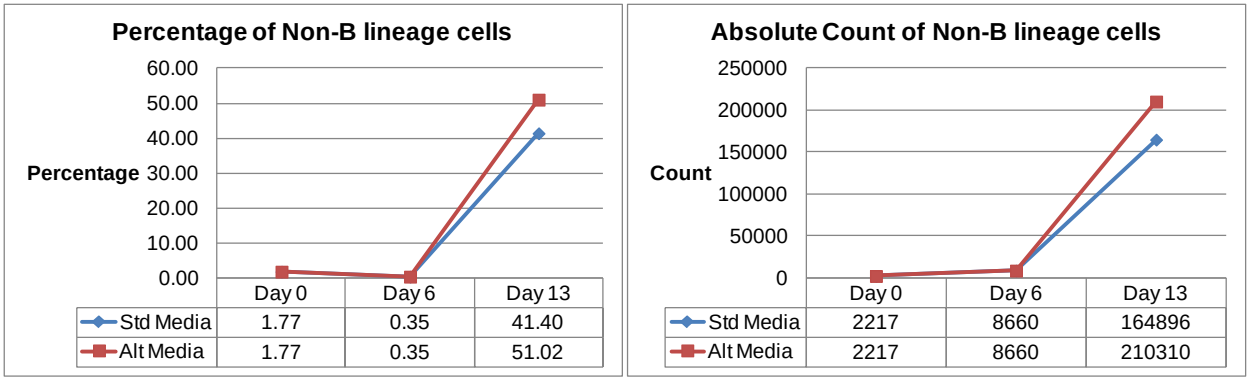

	Day 0	Day 6	Day 13
Std Media	1.77	0.35	41.40
Alt Media	1.77	0.35	51.02

	Day 0	Day 6	Day 13
Std Media	2217	8660	164896
Alt Media	2217	8660	210310

Figure 14.1-1Operator independent expansion of non-B lineage cells

The proportion and absolute count of non-B lineage cells on the days specified with media prepared by self (Std) and media prepared by an experienced operator (Alt).

14.1.2 Expansion of non-B lineage cells is not due to dilution of the initial seeding concentration of cells

To assess whether the dilution in the initial seeding concentration is responsible for the noted expansion between days 6 and 13, B-cells were differentiated from 2 volunteers at standard and one-fifth concentrations. The higher starting dilution did not cause increased expansion as seen in Figure 14.1-2. In fact the higher starting concentration yielded more expansion between day 6 and day 13. This suggests that cell density is a significant determinant of CD19 negative cells expansion, possibly consistent with a cell contact mediated effect.

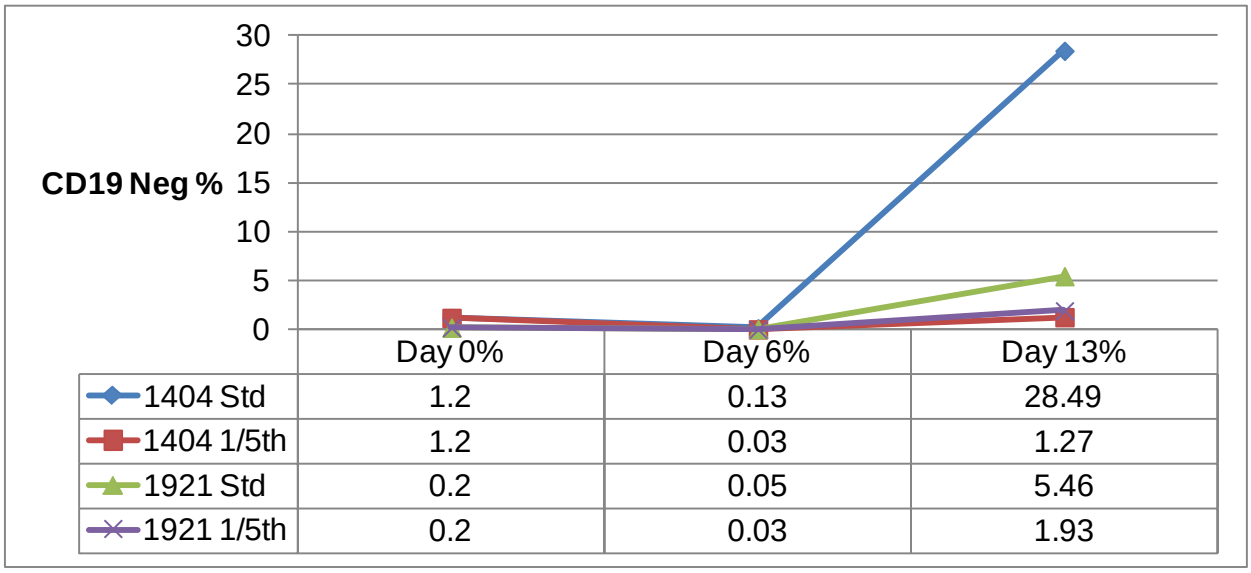

	Day 0%	Day 6%	Day 13%
1404 Std	1.2	0.13	28.49
1404 1/5th	1.2	0.03	1.27
1921 Std	0.2	0.05	5.46
1921 1/5th	0.2	0.03	1.93

Figure 14.1-2 Effect of standard and 1/5th Initial seeding concentrations on non-B lineage cell expansion

Percentage of non-B lineage cell expansion with standard and 1/5th starting cell concentrations from 2 donors is shown.

14.1.3 Expansion of non-B lineage cells is worse with a 48 well plate compared to 24 well plate.

The other variation from the standard protocol for differentiating RA B-cells was to use 48 well plates instead of 24 well plates to try and reduce the volume of blood needed to be collected from patients. The initial seeding concentration was reduced by half for a 48 well plate to account for the difference in surface area of the 24 well plate. Although the increase in absolute numbers of non-B lineage cells was not dramatic, when the fold expansion of the non-B cells from day 0 and day 6 is compared between the two conditions, it becomes clear that the expansion is favoured by the 48 well plate.

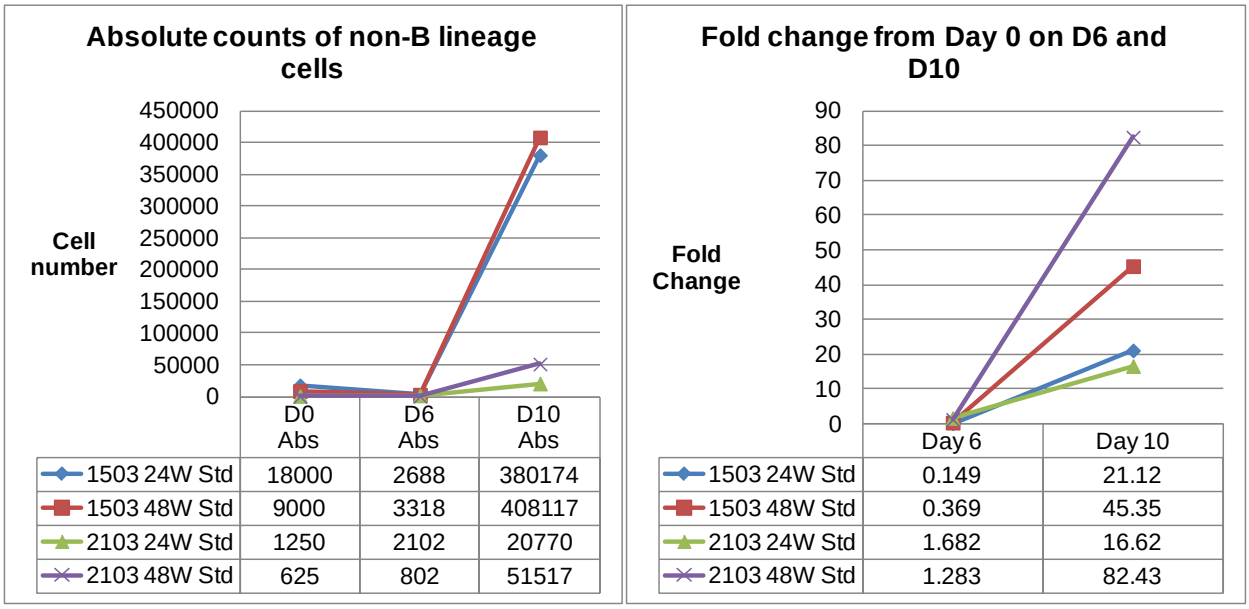

	D0 Abs	D6 Abs	D10 Abs
1503 24W Std	18000	2688	380174
1503 48W Std	9000	3318	408117
2103 24W Std	1250	2102	20770
2103 48W Std	625	802	51517

	Day 6	Day 10
1503 24W Std	0.149	21.12
1503 48W Std	0.369	45.35
2103 24W Std	1.682	16.62
2103 48W Std	1.283	82.43

Figure 14.1-3 Favourable expansion of non-B lineage cells when differentiated on a 48 well plate

B-cells from 2 donors were differentiated in parallel on a 24 and 48 well plate and the change in number of non-B lineage cells is shown in the first graph. Fold increase from day 0 shown in the second graph was calculated as: (Number of cells on day 10 or 6 from a single day 0 well) **/** (Number of cells that started in a single day 0 well)

14.1.4 Expansion of non-B lineage cells can be reduced by swapping from 48 to 24 well plate between day 6 to day 10

Since there was increased expansion of non-B lineage cells with a 48 well plate between day 6 and day 10, the possibility of overcoming this effect by swapping the plates on day 6 was evaluated. Cells differentiated in 24 and 48 wells in parallel were either continued on the same sized plate or swapped to the alternative plate. There was more expansion of the non-B lineage cells when the cells were swapped from 24 well plate to a 48 well plate on day 6 as evidenced by the comparison of fold increase in non-B cells from day 0 to day 10 when they were grown in 24 well plate throughout. It is not as evident in the donor who started with much lower number of non-B cells on day 0. Conversely the expansion could be reduced by swapping from a 48 well plate to a 24 well plate in both donors.

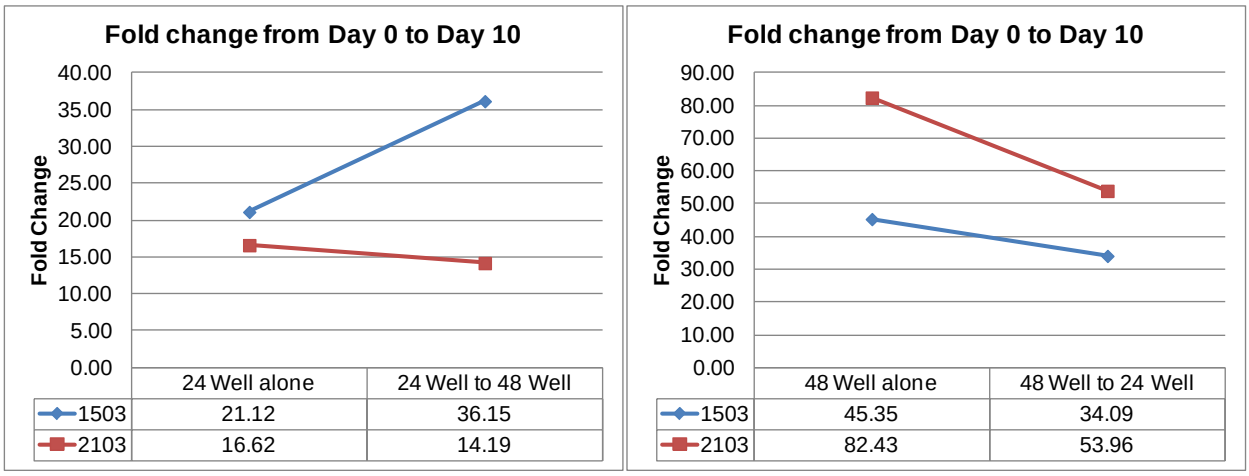

Figure 14.1-4 Reduction in Expansion of non-B lineage cells by swapping to a 24 well plate on day 6

Expansion of non B-lineage cells when they are cultured throughout on 24 or 48 well plates compared with swapping plates on day 6. The numbers shown in tables are fold expansion on day 10 from day 0 calculated as (Number of CD19 negative cells on day 10 from a single day 0 well) **/** (Number of CD19 negative cells that started in a single day 0 well)

14.1.5 Summary

The above experiments show that non-B lineage cell expansion is unlikely to be an operator dependent issue and not due to seeding the cells at a lower concentration. However, it is made worse by using smaller sized wells for the culture and therefore subsequent experiments were performed in a 24 well plate.

14.2 Appendix A – Reagents used

Reagent	Source	Constituents
Lymphoprep	Axis-Shield	Sodium diatrizoate - 9.1% (w/v) Polysaccharide – 5.7% (w/v)
Ammonium Chloride	Sigma-Aldrich	8.6g/l in distilled water
FACSflow	BD Biosciences	
Bovine Serum Albumin	Sigma Aldrich	0.5% in FACSflow
Human Memory B-cell Isolation Kit	Miltenyi Biotec	Biotin Antibody cocktail- Biotinylated mAb against CD2,CD14, CD43, CD16, CD36, Anti-IgE,CD235a Microbead conjugated to monoclonal antibiotin antibodies
Human NK cell Isolation KIt	Miltenyi Biotec	NK cell biotin antibody cocktail NK cell microbead cocktail
IMDM (Iscove's Modified Dulbecco's Medium)	GIBCO	Glycine 30 mg/L L-Alanine 25 mg/L L-Alanyl-L-Glutamine 812 mg/L L-Arginine hydrochloride 84 mg/L L-Asparagine (freebase) 28.4 mg/L L-Aspartic acid 30 mg/L L-Cystine 70 mg/L

		L-Glutamic Acid 75 mg/L L-Histidine hydrochloride-H2O 42 mg/L L-Isoleucine 105 mg/L L-Leucine 105 mg/L L-Lysine hydrochloride 146 mg/L L-Methionine 30 mg/L L-Phenylalanine 66 mg/L L-Proline 40 mg/L L-Serine 42 mg/L L-Threonine 95 mg/L L-Tryptophan 16 mg/L L-Tyrosine disodium salt 104 mg/L L-Valine 94 mg/L Biotin 0.013 mg/L Choline chloride 4 mg/L D-Calcium pantothenate 4 mg/L Folic Acid 4 mg/L Niacinamide 4 mg/L Pyridoxal hydrochloride 4 mg/L Riboflavin 0.4 mg/L Thiamine hydrochloride 4 mg/L Vitamin B12 0.013 mg/L i-Inositol 7.2 mg/L Calcium Chloride (CaCl2-2H2O) 219 mg/L

		Magnesium Sulfate (MgSO4-7H2O) 200 mg/L Potassium Chloride (KCl) 330 mg/L Potassium Nitrate (KNO3) 0.076 mg/L Sodium Bicarbonate (NaHCO3) 3024 mg/L Sodium Chloride (NaCl) 4500 mg/L Sodium Phosphate monobasic (NaH2PO4-2H2O) 141 mg/L Sodium Selenite (Na2SeO3-5H20) 0.017 mg/L D-Glucose (Dextrose) 4500 mg/L HEPES 5958 mg/L Phenol Red 15 mg/L Sodium Pyruvate 110 mg/L
Penicillin Streptomycin	Invitrogen	Penicillin 5000 units Streptomycin 5000 µg/ml
Trypsin-EDTA	Invitrogen	Trypsin 2.5 g/L EDTA 0.38 g/L
Flow Cytometry Absolute Count Standard	Invitrogen Countbright Beads	0.49 - 0.51 X 10^5 particles/50µL
Blocking Buffer	In-house	FACS Buffer 933 µL Normal Mouse Serum 50 µL Human IgG 16.7 µL
Human IgG	Sigma-Aldrich	Human IgG >95% 4.7 mg/ml

Normal Mouse Serum	Invitrogen		
Hybridomax	Gentaur	DMEM/F12 base, HEPES buffer, Insulin, Transferrin, Testosterone, Sodium selenite, Ethanolamine, saturated and unsaturated fatty acids and stabilising proteins	
Lipid Mixture 1, Chemically defined	Sigma Aldrich	Arachidonic acid	2 µg/ml
		Linoleic acid	10 µg/ml
		Linolenic acid	10 µg/ml
		Myristic acid	10 µg/ml
		Oleic acid	10 µg/ml
		Palmitic acid	10 µg/ml
		Stearic acid	10 µg/ml
		Cholesterol	0.22 mg/ml
		Tween-80	2.2 mg/ml
		Tocopherol acetate	70 µg/ml
		Pluronic F-68	100 mg/ml
MEM Amino Acids (50X) Solution	Sigma Aldrich	L-Arginine.Hcl	6.32 g/L
		L-Cystine.2Hcl	1.564 g/L
		L-Histidine.Hcl.H_20	2.1 g/L
		L-Isoleucine	2.625 g/L
		L-Leucine	2.62 g/L
		L-Lysine.Hcl	3.625 g/L
		L-Methionine	0.755 g/L
		L-Phenylalanine	1.65 g/L

		L-Threonine	2.38 g/L
		L-Tryptophan	0.51 g/L
		L-Tyrosine	1.8 g/L
		L-Valine	2.34 g/L

14.3 Appendix B – Details of Antibodies used for flow cytometry

Antigen	Fluorochrome	Volume Per Test (µL)	Clone	Manufacturer	Isotype
BCL2	FITC	2	124	Dako Cytomation	IgG1
CD10	PE	1	HI10a	BD Biosciences	IgG1
CD117	PE-Cy7	5	104D2	BD Biosciences	IgG1
CD11c	APC	1	B-ly6	BD Pharmingen	IgG1
CD126	Alexa Fluor 647	5	BL-126	Biolegend	IgG1
CD126	PE	5	M91	Immunotech	IgG1
CD13	PE	5	L138	BD Biosciences	IgG1
CD130	PE	5	AM64	BD Pharmingen	IgG1
CD137	APC	5	4B4-1	Biolegend	IgG1
CD137	LEAF		4B4-1	Bolegend	IgG1
CD137	Unconjugated		BBK-2	Thermo Scientific	IgG1
CD137L	PE	5	5F4	Biolegend	IgG1
CD138	APC	1	B_B4	Miltenyi	IgG1
CD14	FITC	5	M5E2	BD Pharmingen	IgG2a
CD15	FITC	5	C3D-1	Dako	IgM
CD150	PE	5	A12	BD Pharmingen	IgG1
CD152	PE	5	BNI3	BD Pharmingen	IgG2a
CD16	PE	0.1	3G8	BD Pharmingen	IgG1
CD16	V500	5	3G8	BD Horizon	IgG1
CD184	PE	5	12G5	BD Pharmingen	IgG2a

Antigen	Fluorochrome	Volume Per Test (µL)	Clone	Manufacturer	Isotype
CD19	BV421	1	HIB19	Biolegend	IgG1
CD19	PE	2	LT19	Miltenyi	IgG1
CD19	PE-Cy7	1	SJ225C1	BD Biosciences	IgG1
CD19	PerCP-Cy5.5	2.5	SJ225C1	BD Biosciences	IgG1
CD19	V500	5	HIB19	BD Horizon	IgG1
CD196	Alexa Fluor 647	5	11A9	BD Pharmingen	IgG1
CD2	LEAF		RPA-2.10	Biolegend	IgG1
CD2	PE-Cy7	1	RPA2.10	BD Biosciences	IgG1
CD20	APC-H7	2.5	L27	BD Biosciences	IgG1
CD20	efluor450	2.5	2H7	eBioscience	IgG2b
CD20	Pacific Blue	5	B9E9	IOTest	IgG2a
CD200	APC	5	OX104	Biolegend	IgG1
CD200	APC	5	OX104	eBioscience	IgG1
CD21	FITC	5	LB21	Serotec	IgG1
CD22	APC	1	S-HCL-1	BD Biosciences	IgG2b
CD23	APC	5	EBVCS-5	BD Biosciences	IgG1
CD24	FITC	5	ML5	BD Pharmingen	IgG2a
CD25	APC	5	2A3	BD Biosciences	IgG1
CD25	PE	5	2A3	BD Biosciences	IgG1
CD261	FITC	5	DR-4-02	Exbio	IgG1
CD27	AF 647	5	LT27	AbD Serotec	IgG2a
CD27	BV605	2.5	O323	Biolegend	IgG1

Antigen	Fluorochrome	Volume Per Test (µL)	Clone	Manufacturer	Isotype
CD27	CF594	1	M-T271	BD Horizon	IgG1
CD27	FITC	5	M-T271	BD Pharmingen	IgG1
CD27	PE-Cy7	2.5	M-T271	BD Pharmingen	IgG1
CD27	Qdot605	2.5	CLB-27/1	Invitrogen	IgG2b
CD28	PE	5	L293	BD Biosciences	IgG1
CD3	APC	1	SK7	BD Biosciences	IgG1
CD3	APC-H7	2.5	SK7	BD Biosciences	IgG1
CD3	PE-Cy7	1	SK7	BD Biosciences	IgG1
CD307d	APC	5	413D12	Biolegend	IgG2b
CD31	FITC	5	WM59	BD Pharmingen	IgG1
CD319	PE	5	162.1	Biolegend	IgG2b
CD34	APC	0.5	8G12	BD Biosciences	IgG1
CD37	FITC	5	M-B371	BD Pharmingen	IgG1
CD38	AF700	2.5	HIT2	Biolegend	IgG1
CD38	CF594	1	HIT2	BD Horizon	IgG1
CD38	PE	1	HB7	BD Biosciences	IgG1
CD38	PE-Cy7	0.1	HB7	BD Biosciences	IgG1
CD38	PerCP-Cy5.5	0.5	HIT2	BD Pharmingen	IgG1
CD39	FITC	5	A1	AbD Serotec	IgG1
CD4	PerCP-Cy5.5	5	SK3	BD Biosciences	IgG1
CD43	FITC	5	1G10	BD Pharmingen	IgG1
CD45	APC-H7	2.5	2D1	BD Biosciences	IgG1

Antigen	Fluorochrome	Volume Per Test (µL)	Clone	Manufacturer	Isotype
CD45	V500	5	HI30	BD Horizon	IgG1
CD48	FITC	5	TU145	BD Pharmingen	IgM
CD49d	FITC	5	44H6	AbD Serotec	IgG1
CD5	PerCP-Cy5.5	5	L17F12	BD Biosciences	IgG2a
CD54	APC	5	HA58	BD Pharmingen	IgG1
CD56	BV605	1	HCD56	Biolegend	IgG1
CD56	PE	5	NCAM16.2	BD Biosciences	IgG2b
CD56	PE-Cy7	2.5	NCAM16.2	BD Biosciences	IgG2b
CD56	V450	5	B159	BD Horizon	IgG1
CD57	FITC	5	HNK-1	BD Biosciences	IgM
CD58	PE	5	L306.4	BD Biosciences	IgG2a
CD58	LEAF		TS2/9	Biolegend	IgG1
CD61	APC	5	CLB-thromb/1	Caltag	IgG1
CD62L	FITC	5	DREG-56	BD Pharmingen	IgG1
CD63	PE	5	H5C56	BD Pharmingen	IgG1
CD69	APC	5	L78	BD Biosciences	IgG1
CD73	PE	5	AD2	BD Pharmingen	IgG1
CD79b	PE	5	CB3-1	IOTest	IgG1
CD8	APC	0.5	SK1	BD Biosciences	IgG1
CD80	PE	5	L307.4	BD Pharmingen	IgG1
CD81	FITC	5	JS81	BD Pharmingen	IgG1
CD84	PE	5	CD84.1.21	Biolegend	IgG2a

Antigen	Fluorochrome	Volume Per Test (µL)	Clone	Manufacturer	Isotype
CD85j	FITC	5	GHI/75	BD Pharmingen	IgG2b
CD86	APC	5	2331 (FUN-1)	BD Pharmingen	IgG1
CD94	PE	5	HP-3D9	BD Pharmingen	IgG1
CD95	BV421	1	DX2	Biolegend	IgG1
CD95	Pacific Blue	5	LT95	Exbio	IgG1
CD95	PE	5	DX2	BD Pharmingen	IgG1
CXCR5	Alexa Fluor 647	5	RF8B2	BD Pharmingen	IgG2b
FCRL4	APC	5	580810	R&D Systems	IgG1
Galectin-9	LEAF		9M1-3	Biolegend	IgG1
HLA-DR	FITC	5	G46-6	BD Biosciences	IgG2a
IgA	FITC	5	Polyclonal	Dako	Fab2
IgD	PE	5	IA6-2	BD Pharmingen	IgG2a
IgD	AF700	5	IA6-2	BD Pharmingen	IgG2a
IgG	FITC	5	G18-145	BD Pharmingen	IgG1
IgM	APC	5	G20-127	BD Pharmingen	IgG1
IRF4	Unconjugated	1	M-17	Santa Cruz	Goat IgG
Goat IgG	AF488	1	Polyclonal	Invitrogen	Donkey IgG
Kappa	Pacific Blue	1	A8B5	Exbio	IgG1
Ki67	FITC	5	B56	BD Pharmingen	IgG1
LAIR1	Alexa Fluor 647	1	NKTA255	Biolegend	IgG1
LAIR1	Biotin	1.5	NKTA255	Abcam/Serotec	IgG1
LAIR1	PE	5	DX26	BD Pharmingen	IgG1

Antigen	Fluorochrome	Volume Per Test (µL)	Clone	Manufacturer	Isotype
Lambda	FITC	5	1-155-2	BD Biosciences	IgG1
TIM3	PE / LEAF	5	F38-2E2	Biolegend	IgG1

14.4 Ethical Approval Forms and Consent Forms

NHS

National Research Ethics Service

Harrogate Research Ethics Committee
C/O Leeds (East) Research Ethics Committee
Room 5.2, Clinical Sciences Building
St James's University Hospital
Beckett Street
Leeds
LS9 7TF

Telephone: 0113 2065637
Facsimile: 0113 2066772

28 July 2009

Dr Andrew Rawstron
Leeds Teaching Hospitals NHS Trust
Principle Clinical Scientist
HMDS
Algernon Firth Building
Leeds
LS1 3EX

Dear Dr Rawstron

Study title:	**Characterisation of sub-clinical haematological malignancies in the adult population**
REC reference:	**04/Q1107/40**
Amendment number:	**1: Modified**
Amendment date:	**14 July 2009**

Thank you for submitting the above amendment, which was received on 15 July 2009. It is noted that this is a modification of an amendment previously rejected by the Committee (our letter of 18 June 2009 refers).

The modified amendment was reviewed by the Sub-Committee in correspondence. A list of the members who took part in the review is attached.

Ethical opinion

I am pleased to confirm that the Committee has given a favourable ethical opinion of the modified amendment on the basis described in the notice of amendment form and supporting documentation.

Approved documents

The documents reviewed and approved are:

Document	Version	Date
Correspondence from Melanie Kingston, Ethics and Confidentiality Committee, NIGB		10 July 2009
Modified Amendment		14 July 2009

R&D approval

All investigators and research collaborators in the NHS should notify the R&D office for the relevant NHS care organisation of this amendment and check whether it affects R&D approval of the research.

Statement of compliance

The Committee is constituted in accordance with the Governance Arrangements for Research Ethics Committees (July 2001) and complies fully with the Standard Operating Procedures for Research Ethics Committees in the UK.

04/Q1107/39:	**Please quote this number on all correspondence**

Yours sincerely

Ann Tonley

Miss Amy Beckitt
Committee Assistant Co-ordinator
E-mail: Amy.Beckitt@leedsth.nhs.uk

Enclosures: List of names and professions of members who took part in the review

Copy to: R&D office for Leeds Teaching Hospitals NHS Trust

Leeds (East) Research Ethics Committee

Attendance at Sub-Committee of the REC meeting on 28 July 2009

Committee Members:

Name	*Profession*	*Capacity*
Dr Carol E Chu	Vice Chair: Consultant Clinical Geneticist	Expert
Mrs Caroline Bedford	Pharmacist	Expert

Leeds (East) Research Ethics Committee
Room 5.2, Clinical Sciences Building
St James's University Hospital
Beckett Street
Leeds
LS9 7TF

Tel: 0113 2065652
Fax: 0113 2066772

27 April 2009

Dr Ann Morgan
HEFCE- Clinical Senior Lecturer
Honorary Consultant Rheumatologist
The University of Leeds
St James Hospital
Leeds
LS9 7TF

Dear Dr Morgan

Study title: **Functional characterisation of the genes and proteins involved in the development and severity of autoimmune and (auto)inflammatory diseases**
REC reference: **04/Q1206/107**
Amendment number: **5**
Amendment date: **26 March 2009**

Thank you for your email of 23 April 2009, responding to the Committee's request for further information on the above research and submitting revised documentation.

The further information was considered in correspondence by a sub-committee of the REC.

Ethical opinion

The members of the Committee taking part in the review gave a favourable ethical opinion of the amendment on the basis described in the notice of amendment form and supporting documentation, as revised.

Documents approved

The documents reviewed and approved were:

Document	Version	Date
Participant Information Sheet: Healthy Controls	3	26 March 2009
Participant Information Sheet: Disease Controls	3	26 March 2009
Participant Information Sheet: Patients	3	26 March 2009
Notice of Substantial Amendment (non-CTIMPs)		26 March 2009

Membership of the Committee

The members of the Committee who took part in the review are listed on the attached sheet.

R&D approval

All investigators and research collaborators in the NHS should notify the R&D office for the relevant NHS care organisation of this amendment and check whether it affects R&D approval of the research.

Statement of compliance

The Committee is constituted in accordance with the Governance Arrangements for Research Ethics Committees (July 2001) and complies fully with the Standard Operating Procedures for Research Ethics Committees in the UK.

04/Q1206/107:	**Please quote this number on all correspondence**

Yours sincerely

Ann Tunley
Committee Co-ordinator

E-mail: ann.tunley@leedsth.nhs.uk

Copy to: R&D Office for Leeds Teaching Hospitals NHS Trust

Leeds (East) Research Ethics Committee

Members of the Sub-Committee which reviewed the amendment

Name	*Profession*	*Capacity*
Dr Carol E Chu	Consultant Clinical Geneticist	Expert
Mr Roly Squire	Consultant Paediatric Surgeon	Expert

PATIENT INFORMATION SHEET

Functional characterisation of the genes and proteins involved in the development and severity of autoimmune and (auto) inflammatory diseases.

PART 1

1. Invitation

You are being invited to take part in a research study. Before you decide whether or not to take part, it is important for you to understand why the research is being done and what it will involve. Please take time to read the following information carefully, and discuss it with others if you wish.

PART 1 tells you the purpose of this study and what will happen to you if you take part.

PART 2 gives you more detailed information about the conduct of the study.

Ask us if there is anything that is not clear, or if you would like more information. Take time to decide whether or not you wish to take part.

2. What is the purpose of the study?

Many autoimmune and (auto)inflammatory diseases, such as rheumatoid arthritis, systemic lupus erythematosus, vasculitis and the connective tissue diseases are associated with the presence of specific changes in either an individual's genetic makeup or their immune system. This can lead to alterations in the different components of the immune system or in the proteins that are produced by these genes. We feel these changes may be important for the development of either the disease itself, specific antibodies/ complications or that they may even predispose to or even help us predict more severe disease. We would like to perform some further research to gain a better understanding of their biology and how they may contribute to these various diseases.

3. Why have I been chosen?

You have been chosen because you have a specific autoimmune or inflammatory disease that we are interested in studying further. Alternatively, you may have donated a sample for one of our previous studies and we have already characterised some of your genes. In this study we would like to use your white blood cells to determine if this genetic variant affects the way your cells work. We would also like to store some of your white blood cells and additional components of your blood, such as the proteins and a sample of your DNA and urine. Otherwise, you may be having some fluid drained from one of your joints, an arthroscopy or biopsy to help with the diagnosis of your condition, or as part of your treatment. We would like to be able to use this fluid and/or any surplus tissue samples, which would otherwise be thrown away, for research purposes. These samples will only be used in future studies that continue with this agreed line of research. In order to give us a permanent source of specific genes and proteins we may also like to make some cell-lines from specific proteins or cells from your blood in the laboratory.

4. Do I have to take part?
It is up to you to decide whether or not to take part. If you decide to take part, you will be given this information sheet to keep and be asked to sign a consent form. If you decide to take part, you are still free to withdraw at any time and without giving a reason. This will not affect the standard of care you receive.

5. What will happen to me if I take part?

If you decide to take part you will asked to sign an informed consent sheet, and you will be given a copy of the information sheet to keep. You will be asked to donate a sample of blood (up to 50mls), which will be taken at the same time as your routine clinic blood tests. Alternatively, we may ask for a sample of your urine or the ability to use the surplus joint fluid or tissue removed as part of your routine NHS treatment. Taking part will therefore not involve any extra visits to the clinic.

The blood sample will be used for genetic testing, but this is purely for research purposes and you will not be told the results of the tests on your samples. Insurance companies, however, may ask you whether you have previously had genetic tests. Should this situation arise, we advise you to answer "no" in your insurance policy application form. This is because the genetic tests we are doing, are purely for research purposes and have no bearing whatsoever on your current or future insurance policies.

6 What do I have to do?
Apart from donating a small volume of blood for research, there are no other requirements/ tests.

7. What are the side effects of any treatment received when taking part?
You may develop a bruise at the site of the needle but, as stated above, taking part in this study does not involve any additional blood tests.

8. What are the possible benefits of taking part?
You will not benefit directly from taking part in this research, and all other aspects of your care will be the same as if you did not take part.

9. What if there is a problem?
If you have a concern about any aspect of this study, you should ask to speak with the researchers who will do their best to answer your question. **If you remain unhappy and wish to complain formally, you can do this through the NHS Complaints Procedure. Details can be obtained from the hospital.**

In the event that something does go wrong and you are harmed during the research study there are no special compensation arrangements. If you are harmed and this is due to someone's negligence then you may have grounds for a legal action for compensation but you may have to pay your legal costs. The normal National Health Service complaints mechanisms will still be available to you.

10. Will my taking part in this study be kept confidential?
Yes. All the information about your participation in this study will be kept confidential. The details are included in Part 2.

11. Contact Details

Please do not hesitate to contact your GP or any other independent person if you need advice. For further information on the study please contact Dr Ann W Morgan or Professor Dennis McGonagle on extension 0113 206 5117.

This completes Part 1 of the Information Sheet.

If the information in Part 1 has interested you and you are considering participation, please continue to read the additional information in Part 2 before making any decision.

PART 2

12. Will my part in this study be kept confidential?

If you consent to take part in this study, the records obtained while you are in this study as well as related health records will remain strictly confidential at all times. The information will be held securely on paper and electronically at your treating hospital and the University of Leeds, the main team managing this research under the provisions of the 1998 Data Protection Act. Your name will not be passed to anyone else outside the research team or the sponsor, who is not involved in the research.

Information will be transferred from your hospital site to the team at the University of Leeds organizing the research, to enable processing of blood samples, this will be done by mail, however your name will only appear on your consent form and blood sample until it is separated and stored. All other records will have your name removed and will only feature your initials and date of birth.

Your records will be available to people authorised to work on the trial but may also need to be made available to people authorised by the Research Sponsor, which is the organisation responsible for ensuring that the study is carried out correctly. A copy of your consent form may be sent to the Research Sponsor during the course of the study. By signing the consent form you agree to this access for the current study and any further research that may be conducted in relation to it, even if you withdraw from the current study.

The information collected about you may also be shown to authorised people from the UK Regulatory Authority and Independent Ethics Committee; this is to ensure that the study is carried out to the highest possible scientific standards. All will have a duty of confidentiality to you as a research participant.

In line with Good Clinical Practice guidelines, at the end of the study, your data will be securely archived for a minimum of 15 years. Arrangements for confidential destruction will then be made.

20. What will happen to any samples I give?

Once it is sent to the University of Leeds, your blood sample will anonymised and separated into its component parts so that some of your DNA, serum and cells will be stored to form part of our "disease sample repository" so that we can use it in current and future genetic and immunological studies. Any additional studies will be subject to additional independent ethical committee review.

21. Will any Genetic testing be done?

Yes, once anonymised your DNA will be used in genetic testing aimed at finding out which genes are important in both the development and severity of a number of autoimmune and (auto)inflammatory diseases. Your DNA will only be used in future studies which continue the research themes outlined above.

22. What will happen to the results of this research?

The results of the studies using the "disease sample repository" will usually be published in a medical journal or be presented at a scientific conference. The data will be anonymous and none of the patients involved in the study will be identified in any report or publication.

23. Who is organising and funding this research?

This project is partly being funded by grants from the National Institute for Health Research, Arthritis Research Campaign, Research into Ageing and the University of Leeds.

24. Who has reviewed the study?

This study was given favourable ethical opinion for conduct in the NHS by Leeds (East) Research Ethics Committee. This committee is appointed to determine that research studies are ethical and do not impair the rights or well-being of patients. We have received approval by this committee to be able to do this research study.

25. Contact for further information

You are encouraged to ask any questions you wish, before, during or after your treatment. If you have any questions about the study, please speak to your study nurse or doctor, who will be able to provide you with up to date information about the procedure(s) involved. If you wish to read the research on which this study is based, please ask your study nurse or doctor. If you require any further information or have any concerns while taking part in the study please contact one of the following people:

Dr Ann W Morgan or Professor Dennis McGonagle on 0113 2065117

Alternatively if you or your relatives have any questions about this study you may wish to contact your GP or an organisation that is independent of the hospital at which you are being treated:

Arthritis Research Campaign (***arc***) is a registered charity providing information about all aspects of arthritis for patients and their families. They can provide useful booklets. You can contact them on 0870 850 5000, or access their web site at http://www.arc.org.uk

If you decide you would like to take part then please read and sign the consent form. You will be given a copy of this information sheet and the consent form to keep. A copy of the consent form will be filed in your patient notes, one will be filed with the study records and one may be sent to the Research Sponsor.

You can have more time to think this over if you are at all unsure.

Thank you for taking the time to read this information sheet and to consider this study.

The Leeds Teaching Hospitals NHS
NHS Trust

PATIENT CONSENT FORM

Functional characterisation of the genes and proteins involved in the development and severity of autoimmune and (auto) inflammatory diseases.

Patient ID: …..…….. Initials: …….. Date of Birth: ……..

Patient initial each point

1. I confirm that I have read and understand the information sheet dated 26.03.2009 (version 3.0) for the above study, and have had the opportunity to ask questions. I understand that my participation is voluntary and that I am free to withdraw at any time without my medical care or legal rights being affected. I agree to take part in the study. _____

2. I understand that my medical records may be looked at by authorised individuals from the Sponsor for the study, the UK Regulatory Authority or the Independent Ethics Committee in order to check that the study is being carried out correctly. I give permission, provided that strict confidentiality is maintained, for these bodies to have access to my medical records for the above study and any further research that may be conducted in relation to it. I also give permission for a copy of my consent form to be sent to the Sponsor for the study. _____

3. I understand that even if I withdraw from the above study, the data and samples collected from me will be used in analysing the results of the study, unless I specifically withdraw consent for this. I understand that my identity will remain anonymous. _____

4. I consent to the storage including electronic, of personal information for the purposes of this study. I understand that any information that could identify me will be kept strictly confidential and that no personal information will be included in the study report or other publication. _____

5. I agree to the samples and cell lines being stored for future research. _____

6. I agree to have genetic tests done on samples for research purposes. _____

_____	_____
Name of the patient	Patient's signature and the date the patient signed the Consent form
_____	_____
Name of the Investigator taking written consent	Investigator's signature and date the Investigator signed the consent form

Original to be retained and filed in the site file. 1 copy to patient, 1 copy to be filed in patient's notes, 1 copy for Sponsor